DEFORMATION IN THE HIGH SPEED UPSETTING OF RINGS - A SOLUTION BY WEIGHTED RESIDUALS

By

THANGEVELU RAVINDRANATH

MARCH 1976

A Thesis submitted for the degree of Doctor of Philosophy of the University of London and for the Diploma of the Imperial College

Mechanical Engineering Dept.,
Imperial College,
London SW7 2BX

SYNOPSIS

This thesis is essentially a study of the effects of strain-rate, end friction and consequent temperature rise and the changes in geometry of short hollow cylinders during the high speed upsetting between flat parallel platens. Literature is reviewed to sum up the dynamic behaviour of metals. A numerical solution using the method of weighted residuals is presented. The mathematical treatment and the computational procedure are described in detail. It is also demonstrated how this model could be used to obtain stress, strain, velocity and temperature fields in upsetting in general. The computed results have been verified experimentally and compared with other published work. A linear induction motor was used as an impact device and some aspects of instrumentation and measurement of transient phenomena are also discussed.

CONTENTS

LIST OF ILLUSTRATIONS

NOTATIONS

A - area of cross-section.

α - constant friction factor.

b - bulge parameter.

A_i, B_i, C_i, D_i - parameters of trial function.

C_k - slope of stress-strain curve at room temperature.

C_{kT} - slope of stress-strain curve at temperature T.

D, d - diameters.

D_o - initial diameter.

δ_{ij} - Kronecker delta.

∇^2 - Laplace operator.

E - Young's Modulus.

e - engineering strain.

ε_r - radial strain.

ε_θ - hoops strain.

ε_z - axial strain.

ε_{rz} - shear strain.

$\dot{\varepsilon}$ - strain rate.

$\bar{\varepsilon}$ - equivalent strain.

$\dot{\bar{\varepsilon}}$ - equivalent strain rate.

$\dot{\varepsilon}^P$ - plastic strain rate.

ε^P - plastic strain.

G_n - weighting factors.

J_1 - first invariant of deviatoric stress tensor.

J_2 - second invariant of deviatoric stress tensor.

J_3 - third invariant of deviatoric stress tensor.

Γ - boundary surfaces.

h - heat generated.

H_o - initial height of the specimen.

H_1 - height after deformation.

H - current height of specimen.

h_f - heat transfer film coefficient.

I_1 - first invariant of strain rate tensor.

I_2 - Second invariant of strain rate tensor.

I_3 - third invariant of strain rate tensor.

I_2 - second invariant of strain rate tensor.

i,J,k,m,n - indices.

k - shear yield stress (initial).

k* - shear yield stress (current).

K - thermal conductivity.

Δk - increment in shear yield stress.

ℓ - length of the specimen.

μ - coefficient of friction.

P_{av} - average pressure.

q_g - heat generated due to plastic work.

q_g - heat generated due to work of friction.

r - coordinate in the r-direction.

r_{max} - maximum value of coordinate in r-direction.

R_o - outside radius.

R_i - inside radius.

R_n - neutral radius.

R - residual.

R_T - total residual.

ρ - density of the material.

ρ_s - density of the specimen.

ρ_p - density of the platen.

σ_o - yield stress.

σ_r - radial stress.

σ_θ - hoop stress.

σ_z - axial stress.

σ'_r - deviatoric radial stress.

σ'_θ - deviatoric hoop stress.

σ'_z - deviatoric axial stress.

τ_{rz} - shear stress.

$\bar{\sigma}$ - equivalent stress.

σ_s - flow stress.

T - temperature.

T_o - ambient temperature.

T_I - initial temperature.

T_F - temperature of the surrounding medium.

ΔT - increment in temperature.

t - time.

Δt - time increment.

u_r - radial displacement.

u_z - axial displacement.

$\dot{u}$ - platen velocity.

v - volume or domain.

V_I - impact velocity of platen.

V - current velocity of platen.

V_r - radial velocity.

V_z - axial velocity.

V_θ - circumferential velocity.

$\bar{V}$ - velocity vector.

w - work done.

$\dot{w}$ - power.

W_j - weighting function.

X_{ij}, x_{ij} - coefficients of free parameters in the trial function.

z - coordinate in the z-direction.

z_{max} - maximum value of coordinate in z-direction.

ACKNOWLEDGEMENTS

I wish to express my sincere thanks and gratitude to Dr. B. Lengyel for suggesting this project and for his help and guidance throughout this work.

I gratefully acknowledge Professor J.M. Alexander for his kind permission to use the facilities of the Metalworking Laboratory and the Authorities of the Imperial College for the award of an assistantship.

Thanks are also due to Dr. E.L. Ortiz, Mathematics Department, and Dr. H. Bolton, Electrical Engineering Department, for their help and advice.

The assistance given by all members of staff, in particular M/s. H.A. Pooley, N. Keates, R. Baxter, W.H. Plumb, R. Gunn and S. Pridham and my colleagues, in particular Mr. H. Helman, is gratefully acknowledged.

Finally my thanks are due to Mrs. Shelagh Murdock for typing this manuscript.

T. RAVINDRANATH
March, 1976.

CHAPTER 1

INTRODUCTION

In recent years much research and development work in metal working has been directed at increasing conventional forming speeds and extending the normal range of forming temperatures. In view of the fact that supply and cost of material is becoming critical, the development of forming processes has assumed greater priority. Although the introduction of high energy rate machines a decade or so ago has not been very successful there is a sustained interest in the development of such processes due to the possibility of more compact and cheaper equipment, reduced production cost and better products. Therefore the study of dynamic behaviour of metals at high speed is of interest and value in metalworking.

Considerable effort has been made in the past to collect experimental data to establish the relationship between applied forces and deformation at high strain-rates. Mechanical behaviour of metal is influenced by strain, strain rate, temperature, boundary and inertia restraints and interfacial friction. Research workers have developed ingenious techniques to isolate these variables and study them individually. Data thus generated enable us to sensibly interpret the deformation and apply them to a production situation.

The experimental work has closely been followed by theoretical work and in the early days many mathematical solutions in the closed analytical form were proposed for idealised materials. With computers it has now become possible to employ numerical methods to construct mathematical models which simulate the behaviour of deforming metals very much closer to reality. However, much theoretical work would seem to have been directed mainly at satisfying academic interests.

Nearly all the numerical methods that are in vogue, in particular the most popular and possibly the most powerful method of finite elements, make excessive demands on computer resources. Rewarding intellectual exercises they may be, but outside the academic world the costs will be prohibitive for them to be of much use. This certainly will be so in the case of smaller industrial establishments and less affluent societies. The need to direct research activities into more purposeful channels has been evident for some time and efforts are now made to ensure this.

Insofar as this subject of interest is concerned, the main objectives for further work should be:-

a) As analytical solutions cannot adequately describe the deformation process, to propose numerical

solutions that characterise the deformation in terms of all, or at least the most significant, variables collectively. Thus the concomitant effect of the process variables can be accounted for.

b) To propose models to simulate deformation at high speeds which can be easily adopted for processes at conventional speeds.

c) To adapt or devise methods that can be handled with relative ease and are less demanding on computer resources.

This present work is an attempt to meet some of these requirements. The method of weighted residuals seems to offer the best scope for a solution to this chosen problem of high speed upsetting of rings.

CHAPTER 2

LITERATURE SURVEY

Metal working theories are chiefly concerned with prediction of stresses acting during metal deformation and consequently the forces that must be applied. During plastic deformation there is generation, movement and interlocking of dislocations [1,2] and the material slips along lattice planes in directions related to the structure of the material. With increasing deformation larger numbers of dislocations are produced and hence larger forces must be applied to enforce their movement. This residual effect broadly explains the strain hardening phenomenon. In order to establish this deformation characteristic, it is first necessary to determine the stress-strain relationship from a test with a simple stress system. The tensile test, simplest of all, is limited to relatively small changes in shape and therefore for larger deformations it is necessary to resort to tests of compression or shear type [3].

2.1 QUASI-STATIC COMPRESSION

Contrary to the tensile test in which the ultimate strength is practically independent of the length of the specimen (above a certain length/diameter ratio), in comparison

the stress/strain relationship is strongly influenced by the height (H_o)/Diameter (D_o) ratio of the specimen and the frictional constraints at the tool/specimen interface. These are demonstrated in Fig. 2.1 and Fig. 2.2.

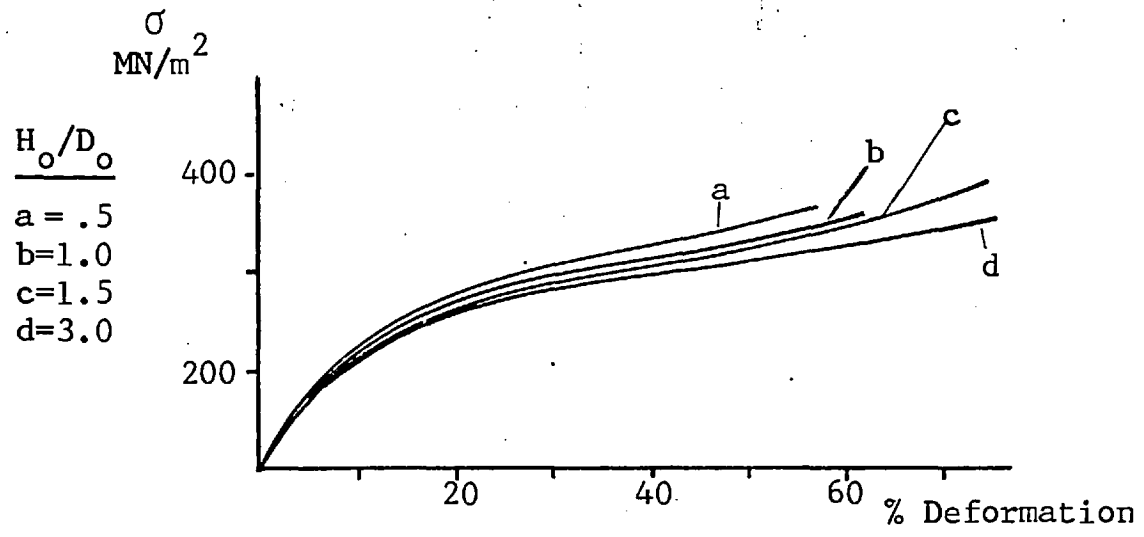

FIG. 2.1 Compression curves of Cu between lapped tools [4].

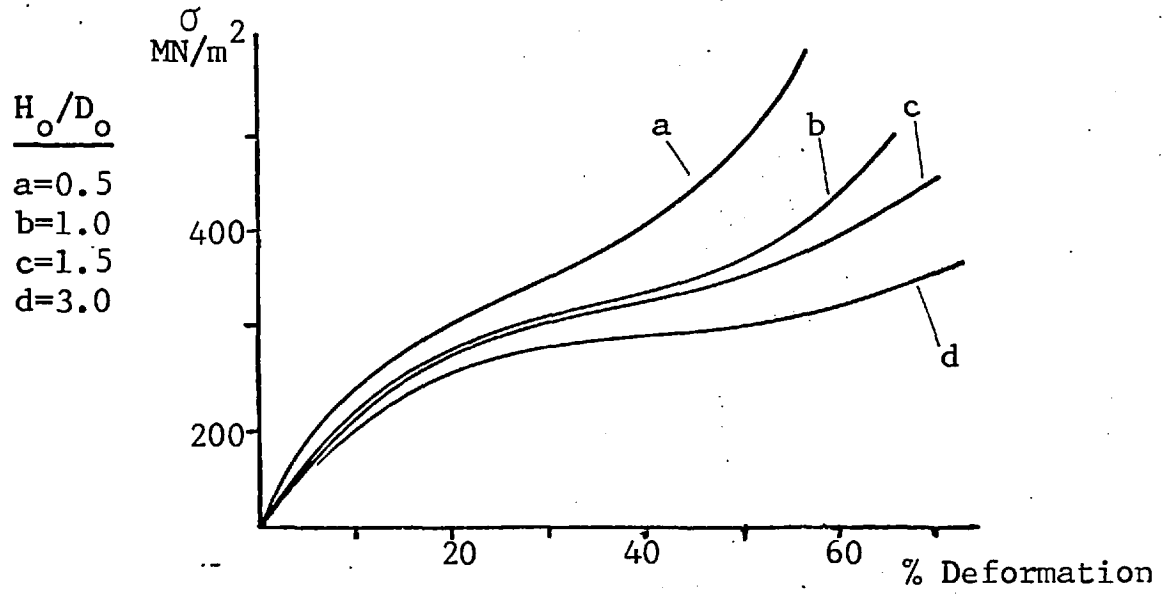

FIG. 2.2 Compression curves of Cu between turned tools [4].

2.1.1 Compression Tests to determine basic Stress/Strain Relationship

Stress/strain relationship unaffected by the aspect ratio and the interface friction will be the "true" or "basic" stress/strain curve. Many ingenious methods have been used to determine the basic relationship. Rummel [5] and Meyer and Nehl [6] suggested that soft compression pieces be placed between tool and specimen to eliminate end friction. Other workers have found that although the bulge was minimised the end faces of the specimen became concave. Siebel and Pomp [7,8] suggested use of conical dies and countersunk specimens and deduced a formula which related the true stress S_o, the diameter to height ratio, the friction angle ϕ and the cone angle α as

$$S = S_o \left[1 + \tfrac{1}{3} \frac{d}{h} \tan(\phi - \alpha) \right] \qquad (2.1)$$

Underwood [9] observed that friction decreases towards the apex of the cone and so suggested the use of hyperboloid-like tools which complicates the procedure even more. Taylor and Quinney [10] used a h/d ratio of unity and to minimise bulge applied the load incrementally and lubricated the specimen between each stage. The specimen was re-machined after 40% deformation to reduce diameter and hence friction effect. The method proposed by Cook and Larke [4] was based on the

work of Sachs [11] who observed that when a number of cylinders, equal in diameter but of various heights, are compressed each stress/strain curve converges towards a lower limit as the h/d ratio increases. The method is indirect and the final results are obtained by extrapolation. Polokowski [12] suggested use of h/d ratio greater than unity and re-machining the specimen after 25% deformation to original h/d ratio. The results will obviously depend upon the care taken to re-machine the specimen.

2.1.2 Measurement of friction

Among the few experimental methods proposed to measure friction, the method suggested by Kunogi, and then Kudo [13] and developed by Male and Cockcroft [14] is probably the most reliable. It was observed that changes in geometry of short hollow cylinders in compression is a measure of friction at the interface. The changes in internal diameter have been calibrated to give numerical values of friction coefficient μ. This method is discussed in detail in Section 2.4.

2.2 DYNAMIC COMPRESSION

The mechanism of deformation in monocrystals of a particular material depends upon the form, rate of

deformation, temperature and boundary restraints. While at slow speeds, the crystal deforms by slip along specific lattice planes at high speeds the deformation is produced by glide on a greater number of closely placed slip bands which are affected by the rate of deformation. Metallurgical [15, 16] studies of the macrostructural changes and motion of dislocations have established the rate-controlling mechanism in terms of the activation energy. Physicists [17] have studied the microstructural changes and explained the metal behaviour in terms of sub-grain and sub-structure formation.

However, from an engineering point of view, the most important material property is the shape of the stress/strain curve. Several techniques [15-30] were developed to establish this dynamic relationship. These and many other works have been reviewed in considerable detail in Stamelos [32] and Mohitpur [31]. Nadai and Manjoine [34] showed that at high speeds as the time taken for deformation decreases, adiabatic heating takes place and results in localised temperature rise. This effect is even more pronounced under conditions of higher friction. Alder and Phillips [35] and Jones et al [36] have clearly demonstrated the dependence of strain-rate sensitivity on temperature. It was reported [35] that for copper and steel the stress for a given strain increased with strain rate, in fair agreement with the power law:

$$\sigma_s = A\,\dot{\varepsilon}^n,$$

where A is a constant, and that the power index 'n' tended to increase with temperature.

Lengyel and Agarwal [37] considered the temperature rise due to deformation and boundary friction in extrusion and reported that the hardness of the product decreased with increase in speed. Finally, another important aspect to consider is the inertia effect at high speeds. The energy required merely to accelerate the material to the working speed could be considerable and further acceleration may occur during the course of this forming process itself as a result of the geometry of the tools enforcing a reduction in cross-sectional area of the billet [38]. Lipman [39] proposed a theory to consider the inertia effects, discussed later in Section 4.7. This was followed up by others [40,41]. Dean [40] observed that the inertia effects became apparent at speeds of 30.0 m/sec. and above.

Some of the formulae proposed to correlate stress, strain, strain rate and temperature are:

i) Ludwik [42]: $\sigma_s = A_1 + B_o \ln \dot{\varepsilon}/\dot{\varepsilon}_o$ (2.2)

where A, B and $_o$ are constants.

ii) Alder and Phillips [35]: $\sigma_s = A\,\dot{\varepsilon}^n$ (2.3)

where A is a constant.

iii) Macgregor and Fisher [44] suggested that increase in strain rate is equivalent to drop in temperature T_m:

$$T_m = T(1 - m \ln \dot{\varepsilon}/\dot{\varepsilon}_o) \qquad (2.4)$$

where T is test temperature and $\dot{\varepsilon}_o$ are constants.

iv) Inouye: $\sigma_s = B_o.\varepsilon^n.\dot{\varepsilon}^m(A/TK)$ (2.5)

where A, B, k, n and m are constants.

2.2.1 Dynamic Compression Test

Many research workers have carried out dynamic tests to collect data and studied strain-rate sensitivity. Usually these have been interpreted in terms of the mean strain rates. Such average values could be misleading in the case of large deformations. Lengyel and Mohitpur [46] adopted an incremental method to obtain stress/strain data to large strains at constant strain-rate and temperature. Their results, Fig. 2.3, clearly demonstrate that strain-rate and temperature vary significantly when the deformation is large.

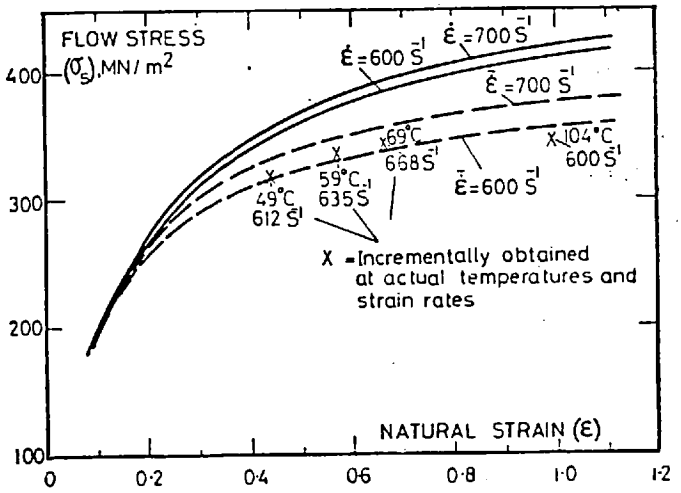

FIG. 2.3 Comparison of Incremental (—) tests and Large Deformation (---) tests.

2.3 NUMERICAL SOLUTIONS

Few numerical solutions [48-53] have been proposed to obtain information regarding bulge, temperature distribution and stress field in compression of cylindrical billets. Some of these solutions are discussed below.

2.3.1 Barreling in compression

Nagamatsu et al [47] analysed the non-uniform flow (barreling of free surfaces) using the method of finite elements. As interface boundary condition they adopted experimentally determined values of slip ratio instead of the usual coefficient of friction. Finite deformation theory was used to allow for geometric changes in the material and elastic plastic analysis was carried out. The results are shown in Fig. 2.4 and Fig. 2.5. The occurrence of double bulge can be seen in Fig. 2.5. Kobayashi et al [48] carried out finite element analysis to study the mode of deformation and observed that the mode changed from single bulge to double bulge for h/d ratios over 1.6.

2.3.2 Temperature distribution

Pohl [49,50] derived a method to determine the heat

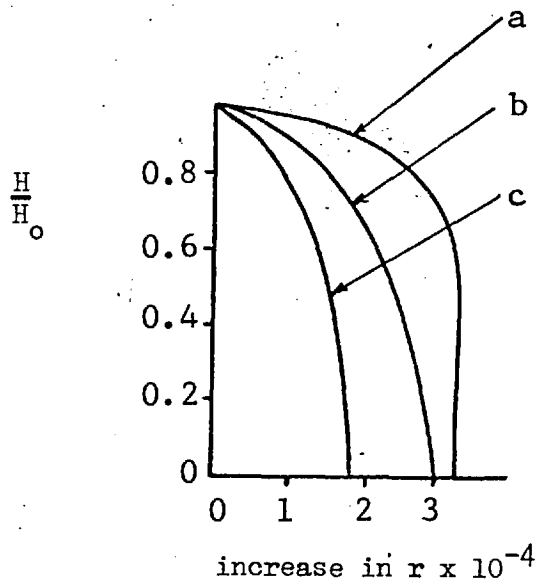

H_o mm
a = 0.25
b = 0.50
c = 2.00

FIG. 2.4 Barreling in compression (sticking) [47]. $\varepsilon = 0.00094$

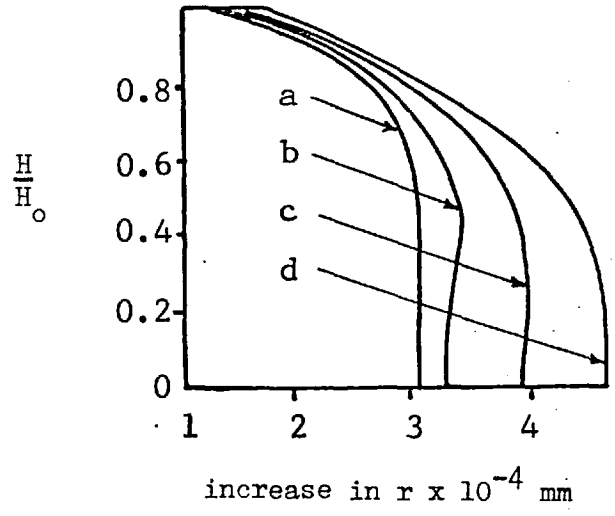

ε
a=0.00091
b=0.00098
c=0.00107
d=0.00116

FIG. 2.5 Bareling in compression (H_o = 2, no lubricant) [47].

generated due to work of deformation and friction at the interface and the resulting temperature distribution in the specimen. The results are shown in Figs. 2.6 to 2.8. It is observed that the temperature rise at the centre of the specimen is over twice as high as that at the tool/specimen interface. This seems to be contrary to what might be expected at higher speeds, particularly as adiabatic heating was assumed. The contribution of the work of friction to heat generation at slow speeds is small, but even so, the difference between the temperature rise at the interface and the centre of the specimen appears rather high. Lengyel and Mohitpur [51] analysed this temperature distribution during high speed upsetting using the method of finite elements. They have clearly demonstrated that those effects of friction at high speeds are quite significant. Their results are compared with the results of this work in Section 7.8.

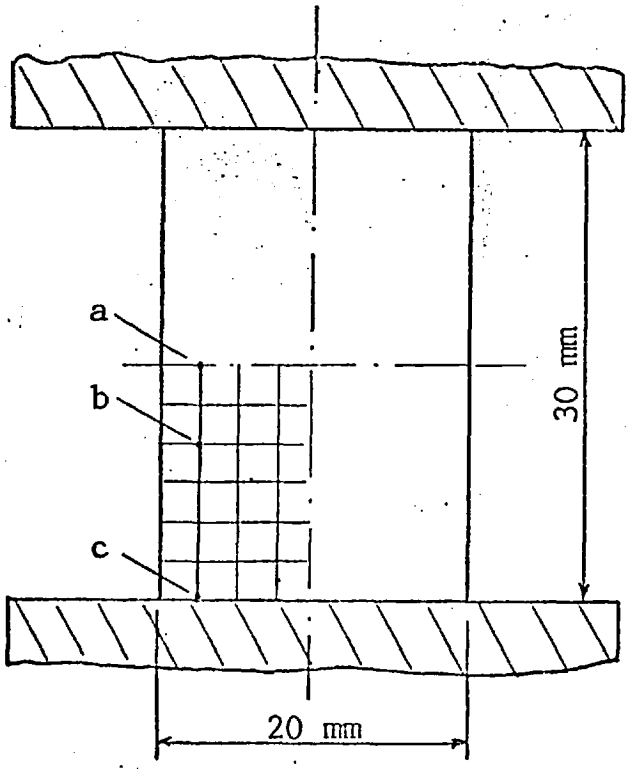

FIG. 2.6 Mesh (material 12CrNi188).

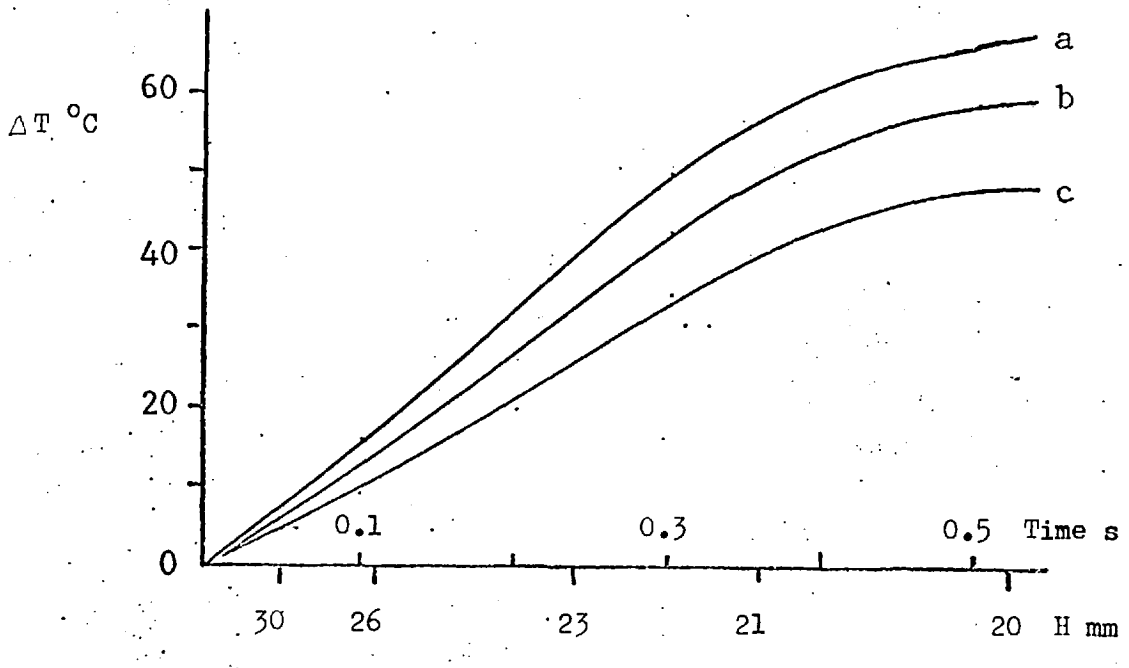

FIG. 2.7 Temperature at specific nodal points in the mesh above [51].

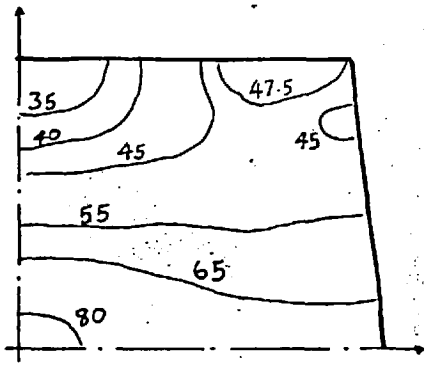

FIG. 2.8 Distribution of increments in temperature [51] Δ T (^{o}C) after 33.3% deformation.

2.3.3 Stress fields

Steck [52,53] used the method of weighted residuals to obtain the stress field, Fig. 2.9. The method of weighted residuals is described in detail in the following chapters.

2.4 RING TESTS

The changes in geometry of a short, hollow cylinder during axisymetric upsetting under frictionless conditions is uniform, i.e. every element flows outwardly in proportion to its distance from the centre, Fig. 2.10(b). However, the existence of end friction makes the process much more complex. As the friction between the die and the specimen increases, the expansion of the hole decreases and eventually the hole begins to contract, Fig. 2.10(c). For a specific geometry under certain conditions of friction the hole may initially increase in

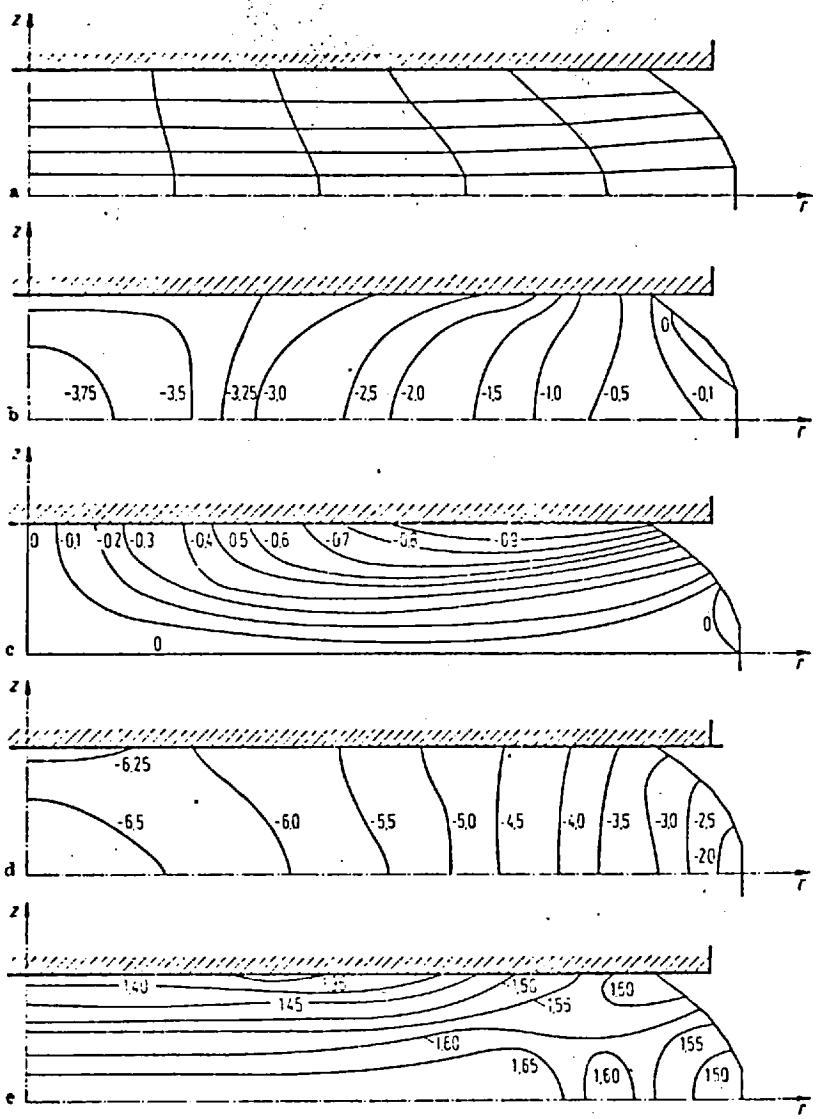

FIG. 2.9 Stress distribution after 50% deformation [51].

a) deformation mode;

b) σ_r/k;

c) τ_{rz}/k;

d) σ_z/k;

e) k^*/k.

diameter and then, as the compression proceeds, begin to contract or begin to contract from the outset of deformation, depending upon the position of neutral surface. The free surface will barrel either way again depending upon the mode of deformation. The two modes of deformation are illustrated in Fig. 2.10.

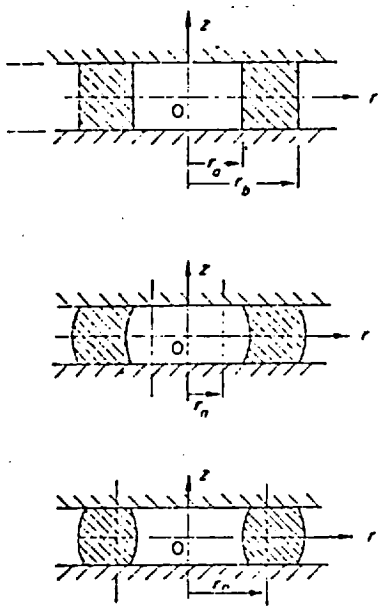

FIG. 2.10 Ring Specimen (a); Deformation Modes (b) and (c).

2.4.1 Experimental calibration

As observed earlier, the ring tests can be effectively used to quantify friction at the tool/billet interface. Male and Cockcroft [14] proposed a method to determine the coefficient of friction by measuring the changes in internal diameter of the ring in compression. A set of experimentally

determined calibration curves are shown in Fig. 2.11. Admittedly, this is an interesting concept in as much as the method of determining the coefficient of friction is independent of the mechanical properties of the material and is dependent only on the geometric configuration, hence has the great

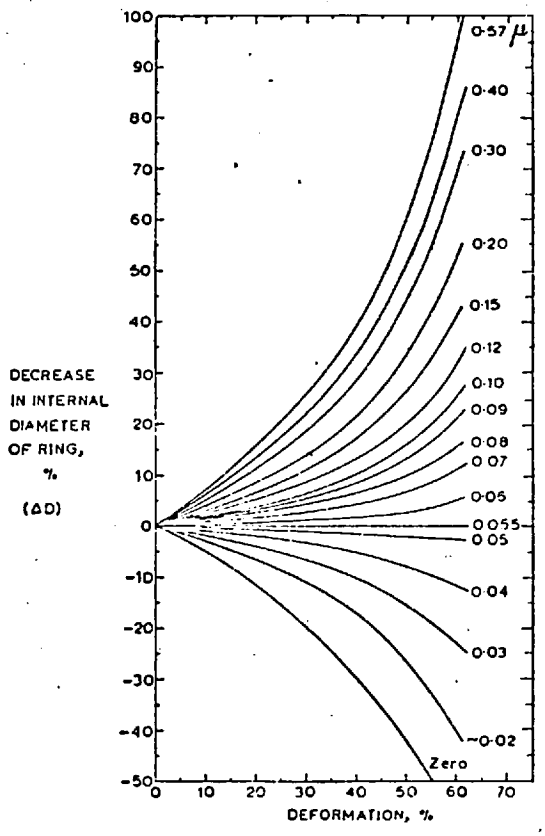

FIG. 2.11 Experimental Calibration Curves [14] for a ring of 6:3:2 ratio. (Outer diameter = 19.05 mm, Inner diameter = 9.53 mm, Height = 6.35 mm).

advantage that no direct measurement of force is required, thus eliminating most of the difficulties in compression

testing at high temperatures and high speeds. However, when this work was first published satisfactory theoretical analysis of rings in compression was not available. Therefore Schroder and Webster [54] analysis for the compression of solid disc was used to compute theoretical average pressure during the compression of rings under different conditions (values of μ) of friction. These were then used for the calibration of experimental results. The need for this indirect method of calibration, which is not entirely satisfactory, has now been eliminated as theoretical analyses of rings are available (Sections 2.4.2 and 2.4.3).

2.4.2 Upper bound solution without bulge

Avitzur [56,57] in the first instance proposed an upper bound solution assuming rigid plastic material, constant shear factor 'm' to characterise friction conditions, and neglecting non-uniform deformation of cylindrical elements. He assumed a kinematically admissible velocity field as

$$V_\theta = 0, \quad V_z = \frac{z}{H}, \quad V_r = V_r(r,z) \tag{2.6}$$

where T is the specimen height.

When appropriate boundary conditions are applied this leads to an expression for power $\dot{W}$ as

$$\dot{W} = \dot{W}(\sigma_o, V, \frac{R_i}{H}, \frac{R_n}{R_o}, \alpha\frac{R_o}{H}) \tag{2.7}$$

The value of r_n that minimises this function for power is considered to be actual. The value of r_n thus determined

can be used to calculate average pressure as follows:

$$\alpha\frac{R_o}{H} \leqslant \frac{1}{2(1 - R_i/R_o)} \ln \frac{3(R_o/R_i)^2}{1+\sqrt{1+3(R_o/R_i)^4}}$$

and

$$\frac{P_{av}}{\sigma_o} = \frac{1}{1-(R_i/R_o)^2}\left\{\sqrt{1+\tfrac{1}{3}(\frac{R_n}{R_o})^4} - \sqrt{(\frac{R_i}{R_o})^4 + \tfrac{1}{3}(\frac{R_n}{R_o})^4} + \frac{2}{3\sqrt{3}}\,\alpha\frac{R_o}{H}\left[1 - (\frac{R_i}{R_o})^3\right]\right\}$$

where

$$(\frac{R_n}{R_o})^2 = \frac{\sqrt{3}}{2}\,\frac{1 - (R_i/R_o)^4 x^2}{\sqrt{x(x-1)\left[1 - (R_i/R_o)^4 x\right]}} \qquad (2.8)$$

$$x = \left\{\frac{R_o}{R_i}\exp\left[-\alpha\frac{R_o}{H}(1 - \frac{R_i}{R_o})\right]\right\}^2$$

When $R_i \leqslant R_n \leqslant R_o$,

$$\alpha\frac{R_o}{H} \geqslant \frac{1}{2(1 - R_i/R_o)} \ln \frac{3(R_o/R_i)^2}{1+\sqrt{1+3(R_o/R_i)^4}}$$

or when $\alpha\frac{R_o}{H} > \frac{1}{2}$

$$\frac{P_{av}}{\sigma_o} = \frac{1}{1-(R_i/R_o)^2}\left\{\sqrt{1+\tfrac{1}{3}(\frac{R_n}{R_o})^4} - \sqrt{(\frac{R_i}{R_o})^4 + \tfrac{1}{3}(\frac{R_n}{R_o})^4} + \frac{2}{3\sqrt{3}}\,\alpha\frac{R_o}{H}\left[1 + (\frac{R_i}{R_o})^3 - 2(\frac{R_n}{R_o})^3\right]\right\}$$

where R_n/R_o is found by successive approximations from

$$2\alpha\frac{R_o}{H}\left(1+\frac{R_i}{R_o}-2\frac{R_n}{R_o}\right)+\ln\left(\frac{R_i}{R_o}\right)^2\left|\frac{(R_n/R_o)^2+\sqrt{3+(R_n/R_o)^4}}{(R_n/R_o)^2+\sqrt{3(R_i/R_o)^4+(R_n/R_o)^4}}\right|=0 \qquad (2.9)$$

Kudo [13] analysed deformation of hollow cylinders assuming that the ring consists of unit deforming regions of annular parts with triangular cross-section. The sides of the triangular sections which are lines of velocity discontinuity are assumed to move as straight lines without changing their angle

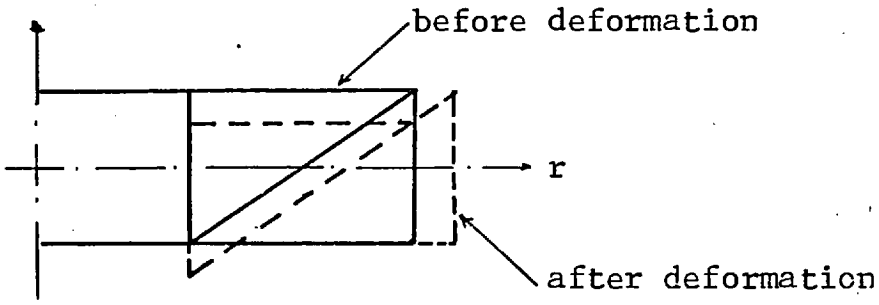

and that the radial velocity component in each part is assumed to be independent of the z-coordinate. The mode of deformation is illustrated above. The velocity field derived for this mode of deformation was then used to obtain an upper bound solution

2.4.3 Equilibrium approach - without bulge

Hawkyard and Johnson [59] proposed a solution from stress equilibrium conditions. They determined calibration (theoretical) comparable with that obtained experimentally in [14]. They also represented the position of neutral surface

graphically, Fig. 2.12. This solution is simpler than those discussed in the previous section and describes the process adequately if the bulge is neglected.

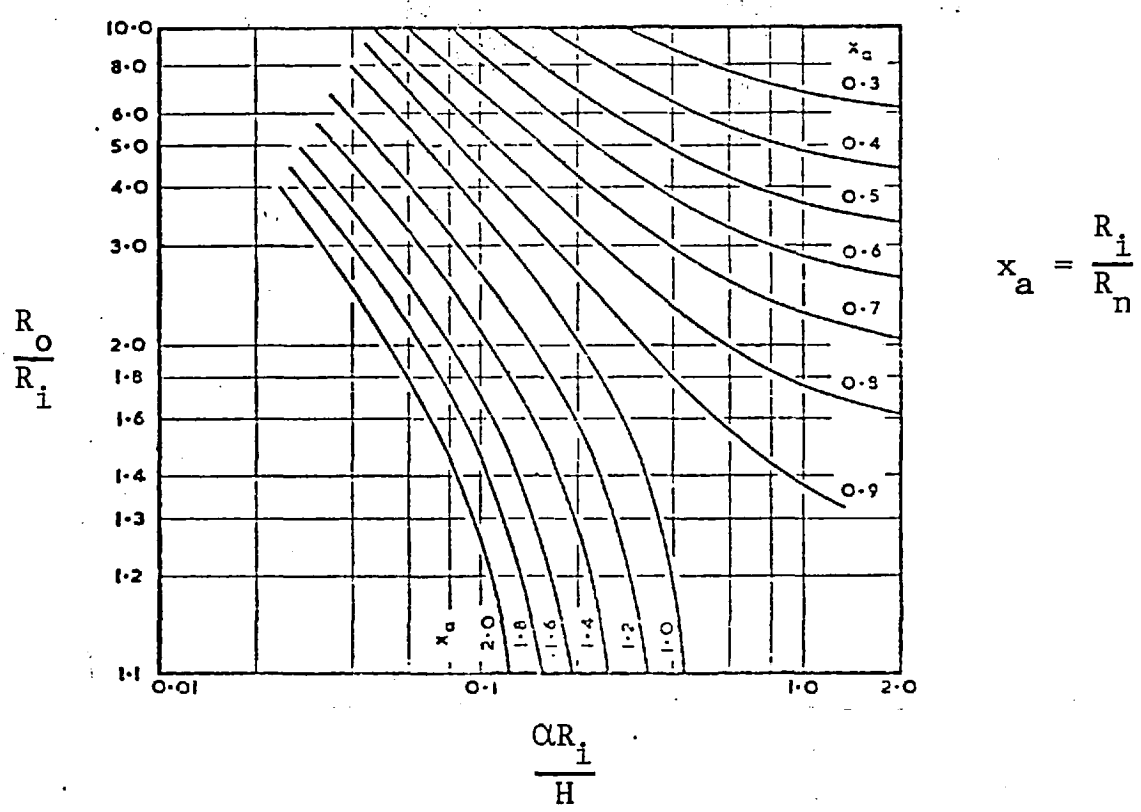

FIG. 2.12 Graphical representation of neutral surfaces [59], 6:3:2 ring.

Burgdorf [60] produced a similar solution assuming constant coefficient of friction, instead of the constant friction factor used in [59]. It is observed that the results of [59] agree more closely with experimental calibration [14]. Therefore it may be concluded that it is better to describe the interface friction in the case of upsetting by constant friction factor.

2.4.4 Upper-bound with bulge

Avitzur [58] extended his solution [57] to take into account the bulge formation at the free surface. He modified the proposed velocity field as:

$$\left.\begin{aligned} V_\theta &= 0 \\ V_r &= -\frac{A}{2}\frac{V}{H} r\left[1-\left(\frac{R_n}{r}\right)^2\right] e^{-bz/H} \\ V_z &= V_z(r,z) \end{aligned}\right\} \text{ for } 0 \leqslant z \leqslant H/2 \qquad (2.10)$$

Constant 'A' can be determined from boundary conditions and the parameter 'b' determines the bulge.

The total internal power $\dot{w} = \dot{w}_i + \dot{w}_f$, where

$$\dot{w} = \dot{w}\left(V, \frac{R_o}{H}, \alpha, \frac{R_n}{R_o}, b, \sigma_o\right) \qquad (2.11)$$

The externally supplied power

$$\dot{w}_e = (R_o^2 - R_i^2) V P_{av} \qquad (2.12)$$

From equations (2.9) and (2.10) an expression for average pressure can be derived as

$$\frac{P_{av}}{\sigma_o} = f\left(\frac{R_o}{R_i}, \frac{R_o}{H}, \alpha, \frac{R_n}{R_o}, b\right) \qquad (2.13)$$

The values chosen for R_n and b are those that minimise the relative pressure and thus the required power.

Hence from

$$\frac{\partial(P_{av}/\sigma_o)}{\partial b} = 0 \qquad (2.14)$$

$$b = b\left(\frac{R_o}{R_i}, \frac{R_o}{H}, \alpha, \frac{R_n}{R_o}\right) \qquad (2.15)$$

Final results are

when $$\alpha\frac{R_o}{H} \leqslant \frac{1}{2(1 - R_i/R_o)} \ln \frac{3(R_o/R_i)^2}{1 + \sqrt{1+3(R_o/R_i)^4}} \qquad (2.16)$$

then $R_n \leqslant R_i$ and

$$\frac{P_{av}}{\sigma_o} = \frac{\frac{1}{\sqrt{3}}(\frac{R_n}{R_o})^2}{1-(\frac{R_i}{R_o})^2} \left\{ + \sqrt{1+3(\frac{R_o}{R_n})^4} - \sqrt{1+3(\frac{R_i}{R_o})^4(\frac{R_o}{R_n})^4} \right.$$

$$- \ln\left[(\frac{R_i}{R_o})^2 \frac{1 + \sqrt{1 + 3(R_o/R_n)^4}}{1 + \sqrt{1+3(R_i/R_o)^4(R_o/R_n)^4}} \right]$$

$$+ \frac{b^2}{4}(\frac{R_o}{H})^2 \frac{1}{\sqrt{1+3(R_o/R_n)^4}} \left\{ \frac{1}{4}(\frac{R_o}{R_n})^4 \left[1 - (\frac{R_i}{R_o})^4 \right] \right.$$

$$- (\frac{R_o}{R_n})^2 \left[1 - (\frac{R_i}{R_o})^2 \right] + \ln\frac{R_o}{R_o} \Big\} + 2\alpha\frac{R_n}{R_o}\frac{R_o}{H} \left\{ \frac{1}{3}(\frac{R_o}{R_n})^3 \left[1 - (\frac{R_i}{R_o})^3 \right] \right.$$

$$\left. \left. - (\frac{R_o}{R_n})(1 - \frac{R_i}{R_o}) \right\} \quad (1 - \frac{b}{4} + \frac{b^2}{48}) \right\} \qquad (2.17)$$

where

$$b = \left[\alpha\left[\tfrac{1}{3}\left(\frac{R_o}{R_n}\right)^2\left(1-\left(\frac{R_i}{R_o}\right)^3\right]-\left(1-\frac{R_i}{R_o}\right)\right]\Bigg/\left\{\frac{\alpha}{6}\left[\tfrac{1}{3}\left(\frac{R_o}{R_n}\right)^2\left[1-\left(\frac{R_i}{R_o}\right)^3\right]\right.\right.$$

$$\left.-\left[1-\frac{R_i}{R_o}\right]\right]+\frac{R_o/H}{\sqrt{1+3(R_o/R_n)^4}}\left[\tfrac{1}{4}\left(\frac{R_o}{R_n}\right)^4\left[1-\left(\frac{R_i}{R_o}\right)^4\right]\right.$$

$$\left.\left.-\left(\frac{R_o}{R_n}\right)^2\left[1-\left(\frac{R_i}{R_o}\right)^2\right]+\ln\frac{R_o}{R_i}\right]\right\} \qquad (2.18)$$

when

$$\alpha\frac{R_n}{H} \geqslant \frac{1}{2(1-R_i/R_o)}\ln\frac{3(R_o/R_i)^2}{1+\sqrt{1+3(R_o/R_i)^4}}$$

or when

$$\alpha\frac{R_o}{H} \geqslant \tfrac{1}{2}$$

then $R_i \leqslant R_n < R_o$ and

$$\frac{P_{av}}{\sigma_o} = \frac{\frac{1}{\sqrt{3}}\left(\frac{R_n}{R_o}\right)^2}{1-(R_i/R_o)^2}\left\{+\sqrt{1+3\left(\frac{R_o}{R_n}\right)^4}-\sqrt{1+3\left(\frac{R_i}{R_o}\right)^4\left(\frac{R_o}{R_n}\right)^4}\right.$$

$$-\ln\left[\left(\frac{R_i}{R_o}\right)^2\frac{1+\sqrt{1+3\left(\frac{R_o}{R_n}\right)^4}}{1+\sqrt{1+3\left(\frac{R_i}{R_o}\right)^4\left(\frac{R_o}{R_n}\right)^4}}\right]+\frac{b^2}{4}\left(\frac{R_o}{H}\right)^2\frac{1}{\sqrt{1+3\left(\frac{R_o}{R_n}\right)^4}}\left\{\tfrac{1}{4}\left(\frac{R_o}{R_n}\right)^4\left[1-\right.\right.$$

$$\left.\left(\frac{R_i}{R_o}\right)^4\right]-\left(\frac{R_o}{R_n}\right)^2\left[1-\left(\frac{R_i}{R_o}\right)^2\right]+\ln\frac{R_o}{R_i}\Bigg\}+2\alpha\frac{R_n}{R_o}\frac{R_o}{H}\left\{\frac{4}{3}+\tfrac{1}{3}\left(\frac{R_o}{R_n}\right)^3\left[1+\left(\frac{R_i}{R_o}\right)^3\right.\right.$$

$$\left.\left.\left.-\left(\frac{R_o}{R_n}\right)\left[1+\frac{R_i}{R_o}\right]\right\}\left[1-\frac{b}{4}+\frac{b^2}{48}\right]\right\} \qquad (2.19)$$

where

$$b = \left\{\alpha\frac{R_n}{R_o}\left[\frac{4}{3}+\tfrac{1}{3}\left(\frac{R_o}{R_n}\right)^3\left[1+\left(\frac{R_i}{R_o}\right)^3\right]-\frac{R_o}{R_n}\left[1+\frac{R_i}{R_o}\right]\right]\right\} \Bigg/ \left\{\frac{\alpha}{6}\frac{R_n}{R_o}\left[\frac{4}{3}+\right.\right.$$

$$+\tfrac{1}{3}\left(\frac{R_o}{R_n}\right)^3\left[1+\left(\frac{R_i}{R_o}\right)^3\right]-\frac{R_o}{R_n}\left[1+\frac{R_i}{R_o}\right]+\frac{R_o/H}{\sqrt{1+3\left(\frac{R_i}{R_n}\right)^4}}\left[\tfrac{1}{4}\left(\frac{R_o}{R_n}\right)^4\left[1-\right.\right.$$

$$\left.\left.\left.-\left(\frac{R_i}{R_o}\right)^4\right]-\left(\frac{R_o}{R_n}\right)^2\left[1-\left(\frac{R_i}{R_o}\right)^2\right]+\ln\frac{R_o}{R_i}\right]\right\}$$

Liu [62] proposed an admissible velocity field as

$$V_\theta = 0$$

$$V_r = \frac{b_1\pi V}{4H\sin\left(\frac{b_1\pi}{2}\right)}\left(\frac{r^2-R_n^2}{r}\right)\cos\left(\frac{b_1\pi z}{H}\right) \qquad (2.20)$$

$$V_v = -\frac{V}{2\sin\left(\frac{b_1\pi}{2}\right)}\sin\left(\frac{b_1\pi z}{H}\right)$$

where b_1 is the parameter which determines bulge.

In general, upper bound solutions are derived assuming Von Mises material. However, Lee and Altan [61] considered the deformation in increments of small steps to account for hardening. For each step a new distribution of $\bar{\sigma}$ was computed and an average value $\bar{\sigma}_{avg}$ was found as follows:

$$\bar{\sigma}_{avg} = \frac{1}{v}\int\bar{\sigma}\,dv \qquad (2.21)$$

2.4.5 Numerical solutions

Hill [64] proposed a general method of analysis where a class of velocity fields are chosen initially and the best approximation taken out eventually. The chosen velocity field must satisfy all kinematic conditions. The chosen velocity field will not necessarily satisfy statical requirements and therefore a criterion must be determined which may be regarded as closely satisfying the statical conditions. Lahothi and Kobayashi [63] applying this method proposed a class of velocity field as

$$\begin{aligned} V_r &= \tfrac{1}{2}\left(r - \frac{R_n^2}{r}\right)\phi'(z) \\ V_z &= -\phi(z) \\ V_\theta &= 0 \end{aligned} \qquad (2.22)$$

and determined the unknown function $\phi(z)$ as

$$\phi(z) = \int_0^z \exp(-az^2)dz \Big/ \int_0^h \exp(-az^2)dz \qquad (2.23)$$

where:

$$a = \pm\frac{\alpha}{\sqrt{3H}} \int r\,dA \Big/ \int \frac{r^2 - R_n^2}{3 + (R_n/r)^2}\,dA$$

2.4.6 Other related work

Male et al [67] reviewed some of the models discussed so far and reported to have found the Avitzur model discussed in Section 2.4.4 to be the most realistic as compared with experimental results. It was also concluded that the concept of defining interface friction by a constant friction factor α to be better than the concept of constant coefficient of friction μ. The variation of friction factor during deformation is shown in Fig. 2.13. Jain and Bramley [65] studied the effects of speed in a ring test and reported that the interface friction decreased with increase in speed and that this effect was more pronounced when lubricants were used. Abdul and Bramley [66] produced a nomogram to determine stress/strain relationship from ring tests, which is an interesting extension of the ring test.

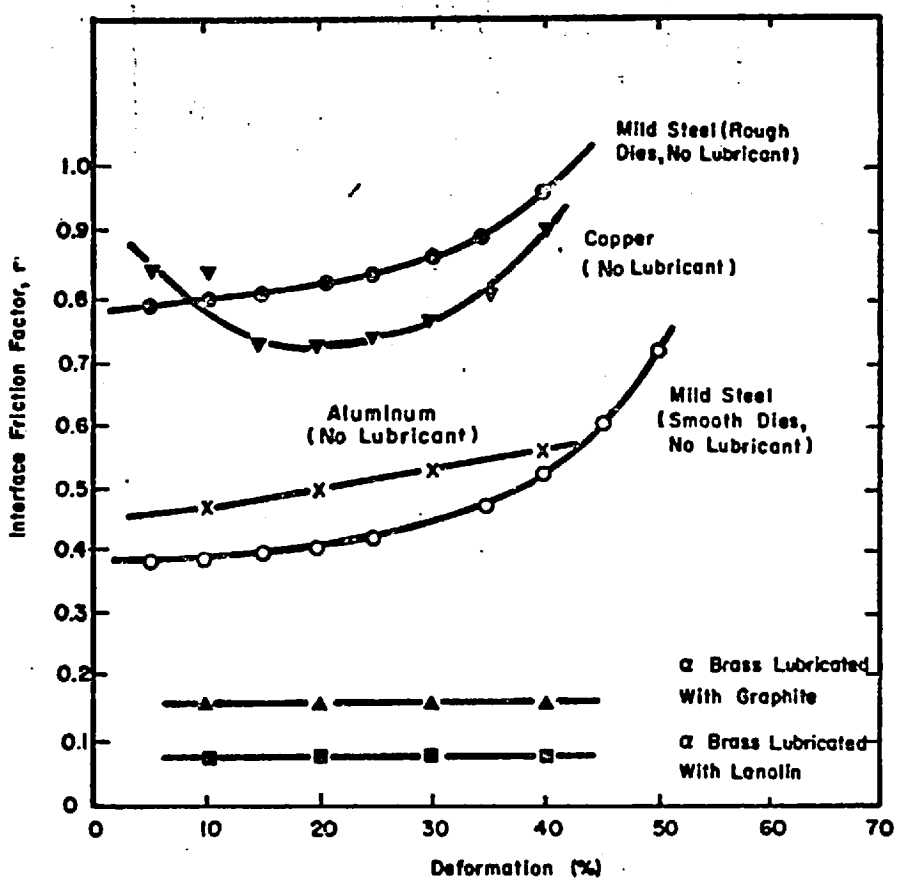

FIG. 2.13 Interface Friction Factor of Various Metals [67].

CHAPTER 3

NUMERICAL METHODS

Analytical solutions to governing differential equations of complex systems are either impossible or too difficult to obtain. Hence it is frequently necessary to use numerical methods to obtain approximate solutions. Usually solutions are proposed in the form of a set of known functions with arbitrary parameters which are then determined so as to satisfy the equations as closely as required or a set of unknown functions are proposed from which the best function is eventually taken out. There are several methods by which approximate solutions can be obtained [75,80]. Generally, the more powerful the method is, the more cumbersome it is to handle. Whenever possible it is best to adopt the simplest method that describes the problem adequately. Advantages gained by using more elaborate methods will be more than offset by the effort, time and computational facilities required and will be of little help in practical situations. Furthermore, methods like finite elements have come to be identified with variational calculus where a functional is derived mathematically and then minimised. In many cases such variational principle does not exist or its existence is not obvious [80] and direct approaches are necessary.

As most problems can be defined by a set of governing equations and boundary conditions a direct approach through the method of weighted residuals presents interesting possibilities. As the method is basically proposing a solution in the form of a series it is inherently capable of converging to exact solution if sufficient number of terms are included in the series [79]. As the solutions obtained by the method of weighted residuals are of analytical form they are more useful than those obtained by numerical integration and usually require much less computing time [75]. If it is necessary to use expansions of higher order to achieve desired accuracy, it might be possible to apply economisation techniques [82].Considering all these, it would seem that the method of weighted residuals is suitable for analysing deformation process of metal in compression and is discussed more fully in the following sections.

3.1 THE METHOD OF WEIGHTED RESIDUALS

The method of weighted residuals is a general method to obtain solutions to the equations of changes in a system. The procedure is to propose an approximate solution in the form of a set of known trial functions with undetermined free parameters. This proposed solution when substituted in the

governing equation results in a "residual" or "error" function. The free parameters are then determined by forcing this residual function to vanish in an average sense.

Consider a differential equation [82]:

$$N(u) - \frac{\partial u}{\partial t} = 0 \qquad x \in V \tag{3.1}$$

where $u = u(x,t)$, $N(-)$ is a general differential operator involving spatial derivatives of 'u'. V is the three-dimensional domain with a boundary s and t is the time.

Let us suppose the initial and boundary conditions are:

$$u(x,0) = u_o(x) \qquad x \in V \tag{3.2}$$

$$u(x,t) = f_s(x,t) \qquad x \in s \tag{3.3}$$

Assume a trial solution

$$u^*(x,t) = u_s(x,t) + \sum_{i=1}^{N} C_i(t)u_i(x,t) \tag{3.4}$$

where the approximating functions u_i are required to satisfy the boundary condition:

$$u_s(x,t) = f_s(x,t) \text{ and } u_i = 0 \qquad x \in s \tag{3.5}$$

Substituting equation (3.4) into (3.1) we obtain the residual function

$$R(u^*) = N(u^*) - \frac{\partial u^*}{\partial t} \neq 0 \qquad (3.6)$$

If the assumed trial functions were the exact solution, then the residual will be zero. To approximate this ideal it is necessary to force the residual to vanish in an average sense over the entire domain of interest. This is done by selecting a set of weighting functions W_j which are orthogonal to the residual functions such that

$$\langle W_j R_j \rangle = 0 \qquad j = 1(1)N \qquad (3.7)$$

and then the weighted integrals are set to zero as

$$\int_V W_j R_j dV = 0 \qquad (3.8)$$

3.2 DIFFERENT METHODS OF WEIGHTING

There are several ways in which the weighting functions may be chosen, each of which corresponds to a different criterion. Once the choice is made, equation (3.4) is reduced to a system of first order equations in N unknowns $C_i(t)$. Some of the more widely used methods are:

i) Collocation

The Dirac delta function $\delta(x-x_1)$ is used as the weighting function so:

$$\int_V \delta(x-x_j)\, R\, dV = R\Big|_{x_j} = 0 \qquad (3.9)$$

i.e., the residual at specified collocation point j is zero. Therefore as many collocation points must be chosen as there are free parameters. However, there exists no rationale [84] for selecting collocation points. In the absence of any special reason, equally spaced collocation points are usually chosen.

ii) Subdomain Method

The domain V is divided into as many subdomains V_j as there are free parameters and the weighting functions are chosen as

$$W_j = \begin{cases} 1 & x \in V_j \\ 0 & x \notin V_j \end{cases}$$

and

$$\int_{V_j} W_j\, R\, dV = 0 \qquad (3.10)$$

Here again it is perhaps best to select uniformly spaced subdomains.

iii) Galerkin Method

The weighting functions are chosen to be the trial function itself in $W_j = C_j$ and:

$$\int_V C_j \, R \, dV = 0 \qquad (3.11)$$

iv) Least Squares Method

The residual is minimised with respect to the free parameters and hence the weighting function is $\frac{\partial R}{\partial C_j}$ and:

$$\frac{\partial R}{\partial C_j} \int_V R^2 \, dV = 0 \qquad (3.12)$$

All these four methods are applied to a simple problem and compared in Section 3.4.

3.3 CHOICE OF TRIAL FUNCTIONS

The choice of trial functions is somewhat arbitrary. The essential condition is that it must be a complete set so that when sufficient number of terms are included in them, the solution will converge to the exact solution. Polynomials are a complete set in as much as any continuous function can be expanded in terms of the polynomials. They are also easy to handle. The trial functions must be linearly independent. Although it is not necessary for them to be linear in free parameters, they are usually chosen to be so to permit easy computation. The trial functions must be chosen to satisfy the governing equation and boundary conditions as closely as possible without unduly complicating the functions. It is not

necessary to satisfy all the boundary conditions in one set of trial functions as they can be treated separately, in which case the total weighted residual function will be the sum of individual weighted residual functions arising from separation, as:

$$G_1 \int_V W_j R \, dV + G_2 \int_S W_j R \, ds = 0 \qquad (3.13)$$

G_1 and G_2 are constants known as "weighting factors". The weighting factors are different from the orthogonalising weighting functions discussed in the previous section. The factors are particularly useful when in the domain of interest only a small proportion of points lie on the boundary one may assign higher weighting factor to ensure that the significance of the particular boundary condition is not lost in the solution. Any symmetry conditions that may exist in the problem must also be satisfied by the trial functions. Finally, it is necessary to ensure that the trial function has no bias in any one particular coordinate direction.

Apart from satisfying these requirements, the choice of the form of trial function is very much left to the intuition and experience of the user. Often the trial functions are based on the simplified analytical solutions to related problems.

3.4 APPLICATION OF DIFFERENT METHODS OF WEIGHTING

In order to illustrate the various methods of selecting weighting functions and to compare them, let us consider the Maxwell's rheological model [83] for the visco-elastic solid

$$\sigma = E\varepsilon + \mu\dot{\varepsilon} \tag{3.14}$$

which may be schematically represented as

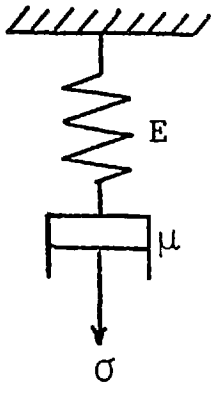

E - Young's Modulus

μ - Viscosity of the damping fluid

The exact solution to this problem is

$$\varepsilon = \frac{\sigma}{E}\left[1 - e^{-Et/\mu}\right] \tag{3.15}$$

where t is time.

To formulate the weighted residual solution we have the governing differential equation

$$\mu\frac{d\varepsilon}{dt} + E\varepsilon(t) - \sigma = 0 \tag{3.16}$$

and the boundary condition

$$\varepsilon(t) = 0\Big|_{t=0} \tag{3.17}$$

Let us consider the time interval

$$0 < t < 1$$

Assume a trial function which satisfies the boundary condition as

$$\varepsilon = \sum_{i=1}^{n} C_i t^i \tag{3.18}$$

Substituting (3.18) in (3.16) we obtain the residual function as in (3.6)

$$R(t) = \mu \sum_{i=1}^{n} C_i\, i\, t^{i-1} + E \sum_{i=1}^{n} C_i t^i - \sigma \neq 0$$

or

$$= \left[\sum_{i=1}^{n} (\mu i\, t^{i-1} + E t^i) C_i \right] - \sigma \tag{3.19}$$

Now we can determine the unknown C_i for i = 1(1)n by applying different weighting functions as follows:

3.4.1 Collocation Method

As we are considering the domain $0 < t < 1$ we can choose 'n' number of collocation points at equal intervals of $\frac{1}{n+1}$. Applying the criterion (3.9) we have $w_j = \delta(t-t_j)$ and

$$R_j = \left[\sum_{i=1}^{n} (\mu_i t_j^{i-1} + E t_j^i) C_i \right] - \sigma = 0$$

$$\text{for } t_j = \frac{1}{n+1}\left(\frac{1}{n+1}\right)\frac{n}{n+1} \qquad (3.20)$$

Thus we have a system of n number of equations which can be solved to determine unknown parameters.

3.4.2 Subdomain Method

Here the subdomain $0 < t < 1$ is divided into equally spaced subdomains of $\frac{1}{n}$. Applying the criterion (3.10) we have

$$W_j = \begin{cases} 1 & t \in j \\ 0 & t \notin j \end{cases}$$

and

$$R_j = \int_{t_{j-1}}^{t_j} \left[\sum_{i=1}^{n} (\mu_i t^{i-1} + E t^i) C_i - \sigma \right] dt = 0$$

$$= \left[\sum_{i=1}^{n} \left(\mu (t_j^i - t_{j-1}^i) + E\left(\frac{t_j^{i+1} - t_{j-1}^{i+1}}{i+1}\right)\right) C_i \right]$$

$$- \sigma (t_j - t_{j-1}) = 0 \quad \text{for} \quad t_j = \frac{1}{n}\left(\frac{1}{n}\right)1 \qquad (3.21)$$

This system of equations can now be solved to determine the free parameters.

3.4.3 Galerkin Method

Applying criterion (3.11) we have

$$W_j = t^j$$

and

$$R_j = \int_0^1 \left[\left(\sum_{i=1}^{n} (\mu_i t^{i-1} + E t^i) C_i \right) t^j - \sigma t^j \right] dt = 0$$

$$= \left[\sum_{i=1}^{n} \left(\frac{\mu_i}{i+j} + \frac{E}{i+j+1} \right) C_i \right] - \frac{\sigma}{j+1} = 0$$

for $j = 1(1)n$ (3.22)

This system of equations can now be solved to determine the free parameters.

3.4.4 Least Square Method

Applying criterion (3.12) we have

$$R_j = \frac{\partial}{\partial A_j} \int R^2 \, dt$$

$$= 2 \int R \frac{\partial R}{\partial A_j} \, dt$$

$$= 2 \int_0^1 \left[\sum_{i=1}^{n} (\mu_i t^{i-1} - E t^i) C_i - \sigma \right] x \left[\mu_j t^{j-1} + E t^j \right] dt = 0$$

$$= \left[\sum_{i=1}^{n} \left(\frac{\mu^2_{ij}}{i+j-1} + \mu E + \frac{E^2}{i+j+1} \right) C_i \right] - \sigma(\mu_j + E) = 0$$

for $j = 1(1)n$ (3.23)

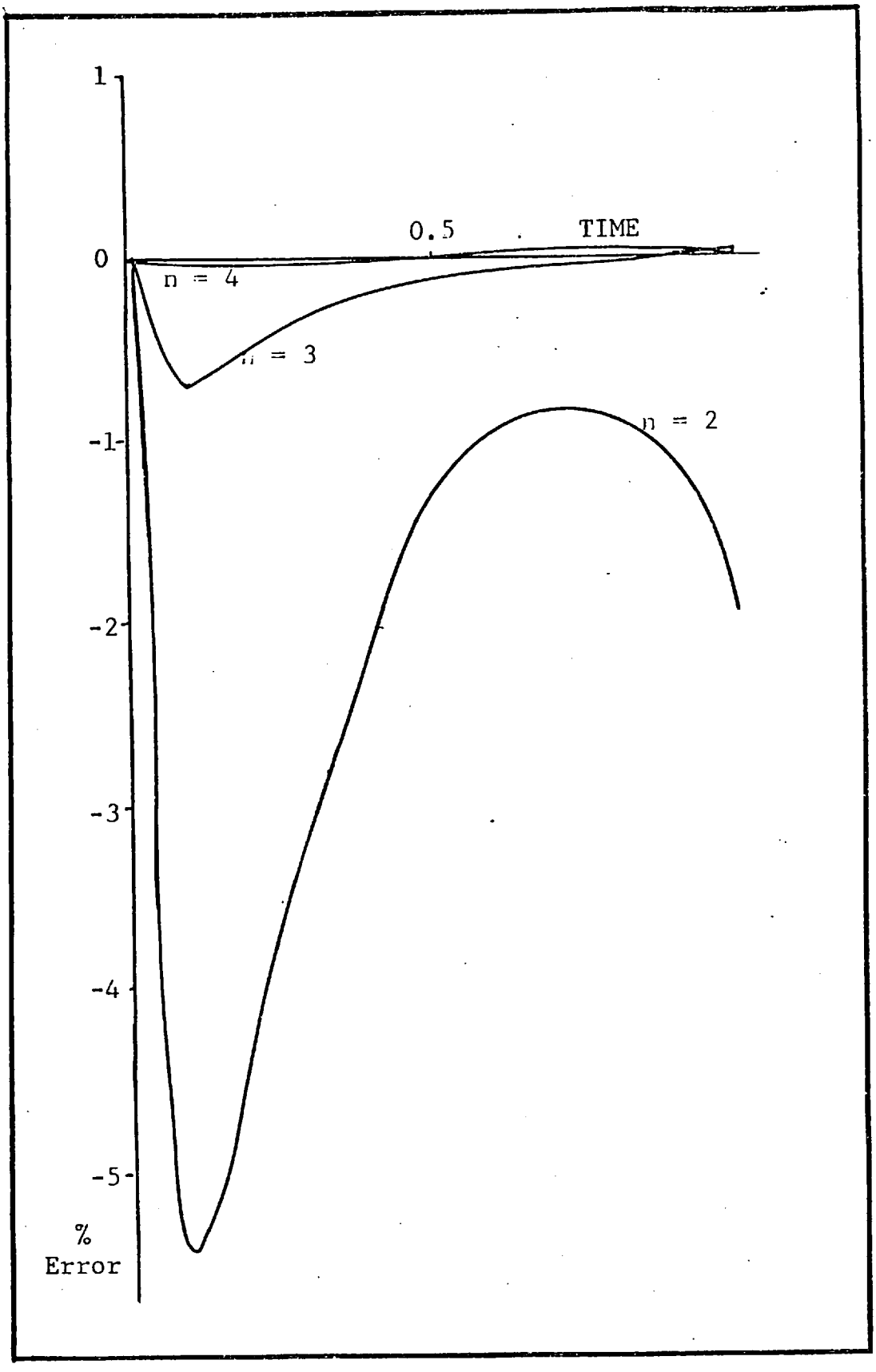

FIG. 3.1 SOLUTION BY COLLOCATION METHOD

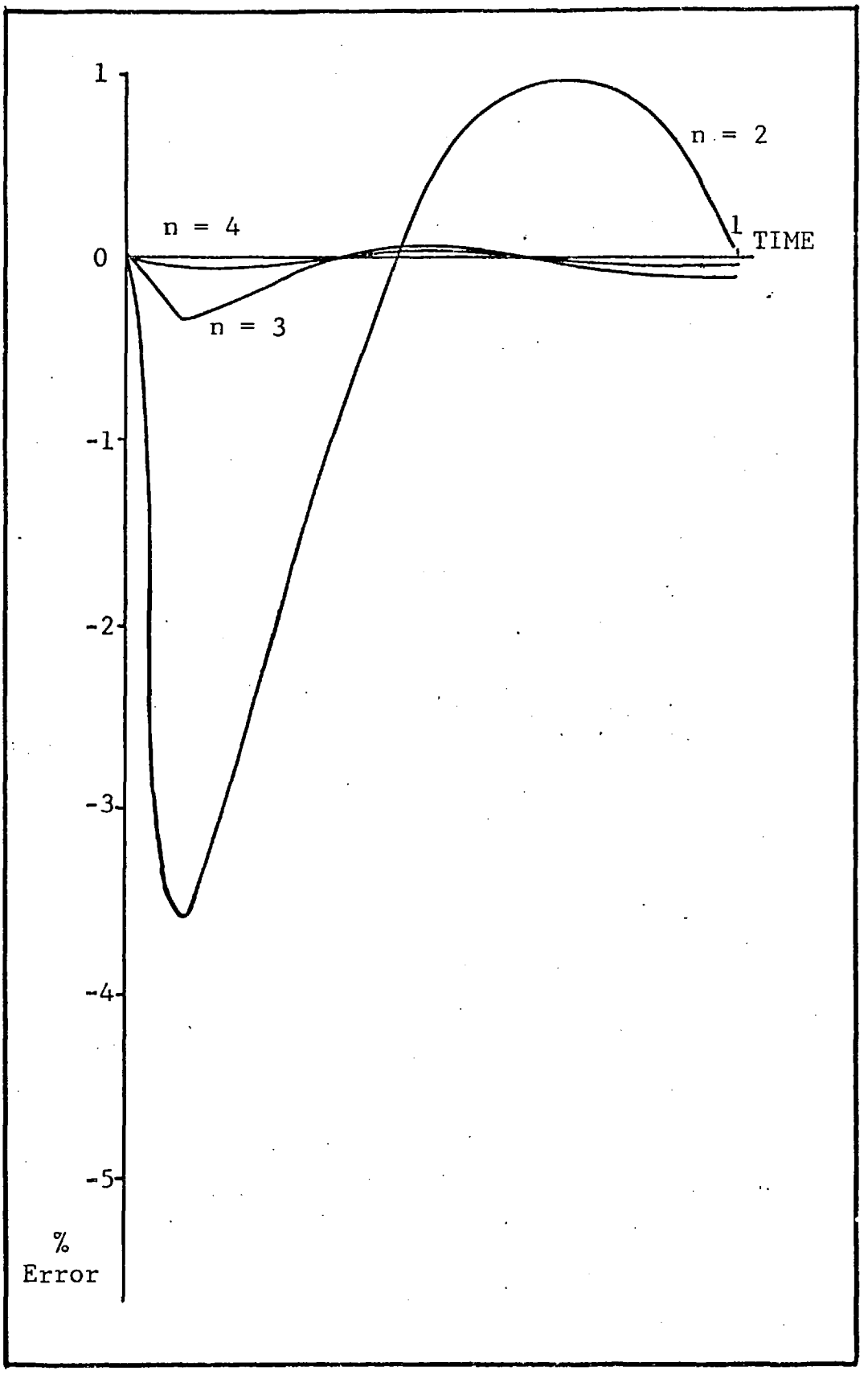

FIG. 3.2 SOLUTION BY SUBDOMAIN METHOD

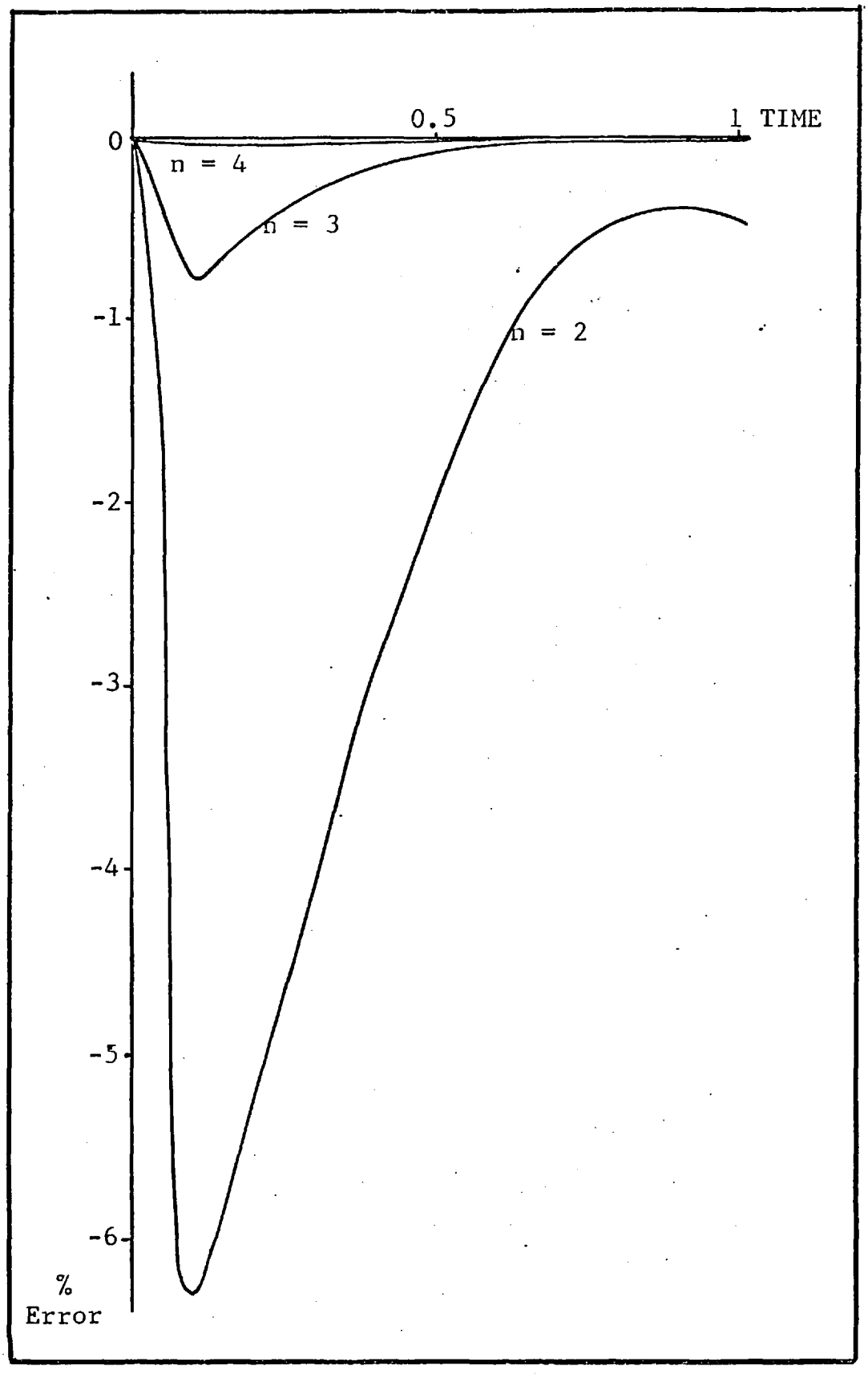

FIG. 3.3 SOLUTION BY GALERKIN METHOD

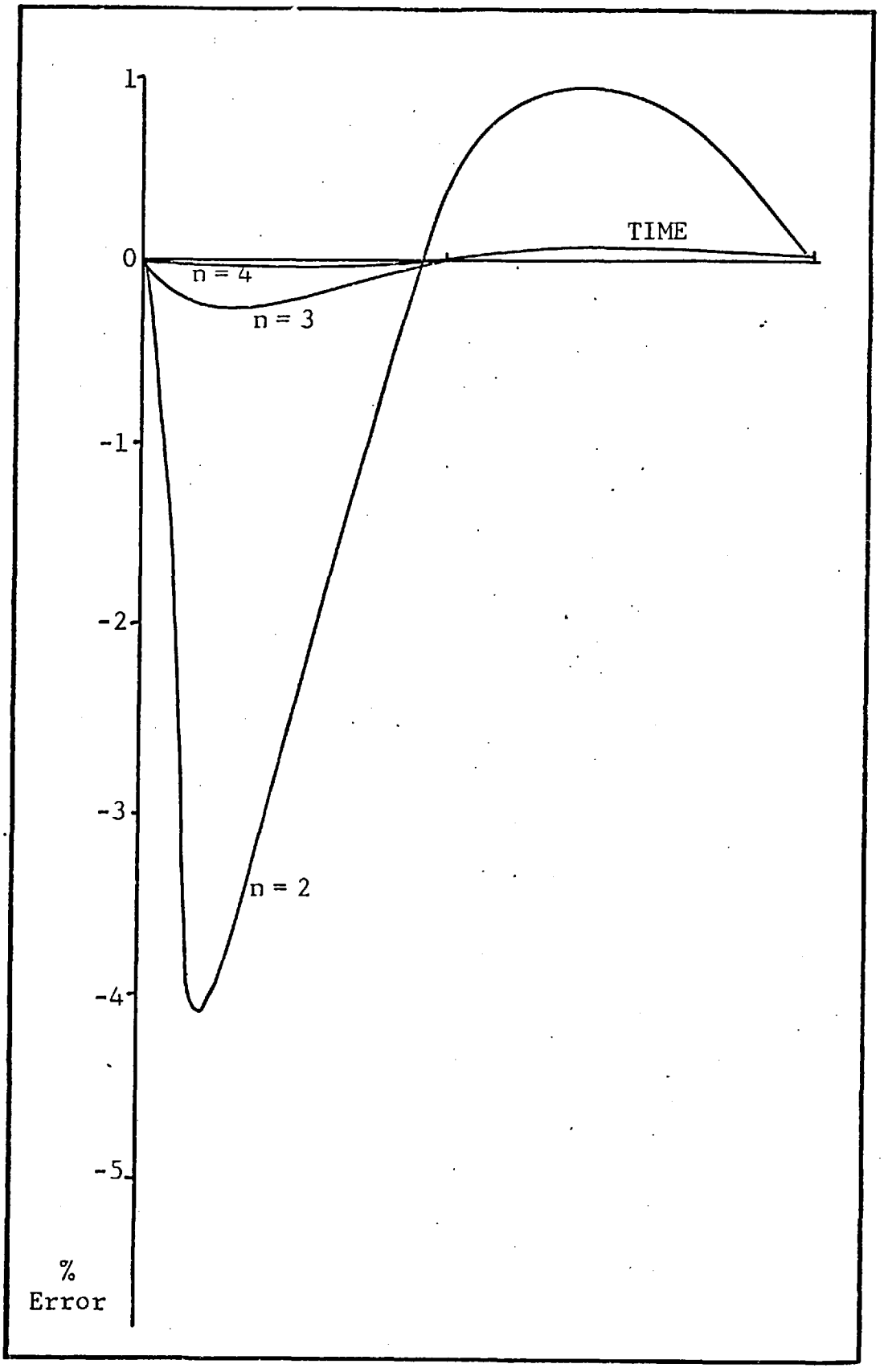

FIG. 3.4 SOLUTION BY LEAST SQUARE METHOD

3.5 COMPARISON OF DIFFERENT METHODS OF WEIGHTING

Solutions to equations (3.20) to (3.23) are represented graphically in Fig. 3.1 to Fig. 3.4 for n = 2, 3 and 4. It is clearly seen that all of them rapidly converge to exact solutions and, as suggested by Finlayson [79], the choice of weighting function is not critical as long as sufficiently high order expansions are used in the trial function. It is observed that the errors are more evenly distributed in the method of least squares and also the mean square residual has theoretical significance as error bounds can sometimes be determined in terms of the residual. Even when error bounds cannot be determined, the mean square residual can be regarded as a measure of accuracy of the solution.

CHAPTER 4

DEFORMATION IN UPSETTING - THEORETICAL CONSIDERATIONS

The elements of continuum mechanics [85,86], theories of plasticity [87-89] and heat transfer [90-92] that are relevant to this work are discussed in this chapter.

4.1 STRESS FIELD

As the subject matter is a study of axisymetric upsetting of rings and cylinders, let us consider the stresses acting on a cylindrical element as in Fig. 4.1.

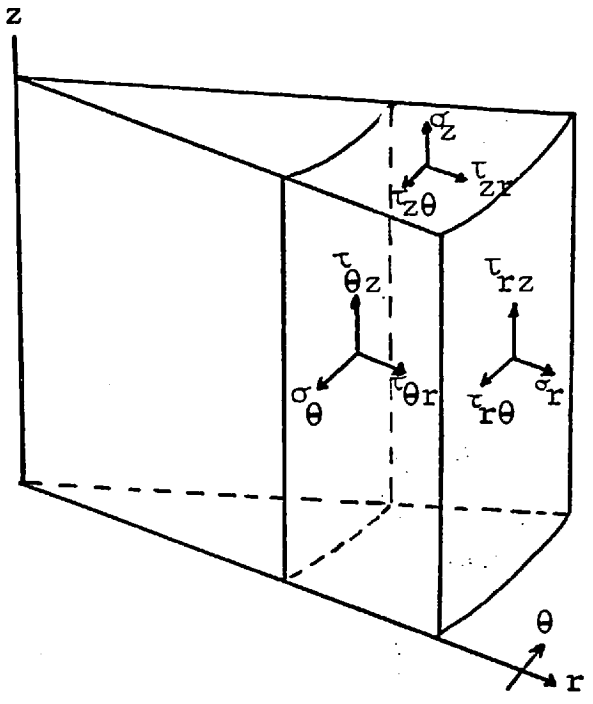

FIG. 4.1 Typical Cylindrical Element.

The distribution of stress in the continuum is defined by Cauchy's stress tensor

$$\sigma_{ij} = \begin{bmatrix} \sigma_{11} & \sigma_{12} & \sigma_{13} \\ \sigma_{21} & \sigma_{22} & \sigma_{23} \\ \sigma_{31} & \sigma_{32} & \sigma_{33} \end{bmatrix} \tag{4.1}$$

is a Cartesian system of coordinates. This second order tensor is symmetric and has the property

$$\sigma_{ij} = \sigma_{ji} \tag{4.2}$$

The principal invariants of this tensor are:

$$\begin{aligned} I_1 &= \sigma_{ii} \\ I_2 &= \tfrac{1}{2}\sigma_{ii}\,\sigma_{jj} - \tfrac{1}{2}\sigma_{ij}\,\sigma_{ij} \\ I_3 &= \det\left[\sigma_{ij}\right] \end{aligned} \tag{4.3}$$

A tensor defined as the 'deviatoric tensor' has the property that its first invariant vanishes. The stress tensor σ_{ij} can be split into two tensors, one of which is the deviatoric tensor and the other is the spherical tensor. Thus

$$\sigma_{ij} = \sigma'_{ij} + \sigma_m\,\delta_{ij} \tag{4.4}$$

where $\sigma_m = \tfrac{1}{3}\sigma_{ii}$

and δ_{ij} is Kronecker delta,

hence the deviatoric stress tensor is

$$\sigma'_{ij} = \sigma_{ij} - \sigma_m\,\delta_{ij} \tag{4.5}$$

whose principal invariants are

$$J_1 = \sigma_{ii} = 0$$
$$J_2 = \tfrac{1}{2}\,\sigma'_{ij}\,\sigma'_{ij} \qquad (4.6)$$
$$J_3 = \det\left[\sigma'_{ij}\right]$$

In a cylindrical coordinate system (r, θ, z) for this element in Fig. 4.1

$$\sigma'_{ij} = \begin{bmatrix} \sigma_r & 0 & \tau_{rz} \\ 0 & \sigma_\theta & 0 \\ \tau_{zr} & 0 & \sigma_z \end{bmatrix} \qquad (4.7)$$

due to symetry

$$\tau_{r\theta} = \tau_{\theta r} = \tau_{\theta z} = \tau_{\theta z} = 0$$

and

$$J_2 = -(\sigma'_r\sigma'_\theta + \sigma'_\theta\sigma'_z + \sigma'_z\sigma'_r) - \tau^2_{rz} \qquad (4.8)$$

Equivalent stress is defined as

$$\bar{\sigma} = \sqrt{3J_2} \qquad (4.9)$$

4.1.1 Stress Function

The equilibrium of stresses acting on the element is given by

$$\frac{\partial \sigma_{ij}}{\partial x_j} + F_j = 0 \qquad \begin{cases} i = 1, 2, 3 \\ j = 1, 2, 3 \end{cases} \tag{4.10}$$

where F is the body force.

The body forces may be neglected for reasons explained in a later section. It is possible to select two scalar functions called 'stress functions' ϕ_1 and ϕ_2 such that

$$\begin{aligned} \sigma_r &= \frac{1}{r}\frac{\partial^2 \phi_1}{\partial r^2} + \frac{\phi_2}{r} = 0 \\ \sigma_\theta &= \frac{\partial \phi_2}{\partial r} \\ \sigma_z &= \frac{1}{r}\frac{\partial^2 \phi_1}{\partial r^2} \\ \sigma_{rz} &= -\frac{1}{r}\frac{\partial^2 \phi_1}{\partial n \partial z} \end{aligned} \tag{4.11}$$

which will automatically satisfy equilibrium of stresses in axisymetric conditions

$$\begin{aligned} &\frac{\partial \sigma_z}{\partial r} + \frac{\partial J_{rz}}{\partial z} + \frac{\sigma_r - \sigma_\theta}{r} = 0 \\ &\frac{\partial \sigma_\theta}{\partial \theta} = 0 \\ &\frac{\partial J_{rz}}{\partial r} + \frac{\partial \sigma_z}{\partial z} + \frac{J_{rz}}{r} = 0 \end{aligned} \tag{4.12}$$

4.2 STRAIN AND STRAIN RATE FIELDS

Cauchy's strain tensor is given by

$$\varepsilon_{ij} = \tfrac{1}{2}\left(\frac{\partial i_i}{\partial x_j} + \frac{\partial u_j}{\partial x_i}\right) \tag{4.13}$$

where u_{ij} is displacement functions.

In cylindrical coordinates and axisymetry

$$\varepsilon_{ij} = \begin{bmatrix} \varepsilon_r & 0 & \varepsilon_{rz} \\ 0 & \varepsilon_\theta & 0 \\ \varepsilon_{rz} & 0 & \varepsilon_z \end{bmatrix} \tag{4.14}$$

The strain rate is defined as

$$\dot{\varepsilon}_{ij} = \frac{\partial \varepsilon_{ij}}{\partial t} \tag{4.15}$$

where t is the time.

This in terms of velocities of displacement v_{ij} is

$$\dot{\varepsilon}'_{ij} = \tfrac{1}{2}\left(\frac{\partial v_i}{\partial x_i} + \frac{\partial v_j}{\partial x_j}\right) \tag{4.16}$$

The assumption that the material is incompressible leads to

$$\dot{\varepsilon}_{ii} = 0 \tag{4.17}$$

The strain rate tensor can also be expressed as deviatoric and spherical components as

$$\varepsilon'_{ij} = \dot{\varepsilon}_{ij} - \dot{\varepsilon}_m \delta_{ij} \tag{4.18}$$

whose principal invariants are

$$
\begin{aligned}
I_1 &= \varepsilon'_{ii} = 0 \\
I_2 &= \tfrac{1}{2}\dot{\varepsilon}'_{ij}\dot{\varepsilon}'_{ij} \\
I_3 &= \det[\dot{\varepsilon}'_{ij}]
\end{aligned}
\tag{4.19}
$$

In axisymetry

$$
I_2 = -(\dot{\varepsilon}'_r\dot{\varepsilon}'_\theta + \dot{\varepsilon}'_\theta\dot{\varepsilon}'_z + \dot{\varepsilon}'_z\dot{\varepsilon}'_r) + \dot{\varepsilon}'^2_{rz} \tag{4.20}
$$

Equivalent strain rate is defined as

$$
\bar{\dot{\varepsilon}} = \frac{2}{\sqrt{3}}\sqrt{I_2} \tag{4.21}
$$

4.2.1 Stream Function

Any strain rate field to be kinematically admissible the continuity equation must be satisfied, which is

$$
\frac{\partial u_r}{\partial r} + \frac{u_r}{r} + \frac{\partial u_z}{\partial z} = 0 \tag{4.22}
$$

in cylindrical coordinates and in axisymetry.

It is possible to choose a stream function ψ such that

$$
\begin{aligned}
v_r &= \frac{1}{r}\frac{\partial\psi}{\partial z} \\
v_z &= -\frac{1}{r}\frac{\partial\psi}{\partial r}
\end{aligned}
\tag{4.23}
$$

which will satisfy equation (4.21).

Expanding equation (4.13) in terms of (4.22) we have

$$\begin{aligned}
\dot{\varepsilon}_r &= \frac{\partial}{\partial r}\left(\frac{1}{r}\frac{\partial \psi}{\partial z}\right) = \frac{\partial v_r}{\partial r} \\
\dot{\varepsilon}_\theta &= \frac{1}{r}\frac{\partial \psi}{\partial z} = \frac{v_r}{r} \\
\dot{\varepsilon}_z &= -\frac{\partial}{\partial z}\left(\frac{1}{r}\frac{\partial \psi}{\partial r}\right) = \frac{\partial v_z}{\partial z} \\
\dot{\varepsilon}_{rz} &= \frac{\partial}{\partial z}\left(\frac{1}{r}\frac{\partial \psi}{\partial z}\right) - \frac{\partial}{\partial r}\left(\frac{1}{r}\frac{\partial \psi}{\partial r}\right) = \frac{\partial v_r}{\partial z} + \frac{\partial v_z}{\partial r}
\end{aligned} \tag{4.24}$$

4.3 YIELD CRITERION

For an isotropic material the scalar function σ_{ij} can be expressed in terms of its principal invariants as

$$f(\sigma_{ij}) = f(J_1, J_2, J_3)$$

Assuming constancy of volume

$$f(\sigma_{ij}) = f(J_1, J_2) \tag{4.25}$$

Von Mises suggested that yielding of the material takes place when the shear energy reaches a maximum. This is given by

$$J_2 - k^2 = 0$$

or

$$\tfrac{1}{2}\,\sigma'_{ij}\,\sigma'_{ij} - k^2 = 0 \tag{4.26}$$

where k is a scalar function depending upon the plastic strain history of the material.

4.4 STRESS STRAIN RELATIONSHIP

An assumption of the infinitesimal elasto plastic theory is that the strain ε_{ij} can be expressed as

$$\varepsilon_{ij} = \varepsilon^E_{ij} + \varepsilon^P_{ij} \tag{4.27}$$

where ε^E_{ij} is the elastic component,

and ε^P_{ij} is the plastic component.

In cases where the plastic strains are much larger than the elastic strains the elastic component may be neglected and then

$$\varepsilon_{ij} = \varepsilon^P_{ij} \tag{4.28}$$

and

$$\dot{\varepsilon}_{ij} = \dot{\varepsilon}^P_{ij} \tag{4.29}$$

For a material that hardens isotropically

$$d\varepsilon^P_{ij} = G \frac{\partial F}{\partial \sigma_{ij}} dF \tag{4.30}$$

Applying the yield criterion (4.26) this can be expressed in terms of strain rates

$$\dot{\varepsilon}^P_{ij} = \Delta \sigma'_{ij} \tag{4.31}$$

where $$\Delta = G \frac{\partial F}{\partial t} = \frac{\sqrt{I_2}}{k}$$

Thus we obtain the Prandtl-Reuss relationship

$$\sigma'_{ij} = \frac{k}{\sqrt{I_2}} \dot{\varepsilon}^P_{ij} \qquad (4.32)$$

4.5 WORK HARDENING

As Von Mises yield criterion has been adopted

$$\bar{\sigma} = Y = \sqrt{3}\,k \qquad (4.33)$$

This is diagrammatically represented in Fig. 4.2.

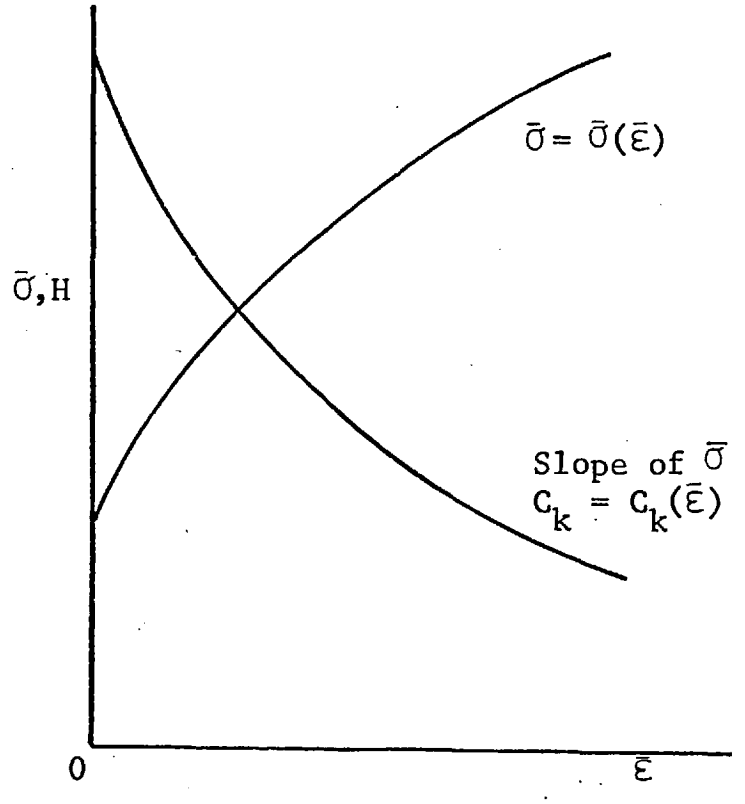

FIG. 4.2 Work Hardening.

From equation (4.21) we have

$$\bar{\varepsilon} = \frac{2}{\sqrt{3}} \int \sqrt{I_2}\, dt \tag{4.34}$$

Assuming $\bar{\sigma} = \bar{\sigma}(\varepsilon)$ we have

$$\bar{\sigma} = \bar{\sigma}_o + \bar{\sigma}(\varepsilon) \tag{4.35}$$

$$\frac{d\bar{\sigma}}{dt} = \frac{d\bar{\sigma}}{d\bar{\varepsilon}} \cdot \frac{d\bar{\varepsilon}}{dt}$$

so

$$\begin{aligned} d\bar{\sigma} &= C_k \dot{\bar{\varepsilon}}\, dt \\ &= C_k \frac{2}{\sqrt{3}} \sqrt{I_2}\, dt \end{aligned} \tag{4.36}$$

In finite increments

$$\Delta\bar{\sigma} = \frac{2}{\sqrt{3}} \cdot C_k \cdot \sqrt{I_2}\, \Delta t \tag{4.37}$$

4.6 STRAIN RATE SENSITIVITY

The strain rate sensitivity of the material is represented in Fig. 4.3.

Now, we can express $\bar{\sigma} = \bar{\sigma}(\bar{\varepsilon}) + \bar{\sigma}(\dot{\bar{\varepsilon}})$ (4.38)

Hence

$$\begin{aligned} \Delta\bar{\sigma} &= \frac{2}{\sqrt{3}} C_k \sqrt{I_2}\, \Delta t + m \frac{2}{\sqrt{3}} \sqrt{I_2} \\ &= \frac{2}{\sqrt{3}} \sqrt{I_2}\, (C_k \Delta t + m) \end{aligned} \tag{4.39}$$

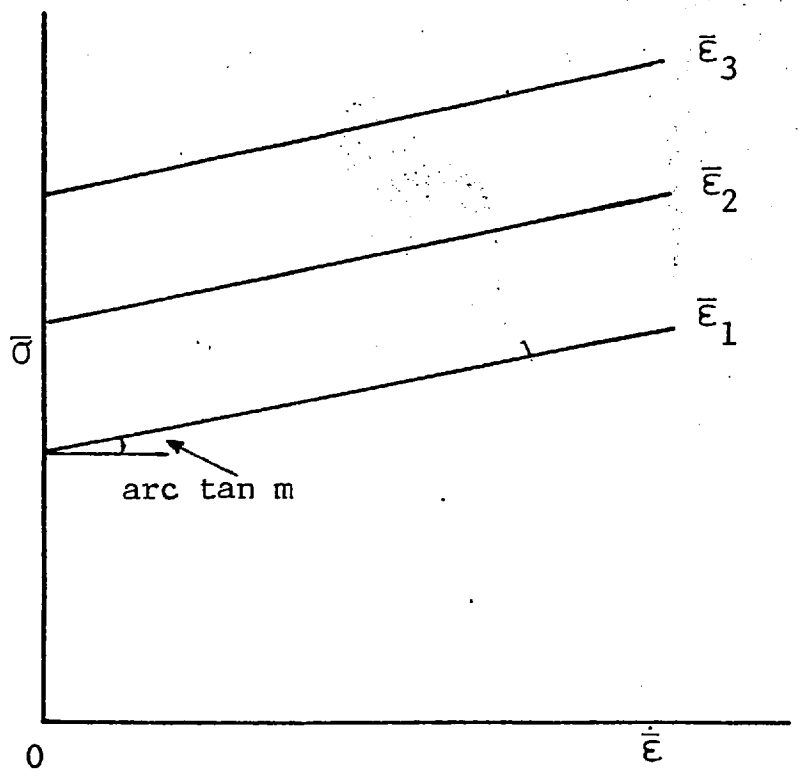

FIG. 4.3 Strain Rate Sensitivity.

4.7 INERTIA FORCES AND STRESS WAVE PROPAGATION

For the purpose of this study it is assumed that the stress waves propagate through the specimen in negligible time and therefore their effects may be ignored. This is a reasonable assumption, since the velocities of stress waves are high enough to establish settled conditions in negligible time [40].

As briefly mentioned in Chapter 2 , analyses have

been carried out taking into account the inertia effects. However, Lippman [39] proposed three dimensionless quantities to determine whether the inertia effect should be considered. They are:

$$\alpha = \frac{\rho V^2}{24\sigma_o \varepsilon}$$

$$\beta = \frac{\rho V^2}{4\sigma_o \varepsilon} \qquad (4.40)$$

$$\gamma = \frac{\rho V^2}{4\sigma_o}\left(\frac{3}{2} - \frac{1}{2\varepsilon}\right)$$

where ρ = density of the material,

σ_o = uniaxial yield stress,

H = height of the billet,

ΔH = reduction in height,

$\varepsilon = \Delta H/H$,

V = velocity of the platen.

It is suggested that if these quantities are $< 10^{-2}$ the inertia effects may be neglected considering that any error introduced by neglecting these effects will be $< 1\%$.

Applying these criteria the inertia effects are negligible as follows [31]:

Copper σ = 600 MN/m^2

ε = 0.1 (increments)

V = 15 m/s

ρ = 8940 kg@m^3

$|\alpha| = 0.15 \times 10^{-2}$

$|\beta| = 0.9 \times 10^{-2}$

$|\gamma| = 3.32 \times 10^{-2}$

Aluminium $\sigma_o = 400\ MN/m^2$

$\varepsilon = 0.1$ (incremental)

$V = 15\ m/s$

$\rho = 2816\ kg/m^3$

$|\alpha| = 0.088 \times 10^{-2}$

$|\beta| = 0.264 \times 10^{-2}$

$|\gamma| = 0.924 \times 10^{-2}$

4.8 POWER OF DEFORMATION

The power of plastic deformation is given by

$$\dot{w} = \int_V \sigma'_{ij}\, \varepsilon^P_{ij}\, dV$$

$$= \int_V 2k\sqrt{I_2}\, dV$$

$$= \frac{2}{\sqrt{3}}\, \sigma_o \int_V \sqrt{\tfrac{1}{2}\varepsilon^P_{ij}\, \varepsilon^P_{ij}} \qquad (4.41)$$

Friction loss is given by

$$\dot{w} = \iint \tau_r\, V_r\, dr\, d\theta \qquad (4.42)$$

4.9 TEMPERATURE FIELD

The effects of temperature on the flow stress are shown in Fig. 4.4. The work due to plastic deformation and

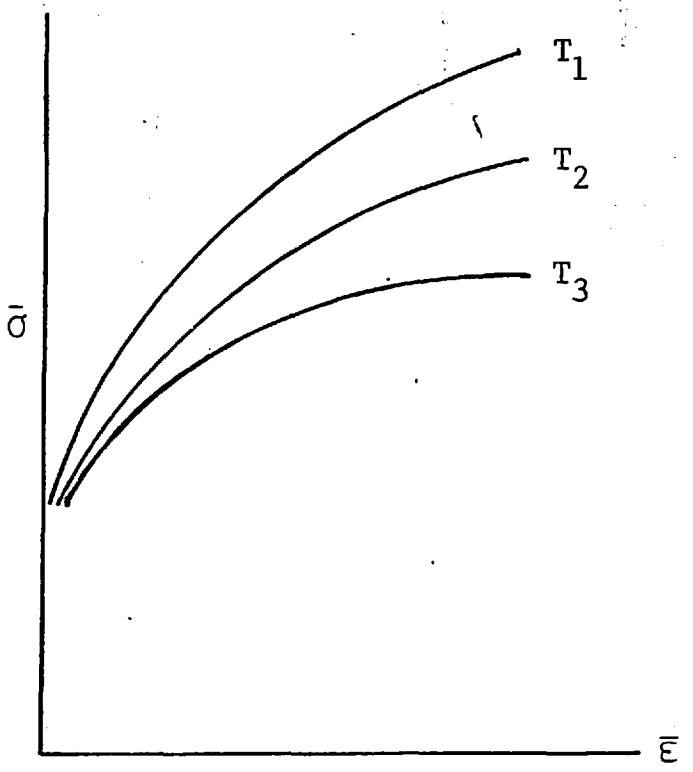

FIG. 4.4 Effects of Temperature.

friction appears as heat. In deformation at high speeds there is little time for this heat to be dissipated to surrounding medium and therefore localised heating takes place. This localised temperature rise results in thermal softening. To be able to account for this it is necessary to determine the temperature distribution in the billet material accounting for

the heat conducted to the dies and heat lost due to convection at the free surfaces.

4.9.1 Heat accumulated

Let us consider a body of volume V in a fixed coordinate system (x,y,z) of reference where a scalar temperature field is defined as

$$T = T(x,y,z,t) \tag{4.43}$$

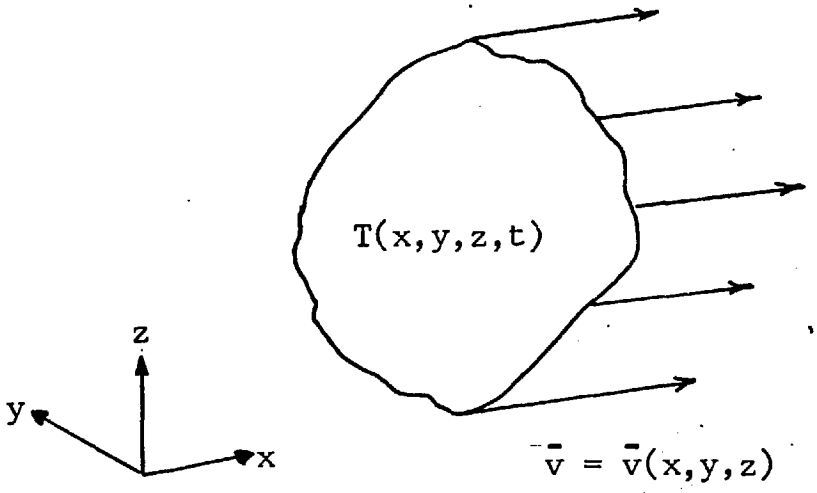

The heat contained in the mass dm

$$dh \propto dm\, T$$

$$h = \iiint_V \rho C T \, dV \tag{4.44}$$

where C is the specific heat,

ρ is density (dm/dV).

The derivative with respect to time

$$\frac{dh}{dt} = \frac{d}{dt} \iiint_V \rho C T \, dV$$

$$= \iiint_V C\rho \frac{dT}{dt} dV$$

as

$$\frac{dT}{dt} = \frac{\partial T}{\partial x} \cdot \frac{dx}{dt} + \frac{\partial T}{\partial x} \cdot \frac{dy}{dt} + \frac{\partial T}{\partial z} \cdot \frac{dz}{dt} + \frac{\partial T}{\partial t}$$

$$\frac{dh}{dt} = (\text{grad}.T \times \bar{V}) + \frac{\partial T}{\partial t}$$

$$\frac{dh}{dt} = \iiint_V C\rho \left(\frac{\partial T}{\partial t} + \bar{V} \, \text{grad} \, T\right) dV \tag{4.45}$$

4.9.2 Heat conducted through the surface

The amount of heat transferred through the surface in some direction $\bar{n}$ is

$$\frac{d^2h}{dsdt} \propto \frac{\partial T}{\partial n} \tag{4.46}$$

$$\frac{d^2h}{dsdt} = k_n \frac{\partial T}{\partial n}$$

where k_n is the thermal conductivity in direction $\bar{n}$. For an isotropic material $k_n = k$ which is the same in all directions.

$$\therefore \quad \frac{dh}{dt} = \iint_S k \frac{\partial T}{\partial n} ds$$

$$= \iint_S k \bar{\nabla} T \bar{n} \, ds$$

$$= \iint_S k \bar{\nabla} T \, ds \qquad (4.47)$$

Applying Gauss theorem we have

$$\frac{dh}{dt} = \iiint_V \operatorname{div}(k \nabla T) dV$$

$$= \iiint_V k \nabla^2 T \, dV \qquad (4.48)$$

4.9.3 Heat generated in the body

If the heat generated in the body due to plastic work is q_g per unit volume then we have

$$h = \iiint_V q_g \, dV \qquad (4.49)$$

$$\frac{dh}{dt} = \iiint_V \dot{q}_g \, dV \qquad (4.50)$$

where $\dot{q}_g = \sigma'_{ij} \dot{\varepsilon}_{ij}$

4.9.4 Heat generated at the surface

If the heat generated at the surface due to friction is q_s per unit surface

$$h = \iint_S q_s \, d_s \qquad (4.51)$$

$$\frac{dh}{dt} = \iint_S \dot{q}_s \, ds$$

$$= \iint_S \dot{q}_s \, \bar{ds}$$

Applying Gauss theorem

$$\frac{dh}{dt} = \iint \mathrm{div}(\dot{q}_s \bar{n}) dV \tag{4.52}$$

For axisymetry

$$\mathrm{div}\, \dot{q}_s = \frac{(\partial \dot{q}_s)_r}{\partial r} + \frac{(\dot{q}_s)_r}{r} + \frac{(\partial \dot{q}_s)_z}{\partial z}$$

In this case

$$\dot{q}_s \bar{n} = \tau v_r(0,0,1)$$

$$\therefore \quad \mathrm{div}\, \dot{q}_s = \frac{\partial \tau v_r}{\partial z} \tag{4.53}$$

4.9.5 Heat convection at the free surface

The heat loss at the free surface due to convection is given by

$$\left(\frac{\partial T}{\partial n}\right)_k = h_f(T-T_F) \tag{4.54}$$

where $\frac{\partial T}{\partial n}$ is the gradient in the direction normal to the surface, h_f is the film coefficient of the material, T is the temperature at the free surface and T_F is the temperature of the surrounding medium.

4.9.6 Temperature distribution

Now, the heat contained in the body (4.43) can be equated to the heat generated (4.48) and (4.50) and heat conducted through the surface (4.46). Thus

$$\iiint_V c\rho\left(\frac{\partial T}{\partial t} + \text{grad}T.\bar{V}\right)dV = \iiint_V k\nabla^2 dV + \iiint_V \dot{q}_g dV + \iiint_V \text{div}\,\dot{\bar{q}}\,dV \qquad (4.55)$$

or

$$\iiint_V \left[-c\rho\left(\frac{\partial T}{\partial t} + \text{grad}T.\bar{V}\right) + k\nabla^2 + \dot{q}_g + \text{div}\,\dot{\bar{q}}_s\right]dV = 0$$

As this is valid for any volume the function itself must vanish.

$$\therefore \quad \nabla^2 T + \frac{\dot{q}_g}{k} + \frac{\text{div}\,\dot{\bar{q}}_s}{k} - \beta\left(\frac{\partial T}{\partial t} + \text{grad}T.\bar{V}\right) = 0$$

where $\beta = \frac{\rho c}{k}$ (4.56)

Expressing (4.56) in cylindrical coordinates and applying equation (4.53) we have the governing differential equation as

$$-\beta\frac{\partial T}{\partial r} + \frac{\partial^2 T}{\partial r^2} + \frac{\partial^2 T}{\partial z^2} + \left(\frac{1}{r} - \beta V_r\right)\frac{\partial T}{\partial r} - \beta V_z \frac{\partial T}{\partial z} + \frac{\dot{q}_g}{k} + \frac{1}{k}\frac{\partial \tau v_r}{\partial z} = 0 \qquad (4.57)$$

and the boundary condition

$$\left(\frac{\partial T}{\partial n}\right)k_n = h_f(T - T_F) \qquad (4.58)$$

CHAPTER 5

SOLUTION BY WEIGHTED RESIDUALS

As explained in Chapter III, the method of weighted residuals provides a viable approach to obtaining numerical solutions to complex problems. Different weighting functions were applied to study the behaviour of visco elastic solids over a continuous domain. However, the domain can also be discretised into a number of nodal points, applying the residual function and the weighting function to each nodal points and minimising their sum as shown in the later sections of this chapter.

Steck [52] applied this discrete method of weighted residuals (least squares) to obtain velocity and stress field during compression of cylindrical billets. His results were shown in Fig. 2.9. The formulation of the problem is discussed here. The continuum was discretised as shown in Fig. 5.1.

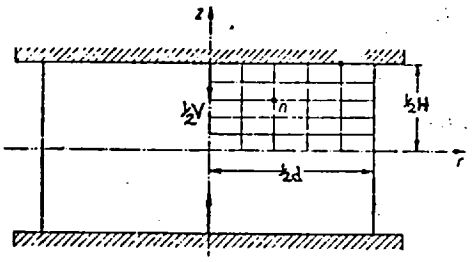

FIG. 5.1 Discretized Continuum.

Stream and stress functions were proposed as follows:

$$\psi = \frac{V_w z}{2h} r^2 z + (z^2 - h^2) \sum^{M} \sum^{N} A_{mn} r^{2m} z^{2n-1} \tag{5.1}$$

$$\phi_1 = -\frac{\sqrt{3}}{6} k r^3 + \sum^{I} \sum^{J} B_{ij} r^{2i-1} z^{2j} \tag{5.2}$$

$$\phi_2 = \sum^{P} \sum^{Q} C_{pq} r^{2p-1} z^{2q} \tag{5.3}$$

where A_{mn}, B_{ij} and C_{pq} are unknown parameters. From equation (5.1) the following can be obtained:

$$\begin{aligned} \dot{\varepsilon}_r &= \dot{\varepsilon}_r(r, z, A_{mn}) \\ \dot{\varepsilon}_\theta &= \dot{\varepsilon}_\theta(r, z, A_{mn}) \\ \dot{\varepsilon}_z &= \dot{\varepsilon}_z(r, z, A_{mn}) \\ \dot{\varepsilon}_{rz} &= \dot{\varepsilon}_{rz}(r, z, A_{mn}) \\ I_2 &= I_2(r, z, A_{mn}) \end{aligned} \tag{5.4}$$

From equations (5.2) and (5.3) the following can be obtained:

$$\begin{aligned} \sigma_r &= \sigma_r(r, z, B_{ij}, C_{pq}) \\ \sigma_\theta &= \sigma_\theta(r, z, C_{pq}) \\ \sigma_z &= \sigma_z(r, z, B_{ij}) \\ \tau_{rz} &= \tau_{rz}(z, r, B_{ij}) \\ \sigma_m &= \sigma_m(r, z, B_{ij}, C_{pq}) \end{aligned} \tag{5.5}$$

Applying stress strain relationship equation (4.32), the following error functions were obtained:

$$F_1 = \sigma_r(r,z,B_{ij},C_{pq}) - \sigma_m(r,z,B_{ij},C_{pq}) \frac{-k}{\sqrt{I_2(r,z,A_{mn})}} \dot{\varepsilon}(r,z,A_{mn}) \qquad (5.7)$$

Similarly, constancy of volume was assumed and the two remaining independent error functions F_2 and F_3 were also obtained from equations (5.4) and (5.5). Applying the following boundary conditions:

$$\tau_{rz} = CV_r\Big|_{z=h} \qquad (5.8)$$

where C is a constant

$$\sigma_r = 0\Big|_{r=d/2} \qquad (5.9)$$

two more error functions F_4 and F_5 were obtained. It was suggested that these equations constitute residual functions as in equation (3. 6) and by applying weighting functions equation (3.12) the unknown parameters A_{mn}, B_{ij} and C_{pq} can be determined. As these equations are non-linear, an iterative procedure illustrated in Fig. 5.2 was employed. The process of deformation was analysed step by step incrementally accounting for the strain hardening as explained in Section 4.5 and updating the nodal coordinates in each step.

Considerable time and effort was spent in trying to reproduce the results obtained by Steck. Two separate computer programmes were developed, one following the iterative

procedure illustrated in Fig. 5.2 and the other a different iterative procedure [51] also suggested by Steck. Neither of these programmes converged to solution. Both programmes produced identical results after the first step of iteration where I_2 is assumed to be equal to unity and the system is equivalent to viscous fluid with viscosity $\eta = k/2$. This may be considered as sufficient proof that there were no programming errors. The programmes were tried for various geometry and friction conditions and in no case could meaningful results be obtained. Although during early attempts for a particular geometry (which happened to be a very thin disc) the results seemed reasonable, they have now been discarded as being unreliable on account of the following explanation.

It is observed that this formulation of the problem is not satisfactory. Equation (5.7) is not the same as residual function, equation (3. 6). It appears as though two sets of approximating functions with unknown parameters were proposed for the same quantity and then the parameters were determined minimising the difference between these two sets of approximating functions. This can be expressed as follows:

$$\lambda[A][X] - [B][Y] = [0] \qquad (5.10)$$

where $\lambda = \lambda(A)$.

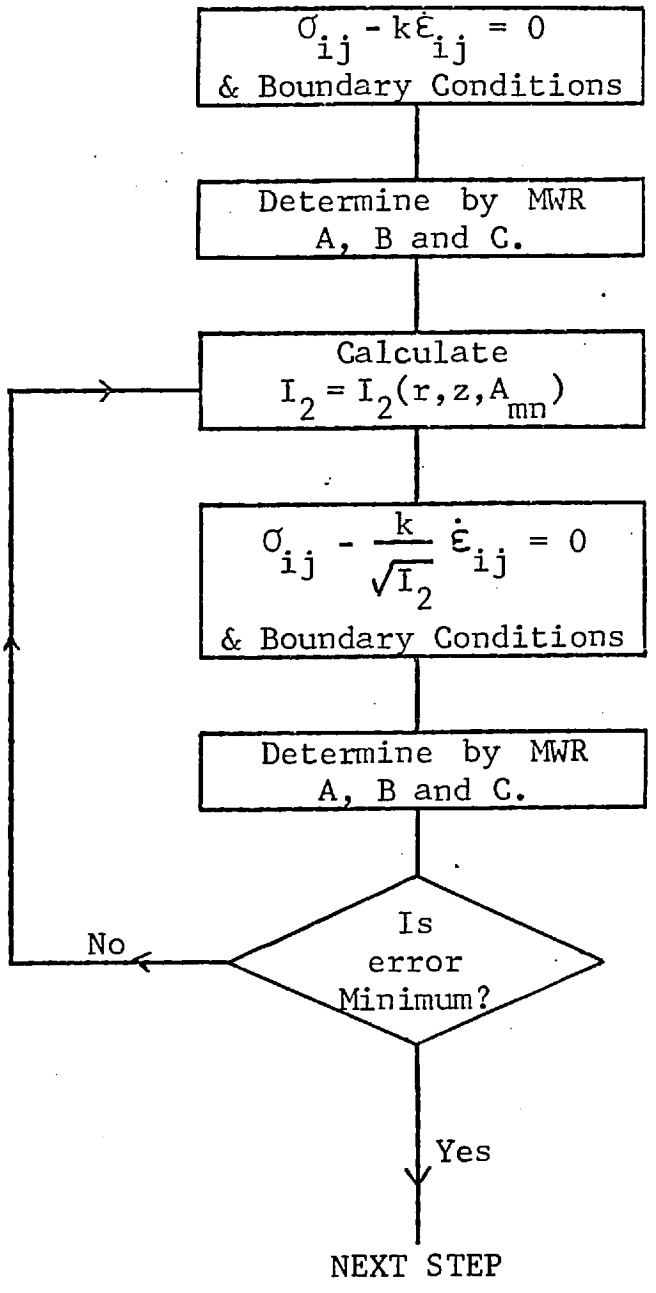

FIG. 5.2 Iterative Procedure [52].

Given X and Y it is possible to determine several sets of A and B satisfying the requirements. Mathematically [93] there is no reason why any of these solutions should be considered unique unless a criterion with a physical meaning is established. Therefore it would seem that this approach is not very sound. It is possible to get around this difficulty by obtaining strain rate field through a predetermined velocity field (which can be obtained by using some other technique discussed in Section 2.4) and construct residual functions of the form

$$\sigma_{ij}(r,z,B_{de},C_{pq}) - K^{*}_{ij} = R \neq 0 \qquad (5.11)$$

where K^{*}_{ij} is a known constant $\frac{k}{\sqrt{I_2}} \dot{\varepsilon}_{ij}$.

5.1 METHOD TO DETERMINE STRESS FIELDS

The modified approach mentioned above is applied to obtain stress fields during deformation of rings and it is then adopted to analyse the deformation of solid billets. The velocity of deformation and frictional conditions are two variable parameters of the process which will enable different conditions to be analysed.

5.1.1 Premises

The following conditions are held to be valid:

1. The material is incompressible.

2. The material is isotropic.

3. The material work hardens as in equation (4.39).

4. The elastic strains are small in comparison with plastic strains and can be neglected.

5. The stress waves propagate through the specimen in negligible time.

6. The inertia effects are not significant.

7. The frictional stress at the tool/billet interface is assumed to be proportional to the shear yield stress of the material.

8. The elements of the forging machine and the anvil are considered to be rigid and stationary at all times.

9. The process of deformation and simultaneous heat generation is considered to take place in steps of small time interval.

5.1.2 Discretisation

The platen and the specimen are divided into a number of nodal points as shown in Fig. 5.3. Due to symmetry only one-quarter of the specimen and platen is considered.

5.1.3 Velocity and Strain Rate Fields

The different forms of velocity fields that have been proposed were discussed in Chapter 2. Male et al [67] analysed these proposed velocity fields and reported that Avitzur's solution (Section 2.4.4) agreed more closely with experimental results. Avitzur's solution is for a rigid, perfectly plastic material, so for a strain hardening material the solution is accurate on the rate of formation of the bulge only at the onset of deformation. It was assumed that any bulge that may exist during deformation in the ring does not influence the velocity field in other parts of the ring, and for theoretical calibration of the ring test only the non-bulged rectangular portion of the ring was considered in each increment of compression. As only the rectangular portion of the ring is considered in each increment, Avitzur's solution (Section 2.4.2) for determining the neutral surface is valid, which was then used to determine the bulge parameter and the velocity field. For this investigation this method was adopted as follows:

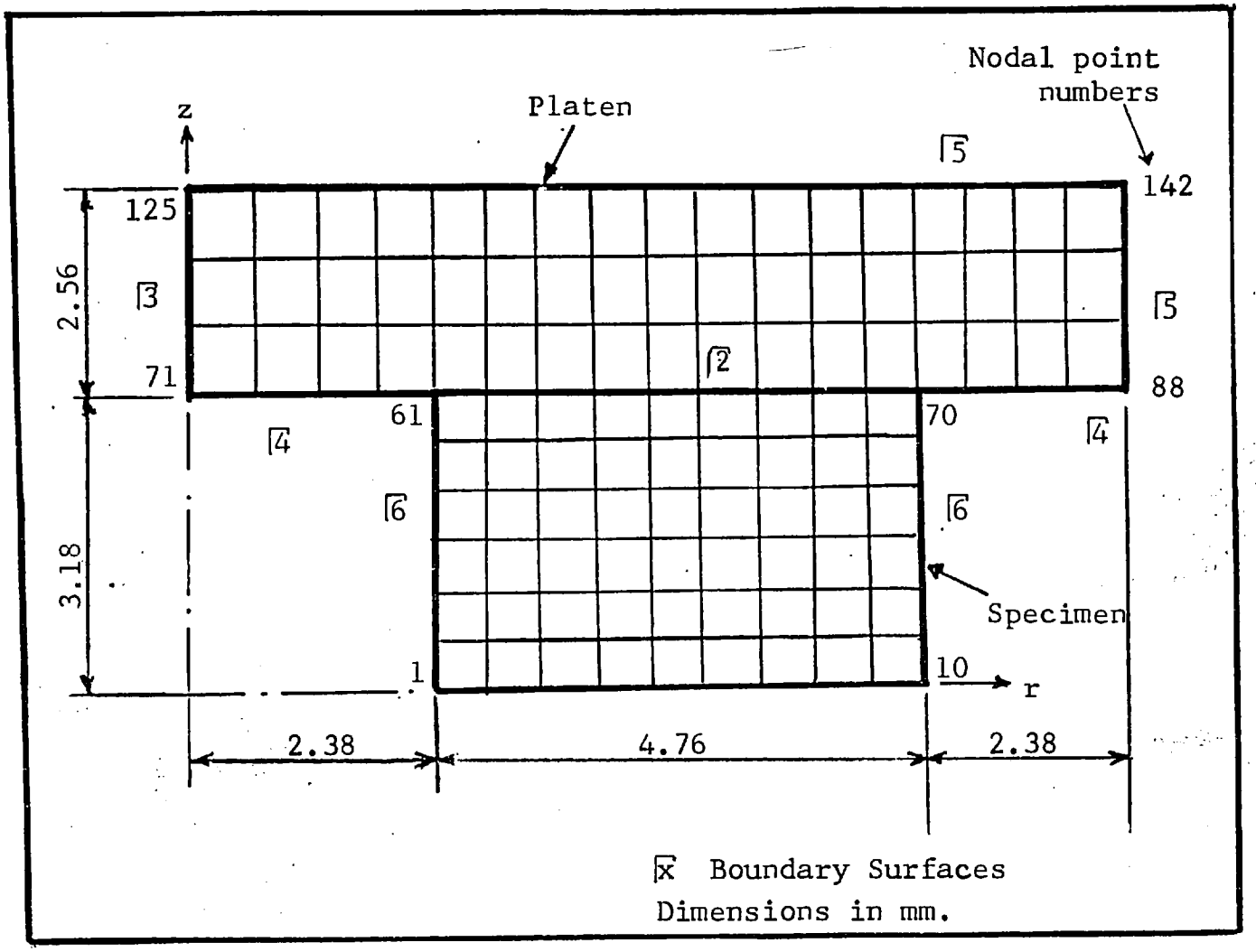

FIG. 5.3 Mesh and Boundary Surfaces for Ring Specimen.

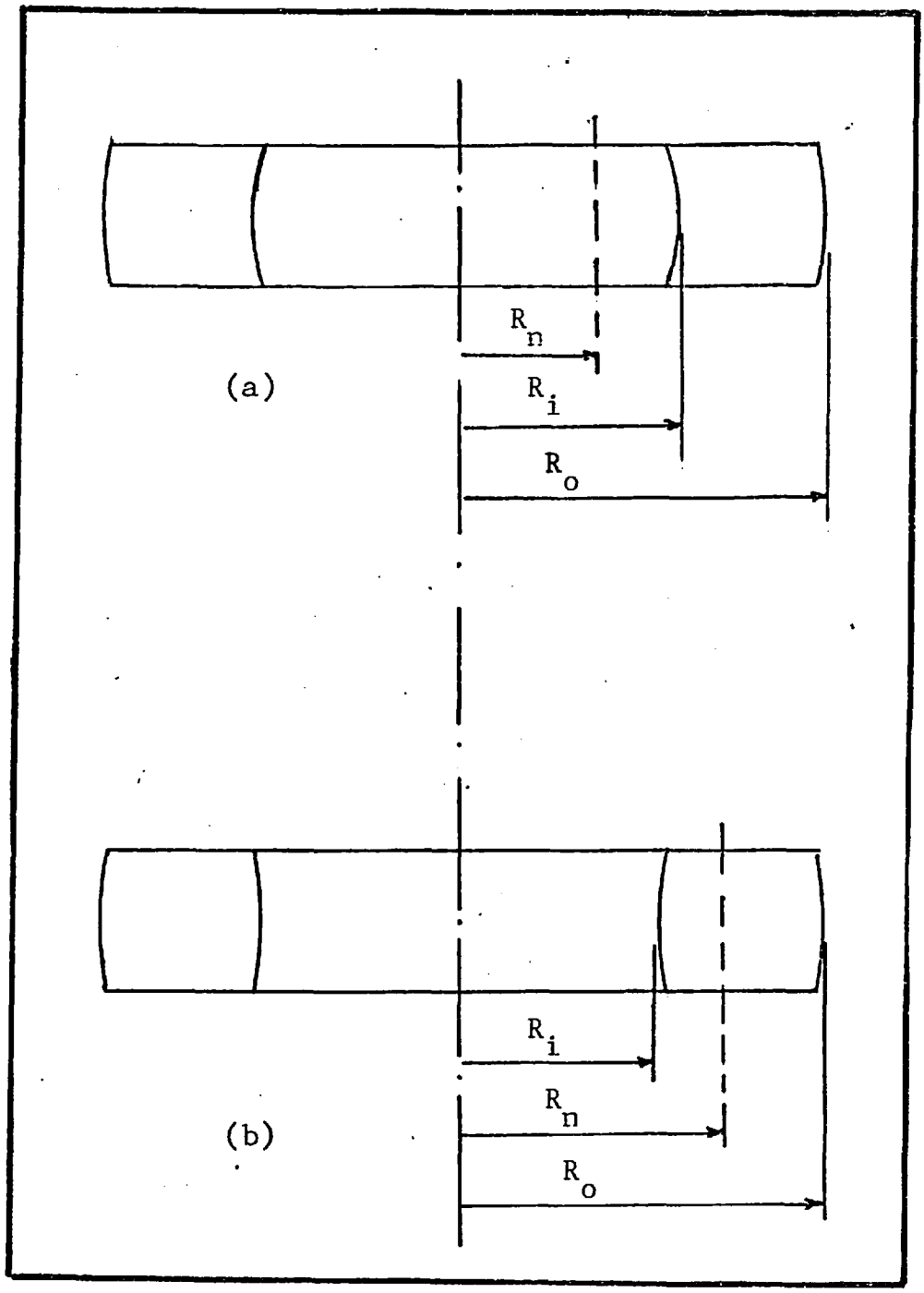

FIG. 5.4 Deformation Modes of Ring in Compression.

The two possible deformation modes are shown in Fig. 5.4. For mode 'a', from equation (2.8) we have, when $R_n \leqslant R_i$:

$$\alpha \frac{R_o}{H} \leqslant \frac{1}{2(1-R_i/R_o)} \ln \frac{3(R_o/R_i)^2}{1+\sqrt{1+3(R_o/R_i)^4}} \tag{5.12}$$

and

$$\frac{P_{ave}}{\sigma_o} = \frac{1}{(1-(R_i/R_o)^2} \left\{ \sqrt{1+\tfrac{1}{3}\left(\frac{R_n}{R_o}\right)^4} - \sqrt{\left(\frac{R_i}{R_o}\right)^4+\tfrac{1}{3}\left(\frac{R_n}{R_o}\right)^4} + \frac{2}{3\sqrt{3}} \alpha \frac{R_o}{H} \left[1-\left(\frac{R_i}{R_o}\right)^3\right] \right\}$$

where $$\left(\frac{R_n}{R_o}\right)^2 = \frac{1-(R_i/R_o)^4 x^2}{\sqrt{x(x-1)\left[1-(R_i/R_o)^4 x\right]}} \frac{\sqrt{3}}{2}$$

$$x = \left\{ \frac{R_o}{R_i} \exp\left[-\alpha \frac{R_o}{H}\left(1-\frac{R_i}{R_o}\right)\right]\right\}^2 \tag{5.13}$$

From equation (2.18)

$$b = \left\{ \alpha \left[\tfrac{1}{3}\left(\frac{R_o}{R_n}\right)^2 \left[1-\left(\frac{R_i}{R_o}\right)^3\right] - \left[1-\frac{R_i}{R_o}\right]\right]\right\} \Bigg/ \left\{ \frac{\alpha}{6} \left[\tfrac{1}{3}\left(\frac{R_o}{R_n}\right)^2 \left[1-\left(\frac{R_i}{R_o}\right)^2\right] - \left[1-\frac{R_i}{R_o}\right]\right] + \frac{R_o/H}{\sqrt{1+3(R_o/R_n)^4}} \left[\tfrac{1}{4}\left(\frac{R_o}{R_n}\right)^4 \left[1-\left(\frac{R_i}{R_o}\right)^4\right] - \left(\frac{R_o}{R_n}\right)^2 \left[1-\left(\frac{R_i}{R_o}\right)^2\right] + \ln\frac{R_o}{R_i}\right]\right\} \tag{5.14}$$

For mode 'b', from equation (2.9), when $R_i \leqslant R_n \leqslant R_o$,

$$\frac{R_o}{H}\ \frac{1}{2(1-R_i/R_o)}\ln\frac{3(R_o/R_i)^2}{1+\sqrt{1+3(R_o/R_i)^4}} \tag{5.15}$$

$$\frac{P_{av}}{\sigma_o} = \frac{1}{1-(R_i/R_o)^2}\left\{\sqrt{1+\tfrac{1}{3}\left(\frac{R_n}{R_o}\right)^4}-\sqrt{\left(\frac{R_i}{R_o}\right)^4+\tfrac{1}{3}\left(\frac{R_n}{R_o}\right)^4}\right.$$

$$\left.+\frac{2}{3\sqrt{3}}\alpha\frac{R_o}{H}\left[1+\left(\frac{R_i}{R_o}\right)-2\left(\frac{R_n}{R_o}\right)^3\right]\right\}$$

where R_n/R_o is found by successive approximation from

$$\alpha\frac{R_o}{H}\left(1+\frac{R_i}{R_o}-2\frac{R_n}{R_o}\right)$$

$$+\ln\left|\left(\frac{R_i}{R_o}\right)^2\frac{(R_n/R_o)^2+\sqrt{3+(R_n/R_o)^4}}{(R_n/R_o)^2+\sqrt{3(R_i/R_o)^4+(R_n/R_o)^4}}\right| = 0 \tag{5.16}$$

As a first approximation,

$$\frac{R_n}{R_o} = \frac{2\sqrt{3}\alpha R_o/H}{(R_o/R_i)^2-1}\left\{1+\frac{(1+R_i/R_o)(R_o/R_i)^2-1}{2\sqrt{3}\,\alpha R_o/H}-1\right\}$$

From equation (2.19)

$$b = \left\{\alpha\frac{R_n}{R_o}\left[\frac{4}{3}+\tfrac{1}{3}\left(\frac{R_o}{R_n}\right)^3\left[1-\left(\frac{R_i}{R_o}\right)^3\right]-\frac{R_o}{R_n}\left[1+\frac{R_i}{R_o}\right]\right]\right\}\Bigg/\left\{\frac{\alpha}{6}\,\frac{R_n}{R_o}\left[\frac{4}{3}\right.\right.$$

$$+\tfrac{1}{3}\left(\frac{R_o}{R_n}\right)^2\left[1+\left(\frac{R_i}{R_o}\right)^2\right]-\frac{R_o}{R_n}\left[1+\frac{R_i}{R_o}\right]+\frac{R_o/H}{\sqrt{1+3\left(\frac{R_o}{R_n}\right)^4}}\left[\tfrac{1}{4}\left(\frac{R_o}{R_n}\right)^4\left[1-\right.\right.$$

$$\left.\left.\left.-\left(\frac{R_i}{R_o}\right)^2\right]-\left(\frac{R_o}{R_n}\right)^2\left[1-\left(\frac{R_i}{R_o}\right)^2\right]+\ln\frac{R_o}{R_i}\right]\right\} \tag{5.17}$$

The velocity field is given by

$$V_r = \frac{b}{4}\frac{V}{H} r\left[1 - \left(\frac{R_n}{r}\right)^2\right] \frac{e^{-bz/H}}{1 - e^{-b/2}} \tag{5.18}$$

$$V_z = -\left(\frac{V}{2}\right) \frac{1-e^{-bz/H}}{1 - e^{-b/2}} \tag{5.19}$$

$$V_\theta = 0 \tag{5.20}$$

where V = platen relative velocity,

r, z = nodal coordinates.

This satisfies the boundary condition

$$V_z = -\frac{V}{2}\Big|_{z=H/2} \tag{5.21}$$

$$V_z = 0\Big|_{z=0} \tag{5.22}$$

The strain rate field (4.24) can be obtained as

$$\dot{\varepsilon}_r = \frac{b}{4}\frac{V}{H}\left[1 + \left(\frac{R_n}{r}\right)^2\right] \frac{e^{-bz/H}}{1 - e^{-b/2}} \tag{5.23}$$

$$\dot{\varepsilon}_\theta = \frac{b}{4}\frac{V}{H}\left[1 - \left(\frac{R_n}{r}\right)^2\right] \frac{e^{-bz/H}}{1 - e^{-b/2}} \tag{5.24}$$

$$\dot{\varepsilon}_z = -\frac{b}{2}\frac{V}{H} \frac{e^{-bz/H}}{1 - e^{-b/2}} \tag{5.25}$$

$$\dot{\varepsilon}_{rz} = -\frac{b^2}{8}\frac{V}{H^2} r\left[1 - \left(\frac{R_n}{r}\right)^2\right] \frac{e^{-bz/H}}{1 - e^{-b/2}} \tag{5.26}$$

Hence for any nodal point the principal invariant of the strain rate tensor I_2 can be determined and $\bar{k}$, the mean shear yield stress, is the same at all points at the onset of deformation. Given these two, one can estimate the stress field by the method of weighted residuals.

5.1.4 Governing equations and boundary conditions

The Prandtl-Reuss relationship (4.32) can be written as

$$\sigma_{ij} - \sigma_m \delta_{ij} = \frac{k}{\sqrt{I_2}} \dot{\varepsilon}_{ij} \tag{5.27}$$

The boundary conditions are

$$\begin{aligned} \tau_{rz} &= \alpha k && n \in \overline{2} \\ \sigma_r &= 0 && n \in \overline{6} \end{aligned} \tag{5.28}$$

where α is a constant,

n is any nodal point.

This leads to governing equations

$$\begin{aligned} \sigma_r - \sigma_m - \frac{k}{\sqrt{I_2}} \dot{\varepsilon}_r &= 0 \\ \sigma_\theta - \sigma_m - \frac{k}{\sqrt{I_2}} \dot{\varepsilon}_\theta &= 0 \\ \sigma_z - \sigma_m - \frac{k}{\sqrt{I_2}} \dot{\varepsilon}_z &= 0 \\ \tau_{rz} - \frac{k}{\sqrt{I_2}} \dot{\varepsilon}_{rz} &= 0 \end{aligned} \tag{5.29}$$

and boundary conditions

$$\begin{aligned} \tau_{rz} + \alpha k &= 0 \\ \sigma_r &= 0 \end{aligned} \tag{5.29}$$

These equations are comparable to equations (3.16) and (3.17). As constancy of volume is assumed, the equation corresponding to $(\sigma_z - \sigma_m)$ need not be considered.

5.1.5 Residual functions

To obtain a solution for equations (5.29) it is necessary to select a set of trial functions which can be used to construct this residual function. As already seen, stress functions ϕ_1 and ϕ_2 selected according to equation (4.11) will satisfy the equilibrium conditions (4.12). Therefore ϕ_1 and ϕ_2 are chosen as trial functions as below:

$$\phi_1 = -\frac{\sqrt{3}}{6} k r^3 + \sum^{D} \sum^{E} B_{de} r^{2e-1} z^{2d} \tag{5.30}$$

$$\phi_2 = \sum^{P} \sum^{Q} C_{pq} r^{2p-1} z^{2q} \tag{5.31}$$

Applying equation (4.11) we have

$$\sigma_r = \sum^{D} \sum^{E} B_{de} r^{2e-2}(4d^2-2d) z^{2d-2} + \sum^{P} \sum^{Q} C_{pq} r^{2p-2} z^{2q} \tag{5.32}$$

$$\sigma_\theta = \sum^{P} \sum^{Q} C_{pq}(2p-1) r^{2p-2} z^{2q} \tag{5.33}$$

$$\sigma_z = -\sqrt{3}k + \sum^{D}\sum^{E} B_{de}(2e-1)(2e-2)r^{2e-4}z^{2d} \quad (5.34)$$

$$\tau_{rz} = \sum^{D}\sum^{E} B_{de}2d(2e-1)r^{2e-3}z^{2d-1} \quad (5.35)$$

Obviously the functions ϕ_1 and ϕ_2 are chosen to be polynomial expressions as they satisfy the requirement that the trial function should be a complete set and they are relatively easy to handle. The index of r is (2e-1) and that of z is 2d so that the resulting functions for σ_r and σ_z are even. This is a necessary condition for axisymetry, i.e. the functions are identical for negative and positive values of r and z. The expression for σ_z will satisfy the condition that $\sigma_z = -\sqrt{3}k\big|_{r=0}$. It is also necessary that σ_r is a function z alone when r = 0 and σ_z is a function of r alone when z = 0. This can be achieved by making the corresponding indices go through zero. This will, however, lead to difficulty in computation as some of the terms will be of the form 0^0. This can be overcome by replacing the values of r and z when they are equal to zero by a very small value (say 10^{-10}). Any error resulting from this adjustment will be insignificant and may be ignored.

Having satisfied all the requirements a set of residual functions can be assembled for each generic nodal point n as follows:

$$R_{1n} = \sigma_r(r_n, z_n, B_{de}, C_{pq}) - \sigma_m(r_n, z_n, B_{de}, C_{pq}) - \frac{k}{\sqrt{I_2}} \dot{\varepsilon}_r \qquad (5.36)$$

$$R_{2n} = \sigma_\theta(r_n, z_n, C_{pq}) - \sigma_m(r_n, z_n, B_{de}, C_{pq}) - \frac{k}{\sqrt{I_2}} \dot{\varepsilon}_\theta \qquad (5.37)$$

$$R_{3n} = \tau_{rz}(r_n, z_n, B_{de}) - \frac{k}{\sqrt{I_2}} \dot{\varepsilon}_{rz} \qquad (5.38)$$

$$R_{4n} = \tau_{rz}(r_n, z_n, B_{de}) - \alpha k \qquad n \in \boxed{2} \qquad (5.39)$$

$$R_{5n} = \sigma(r_n, z_n, C_{pq}) \qquad n \in \boxed{6} \qquad (5.40)$$

The sum total of the residual over the entire discretised domain

$$R_T = \sum_{m=1}^{M} \sum_{n=1}^{N} G_m R_{mn}(r_n, z_n, B_{de}, C_{pq}) \qquad (5.41)$$

where G_m is the weighting factor discussed in Section (3.3). The nodal points lying on the surfaces $\boxed{2} + \boxed{6}$ are relatively few. The significance of boundary conditions associated with these may be lost in this solution. Therefore the weighting factors G_m are determined as

$$G_m = \frac{N}{N_m} \qquad \begin{array}{l} N = \text{total number of nodal points,} \\ N_m = \text{number of nodal points on the boundary.} \end{array} \qquad (5.42)$$

The total residual R_T when expanded will be of the form

$$R_T = A_i X_i + C \geqslant 0 \text{ for } i = 1(1)k \qquad (5.43)$$

where k = the total number of free parameters,

A_i replaces B_{de} and C_{pq},

C is the constant term.

5.1.6 Solution (rings)

Given a residual function $R = R(A_p)$, a suitable weighting function can be chosen to force the residual to be zero in an average sense over the domain of interest. Applying the criterion (3.12) we have

$$\frac{\partial}{\partial A_p} \int_V R^2(A_p) = 0 \tag{5.44}$$

In a discrete domain this can be expressed as

$$\frac{\partial}{\partial A_p} \sum_{i=1}^{N} R_i^{\,2}(A_p) = 0 \tag{5.45}$$

$$= \frac{\partial R_T^{\,2}}{\partial A_p} \quad \text{where } R_T = \sum_{i=1}^{N} R_i(A_p) \tag{5.46}$$

From equation (5.43) we have

$$R_T = A_i X_i + C$$

$$R_T^{\,2} = A_i A_j X_i X_j + 2CA_i X_i + C^2 \tag{5.47}$$

$$\frac{\partial R_T^{\,2}}{\partial A_p} = \delta_{ip} A_j X_p X_j + \delta_{jp} A_i X_i X_p + 2CX_p$$

$$= 2A_i X_i X_p + 2CX_p = 0 \tag{5.48}$$

or

$$\frac{\partial R_T^2}{\partial A_p} = A_i X_i X_p + C X_p = 0 \qquad (5.49)$$

This system of equations can be solved to determine the unknown free parameters A_i. Once these are determined the stress field can be determined from equations (5.32) to (5.35). The complete sequence is summarised in the form of a flow chart in Fig. 5.5, which corresponds to the computer programme given in Appendix A.

5.1.7 Solution (solid billets)

The solution for a stress field during upsetting of solid billets is identical to that of rings except that the inside radius and neutral surface are equal to zero. The specimen and the dies are divided into a number of nodal points as shown in Fig. 5.6.

For $R_I = R_n = 0$, equation (2.18) reduces to

$$b = \frac{4(\alpha/\sqrt{3})(h/R_o)}{1+\frac{2}{3}\frac{\alpha}{\sqrt{3}}(h/R_o)} \qquad (5.50)$$

The velocity field becomes

$$v_r = \dot{\gamma}\frac{b}{4}\frac{re^{-bz/h}}{1-e^{-b/2}} \qquad (5.51)$$

$$v_z = -(\frac{v}{2})\frac{1-e^{-bz/h}}{1-e^{-b/2}} \qquad (5.52)$$

$$v_\theta = 0 \qquad (5.53)$$

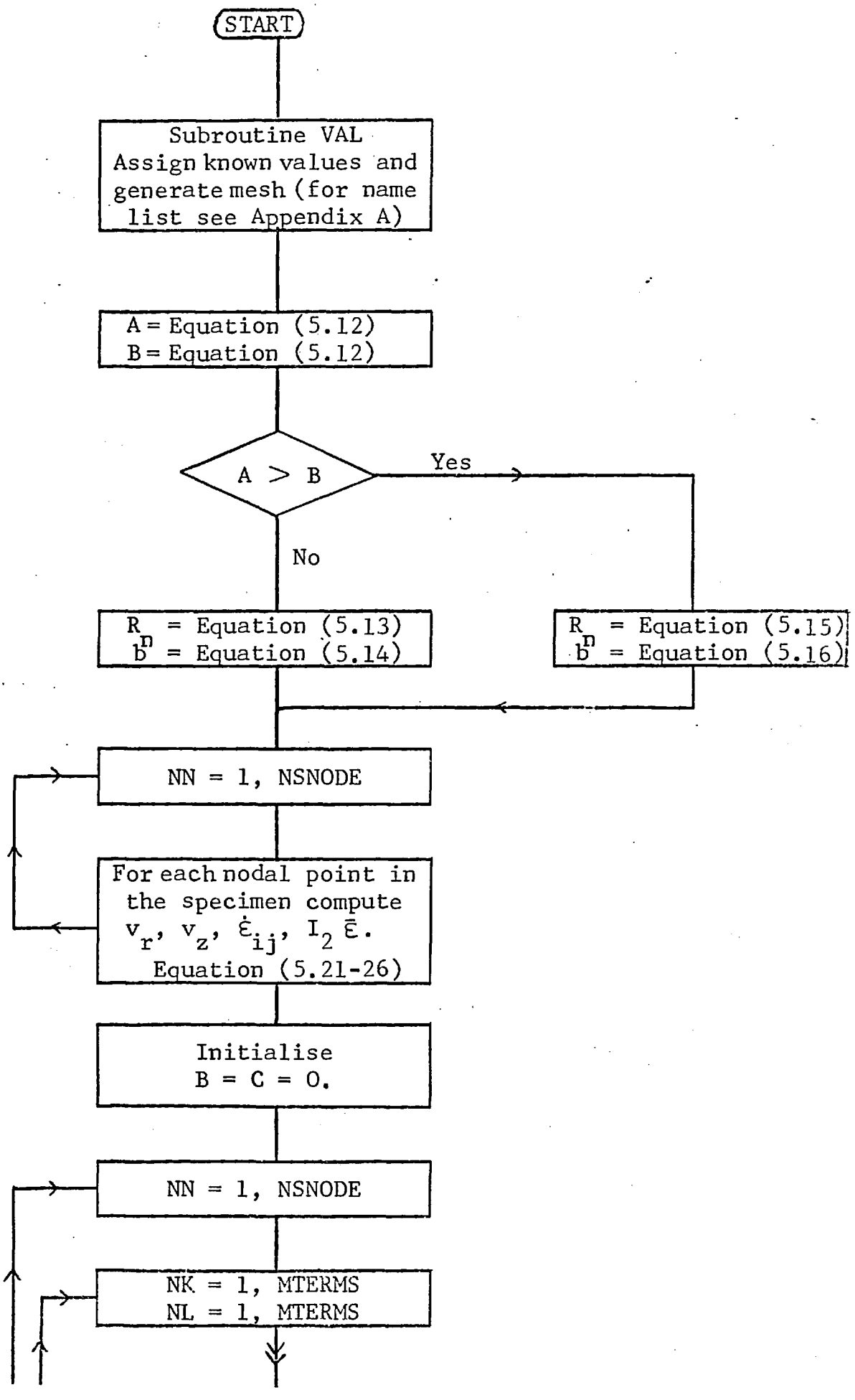
START
Subroutine VAL
Assign known values and generate mesh (for name list see Appendix A)
A = Equation (5.12)
B = Equation (5.12)
A > B
Yes
No
R_n = Equation (5.13)
b^n = Equation (5.14)
R_n = Equation (5.15)
b^n = Equation (5.16)
NN = 1, NSNODE
For each nodal point in the specimen compute v_r, v_z, $\dot{\varepsilon}_{ij}$, I_2 $\bar{\varepsilon}$.
Equation (5.21-26)
Initialise
B = C = 0.
NN = 1, NSNODE
NK = 1, MTERMS
NL = 1, MTERMS

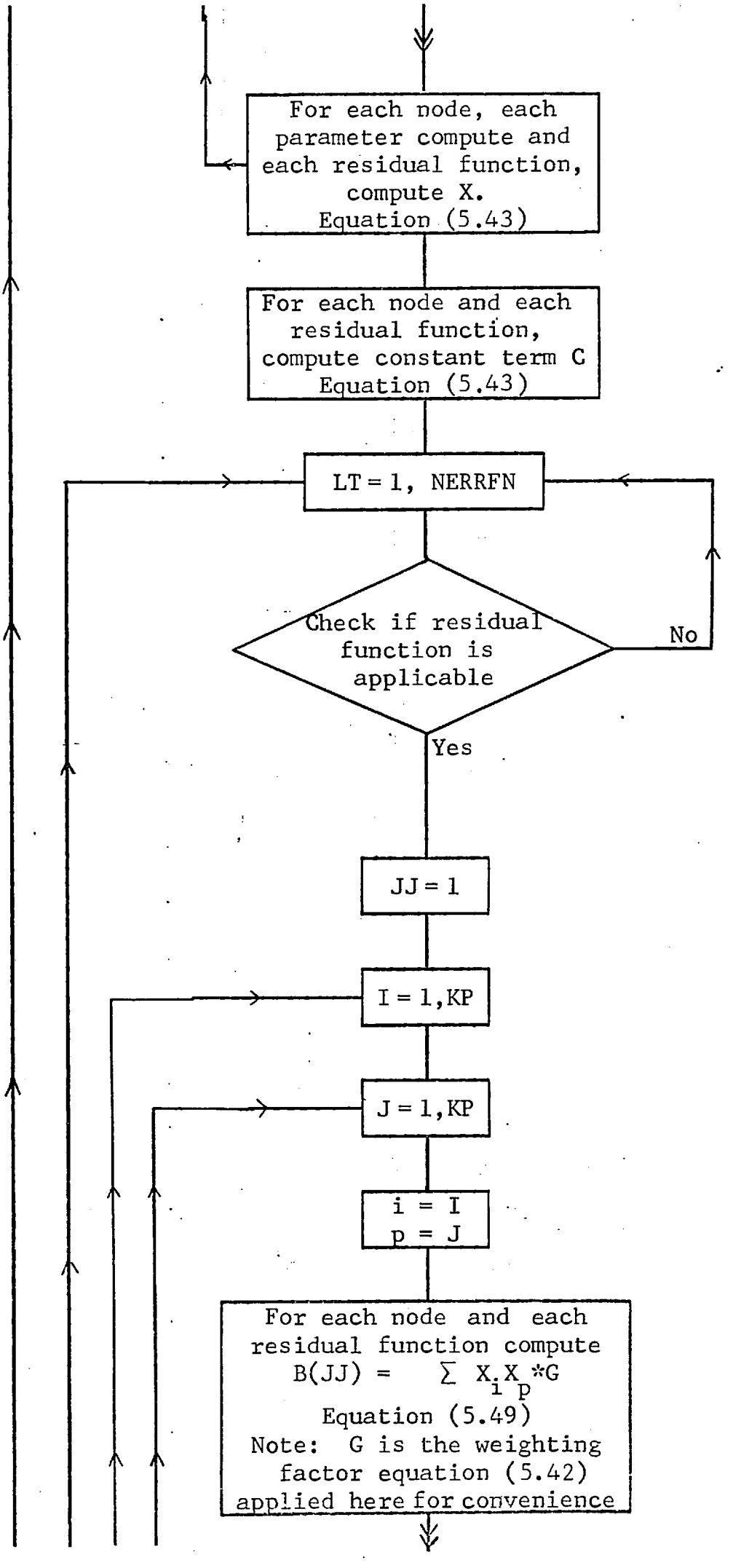
For each node, each parameter compute and each residual function, compute X.
Equation (5.43)
For each node and each residual function, compute constant term C
Equation (5.43)
LT = 1, NERRFN
Check if residual function is applicable
No
Yes
JJ = 1
I = 1,KP
J = 1,KP
i = I
p = J
For each node and each residual function compute
B(JJ) = Σ X_i X_p *G
Equation (5.49)
Note: G is the weighting factor equation (5.42) applied here for convenience

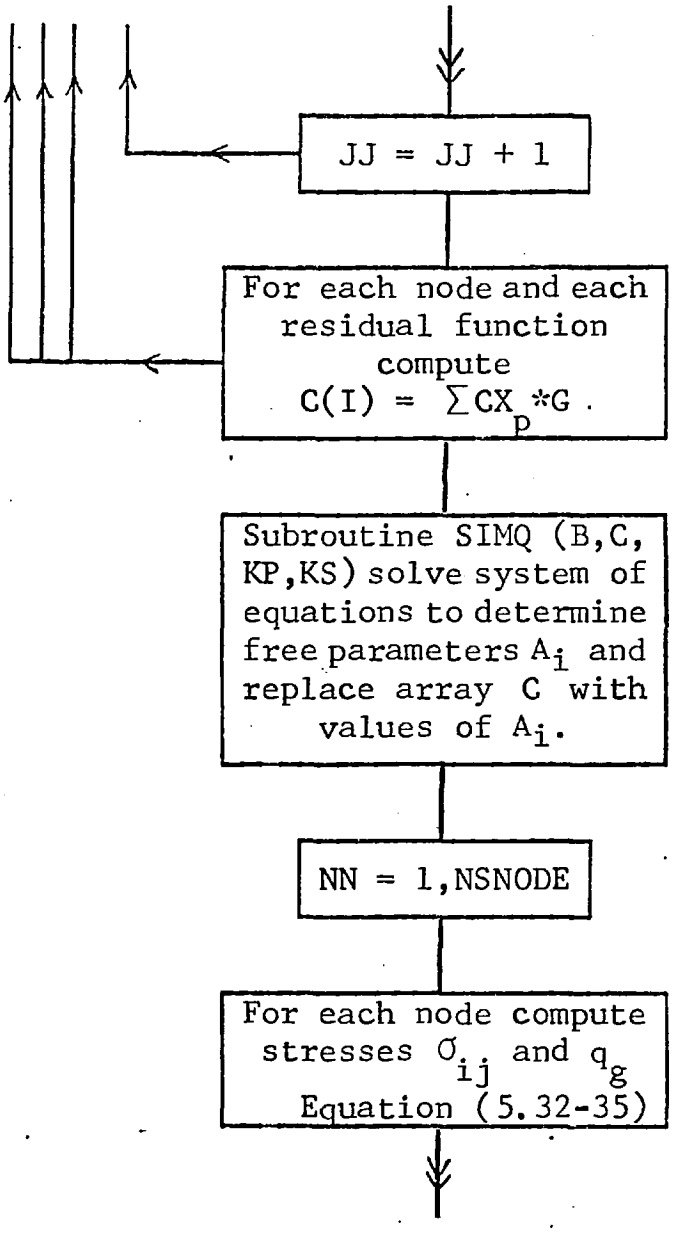

NEXT STAGE DETERMINE
TEMPERATURE FIELD
FIG. (5.7)

FIG. 5.5 Flow Chart, computation of Stress Field.

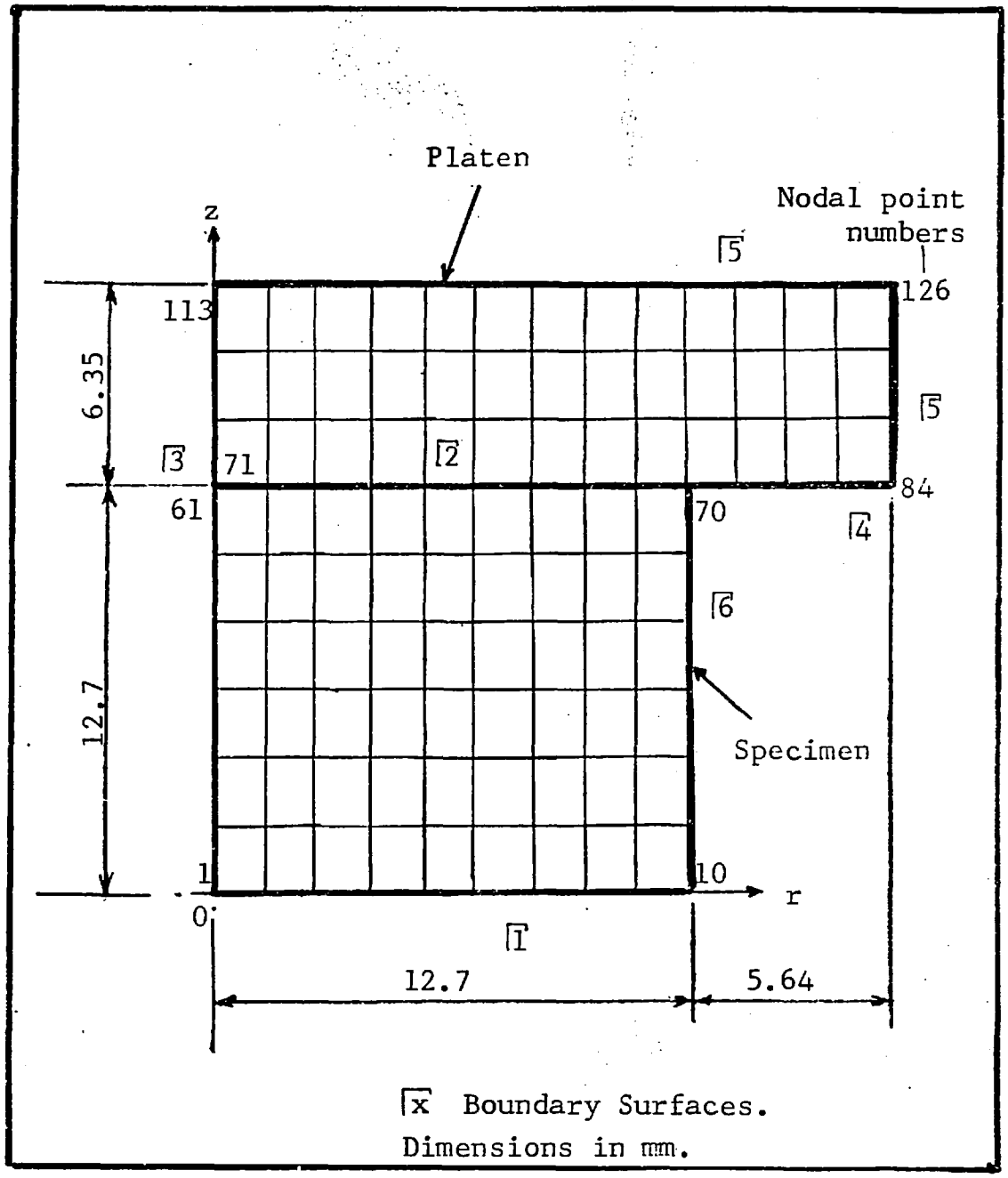

FIG. 5.6 Mesh and Boundary Surfaces for Solid Specimen.

The strain rate field is given by

$$\dot{\varepsilon}_r = \frac{b}{4}\frac{v}{h}\frac{e^{-bz/h}}{1-e^{-b/2}} \tag{5.54}$$

$$\dot{\varepsilon}_\theta = \frac{b}{4}\frac{v}{h}\frac{e^{-bz/h}}{1-e^{-b/2}} \tag{5.55}$$

$$\dot{\varepsilon}_z = -\frac{b}{2}\frac{v}{h}\frac{e^{-bz/h}}{1-e^{-b/2}} \tag{5.56}$$

$$\dot{\varepsilon}_\theta = -\frac{b^2}{8}\frac{v}{h^2}r\frac{e^{-bz/h}}{1-e^{-b/2}} \tag{5.57}$$

The rest of the procedure is the same as in the case of rings.

5.2 METHOD TO DETERMINE TEMPERATURE FIELD

Heat generated due to work of plastic deformation and friction often results in localised temperature rise, particularly at large strains and high strain rates. A method to determine this temperature field by weighted residuals is discussed in the following sections.

5.2.1 Premises

The following are held to be valid:

1. The material is thermally isotropic.

2. The work due to plastic work and friction is entirely converted into heat and transported simultaneously. In order to be able to analyse the process incrementally and to take into account the thermal softening, the heat generated during any particular increment of deformation is assumed to be transported instantaneously [103,105].

3. The thermal conductivity and the specific heat of the material are assumed to vary linearly with temperature (as illustrated in the Appendix).

4. The strain rate sensitivity is unaffected by rise in temperature up to 400°C [36,32].

5.2.2 Discretisation

The specimen and the platen are discretised as shown in Fig. 5.3 and Fig. 5.6 except that the nodal points lying on the r and z axes are not considered. As explained later in Section 5.2.4, this is equivalent to considering all four quarters of the specimen and platen together without having any nodal points on the axis.

5.2.3 Governing differential equation and boundary conditions

As it is considered that the heat generated is transported instantaneously, from equation (4.57) the governing differential equation may be obtained as

$$\frac{\partial^2 T}{\partial r^2}+\frac{\partial^2 T}{\partial z^2}+(\frac{1}{r}-V_r)\frac{\partial T}{\partial r}-V_z\frac{\partial T}{\partial z}+\frac{\dot{q}_g}{k}+\frac{\partial(\tau v_r)}{\partial z}=0 \qquad (5.58)$$

and for convection at the free surfaces Γ_6 and Γ_4

$$(\frac{\partial T}{\partial r})k = h_g(T-T_f)$$

$$-(\frac{\partial T}{\partial z})k = h_f(T-T_f) \qquad (5.59)$$

It is also assumed that the temperature at the surface Γ_5 remains equal to ambient temperature. So we have

$$T\Big|_{r=r_{max}} = T_o$$

$$T\Big|_{z=z_{max}} = T_o \qquad (5.60)$$

5.2.4 Residual functions

To obtain a solution a trial function approximating the temperature field is proposed as

$$T = T_o + (r^2-r_{max}^2)(z^2-z_{max}^2)\sum_{\ell=1}^{L}\sum_{m=1}^{M} A_{\ell m} r^{2\ell} z^{2m} \qquad (5.61)$$

This function is even in r and z, which is a necessary condition for axisymmetry and also satisfies the equation (5.60). However, there is an anomaly in that when r = 0 and z = 0 the increment in temperature will be equal to zero. In principle it should be possible to get around this difficulty by selecting values for ℓ and m as 0, 1, 2, ... so that there will be one term in the series which is a function of z only when r = 0 and vice versa. This technique was found to be unsatisfactory as the solution was unstable even for expansions of the 5^{th} order. An alternative to this will be to consider the entire cross-section of the specimen (rather than just one quarter), selecting a mesh which does not have any nodes lying on the axes. As the nodal points lying immediately beside the axes are close to the axis itself and as there are no essential conditions that need to be imposed upon at the axes, the continuum may be considered to be well represented in this case as well. Due to the even nature of the function and the fact that total residual is the algebraic sum of residuals at all nodes, identical results can be achieved by considering just one quarter of the specimen and simply omitting the nodal points that lie on the axes.

Referring to equations (4.14), (4.42), (4.53) and (5.51), we have

$$\dot{q}_g = \sigma'_{ij} \dot{\varepsilon}'_{ij} \tag{5.62}$$

$$\tau = \alpha (\sigma_o/\sqrt{3}) \tag{5.63}$$

$$\frac{\partial \tau v_r}{\partial z} = \tau v_r(-\frac{b}{h}) \tag{5.64}$$

Having satisfied some of the boundary conditions it is now necessary to set up three residual functions, one of them approximates the governing differential equations (5.58) and the other two approximate the boundary condition equation (5.60), which have not been satisfied by the proposed trial function, which are

$$\begin{aligned} R_1 = T_o + \sum_{\ell=1}^{L}\sum_{m=1}^{M} A_{\ell m}\Big[& 2(z^2-z_{max}^2)r^{2\ell}z^{2m} \\ & + 8r\ell(z^2-z_{max}^2)r^{2\ell-1}z^{2m}+2\ell(2\ell-1)(r^2-r_{max}^2) \\ & (z^2-z_{max}^2)r^{2\ell-2}z^{2m}+2(r^2-r_{max}^2)r^{2\ell}z^{2m} \\ & +8zm(r^2-r_{max}^2)z^{2m-1}r^{2\ell}+2m(2m-1)(r^2-r_{max}^2) \\ & (z^2-z_{max}^2)z^{2m-2}r^{2\ell}+(\frac{1}{r}-\beta V_r)\{2r(z^2-z_{max}^2)r^{2\ell}z^{2m} \\ & +2\ell(r^2-r_{max}^2)z^2-z_{max}^2)r^{2\ell-1}z^{2m}\} - \beta V_z\{2z(r^2 \\ & -r_{max}^2)r^{2\ell}z^{2m}+2m(r^2-r_{max}^2)(z^2-z_{max}^2)z^{2m-1}r^{2\ell}\Big] \\ & + \frac{\sigma'_{ij}\dot{\varepsilon}'_{ij}}{k} - \frac{JV_r b}{h} \end{aligned} \tag{5.65}$$

at the surface Γ_6

$$\begin{aligned} R_2 = \sum_{\ell=1}^{L}\sum_{m=1}^{M} A_{\ell m}\Big[& 2r(z^2-z_{max}^2)r^{2\ell}z^{2m}+2\ell(r^2-r_{max}^2) \\ & (z^2-z_{max}^2)r^{2\ell-1}z^{2m}\Big] - \frac{h_f}{k}(T-T_f) \end{aligned} \tag{5.66}$$

at the surface Γ_4.

$$\begin{aligned} R_3 = \sum_{\ell=1}^{L}\sum_{m=1}^{M} -A_{\ell m}\Big[& 2z(r^2-r_{max}^2)r^{2\ell}z^{2m}+2m(r^2-r_{max}^2) \\ & (z^2-z_{max}^2)z^{2m-1}r^{2\ell}\Big] - \frac{h_f}{k}(T-T_f) \end{aligned} \tag{5.67}$$

The total residual $R_T = R_1 + R_2 + R_3$.

5.2.5 Solution

As explained in Section 5.1.6, the residual functions can now be assembled and weighting functions applied which will lead to solution. The procedure is summarised in the form of a flow chart, Fig. 5.7, which corresponds to a sub-routine (Appendix B).

It should be noted that the terms corresponding to heat generation (equation 5.66) apply only to nodal points that are in the specimen and that the platen velocities $v_r = 0$ and $v_z = v$. These conditions are taken into account as shown in the flow chart.

5.3 COMPLETE SOLUTION FOR THE DEFORMATION IN UPSETTING

The stress field and temperature field determined as above can be extended to analyse the deformation process incrementally step by step accounting for strain hardening, strain rate sensitivity and thermal softening.

The increment Δk is calculated as illustrated in Appendix B. The changes in geometry can be calculated as

$$\begin{aligned} \Delta r &= V_r \times \Delta t \\ \Delta z &= V_z \times \Delta t \end{aligned} \qquad (5.70)$$

The complete sequence of computation is illustrated in Fig. 5.8.

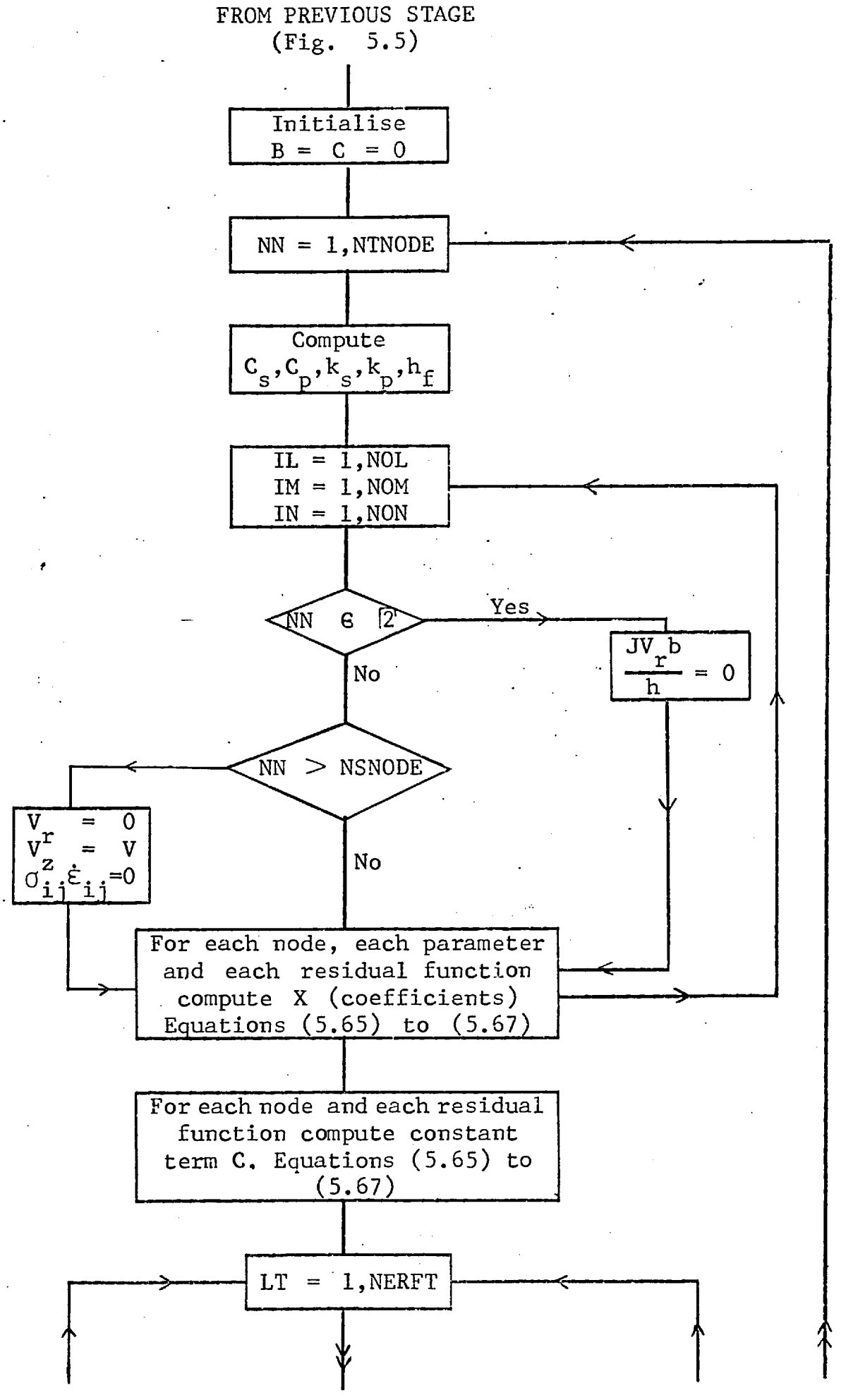
FROM PREVIOUS STAGE
(Fig. 5.5)
Initialise
B = C = 0
NN = 1,NTNODE
Compute
C_s, C_p, k_s, k_p, h_f
IL = 1,NOL
IM = 1,NOM
IN = 1,NON
NN ∈ Γ2'
Yes
No
$\frac{JV_r b}{h} = 0$
NN > NSNODE
No
$V_z = 0$
$V^r = V$
$\sigma_{ij}\dot{\varepsilon}_{ij} = 0$
For each node, each parameter and each residual function compute X (coefficients) Equations (5.65) to (5.67)
For each node and each residual function compute constant term C. Equations (5.65) to (5.67)
LT = 1,NERFT

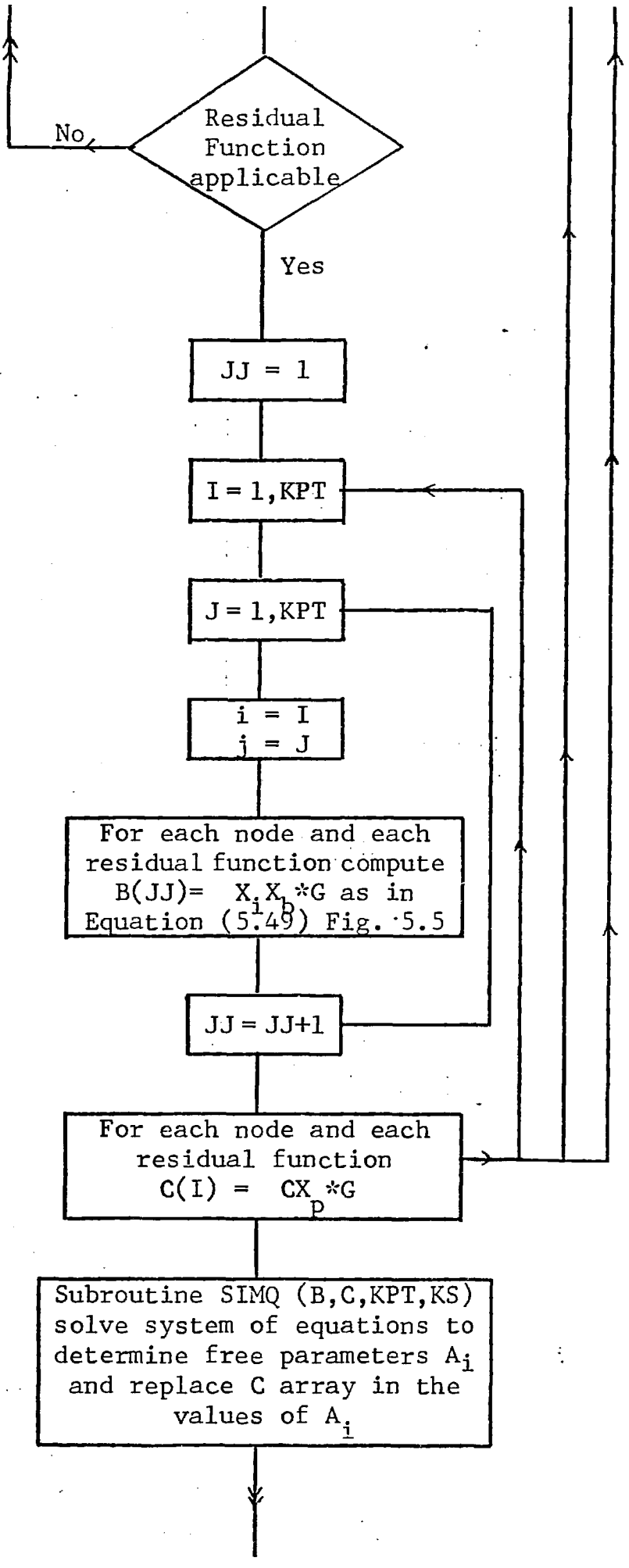
Residual Function applicable
No
Yes
JJ = 1
I = 1,KPT
J = 1,KPT
i = I
j = J
For each node and each residual function compute B(JJ)= $X_i X_b$ *G as in Equation (5.49) Fig. 5.5
JJ = JJ+1
For each node and each residual function C(I) = CX_p *G
Subroutine SIMQ (B,C,KPT,KS) solve system of equations to determine free parameters A_i and replace C array in the values of A_i

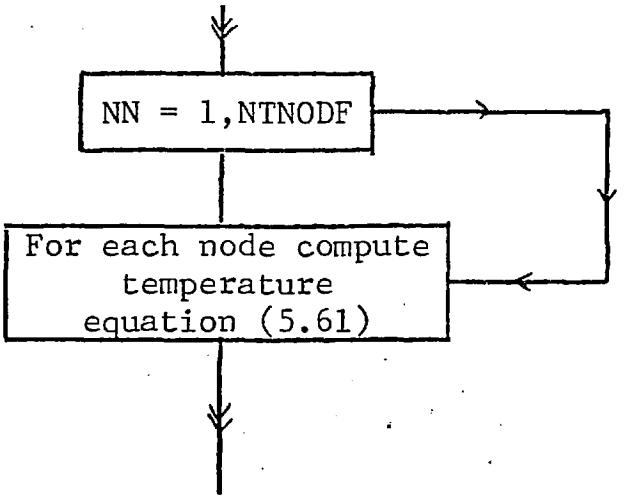

FIG. 5.7 Flow Chart, Computation of Temperature Field.

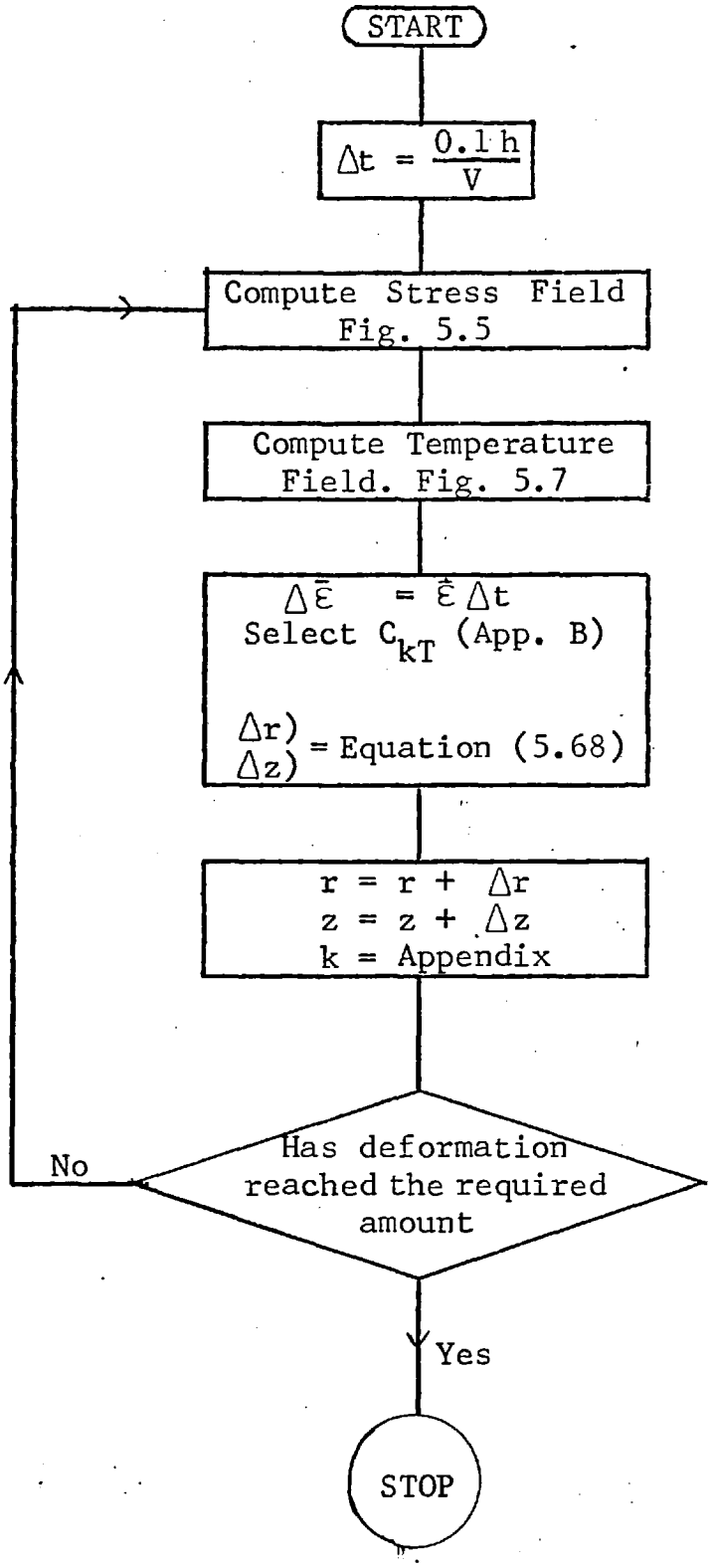

FIG. 5.8 Flow Chart - Complete Solution.

CHAPTER 6

EXPERIMENTAL EQUIPMENT AND PROCEDURE

Features of experimental rig and measurement of transient phenomena are discussed in this chapter.

6.1 EXPERIMENTAL EQUIPMENT

A linear induction motor was used as an experimental forging machine. This particular machine was designed and developed by Johnson et al [94] for use as a horizontal impact extrusion machine. The stator windings were modified to improve performance and the machine was mounted vertically in a framework as a high speed forging machine.

6.1.1 Linear induction motor

Linear motors can be considered as a planar development of conventional rotary machines. Any rotary electrical machine can be manufactured as a developed or linear machine [95]. As most conventional rotary motors are induction motors, their linear counterpart has become more popular. In a rotary machine the sinusoidally distributed flux density in the air gap produces a wave front which rotates at synchronous speed. Similarly in a linear stator wound with

three-phase system of coils produces a wave front, which travels linearly along the stator at synchronous speed. This speed is given by:

$$u_s = 2pf \qquad (6.1)$$

where p = pole pitch,

f = supply frequency.

The secondary member of the linear machine, not necessarily the moving member, is often called the "translator".

The linear induction motor can be broadly classified into two categories as:

i) Short stator machines, and

ii) Short translator (rotor) machines.

In general the first type is used in applications where long travel is required, e.g. overhead cranes, conveyors, etc. The second type characterised by short secondary may be used when only a short travel is required, as in the case of forging.

The linear induction motors the double-sided stator arrangement, Fig. 6.1, is a natural choice in which the corresponding poles of the two stators are of opposite instantaneous polarity so they assist each other in forcing

the flux through the translator. Magnetic circuit for such a double-sided arrangement is complete whether or not the translator is between them. This permits use of non-ferrous translators which are conducting material like copper and aluminium, thus eliminating undesirable magnetic forces in the direction normal to the motion.

The linear induction motor used in the rig is a twin arrangement of two double-sided machines as shown in Fig. 6.1. The dual translator carries a ramhead (serves as an impact hammer) which travels between parallel guides.

Specification of the motor:

Supply:	3 phase, 440 V, 50 Hz.
Maximum current:	160 A.
No. of stators:	4
No. of slots in each stator:	36
No. of coils in each slot:	2
Each coil:	50 turns, 20 SWG (0.914 mm.), triple-stranded insulated Cu wire.
Pole pitch:	152.4 mm.
Synchronous speed:	15.24 m/s.
Translator:	450 mm. x 225 mm. x 5 mm. Al. Total weight including ram head is 11.1 kg.

6.1.2 Stator winding

The main difference between short stator and short translator machines lies in the distribution of magnetic flux in the air gap and the current in the stator conductor. The driving force on the secondary depends upon the flux penetrating and the copper losses mainly on the stator current and the electrical and magnetic transients produced at the edges. In a parallel connection the flux density is distributed evenly as shown in Fig. 6.2. This is due to the fact that flux density is proportional to voltage, which is the same in each coil. Consequently, the current in the secondary zone is higher than the current in the inactive zone which reduces copper losses. Therefore this type of connection is in general suitable for short translator machines. In a series connection the distribution of flux density will be less in the secondary zone than in the inactive part due to the demagnetising effect of the secondary current. This type of connection is in general suitable for a short stator machine.

Originally all the coils of this particular machine were connected in parallel. It is observed that the length of translator is 1.5 times the pole pitch, which is the suggested [96] minimum to reduce the dolphin effect (the

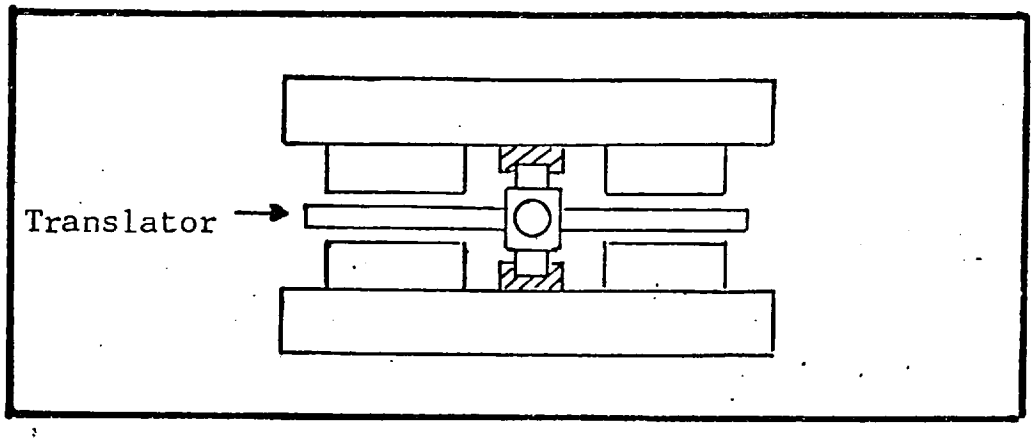

FIG. 6.1 Twin arrangements of Linear Motor.

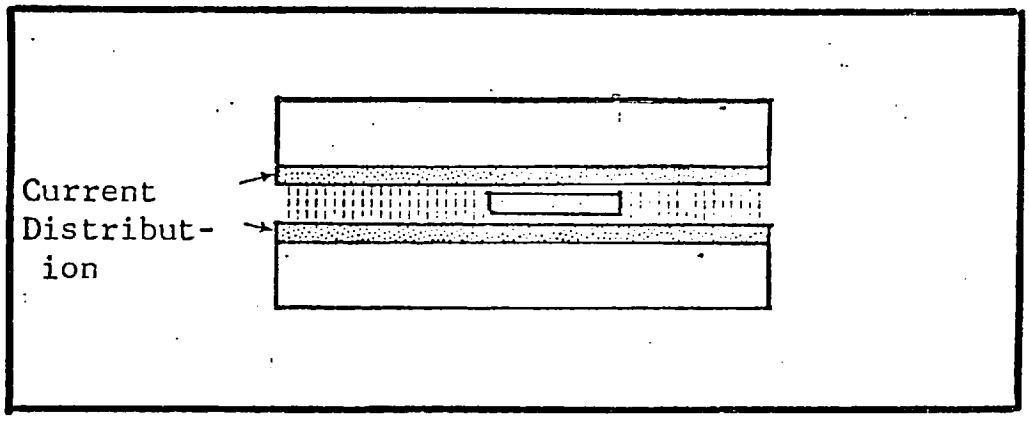

FIG. 6.2 Parallel Connection.

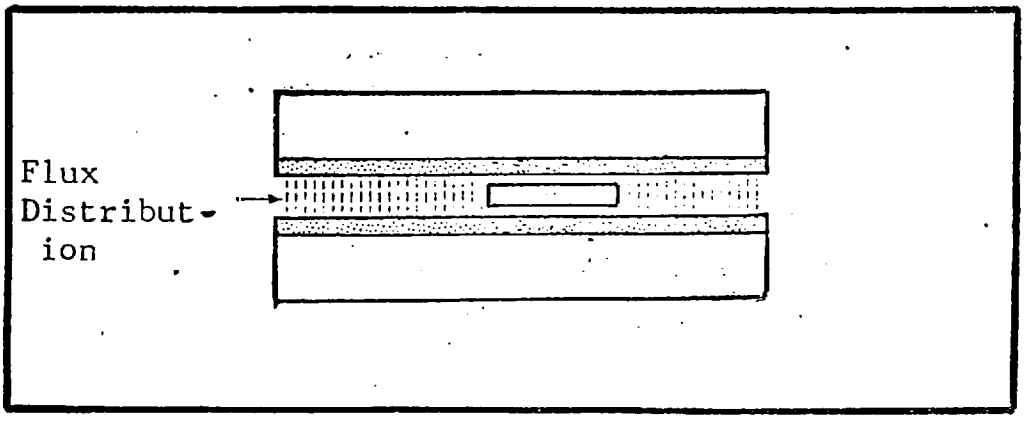

FIG. 6.3 Series Connection.

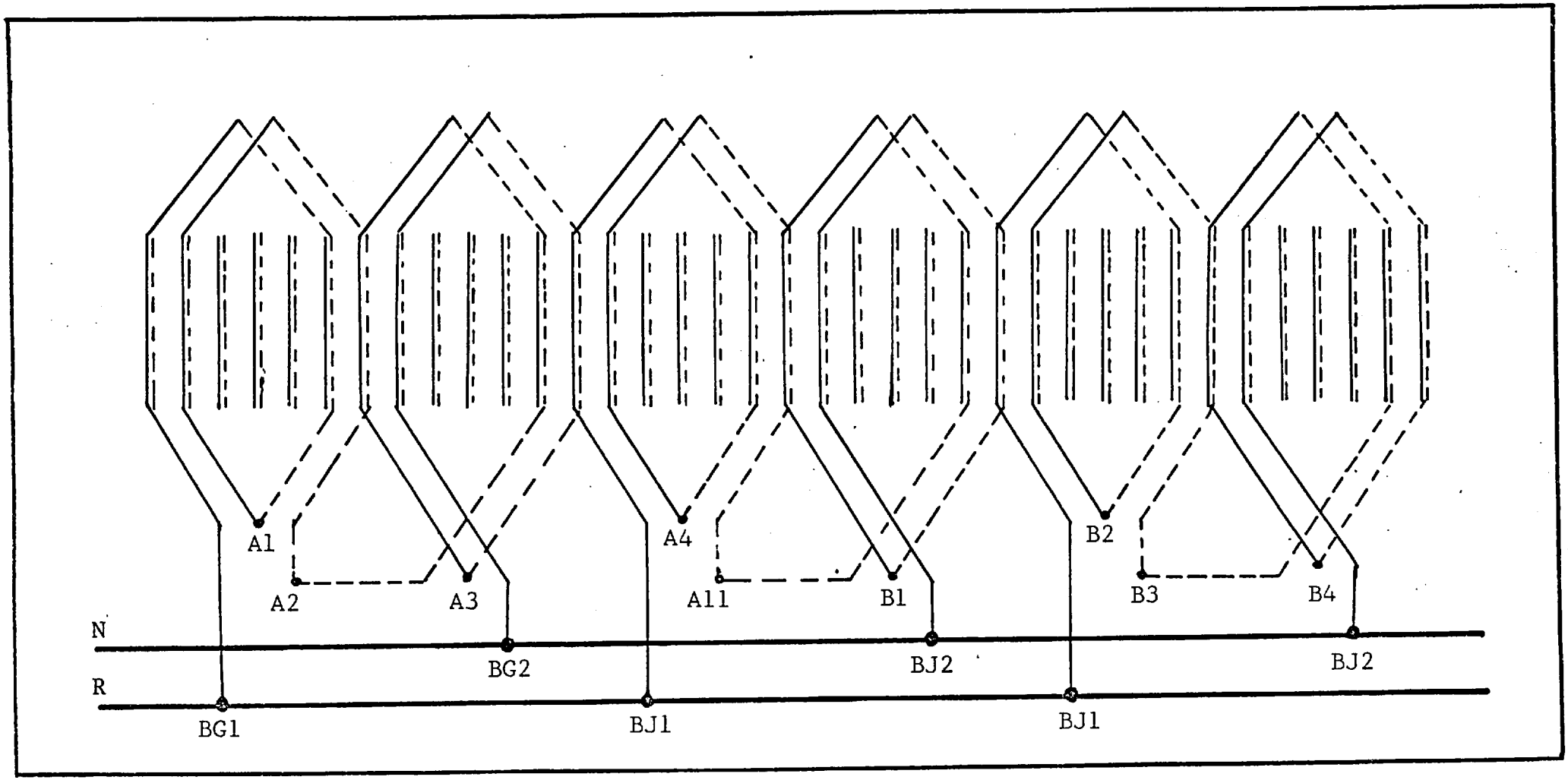

FIG. 6.4 Stator Winding - Red Phase of Stator No. 1.

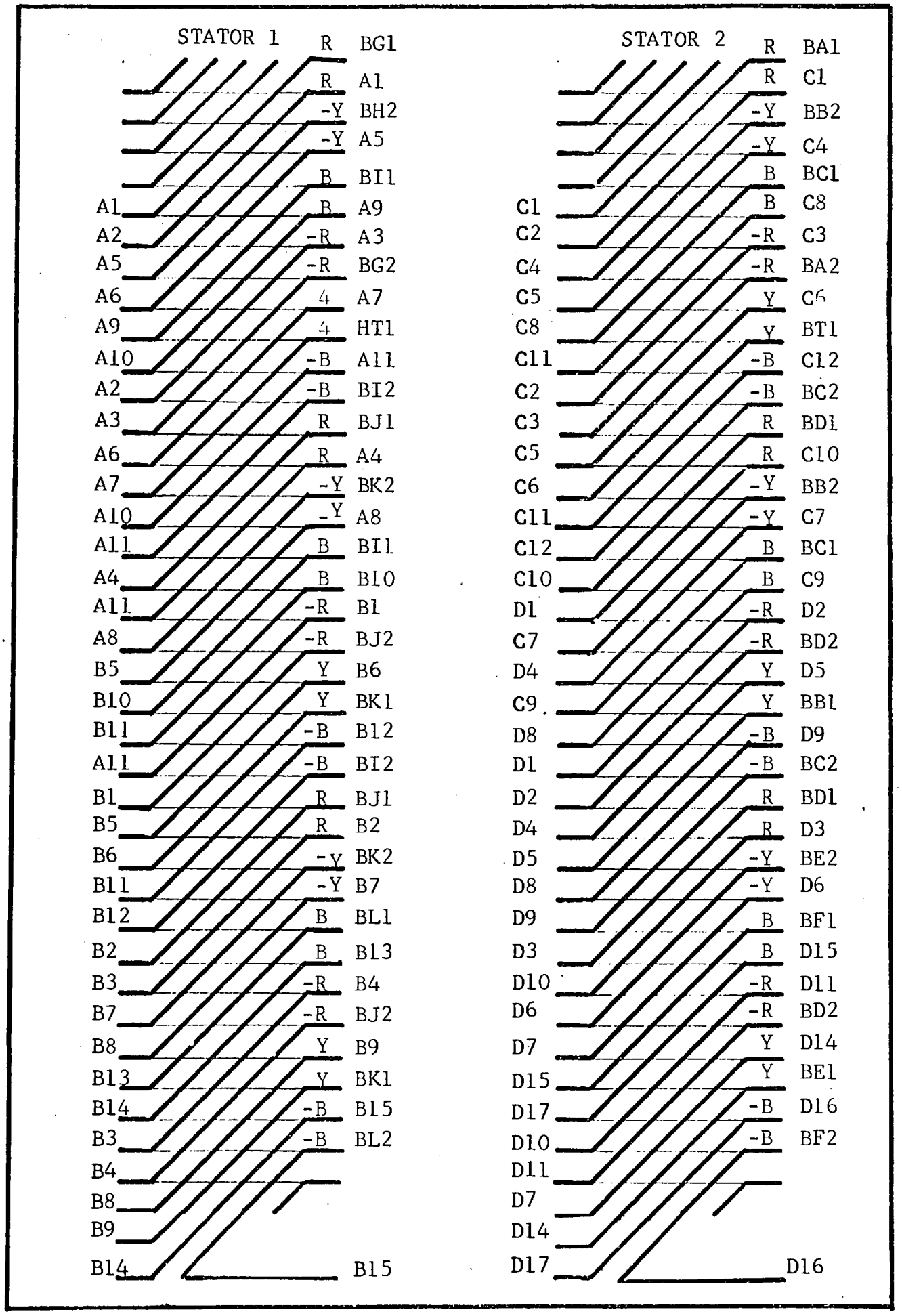

FIG. 6.5 Connection Diagram.

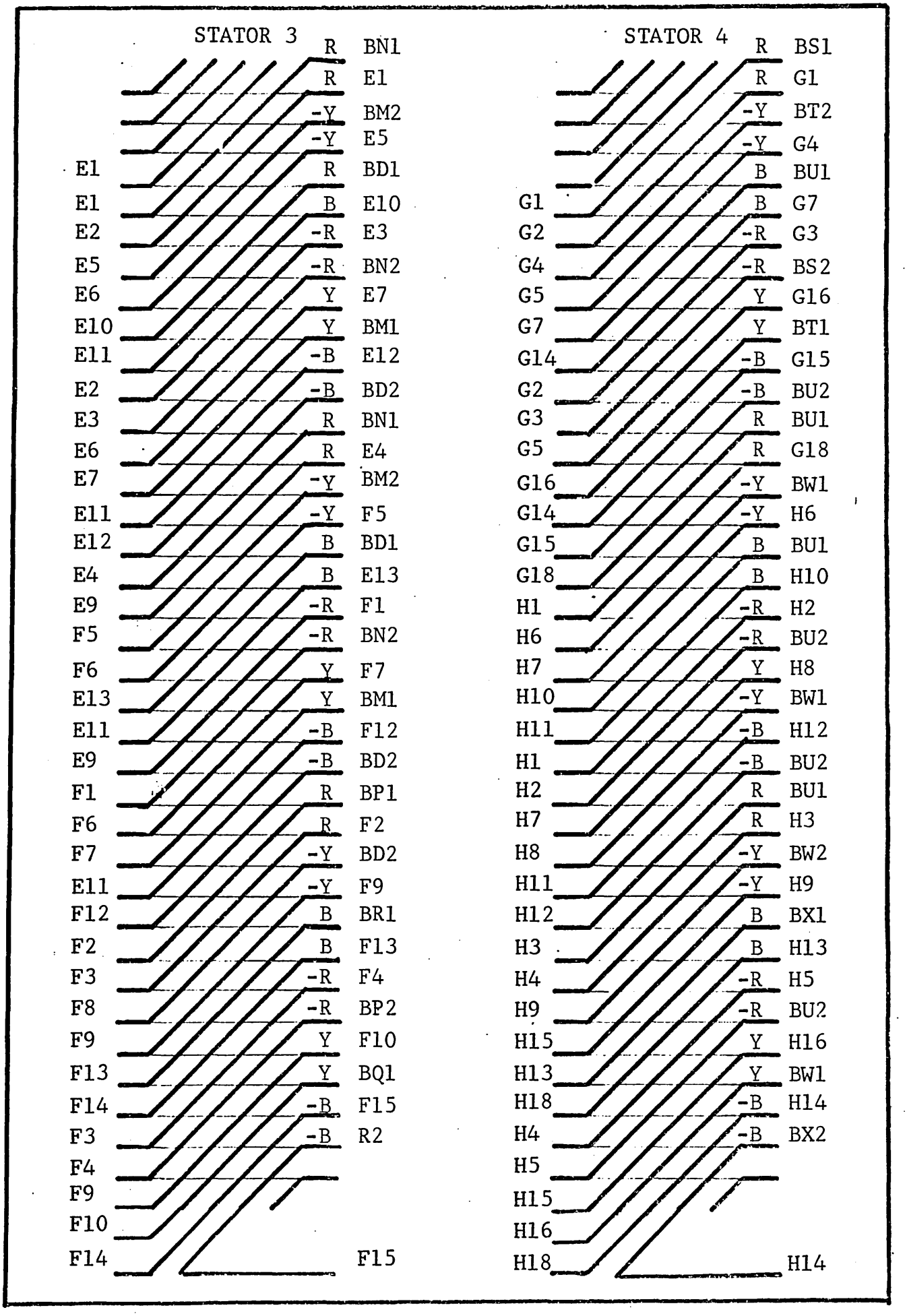

FIG. 6.6 Connection Diagram.

dipping of leading edge). As this length is not an exact multiple of the pole pitch undesirable effects are introduced. The length of the translator can not be increased much more in the present set-up due to other design considerations such as weight to strength ratio. Therefore it is necessary to combine series and parallel connections [97] to minimise losses.

The stator coils are connected as shown in Fig. 6.4. Each phase of each stator has six coil groups which are connected in the form of three parallel paths and each path is composed of two coil groups in series. Incidentally the double-layer system (two coils per slot) permits chording, which will also reduce machine losses. The coils are 5/6 chorded (i.e. the span is 150^{o} instead of 180^{o}).

As shown in the connection diagrams, Fig. 6.5 and Fig. 6.6, five coil sides on each end of the stator are not accommodated in the slots, and four coils at one end and one coil at the other end are left open (to ensure that there are the same number of coils in each phase). This arrangement allows some flexibility inasmuch as one can choose to obtain maximum force at the instant of switching on or reduce rebound at the end of the stroke.

6.1.3 Experimental rig

The general front view of the rig is shown in Fig. 6.8. The linear induction motor is mounted vertically in a framework. A rigid table fixed to the floor serves as an anvil which carries the sub-press and is aligned to be directly under the ram head carried by the translator. The sub-press is of standard type. The bottom platen is fixed to the anvil and the top platen, supported by springs, moves up and down in guide pillars. The translator and the ram head are held at the top by a spring-loaded latch, Fig. 6.9. The latch is held in position by a solenoid, Fig. 6.10. When the motor is switched on, the translator is released and is driven down and the ram head strikes the sub-press and the work piece placed in between the platens is thus forged.

In the past the speed of the motor was varied by changing the supply voltage. This meant the use of an expensive transformer. The need for the transformer was eliminated by use of a simple system of relays. When the motor is connected directly to the mains a maximum speed of 15 metres/second ($\approx$ synchronous speed) can be reached. Therefore it is only necessary to reduce the speed of operation. The acceleration and therefore the speed depends

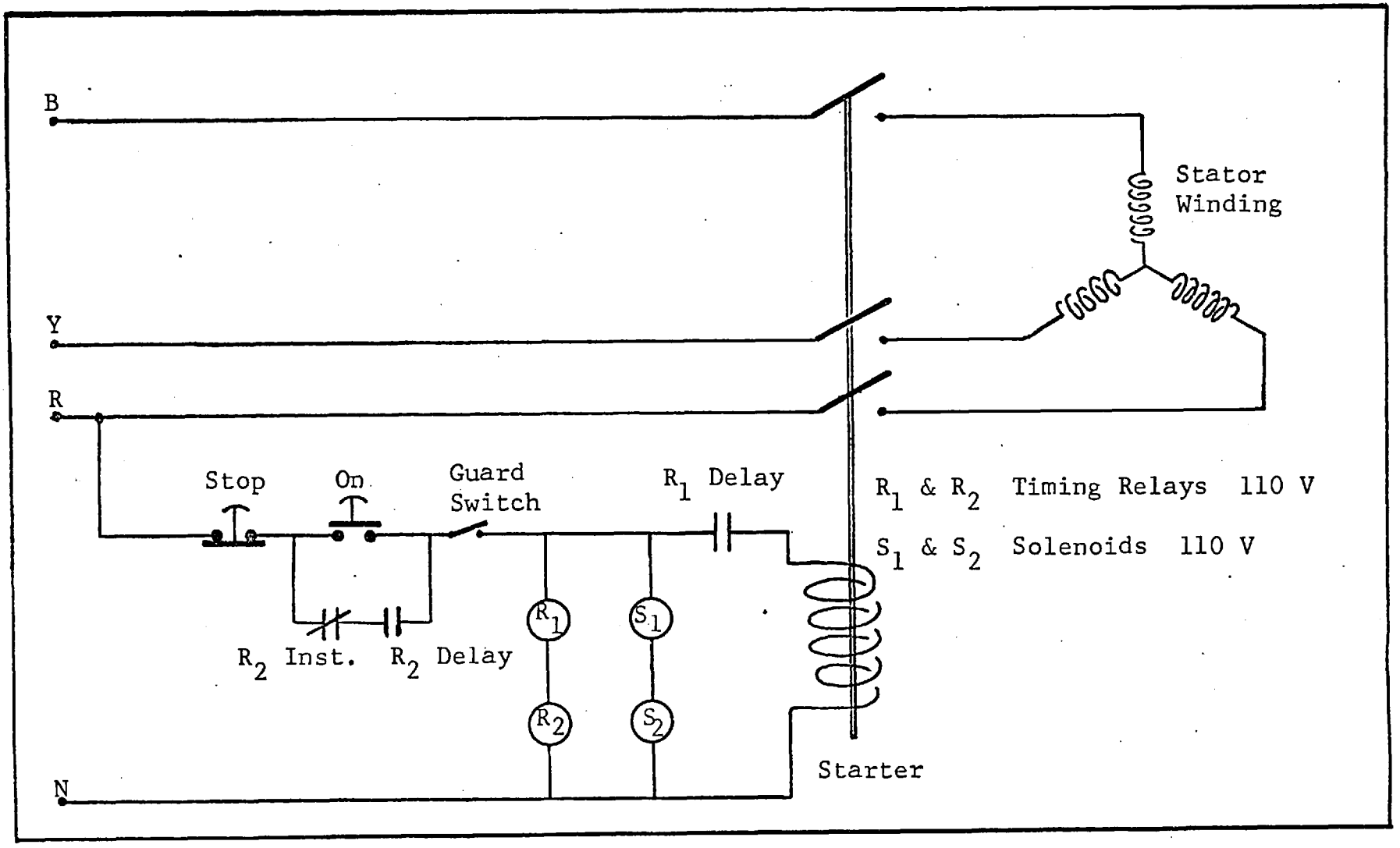

FIG. 6.7 Circuit Diagrams to start the nachine and control speed.

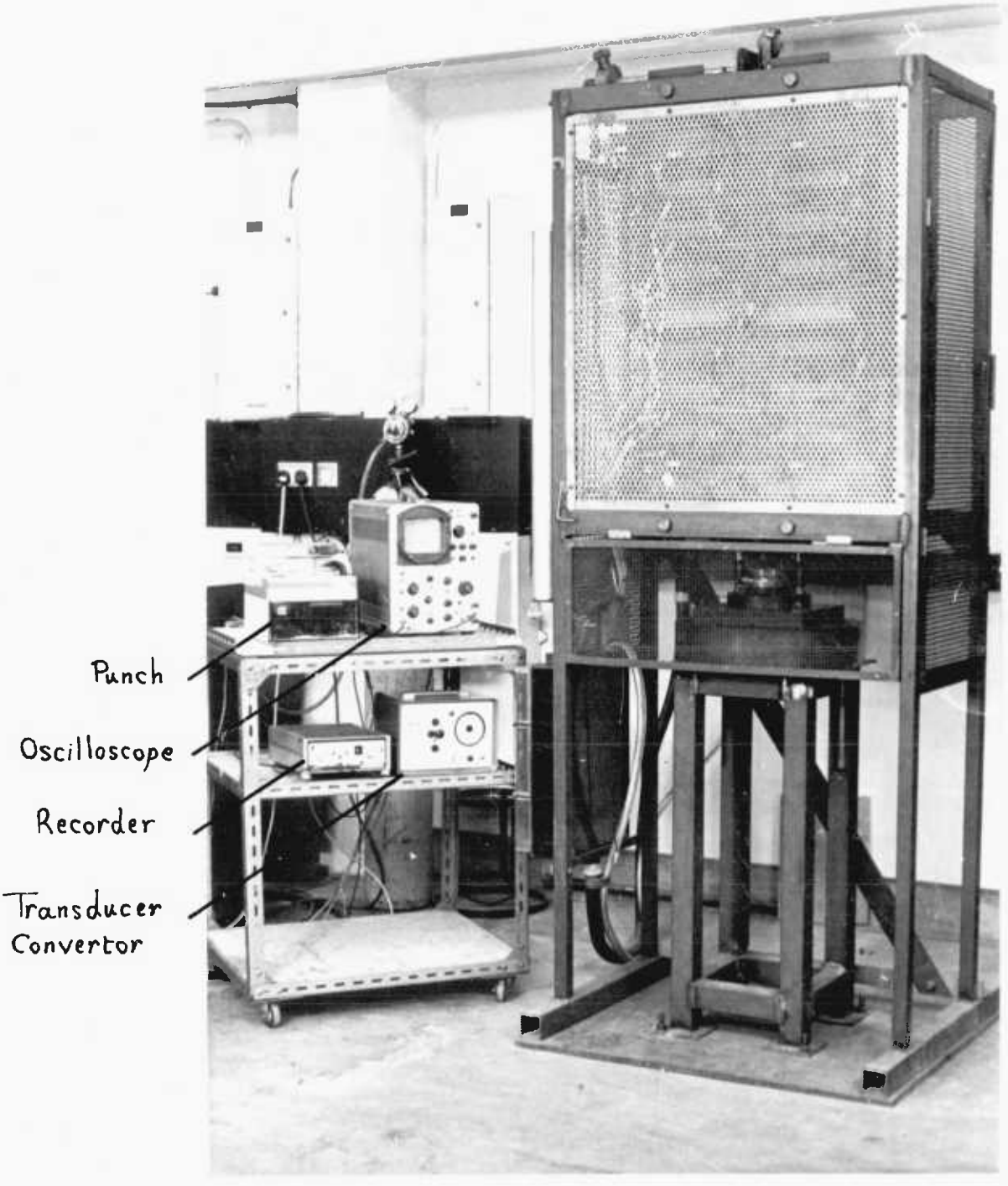

Figure 6.8: General View of the Experimental Rig

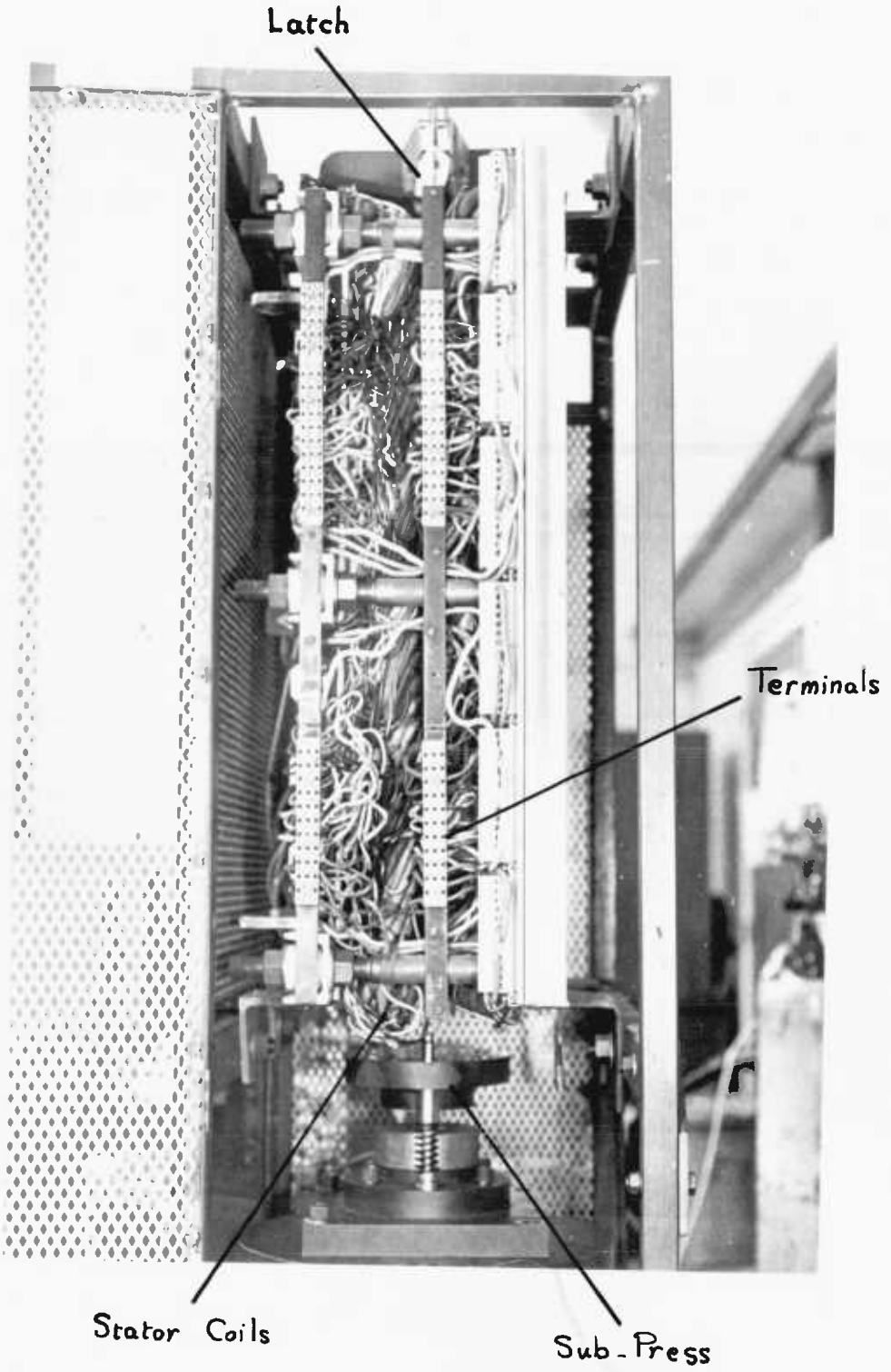

Figure 6.9: Side View of the Linear Induction Motor

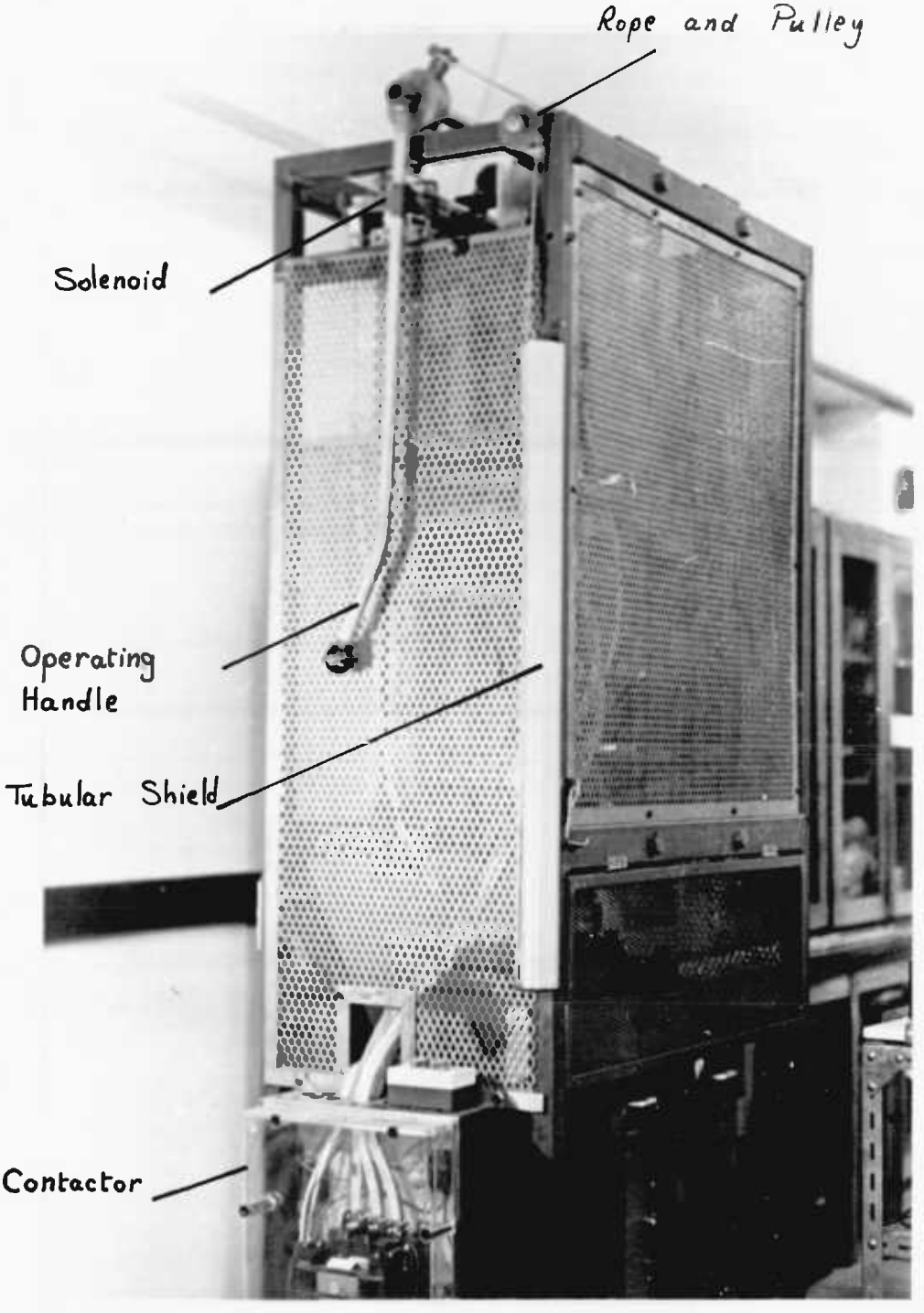

Figure 6.10: Side View of the Experimental Rig

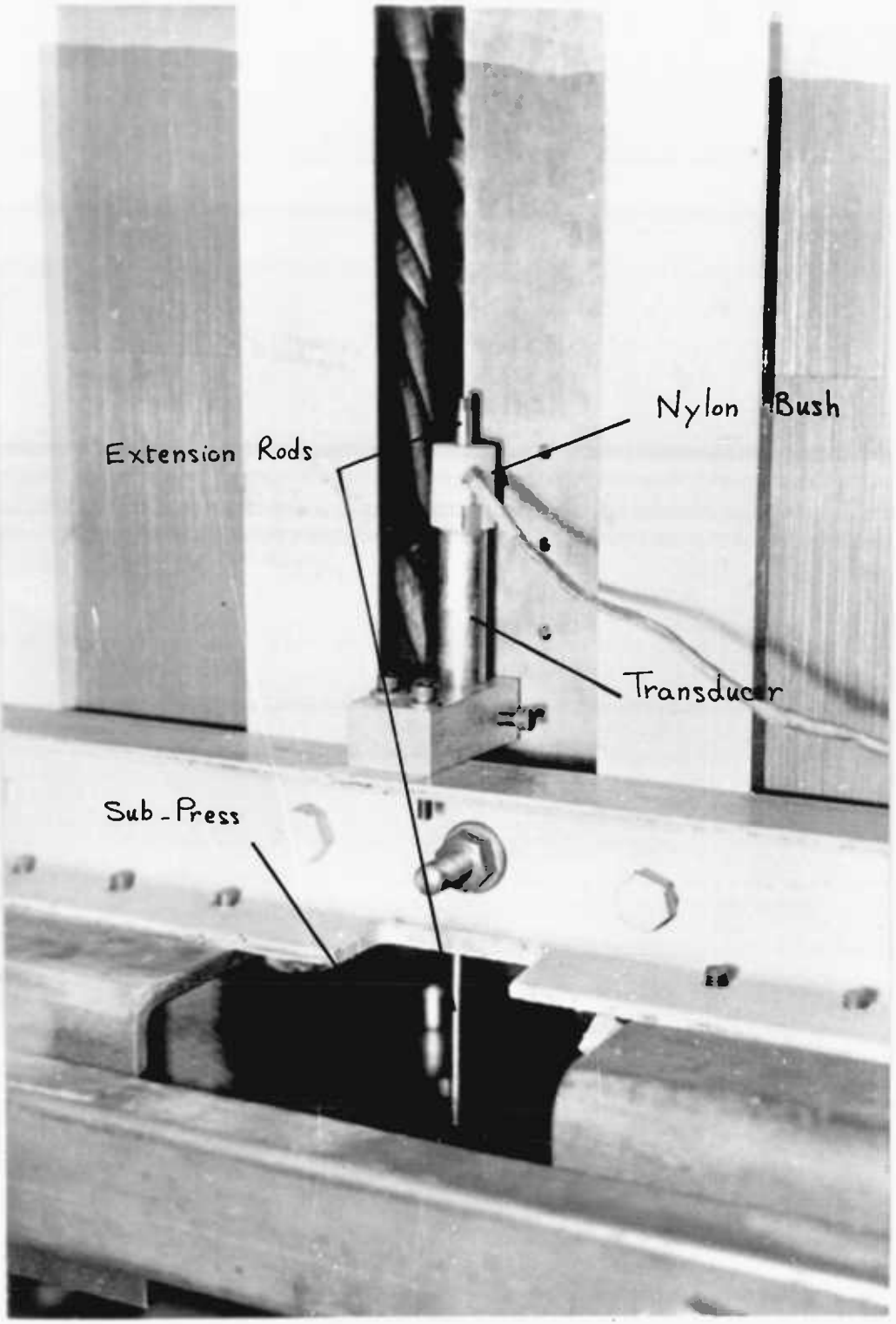

Figure 6.11: Transducer Mounting

H_o = 6.35 mm, OD = 19.05 mm

H_1 = 3.86 mm, No Lub.

H_1 = 4.45 mm, Lub. Moly Slip

H_1 = 3.35 mm, No Lub.

H_1 = 4.03 mm, Lub. Moly Slip

Figure 6.12: Test Specimens - 6:3:2 ratio

upon the distance through which the translator is propelled. If the translator is allowed to fall free, the motor can be switched on for any desired duration of time during its flight downwards and thereby vary the acceleration and speed. This is done by using a system of timing relays as shown in the circuit diagram, Fig. 6.7. The instant the machine is switched on the two relays and the solenoid are energised. The solenoid instantly releases the translator which begins to fall by gravity. The relay R1 can be set to operate after any desired time delay (or instantly) which will complete the circuit and energise the starter of the motor. The relay R2 has two terminals, one of which can be delayed. This will determine when the machine is to be switched off. The other terminal, which operates instantly, is used to hold the supply until the machine is switched off. An emergency stop and a limit switch operated by the guard are also used in the circuit in order to ensure safety. After each operation the translator is retrieved to the top position by means of rope and pulley mechanism. The free end of the rope attached to a rubber ball is guided inside a shield, Fig. 6.10. The relays are mounted on a wall panel and dial clocks are provided to adjust timing.

6.2 INSTRUMENTATION

Measurement systems are basically a transducer, signal conditioning equipment and a read out, which correspond to information acquisition, information processing and information output. In any measurement system there is always a degree of uncertainty resulting from measurement error [102]. Errors can be broadly classified as static errors and dynamic errors. Static errors stem from three basic sources: reading error, characteristic error and environmental error. Reading error arises from such factors as parallax, interpolation and optical resolving power. It is now possible to completely eliminate this by obtaining a digital readout. Gain errors, hysteresis, linearity, etc. are a part of characteristic errors, which will depend very much upon the construction and quality of equipment used. Environmental errors relate to external influences such as magnetic fields. These can be minimised by adequate shielding. Dynamic errors are caused by time variations in the measurement and are characterised by the frequency response of the system. It is necessary to ensure that the frequency response of the system is higher than the highest modulation of frequency of the measurement.

With these considerations in view a measuring system illustrated in Fig. 6.13 was designed. Salient

features of the equipment used are discussed in the following sections.

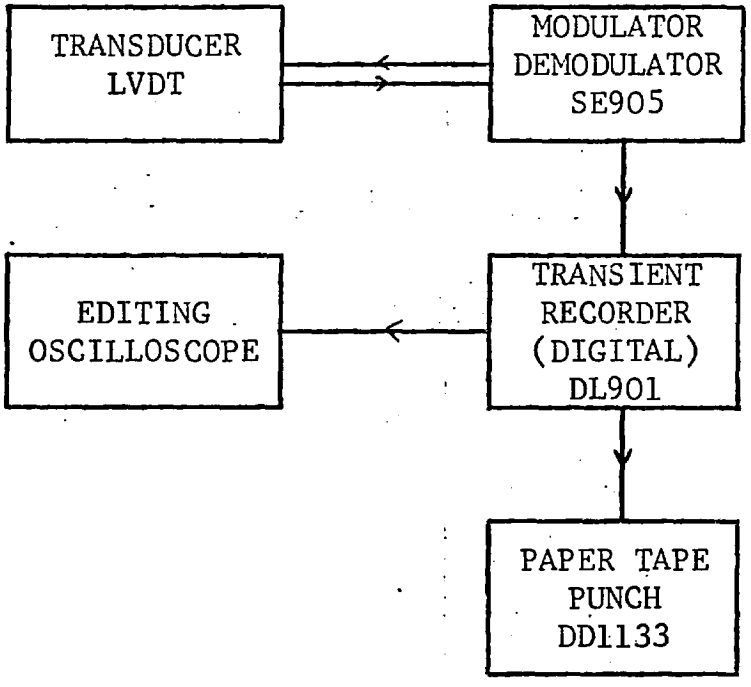

FIG. 6.13 Measuring System.

6.2.1 Displacement transducer

Insofar as this work is concerned displacement, velocity and acceleration are the three quantities of

interest. As these quantities are interrelated by a simple differentiating and integrating operations and as we have digital output, it does not matter which one of these is actually measured. Among the many devices available on the market the Linear Variable Differential Transformer manufactured by Electro Mechanisms Ltd., Slough, Bucks., seemed most suitable. The transducer mounting is shown in Fig. 6.11.

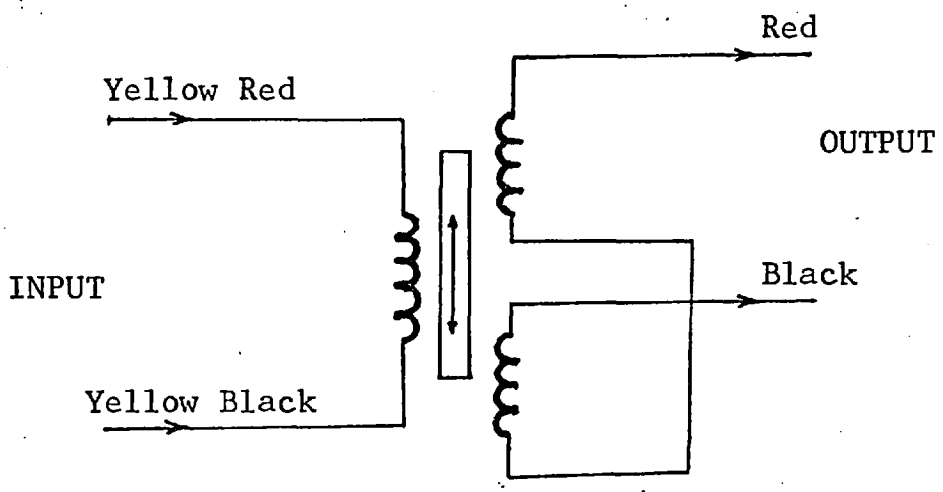

FIG. 6.14 Connection Diagram of LVDT,

LVDT Specification

AC Series D50 1 (Serial No. 170F).

Range ± 25.4 mm.

Core Length 100 mm.

Frequency response depends upon primary excitation.

Null voltage 1.6 mV.

Primary excitation 6 V RMS.

Secondary load 600 k.ohms.

Differential output 2.235 V.

Shock up to 1000 g.

The specifications as listed is quite adequate for this particular application. When an AC carrier excitation is applied to the transducer it produces an electrical output proportional to the displacement of the movable core. The transducer body was mounted to the rigid frame of the machine and the core was fixed to the top platen, which is the moving member of the sub-press. Thus displacement could be recorded against time during deformation. The LVDTs are insensitive to lateral movement. However, the extension rods (non-magnetic stainless steel) of the core were guided between nylon bushes. The LVDT is adequately shielded from any surrounding magnetic field. As explained earlier, the linear induction motor of the experimental rig was always

switched off before impact and therefore the output of the transducer is unaffected by the operation of the motor.

6.2.2 Modulator/demodulator

As the LVDT is a passive device it is necessary to apply an excitation voltage to obtain a response which is then demodulated before being input into the recording device. A S.E. laboratory transducer convertor SE905 was used for this purpose. This generates a carrier of 6 V at 5 kHz and a maximum attenuation of 54 db is available. The main consideration for selection of this equipment is that the carrier wave frequency should be something like ten times as high as the highest modulation frequency of the signal to be measured.

6.2.3 Transient recorder

In general storage oscilloscopes are used to record transient signals and the photographs of the trace used for further analysis. This is not entirely satisfactory as the resolution is very poor and reading errors may also be introduced. Furthermore, it is difficult to trigger at the correct instant and usually some of the available time base is lost on account of this. However, nowadays digital

transient recorders are available which completely eliminate this difficulty. The digital output enables one to perform such operations as numerical differentiation.

A Data Laboratory transient recorder DL901 was selected for use. Main considerations for selection of this equipment are high sampling rate, high resolution and some flexibility in the mode of recording. The sampling rate of this particular machine is 5 to 200,000 (slower rates can be obtained by using external pulse train). The two modes of recording 'delayed mode' and 'pre-trigger mode' that are available allow some flexibility inasmuch as the recording can either be delayed or part of the output prior to the event can be retained in the memory. As the memory is 1024 words long, this facility makes recording very much easier. The operation of this device is represented schematically in Fig. 6.15.

Due to the discrete nature of sampling, it is necessary to ensure that 'aliasing' (incomplete definition of the signal) does not occur. If further analyses are to be carried out on a digital computer the selected sampling rate should be such that at least two samples are taken to define the maximum frequency contained in the signal. Insofar as the present work is concerned, in all cases at least 50 samples define the displacement in the zone of interest.

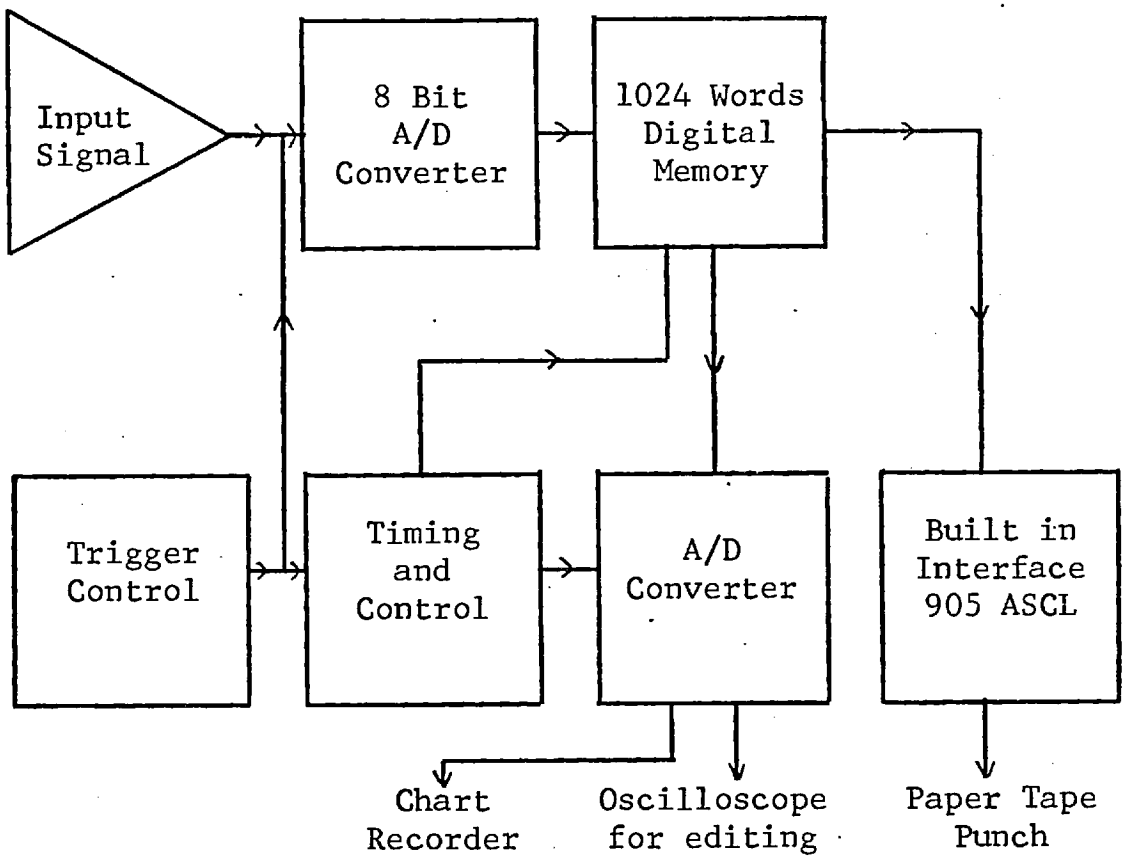

FIG. 6.15 Operation of Transient Recorder.

It may be of interest to record the fact that a FM tape recorder was also considered. This seemed an attractive proposition as the time base can be expanded after recording. The recorded signals were digitised and processed on a PDP15 mini-computer. Although satisfactory

analysis could be carried out the procedure was found to be too cumbersome and time-consuming.

6.2.4 Triggering

In order to be able to capture a transient phenomenon it is necessary to trigger the recording device at the correct instant. Devices such as micro-switches, photoelectric cells, were found unsuitable as the electrical transients produced during switching on and operation of the motor usually caused triggering before the event. A compression type piezoelectric accelerometer was used as a triggering device, which produces a voltage when subjected to shock. The accelerometer was mounted on the anvil which produced the triggering signal on impact. The 'pre-triggering' mode available in the transient recorder enabled retention of a part of the signal immediately prior to the moment of impact, as illustrated in Fig. 6.16.

6.2.5 Editing and output

The recorded signal was first scrutinised with the aid of an oscilloscope. To obtain a permanent record of useful signals a Data Dynamics 1133 paper tape punch was used. The output is ASCII coded, a format suitable for computer analysis.

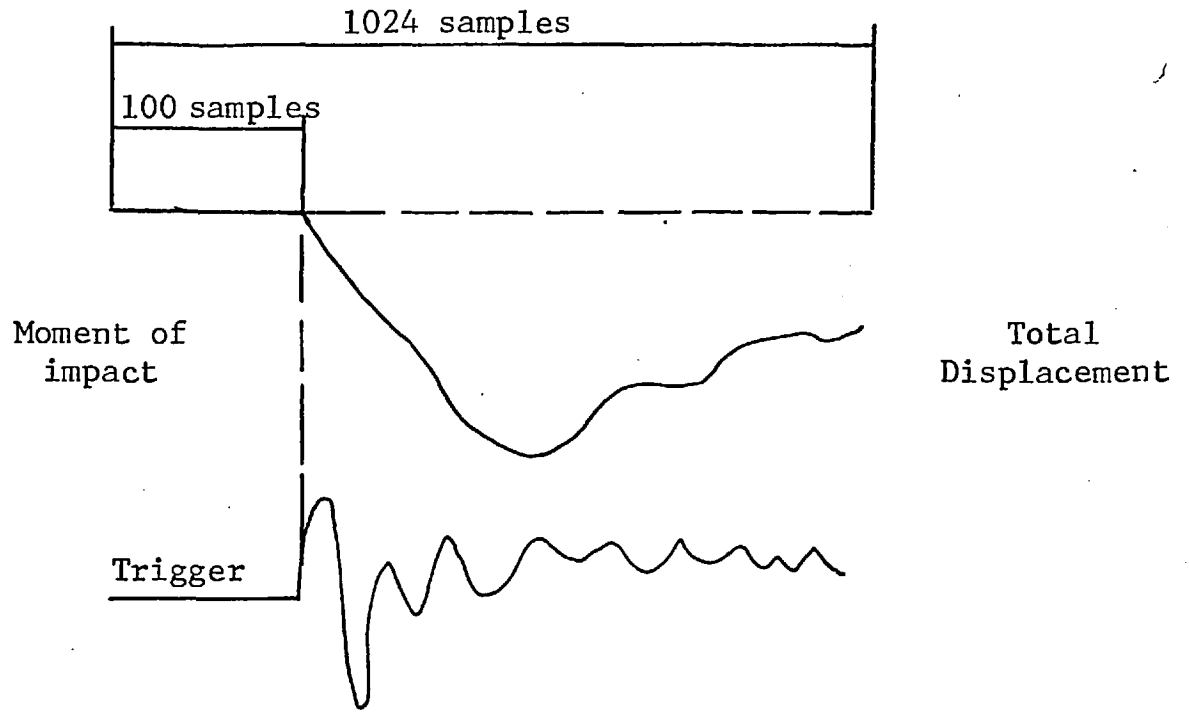

FIG. 6.16 Mode of Recording.

6.3 CALIBRATION AND TESTING

The output of the displacement transducer was statically calibrated before each series of experiments. The calibration was carried out in situ using distance pieces of various thickness between the platens of the sub-press. A typical calibration curve is shown in Fig. 6.17. The digital output value of 256 corresponds to the full scale voltage setting on the recorder. The dynamic response

of the transducer was checked by upsetting specimens at various speeds. There was no significant difference between dynamic and static response of the transducer.

Specimens of commercially pure aluminium and high conductivity copper were machined from cold drawn bars. The rings were of 6:3:2 ratio (19.05 mm O.D., 9.525 mm. I.D., 6.35 mm. height), which is in keeping with most of the published work on ring tests. A circular grid as shown in Fig. 6.12 was inscribed on each face of the specimen. A thread chaser of 0.508 mm. pitch (50 TPI) was used for this purpose. The grooves were 0.05 mm. deep and 0.05 mm. wide. The solid specimens were 12.7 mm. in diameter and 12.7 mm. in height. The aluminium specimens were annealed at 360°C for one hour and the copper specimens were annealed at 600°C for one hour. A vacuum furnace was used for annealing.

Before each dry test without lubricant the platens and the specimen were cleaned with trichloroethylene to ensure that they were clean and perfectly dry. For tests with lubricant molybdenum disulphide grease (Moly Slip) was used. Tests on copper and aluminium specimens were carried out at four different speeds and four different reductions in height for each case. Crash rings were used to limit deformation to the required degree.

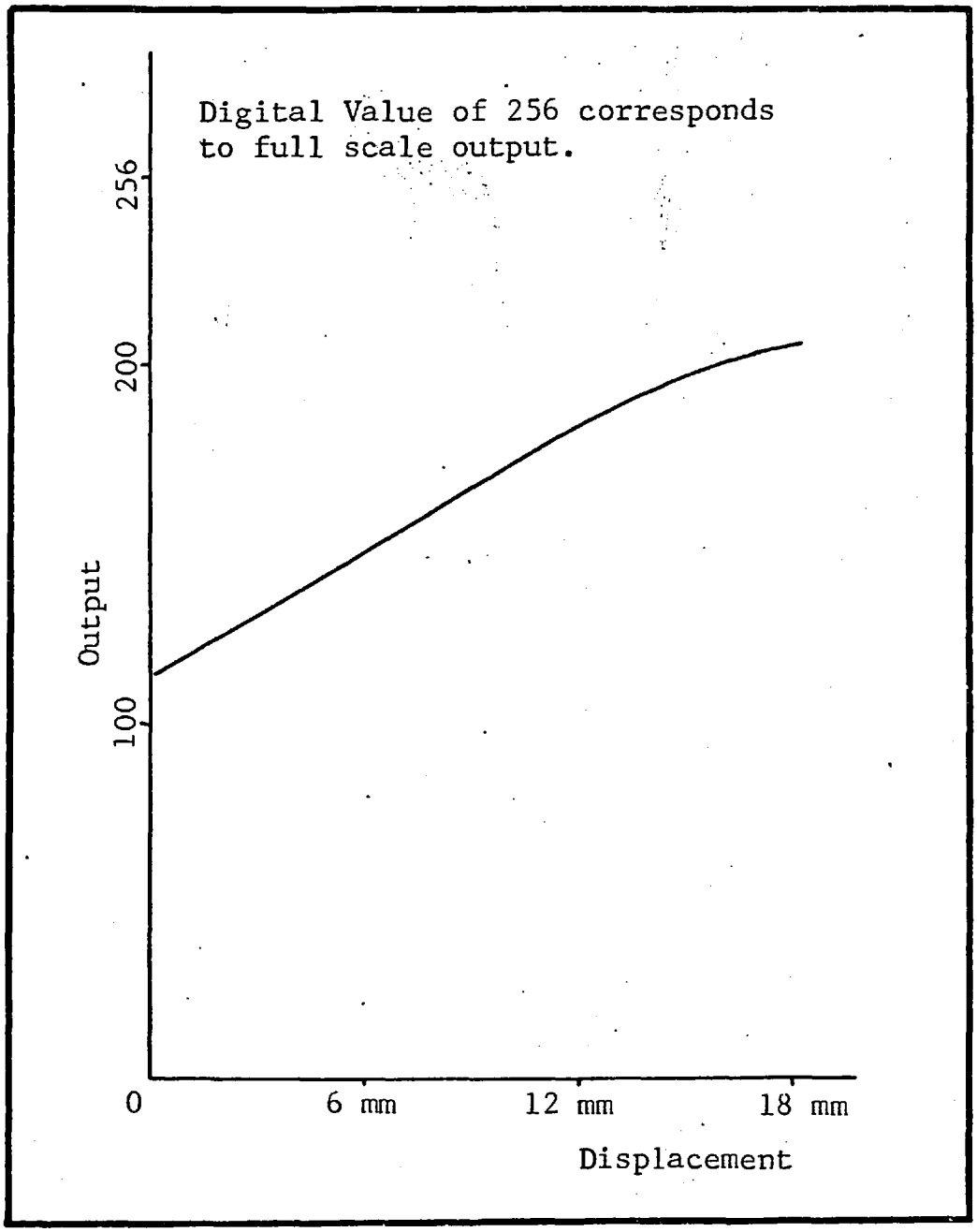

FIG. 6.17 Typical Calibration.

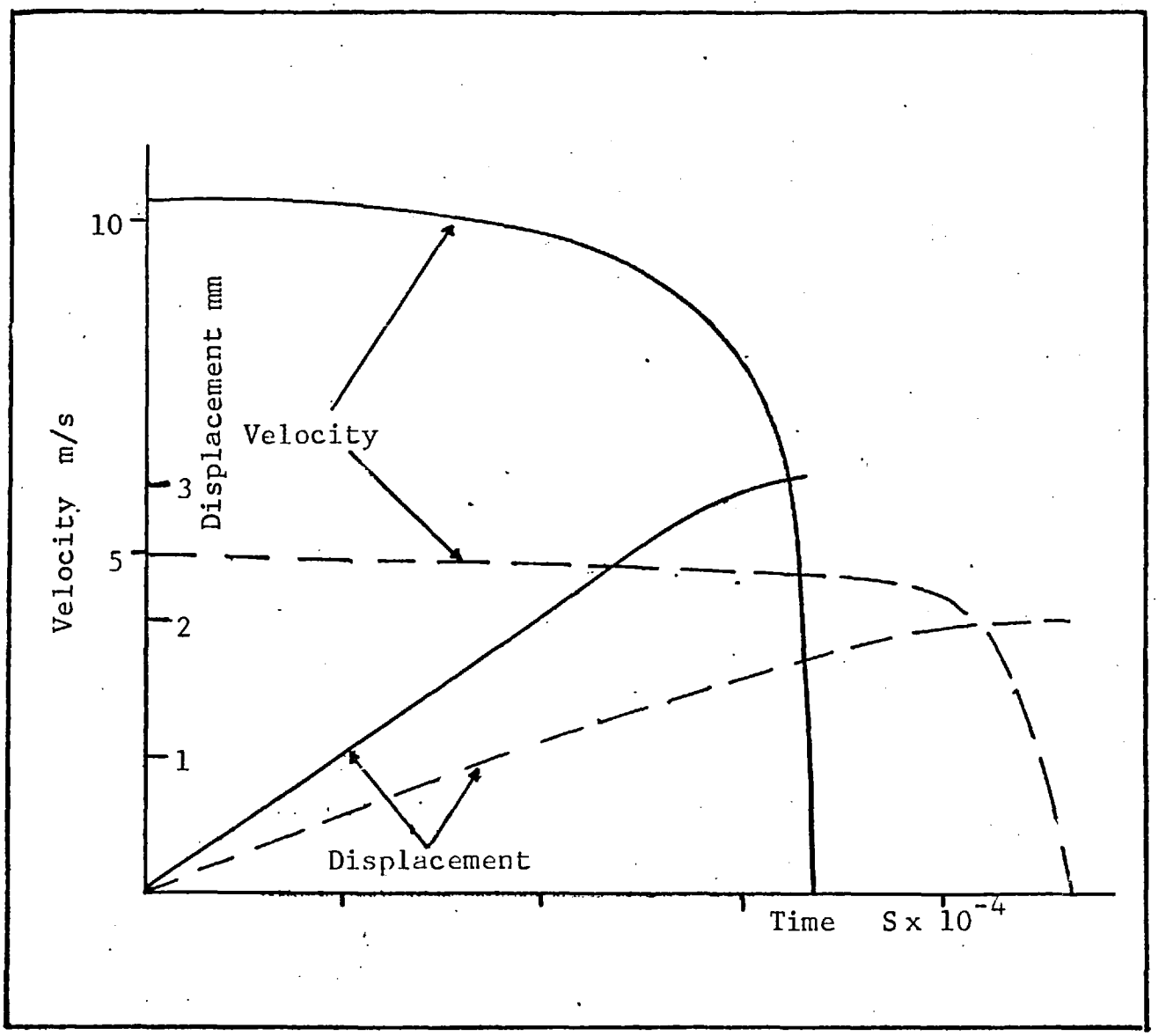

Fig. 6.18 Typical Analysis of Displacement Time Recording.

The displacement/time recording was numerically differentiated to obtain velocity/time curve.

An example of derived results is shown in Fig. 6.18.

CHAPTER 7

RESULTS AND DISCUSSION

Theoretical solutions were computed for upsetting of copper specimens only. The stress/Strain relationship and other material properties used in computation are given in Appendix B. All the stress fields and temperature fields illustrated in this chapter are for upsetting of copper rings, Fig. 5.3, except those in Sections 7.7 and 7.8 which correspond to solid specimens as described therein. The illustrations of stress fields show the top right-hand quarter of the specimen and the illustrations of the temperature fields show the top right-hand quarter of the specimen and a part of the platen as required.

6.1 EXPERIMENTAL VERIFICATION

The experiments were carried out mainly to measure the changes in geometry of rings during compression at different speeds to verify the suitability of the assumed velocity field and to determine friction factor 'α' for the dry and lubricated conditions. Experiments were carried out on both copper and aluminium rings so as to verify the assumption that the velocity field is independent of the mechanical properties of the material and that it is affected only by the frictional restraints at the interface.

The circular grid marked on the face of each specimen was measured at different stages of deformation at selected speeds. From these measurements, the neutral surface was determined either by interpolation (when $R_n > R_i$) or extrapolation (when $R_n < R_i$). Besides being relatively easy to measure, the position of R_n is considered to be a more reliable measure than the change in internal diameter, more so when the bulge at the free surface is pronounced. There is some scatter in the experimental results. This may be attributed to the fact that the test specimens were rather small and measurement errors are inevitable. Unfortunately, larger test specimens could not be used on account of the limited capacity of the experimental rig. The experiments were repeated three or four times for each condition and their mean values were used. The maximum observed variation from these mean values is 8%.

Experimentally measured values of R_n are compared with theoretical values in Figs. 7.1 to 7.4. The bulge profiles were measured on a measuring projector (with magnification of 20) and are compared with theoretical profiles in Figs. 7.5 to 7.12. No discernible effect of speed was observed in the range of up to 12 m/s. Considering the fact that numerical solutions are unlikely to be accurate

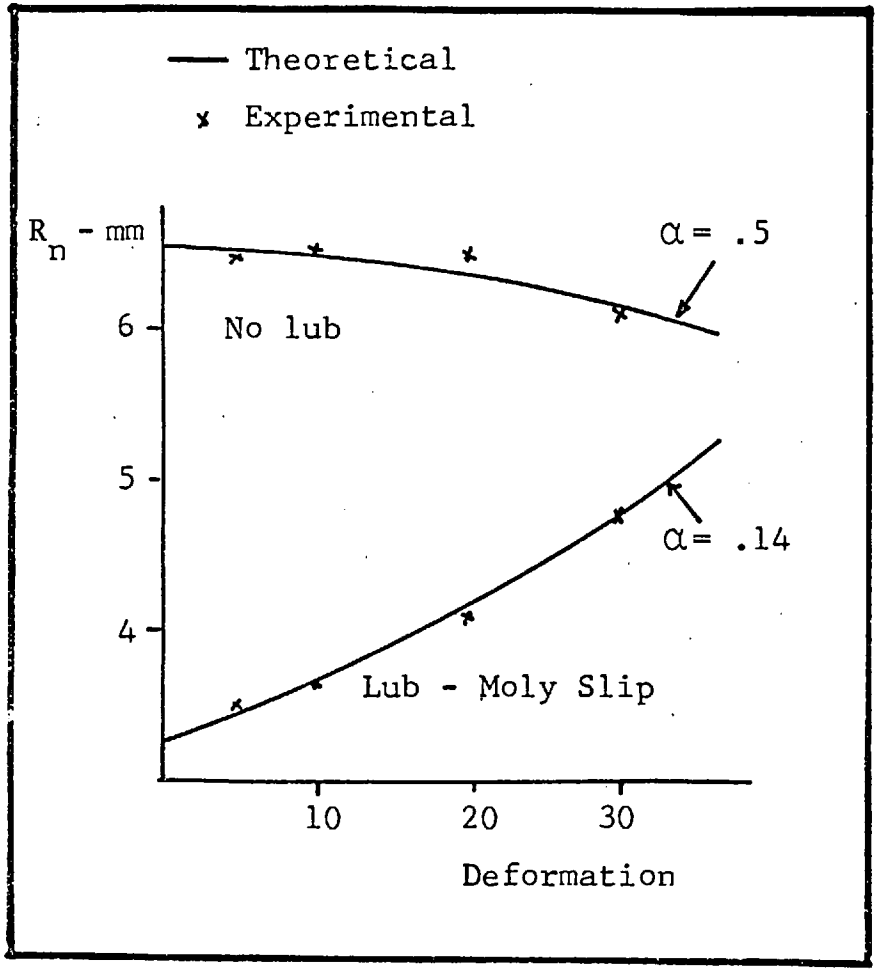

FIG. 7.1 Position of R_n during deformation of 6:3:2 Al ring. V_I = 5.0 m/s.

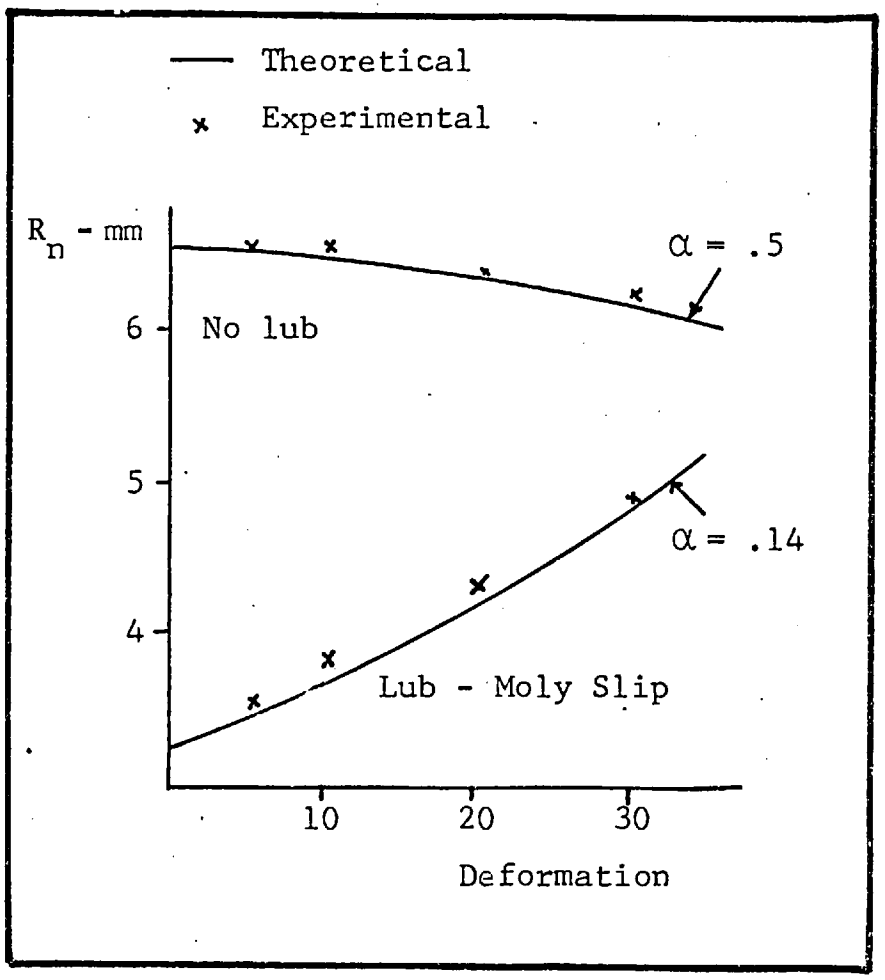

FIG. 7.2 Position of R_n during deformation of 6:3:2 Al ring. V_I = 10.3 m/s.

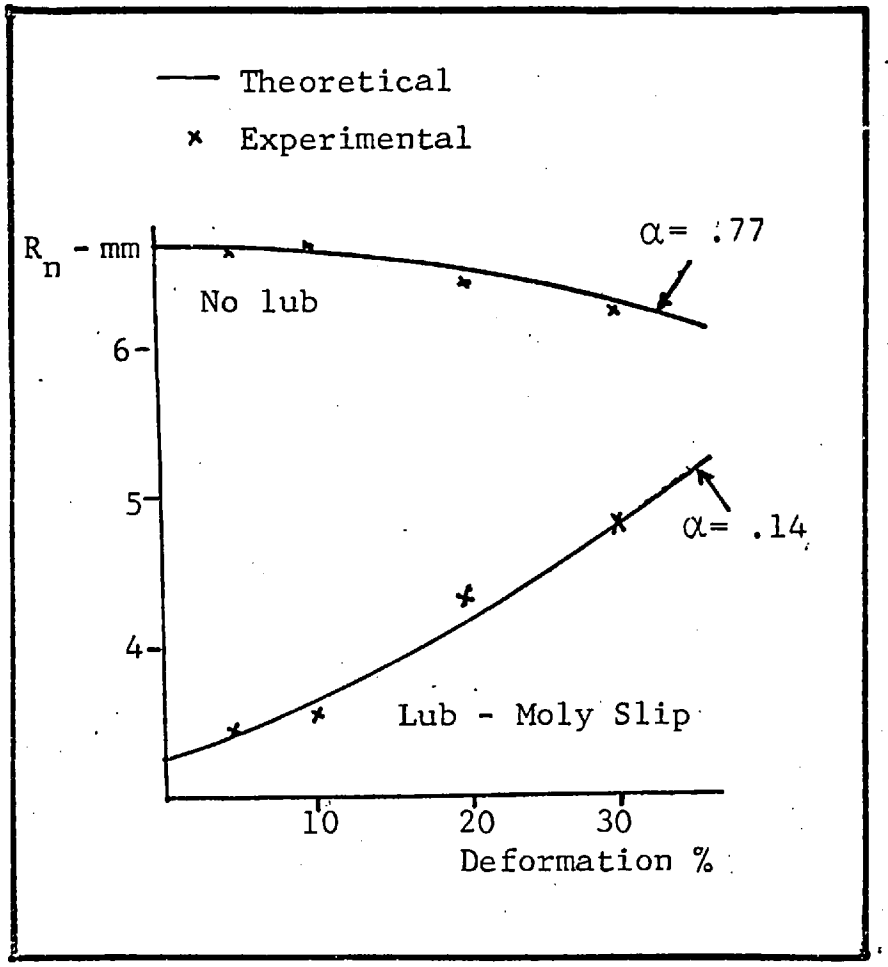

FIG. 7.3 Position of R_n during deformation of 6:3:2 Cu ring. V_I = 5 m/s.

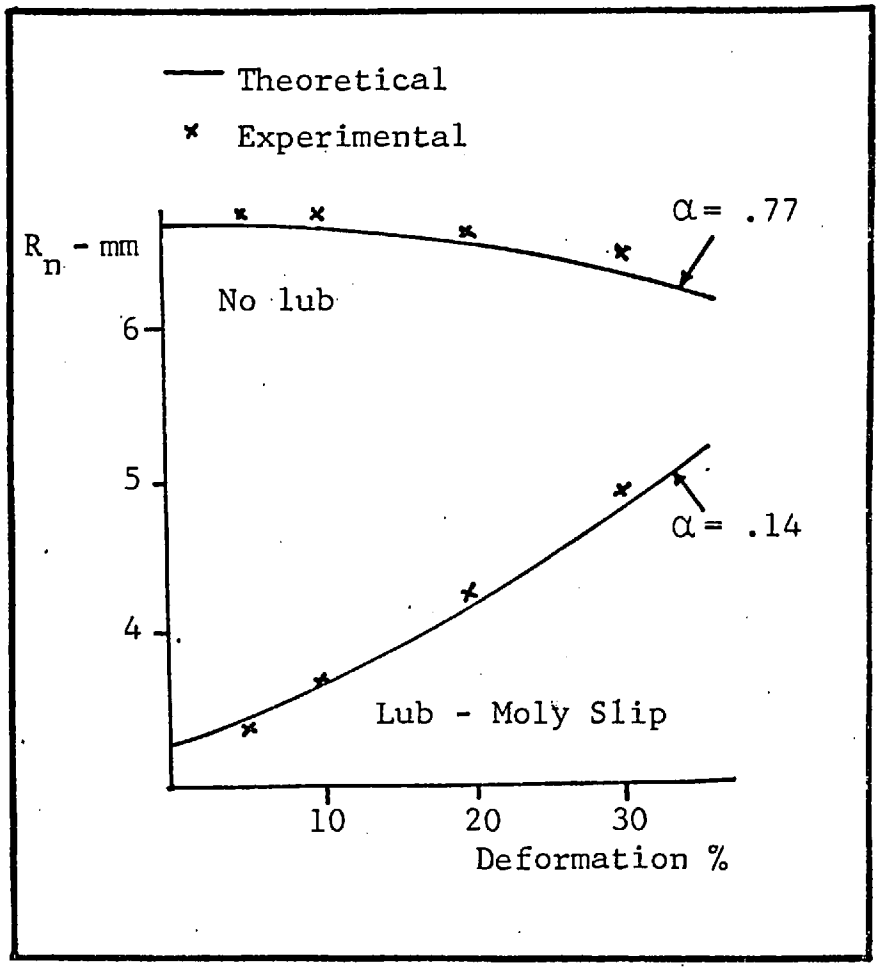

FIG. 7.4 Position of R_n during deformation of 6:3:2 ring. V_I = 10.3 m/s.

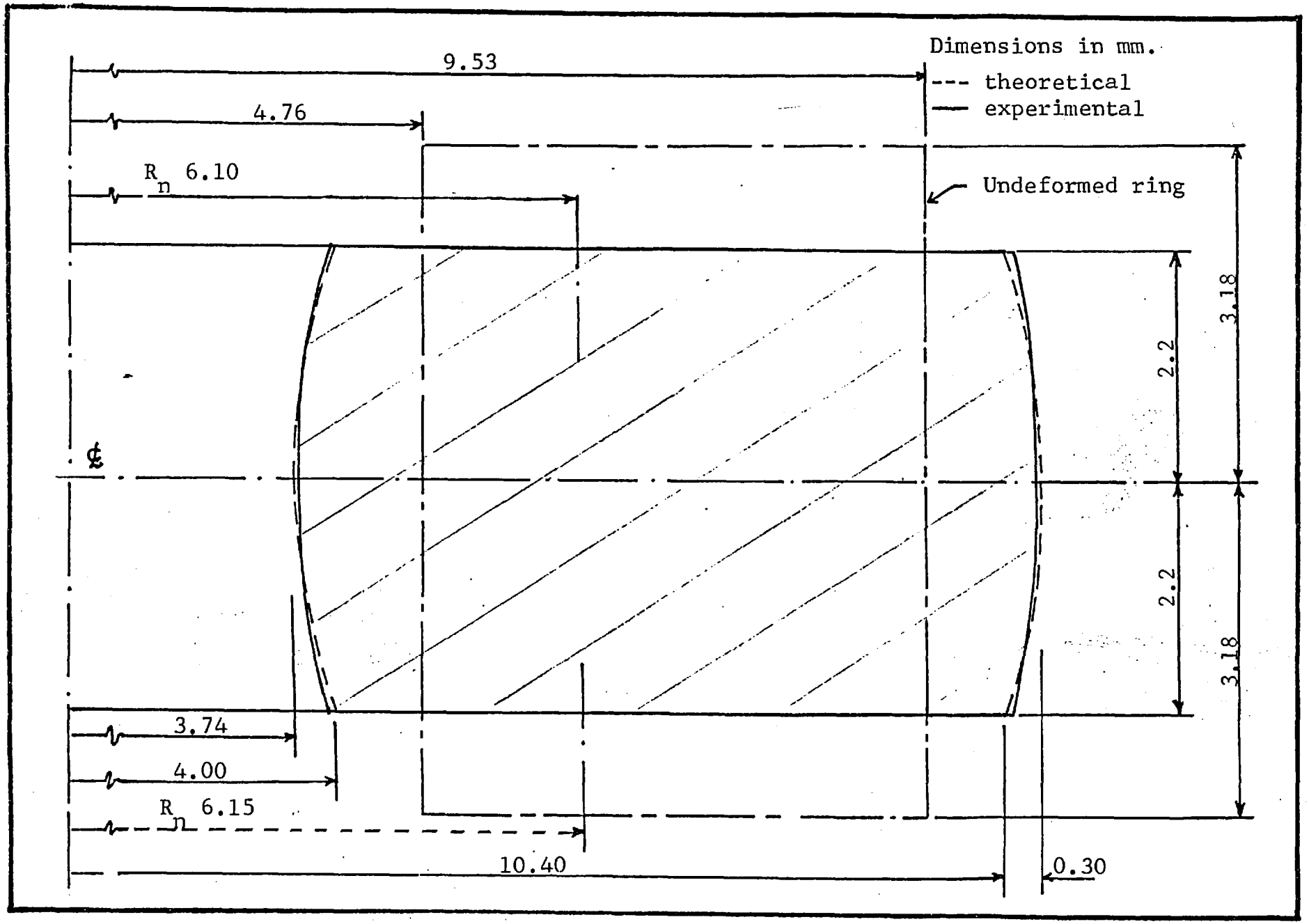

FIG. 7.5 Bulge Profile (A1; No Lub; V_I = 5.0 m/s).

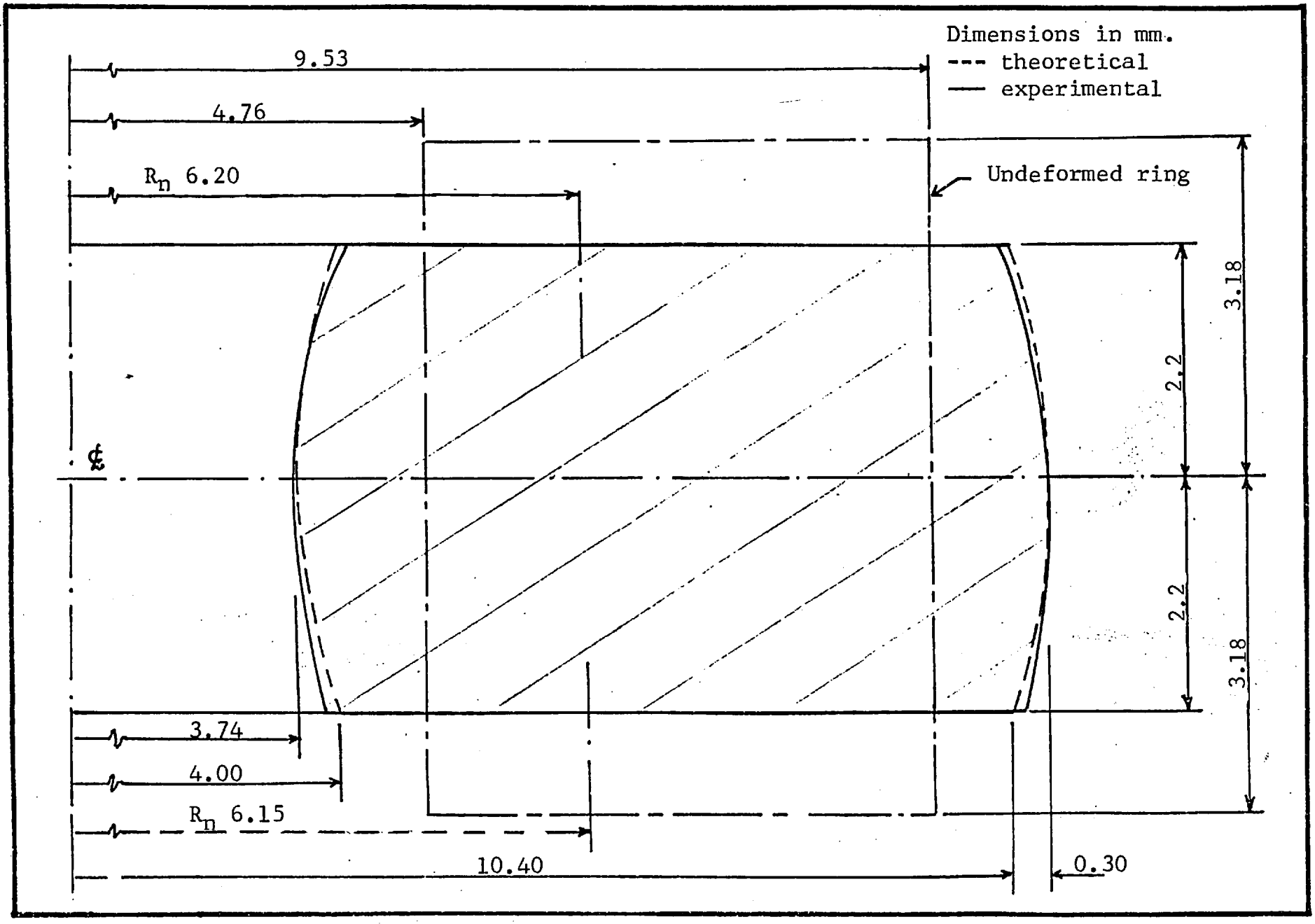

FIG. 7.6 Bulge Profile (A1; No Lub; V_I = 10.3 m/s).

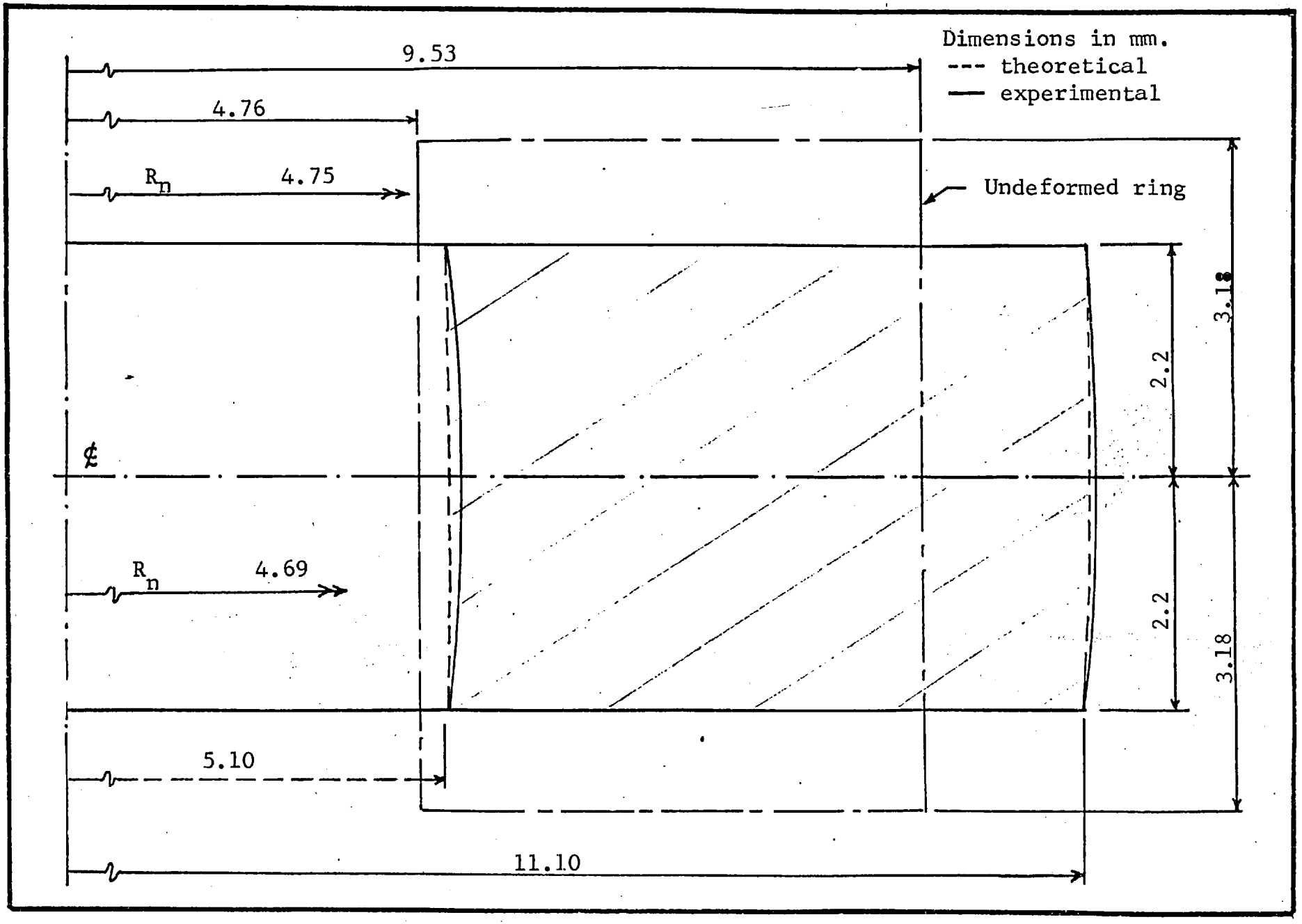

FIG. 7.7 Bulge Profile (A1; Lub, Moly Slip; V_I = 5.0 m/s).

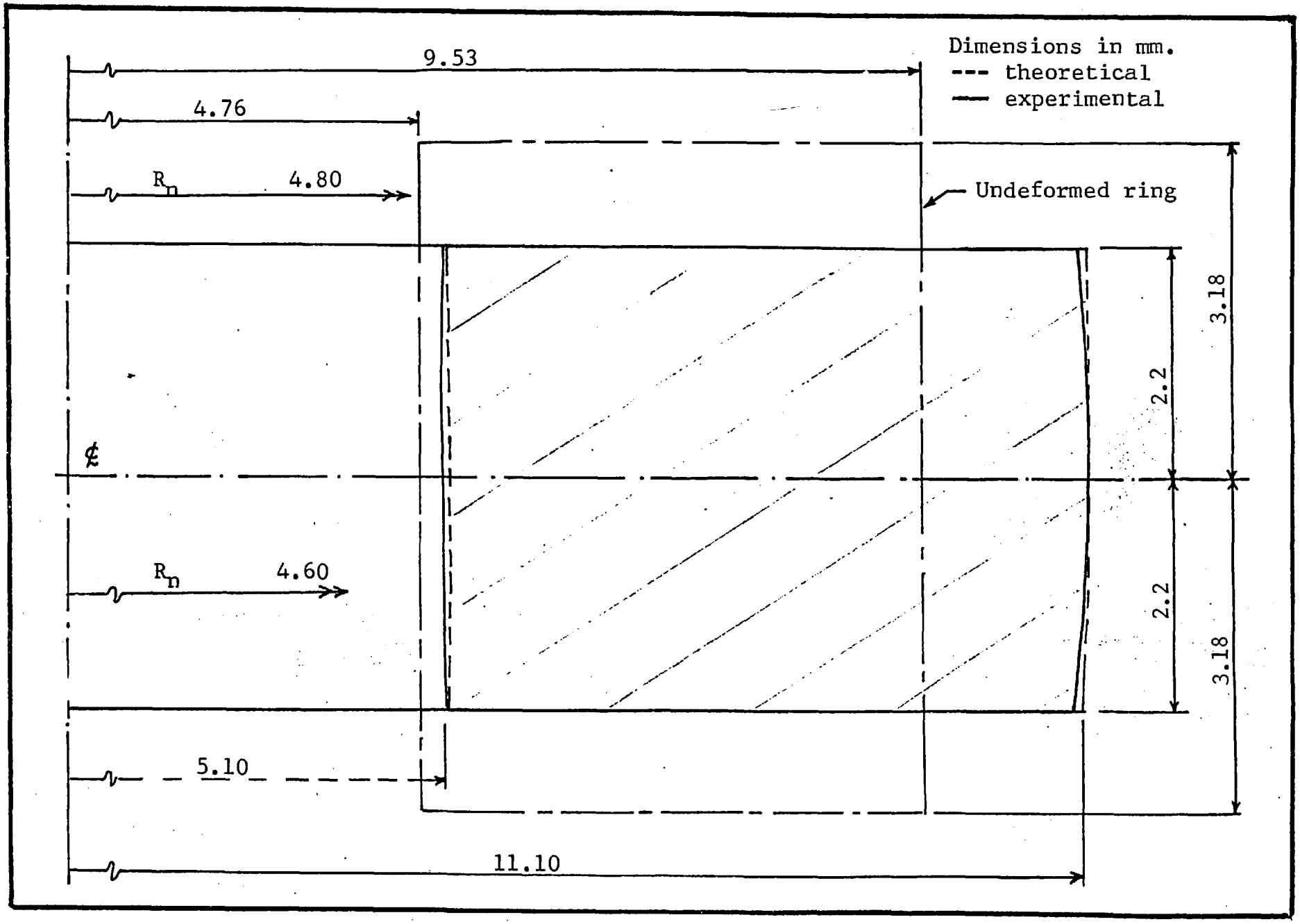

FIG. 7.8 Bulge Profile (Al; Lub, Moly Slip; V_I = 10.3 m/s).

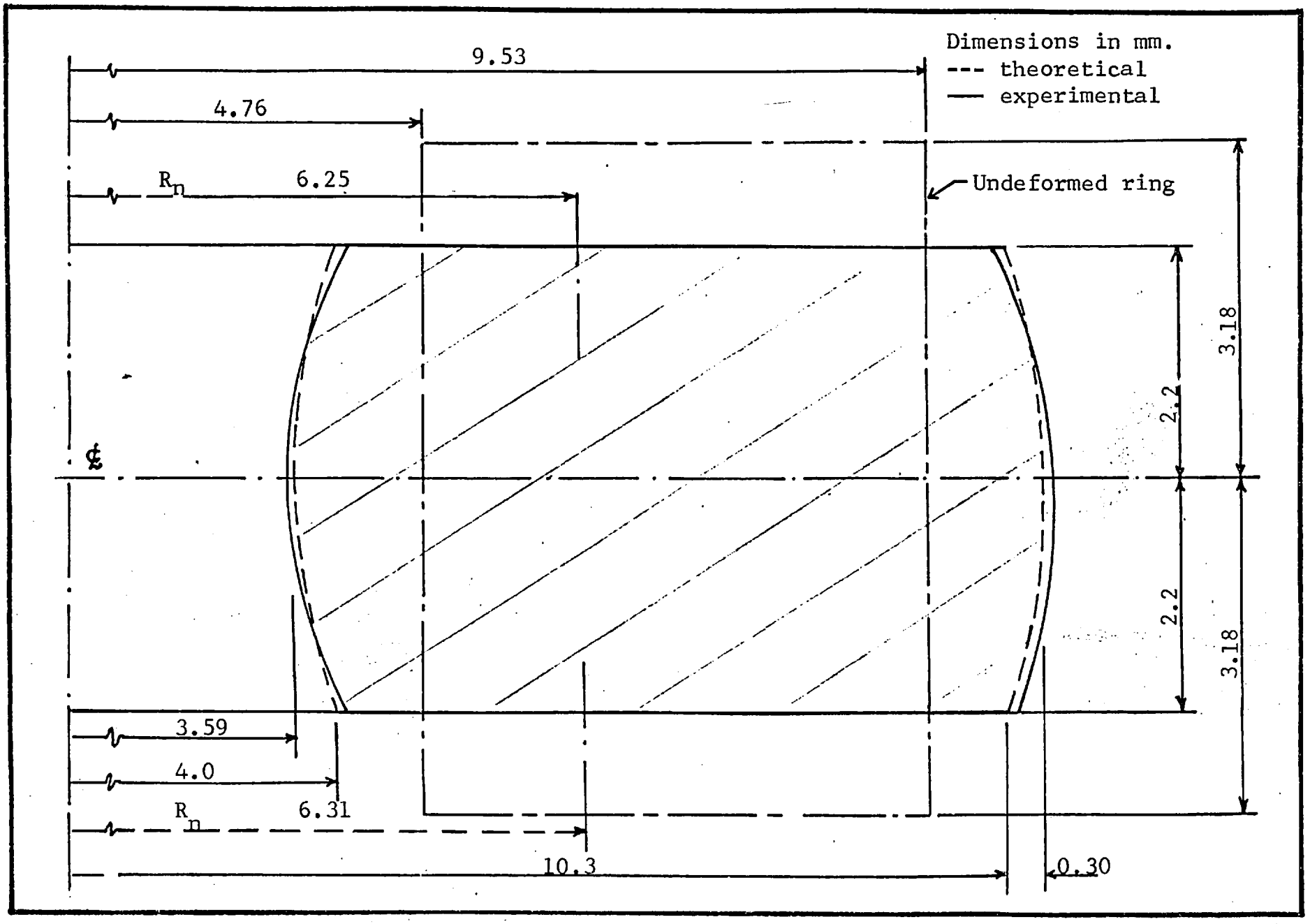

FIG. 7.9 Bulge Profile (Cu; No Lub; V_I = 5.3 m/s).

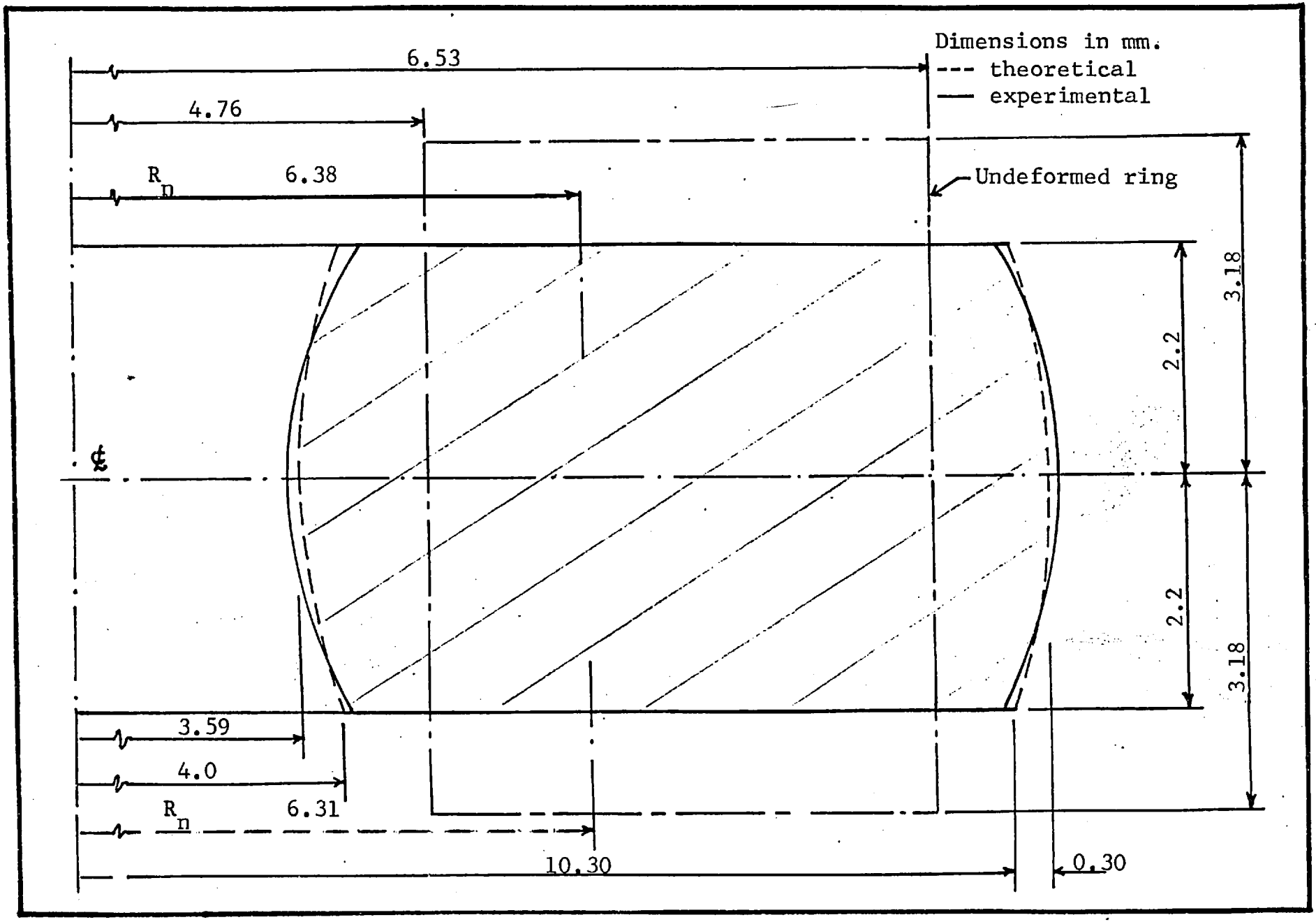

FIG. 7.10 Bulge Profile (Cu; No Lub; V_i = 10.3 m/s).

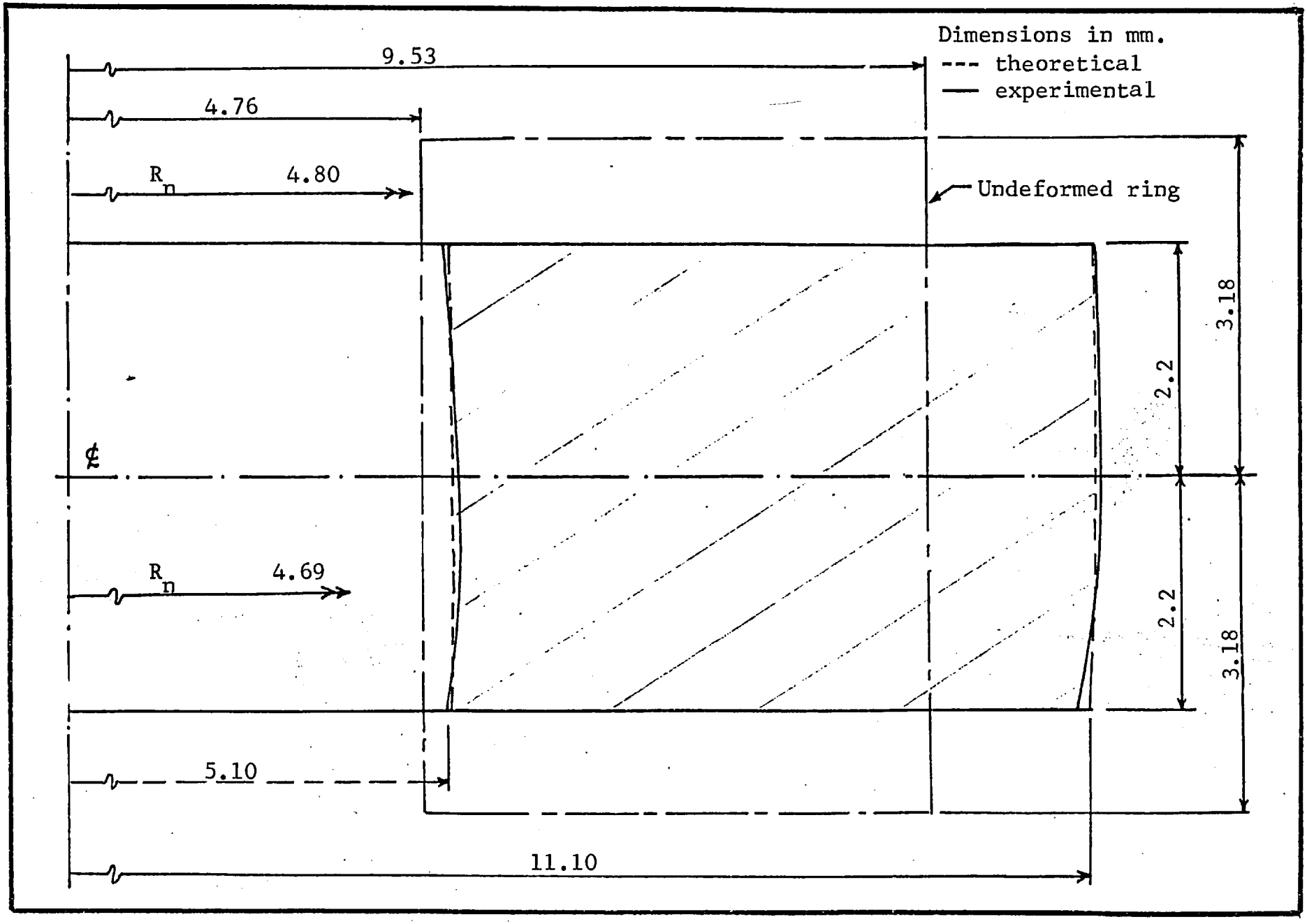

FIG. 7.11 Bulge Profile (Cu; Lub, Moly Slip; V_I = 5.3 m/s).

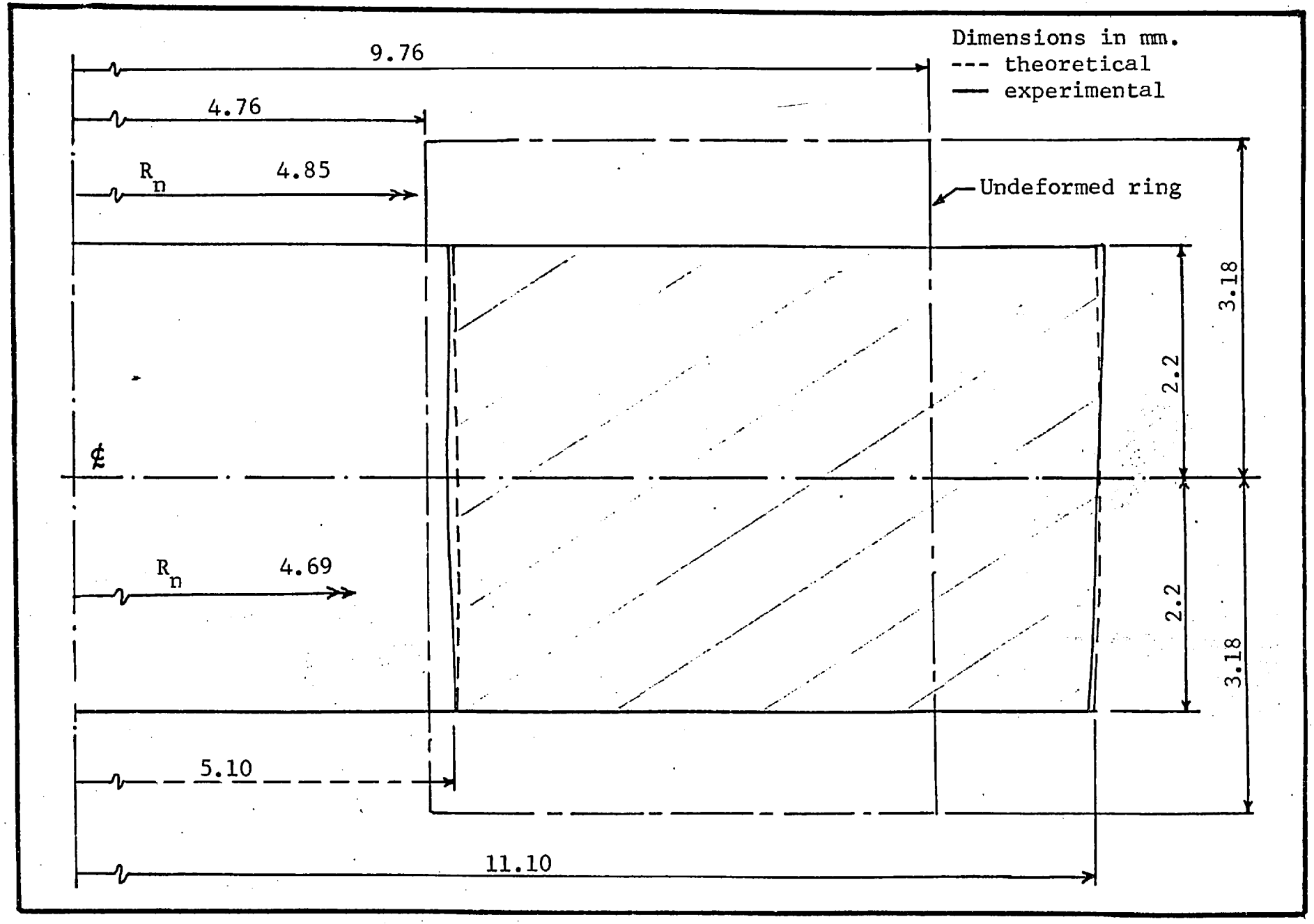

FIG. 7.12 Bulge Profile (Cu; Lub, Moly Slip; V_I = 10.3 m/s).

enough to respond to small variations recorded during these tests, it is suggested that the following values of friction factor will adequately describe the conditions:

1) For copper and aluminium with lubricant (Moly Slip) $\alpha = 0.14$.

2) For copper without lubricant, $\alpha = 0.77$.

3) For aluminium without lubricant, $\alpha = 0.50$.

7.2 VERIFICATION OF THE ALGORITHM AND THE METHOD

As it is not possible to verify experimentally the numerical solutions for stress and temperature fields, it is necessary to resort to indirect methods to establish the reliability of such solutions. In this particular case it is possible to verify the algorithm by comparing the computed average pressure for simplified cases with prescribed stress/strain relationship (experimental) of the material. Stress fields were computed by the method of weighted residuals simulating quasi-static deformation at constant temperature as follows:

1) $V = 1.0$ mm/s, $\alpha = 0.001$, $T = 120^{\circ}C$.

2) $V = 1.0$ mm/s, $\alpha = 0.001$, $T = 320^{\circ}C$.

From these stress fields, average pressure was

calculated at different strains. The results as shown in Appendix Fig. B.1 compare well with known (experimental) material properties. This may be considered as adequate proof that there are no programming errors.

It is possible to compute deviatoric stresses at the onset of deformation from Avitzur's velocity field, equations (5.18) and (5.19), and compare them with those derived from the total stresses, equation (4.5), computed by the method of weighted residuals. These are shown in Tables 7.1 to 7.4 for the following cases:

i) $V = 4.5$ m/s and $\alpha = 0.001$.

ii) $V = 4.5$ m/s and $\alpha = 0.14$.

It is observed that when the friction is low the results of the method of weighted residuals, Table 7.2, are almost identical to those computed directly from the velocity field, Table 7.1, and the stress field is uniform throughout the continuum. It is also observed that the yield criterion, equation (4.26), has been satisfied exactly at all nodal points. When the friction is higher ($\alpha = 0.14$) the two results agree quite well. The error in the yield criterion lies between -8.8% and +2.6%. Although this range is somewhat large, it should be noted that the yield criterion is satisfied much

NODE	σ'_r	σ'_θ	σ'_z	k^2	J_2
1	.369E+08	.369E+08	-.739E+08	.409E+16	.409E+16
2	.369E+08	.369E+08	-.739E+08	.409E+16	.409E+16
3	.369E+08	.369E+08	-.739E+08	.409E+16	.409E+16
4	.369E+08	.369E+08	-.739E+08	.409E+16	.409E+16
5	.369E+08	.369E+08	-.739E+08	.409E+16	.409E+16
6	.369E+08	.369E+08	-.739E+08	.409E+16	.409E+16
7	.369E+08	.369E+08	-.739E+08	.409E+16	.409E+16
8	.369E+08	.369E+08	-.739E+08	.409E+16	.409E+16
9	.369E+08	.369E+08	-.739E+08	.409E+16	.409E+16
10	.369E+08	.369E+08	-.739E+08	.409E+16	.409E+16
11	.369E+08	.369E+08	-.739E+08	.409E+16	.409E+16
12	.369E+08	.369E+08	-.739E+08	.409E+16	.409E+16
13	.369E+08	.369E+08	-.739E+08	.409E+16	.409E+16
14	.369E+08	.369E+08	-.739E+08	.409E+16	.409E+16
15	.369E+08	.369E+08	-.739E+08	.409E+16	.409E+16
16	.369E+08	.369E+08	-.739E+08	.409E+16	.409E+16
17	.369E+08	.369E+08	-.739E+08	.409E+16	.409E+16
18	.369E+08	.369E+08	-.739E+08	.409E+16	.409E+16
19	.369E+08	.369E+08	-.739E+08	.409E+16	.409E+16
20	.369E+08	.369E+08	-.739E+08	.409E+16	.409E+16
21	.369E+08	.369E+08	-.739E+08	.409E+16	.409E+16
22	.369E+08	.369E+08	-.739E+08	.409E+16	.409E+16
23	.369E+08	.369E+08	-.739E+08	.409E+16	.409E+16
24	.369E+08	.369E+08	-.739E+08	.409E+16	.409E+16
25	.369E+08	.369E+08	-.739E+08	.409E+16	.409E+16
26	.369E+08	.369E+08	-.739E+08	.409E+16	.409E+16
27	.369E+08	.369E+08	-.739E+08	.409E+16	.409E+16
28	.369E+08	.369E+08	-.739E+08	.409E+16	.409E+16
29	.369E+08	.369E+08	-.739E+08	.409E+16	.409E+16
30	.369E+08	.369E+08	-.739E+08	.409E+16	.409E+16
31	.369E+08	.369E+08	-.739E+08	.409E+16	.409E+16
32	.369E+08	.369E+08	-.739E+08	.409E+16	.409E+16
33	.369E+08	.369E+08	-.739E+08	.409E+16	.409E+16
34	.369E+08	.369E+08	-.739E+08	.409E+16	.409E+16
35	.369E+08	.369E+08	-.739E+08	.409E+16	.409E+16
36	.369E+08	.369E+08	-.739E+08	.409E+16	.409E+16
37	.369E+08	.369E+08	-.739E+08	.409E+16	.409E+16
38	.369E+08	.369E+08	-.739E+08	.409E+16	.409E+16
39	.369E+08	.369E+08	-.739E+08	.409E+16	.409E+16
40	.369E+08	.369E+08	-.739E+08	.409E+16	.409E+16
41	.369E+08	.369E+08	-.739E+08	.409E+16	.409E+16
42	.369E+08	.369E+08	-.739E+08	.409E+16	.409E+16
43	.369E+08	.369E+08	-.739E+08	.409E+16	.409E+16
44	.369E+08	.369E+08	-.739E+08	.409E+16	.409E+16
45	.369E+08	.369E+08	-.739E+08	.409E+16	.409E+16
46	.369E+08	.369E+08	-.739E+08	.409E+16	.409E+16
47	.369E+08	.369E+08	-.739E+08	.409E+16	.409E+16
48	.369E+08	.369E+08	-.739E+08	.409E+16	.409E+16
49	.369E+08	.369E+08	-.739E+08	.409E+16	.409E+16
50	.369E+08	.369E+08	-.739E+08	.409E+16	.409E+16
51	.369E+08	.369E+08	-.739E+08	.409E+16	.409E+16
52	.369E+08	.369E+08	-.739E+08	.409E+16	.409E+16
53	.369E+08	.369E+08	-.739E+08	.409E+16	.409E+16
54	.369E+08	.369E+08	-.739E+08	.409E+16	.409E+16
55	.369E+08	.369E+08	-.739E+08	.409E+16	.409E+16
56	.369E+08	.369E+08	-.739E+08	.409E+16	.409E+16
57	.369E+08	.369E+08	-.739E+08	.409E+16	.409E+16
58	.369E+08	.369E+08	-.739E+08	.409E+16	.409E+16
59	.369E+08	.369E+08	-.739E+08	.409E+16	.409E+16
60	.369E+08	.369E+08	-.739E+08	.409E+16	.409E+16
61	.369E+08	.369E+08	-.739E+08	.409E+16	.409E+16
62	.369E+08	.369E+08	-.739E+08	.409E+16	.409E+16
63	.369E+08	.369E+08	-.739E+08	.409E+16	.409E+16
64	.369E+08	.369E+08	-.739E+08	.409E+16	.409E+16
65	.369E+08	.369E+08	-.739E+08	.409E+16	.409E+16
66	.369E+08	.369E+08	-.739E+08	.409E+16	.409E+16
67	.369E+08	.369E+08	-.739E+08	.409E+16	.409E+16
68	.369E+08	.369E+08	-.739E+08	.409E+16	.409E+16
69	.369E+08	.369E+08	-.739E+08	.409E+16	.409E+16
70	.369E+08	.369E+08	-.739E+08	.409E+16	.409E+16

TABLE 7.1 Deviatoric Stress from Avitzur's Velocity Field ($V = 4.5$ m/s and $\alpha = 0.001$).

NODE	σ'_r	σ'_θ	σ'_z	k^2	J_2
1	.3695E+08	.3695E+08	-.7390E+08	.4095E+16	.4095E+16
2	.3695E+08	.3695E+08	-.7390E+08	.4095E+16	.4095E+16
3	.3695E+08	.3695E+08	-.7390E+08	.4095E+16	.4095E+16
4	.3695E+08	.3695E+08	-.7390E+08	.4095E+16	.4095E+16
5	.3695E+08	.3695E+08	-.7390E+08	.4095E+16	.4095E+16
6	.3695E+08	.3695E+08	-.7390E+08	.4095E+16	.4095E+16
7	.3695E+08	.3695E+08	-.7390E+08	.4095E+16	.4095E+16
8	.3695E+08	.3695E+08	-.7390E+08	.4095E+16	.4095E+16
9	.3695E+08	.3695E+08	-.7390E+08	.4095E+16	.4095E+16
10	.3695E+08	.3695E+08	-.7390E+08	.4095E+16	.4095E+16
11	.3695E+08	.3695E+08	-.7390E+08	.4095E+16	.4095E+16
12	.3695E+08	.3695E+08	-.7390E+08	.4095E+16	.4095E+16
13	.3695E+08	.3695E+08	-.7390E+08	.4095E+16	.4095E+16
14	.3695E+08	.3695E+08	-.7390E+08	.4095E+16	.4095E+16
15	.3695E+08	.3695E+08	-.7390E+08	.4095E+16	.4095E+16
16	.3695E+08	.3695E+08	-.7390E+08	.4095E+16	.4095E+16
17	.3695E+08	.3695E+08	-.7390E+08	.4095E+16	.4095E+16
18	.3695E+08	.3695E+08	-.7390E+08	.4095E+16	.4095E+16
19	.3695E+08	.3695E+08	-.7390E+08	.4095E+16	.4095E+16
20	.3695E+08	.3695E+08	-.7390E+08	.4095E+16	.4095E+16
21	.3695E+08	.3695E+08	-.7390E+08	.4095E+16	.4095E+16
22	.3695E+08	.3695E+08	-.7390E+08	.4095E+16	.4095E+16
23	.3695E+08	.3695E+08	-.7390E+08	.4095E+16	.4095E+16
24	.3695E+08	.3695E+08	-.7390E+08	.4095E+16	.4095E+16
25	.3695E+08	.3695E+08	-.7390E+08	.4095E+16	.4095E+16
26	.3695E+08	.3695E+08	-.7390E+08	.4095E+16	.4095E+16
27	.3695E+08	.3695E+08	-.7390E+08	.4095E+16	.4095E+16
28	.3695E+08	.3695E+08	-.7390E+08	.4095E+16	.4095E+16
29	.3695E+08	.3695E+08	-.7390E+08	.4095E+16	.4095E+16
30	.3695E+08	.3695E+08	-.7390E+08	.4095E+16	.4095E+16
31	.3695E+08	.3695E+08	-.7390E+08	.4095E+16	.4095E+16
32	.3695E+08	.3695E+08	-.7390E+08	.4095E+16	.4095E+16
33	.3695E+08	.3695E+08	-.7390E+08	.4095E+16	.4095E+16
34	.3695E+08	.3695E+08	-.7390E+08	.4095E+16	.4095E+16
35	.3695E+08	.3695E+08	-.7390E+08	.4095E+16	.4095E+16
36	.3695E+08	.3695E+08	-.7390E+08	.4095E+16	.4095E+16
37	.3695E+08	.3695E+08	-.7390E+08	.4095E+16	.4095E+16
38	.3695E+08	.3695E+08	-.7390E+08	.4095E+16	.4095E+16
39	.3695E+08	.3695E+08	-.7390E+08	.4095E+16	.4095E+16
40	.3695E+08	.3695E+08	-.7390E+08	.4095E+16	.4095E+16
41	.3695E+08	.3695E+08	-.7390E+08	.4095E+16	.4095E+16
42	.3695E+08	.3695E+08	-.7390E+08	.4095E+16	.4095E+16
43	.3695E+08	.3695E+08	-.7390E+08	.4095E+16	.4095E+16
44	.3695E+08	.3695E+08	-.7390E+08	.4095E+16	.4095E+16
45	.3695E+08	.3695E+08	-.7390E+08	.4095E+16	.4095E+16
46	.3695E+08	.3695E+08	-.7390E+08	.4095E+16	.4095E+16
47	.3695E+08	.3695E+08	-.7390E+08	.4095E+16	.4095E+16
48	.3695E+08	.3695E+08	-.7390E+08	.4095E+16	.4095E+16
49	.3695E+08	.3695E+08	-.7390E+08	.4095E+16	.4095E+16
50	.3695E+08	.3695E+08	-.7390E+08	.4095E+16	.4095E+16
51	.3695E+08	.3695E+08	-.7390E+08	.4095E+16	.4095E+16
52	.3695E+08	.3695E+08	-.7390E+08	.4095E+16	.4095E+16
53	.3695E+08	.3695E+08	-.7390E+08	.4095E+16	.4095E+16
54	.3695E+08	.3695E+08	-.7390E+08	.4095E+16	.4095E+16
55	.3695E+08	.3695E+08	-.7390E+08	.4095E+16	.4095E+16
56	.3695E+08	.3695E+08	-.7390E+08	.4095E+16	.4095E+16
57	.3695E+08	.3695E+08	-.7390E+08	.4095E+16	.4095E+16
58	.3695E+08	.3695E+08	-.7390E+08	.4095E+16	.4095E+16
59	.3695E+08	.3695E+08	-.7390E+08	.4095E+16	.4095E+16
60	.3695E+08	.3695E+08	-.7390E+08	.4095E+16	.4095E+16
61	.3695E+08	.3695E+08	-.7390E+08	.4095E+16	.4095E+16
62	.3695E+08	.3695E+08	-.7390E+08	.4095E+16	.4095E+16
63	.3695E+08	.3695E+08	-.7390E+08	.4095E+16	.4095E+16
64	.3695E+08	.3695E+08	-.7390E+08	.4095E+16	.4095E+16
65	.3695E+08	.3695E+08	-.7390E+08	.4095E+16	.4095E+16
66	.3695E+08	.3695E+08	-.7390E+08	.4095E+16	.4095E+16
67	.3695E+08	.3695E+08	-.7390E+08	.4095E+16	.4095E+16
68	.3695E+08	.3695E+08	-.7390E+08	.4095E+16	.4095E+16
69	.3695E+08	.3695E+08	-.7390E+08	.4095E+16	.4095E+16
70	.3695E+08	.3695E+08	-.7390E+08	.4095E+16	.4095E+16

TABLE 7.2 Deviatoric Stresses - Method of Weighted Residuals (V = 4.5 m/s and $\alpha = 0.001$).

NODE	σ'_r	σ'_θ	σ'_z	k^2	J_2
1	.369E+08	.369E+08	-.739E+08	.409E+16	.409E+16
2	.369E+08	.369E+08	-.739E+08	.409E+16	.409E+16
3	.369E+08	.369E+08	-.739E+08	.409E+16	.409E+16
4	.369E+08	.369E+08	-.739E+08	.409E+16	.409E+16
5	.369E+08	.369E+08	-.739E+08	.409E+16	.409E+16
6	.369E+08	.369E+08	-.739E+08	.409E+16	.409E+16
7	.369E+08	.369E+08	-.739E+08	.409E+16	.409E+16
8	.369E+08	.369E+08	-.739E+08	.409E+16	.409E+16
9	.368E+08	.368E+08	-.737E+08	.409E+16	.409E+16
10	.369E+08	.369E+08	-.739E+08	.409E+16	.409E+16
11	.369E+08	.369E+08	-.739E+08	.409E+16	.409E+16
12	.369E+08	.369E+08	-.739E+08	.409E+16	.409E+16
13	.369E+08	.369E+08	-.739E+08	.409E+16	.409E+16
14	.369E+08	.369E+08	-.739E+08	.409E+16	.409E+16
15	.369E+08	.369E+08	-.738E+08	.409E+16	.409E+16
16	.369E+08	.369E+08	-.739E+08	.409E+16	.409E+16
17	.369E+08	.369E+08	-.738E+08	.409E+16	.409E+16
18	.369E+08	.369E+08	-.737E+08	.409E+16	.409E+16
19	.368E+08	.368E+08	-.737E+08	.409E+16	.409E+16
20	.368E+08	.369E+08	-.736E+08	.409E+16	.409E+16
21	.369E+08	.369E+08	-.739E+08	.409E+16	.409E+16
22	.369E+08	.369E+08	-.739E+08	.409E+16	.409E+16
23	.369E+08	.369E+08	-.739E+08	.409E+16	.409E+16
24	.369E+08	.369E+08	-.739E+08	.409E+16	.409E+16
25	.369E+08	.369E+08	-.739E+08	.409E+16	.409E+16
26	.369E+08	.369E+08	-.738E+08	.409E+16	.409E+16
27	.369E+08	.369E+08	-.738E+08	.409E+16	.409E+16
28	.369E+08	.369E+08	-.737E+08	.409E+16	.409E+16
29	.368E+08	.368E+08	-.737E+08	.409E+16	.409E+16
30	.368E+08	.368E+08	-.736E+08	.409E+16	.409E+16
31	.369E+08	.369E+08	-.739E+08	.409E+16	.409E+16
32	.369E+08	.369E+08	-.739E+08	.409E+16	.409E+16
33	.369E+08	.369E+08	-.739E+08	.409E+16	.409E+16
34	.369E+08	.369E+08	-.738E+08	.409E+16	.409E+16
35	.369E+08	.369E+08	-.738E+08	.409E+16	.409E+16
36	.369E+08	.369E+08	-.739E+08	.409E+16	.409E+16
37	.369E+08	.369E+08	-.739E+08	.409E+16	.409E+16
38	.369E+08	.369E+08	-.737E+08	.409E+16	.409E+16
39	.368E+08	.368E+08	-.737E+08	.409E+16	.409E+16
40	.368E+08	.368E+08	-.736E+08	.409E+16	.409E+16
41	.369E+08	.369E+08	-.739E+08	.409E+16	.409E+16
42	.369E+08	.369E+08	-.739E+08	.409E+16	.409E+16
43	.369E+08	.369E+08	-.739E+08	.409E+16	.409E+16
44	.369E+08	.369E+08	-.739E+08	.409E+16	.409E+16
45	.369E+08	.369E+08	-.739E+08	.409E+16	.409E+16
46	.369E+08	.369E+08	-.739E+08	.409E+16	.409E+16
47	.369E+08	.369E+08	-.739E+08	.409E+16	.409E+16
48	.369E+08	.369E+08	-.737E+08	.409E+16	.409E+16
49	.368E+08	.368E+08	-.737E+08	.409E+16	.409E+16
50	.368E+08	.368E+08	-.736E+08	.409E+16	.409E+16
51	.369E+08	.369E+08	-.739E+08	.409E+16	.409E+16
52	.369E+08	.369E+08	-.739E+08	.409E+16	.409E+16
53	.369E+08	.369E+08	-.739E+08	.409E+16	.409E+16
54	.369E+08	.369E+08	-.738E+08	.409E+16	.409E+16
55	.369E+08	.369E+08	-.738E+08	.409E+16	.409E+16
56	.369E+08	.369E+08	-.739E+08	.409E+16	.409E+16
57	.369E+08	.369E+08	-.739E+08	.409E+16	.409E+16
58	.369E+08	.369E+08	-.737E+08	.409E+16	.409E+16
59	.368E+08	.368E+08	-.737E+08	.409E+16	.409E+16
60	.368E+08	.368E+08	-.736E+08	.409E+16	.409E+16
61	.369E+08	.369E+08	-.739E+08	.409E+16	.409E+16
62	.369E+08	.369E+08	-.739E+08	.409E+16	.409E+16
63	.369E+08	.369E+08	-.739E+08	.409E+16	.409E+16
64	.369E+08	.369E+08	-.739E+08	.409E+16	.409E+16
65	.369E+08	.369E+08	-.739E+08	.409E+16	.409E+16
66	.369E+08	.369E+08	-.739E+08	.409E+16	.409E+16
67	.369E+08	.369E+08	-.738E+08	.409E+16	.409E+16
68	.369E+08	.369E+08	-.737E+08	.409E+16	.409E+16
69	.368E+08	.368E+08	-.737E+08	.409E+16	.409E+16
70	.368E+08	.368E+08	-.736E+08	.409E+16	.409E+16

TABLE 7.3 Deviatoric Stresses from Avitzur's Velocity Field (V = 4.5 m/s and α= 0.14).

NODE	σ'_r	σ'_θ	σ'_z	k^2	J_2
1	.369E+08	.369E+08	-.739E+08	.409E+16	.409E+16
2	.370E+08	.369E+08	-.739E+08	.409E+16	.409E+16
3	.371E+08	.369E+08	-.739E+08	.409E+16	.410E+16
4	.373E+08	.369E+08	-.740E+08	.409E+16	.411E+16
5	.375E+08	.366E+08	-.742E+08	.409E+16	.413E+16
6	.379E+08	.365E+08	-.743E+08	.409E+16	.414E+16
7	.382E+08	.363E+08	-.745E+08	.409E+16	.416E+16
8	.385E+08	.362E+08	-.746E+08	.409E+16	.418E+16
9	.389E+08	.360E+08	-.748E+08	.409E+16	.420E+16
10	.391E+08	.358E+08	-.750E+08	.409E+16	.422E+16
11	.368E+08	.368E+08	-.736E+08	.409E+16	.407E+16
12	.368E+08	.369E+08	-.736E+08	.409E+16	.407E+16
13	.370E+08	.368E+08	-.737E+08	.409E+16	.407E+16
14	.371E+08	.367E+08	-.739E+08	.409E+16	.408E+16
15	.373E+08	.366E+08	-.739E+08	.409E+16	.410E+16
16	.376E+08	.365E+08	-.741E+08	.409E+16	.412E+16
17	.379E+08	.364E+08	-.743E+08	.409E+16	.414E+16
18	.382E+08	.363E+08	-.745E+08	.409E+16	.416E+16
19	.385E+08	.362E+08	-.747E+08	.409E+16	.419E+16
20	.388E+08	.362E+08	-.749E+08	.409E+16	.421E+16
21	.365E+08	.365E+08	-.731E+08	.409E+16	.401E+16
22	.366E+08	.365E+08	-.731E+08	.409E+16	.401E+16
23	.366E+08	.365E+08	-.731E+08	.409E+16	.401E+16
24	.367E+08	.365E+08	-.732E+08	.409E+16	.402E+16
25	.369E+08	.365E+08	-.734E+08	.409E+16	.404E+16
26	.371E+08	.365E+08	-.735E+08	.409E+16	.406E+16
27	.373E+08	.365E+08	-.737E+08	.409E+16	.408E+16
28	.375E+08	.365E+08	-.740E+08	.409E+16	.411E+16
29	.377E+08	.367E+08	-.744E+08	.409E+16	.415E+16
30	.379E+08	.369E+08	-.748E+08	.409E+16	.420E+16
31	.363E+08	.363E+08	-.727E+08	.409E+16	.396E+16
32	.363E+08	.363E+08	-.727E+08	.409E+16	.396E+16
33	.363E+08	.364E+08	-.727E+08	.409E+16	.397E+16
34	.364E+08	.364E+08	-.728E+08	.409E+16	.397E+16
35	.364E+08	.365E+08	-.729E+08	.409E+16	.398E+16
36	.364E+08	.366E+08	-.730E+08	.409E+16	.400E+16
37	.365E+08	.367E+08	-.732E+08	.409E+16	.402E+16
38	.366E+08	.369E+08	-.735E+08	.409E+16	.405E+16
39	.368E+08	.371E+08	-.738E+08	.409E+16	.410E+16
40	.370E+08	.373E+08	-.743E+08	.409E+16	.415E+16
41	.364E+08	.364E+08	-.729E+08	.409E+16	.398E+16
42	.364E+08	.365E+08	-.729E+08	.409E+16	.399E+16
43	.363E+08	.365E+08	-.729E+08	.409E+16	.399E+16
44	.362E+08	.366E+08	-.729E+08	.409E+16	.398E+16
45	.361E+08	.368E+08	-.729E+08	.409E+16	.398E+16
46	.360E+08	.369E+08	-.729E+08	.409E+16	.399E+16
47	.359E+08	.370E+08	-.730E+08	.409E+16	.399E+16
48	.359E+08	.371E+08	-.730E+08	.409E+16	.401E+16
49	.361E+08	.371E+08	-.732E+08	.409E+16	.402E+16
50	.365E+08	.369E+08	-.734E+08	.409E+16	.405E+16
51	.368E+08	.368E+08	-.737E+08	.409E+16	.407E+16
52	.368E+08	.369E+08	-.737E+08	.409E+16	.407E+16
53	.366E+08	.370E+08	-.736E+08	.409E+16	.407E+16
54	.364E+08	.371E+08	-.735E+08	.409E+16	.405E+16
55	.361E+08	.373E+08	-.734E+08	.409E+16	.404E+16
56	.358E+08	.374E+08	-.732E+08	.409E+16	.402E+16
57	.356E+08	.374E+08	-.730E+08	.409E+16	.399E+16
58	.355E+08	.372E+08	-.727E+08	.409E+16	.396E+16
59	.357E+08	.367E+08	-.723E+08	.409E+16	.393E+16
60	.362E+08	.365E+08	-.719E+08	.409E+16	.389E+16
61	.371E+08	.371E+08	-.742E+08	.409E+16	.413E+16
62	.370E+08	.371E+08	-.741E+08	.409E+16	.412E+16
63	.368E+08	.372E+08	-.740E+08	.409E+16	.411E+16
64	.364E+08	.373E+08	-.738E+08	.409E+16	.408E+16
65	.360E+08	.375E+08	-.734E+08	.409E+16	.405E+16
66	.355E+08	.375E+08	-.730E+08	.409E+16	.400E+16
67	.350E+08	.375E+08	-.725E+08	.409E+16	.394E+16
68	.347E+08	.372E+08	-.719E+08	.409E+16	.389E+16
69	.346E+08	.366E+08	-.712E+08	.409E+16	.381E+16
70	.349E+08	.356E+08	-.705E+08	.409E+16	.373E+16

TABLE 7.4 Deviatoric Stresses - Method of Weighted Residuals (V = 4.5 m/s and α = 0.14).

more closely at most nodal points. Besides it is an essential feature of the method of weighted residuals to force these errors to vanish in an average sense over the entire continuum. As it is not possible to include the frictional restraints in the governing equation, it was necessary to treat it as a boundary condition leading to a separate residual function as in equation (3.13). Presumably this introduces some error in the solution when friction is high. However, these errors were no higher than the values mentioned above, even for very high values of friction $\alpha = 0.77$. Therefore it would seem reasonable to suggest that the method of weighted residuals is quite adequate for this purpose.

The method of weighted residuals was used [81] to solve the elliptic partial differential equation

$$\nabla^2 F = \frac{\partial^2 F}{\partial r^2} + \frac{\partial^2 F}{\partial z^2} = -A \qquad (7.1)$$

where $F = F(r,z)$ and A is a constant.

The results were compared with known solutions and found to agree within $\pm 1\%$.

The above equation (7.1) also describes the temperature distribution in a plane section with uniform source of heat all over the surface, in which case the governing

differential equation is

$$\nabla^2 T = -\frac{h}{k} \tag{7.2}$$

The equation (7.2) is a special case of equation (5.58) and hence the method of weighted residuals could be used with some confidence to obtain a solution to the equation (5.58) as well.

In view of the above-mentioned facts, the results of this work can be considered as reliable.

7.3 EQUIVALENT STRESS AND TEMPERATURE DISTRIBUTION

The temperature distribution as computed by the method of weighted residuals is illustarted in Figs. 7.13 to 7.18 for different cases. The ambient temperature is taken to be $18^{o}C$. The results indicate that the temperature rise is quite significant, and the temperatures at the tool/specimen interface are much higher than temperatures in the rest of the specimen, and that the conduction of heat into the die is very slow as observed by others in upsetting [31] and extrusion [102,103]. The temperature fields obtained in this work are compared with those obtained by the finite element method [31] in Section 7.8.

The equivalent stress as given by equation (4.19)

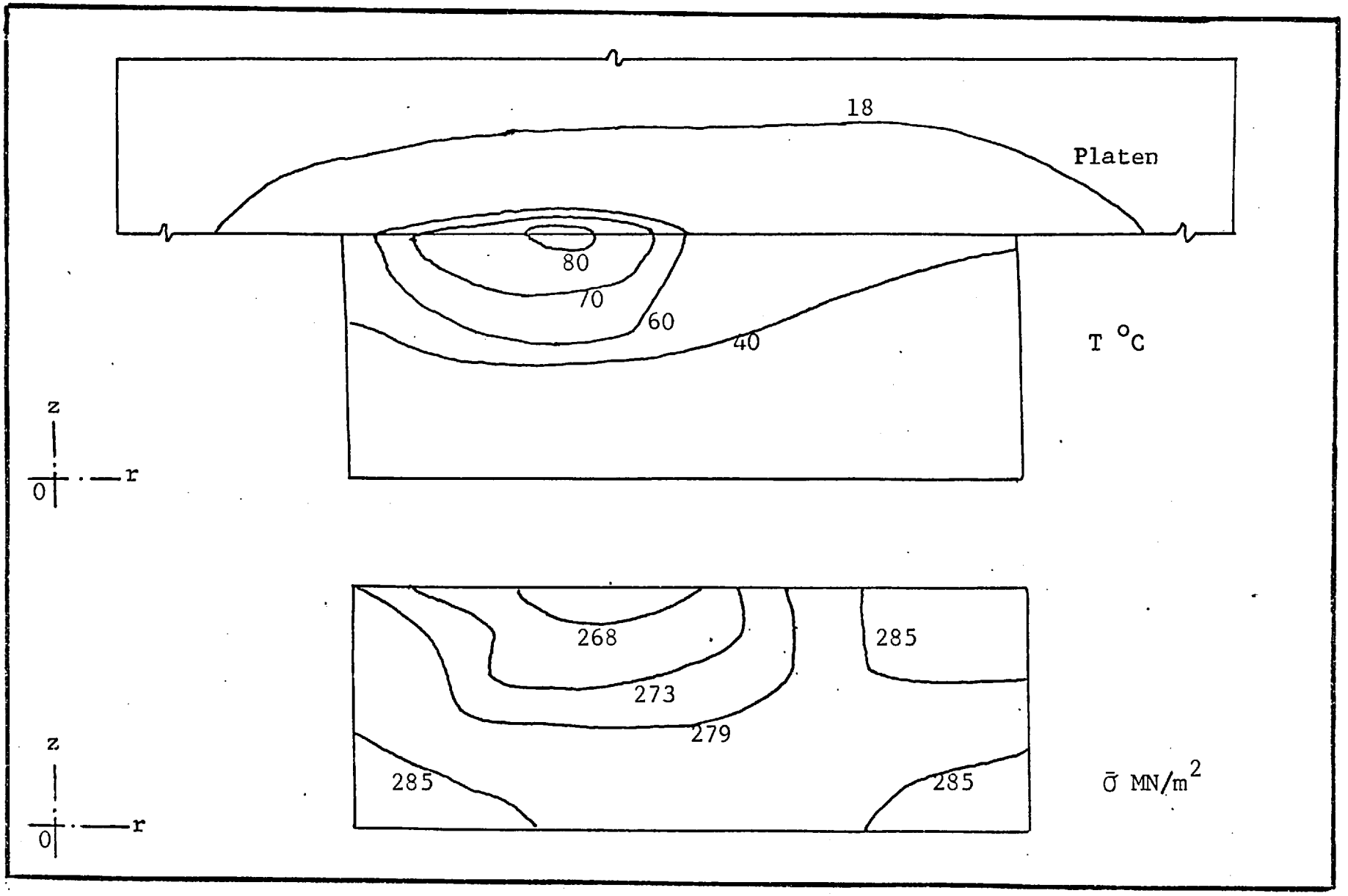

FIG. 7.13 Equivalent Stress and Temperature Fields
(V = 5.0 m/s; α = 0.14; 31.5% Deformation).

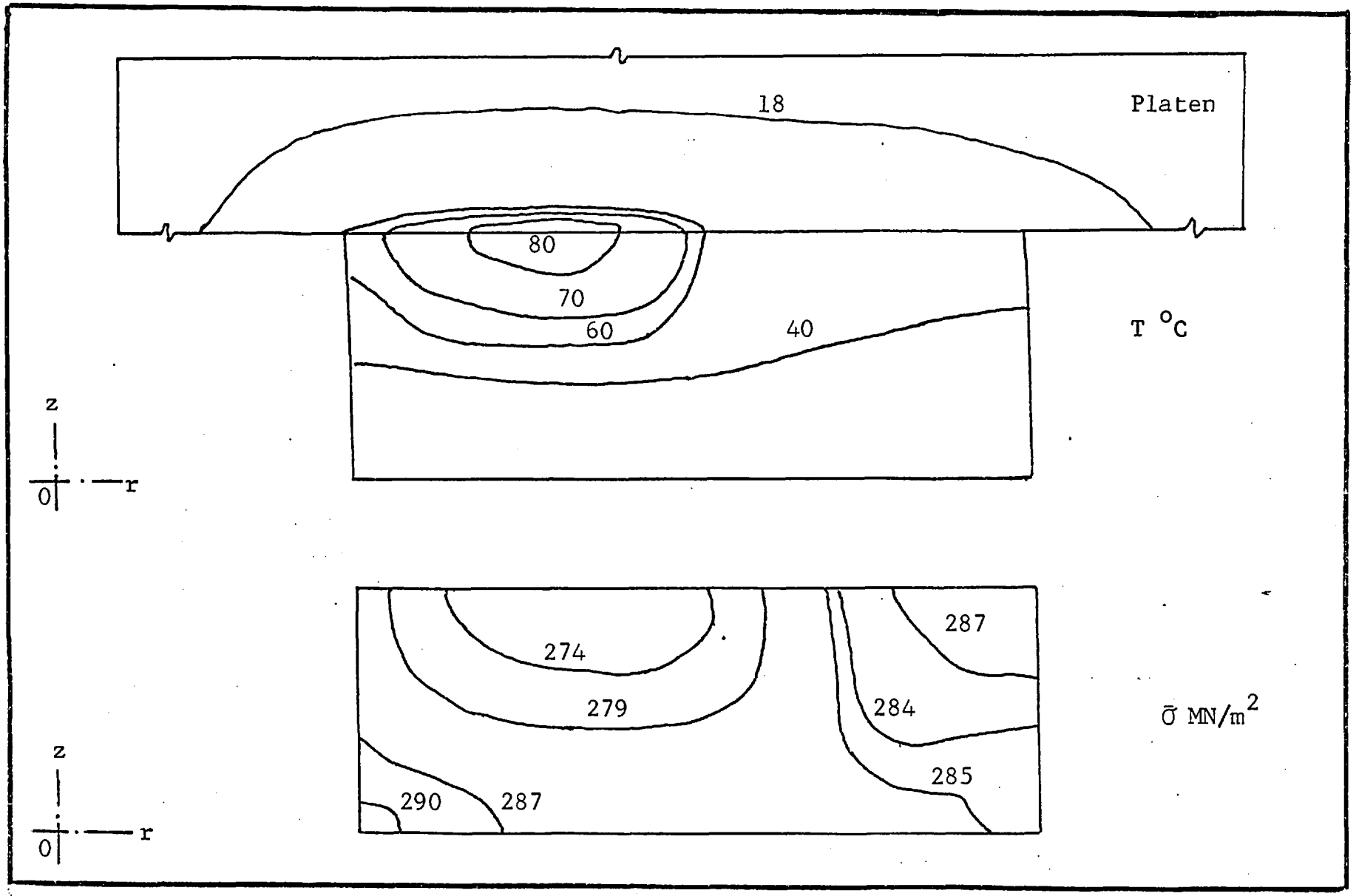

FIG. 7.14 Equivalent Stress and Temperature Fields
(V_I = 10.3 m/s; α = 0.14; 31.5% Deformation).

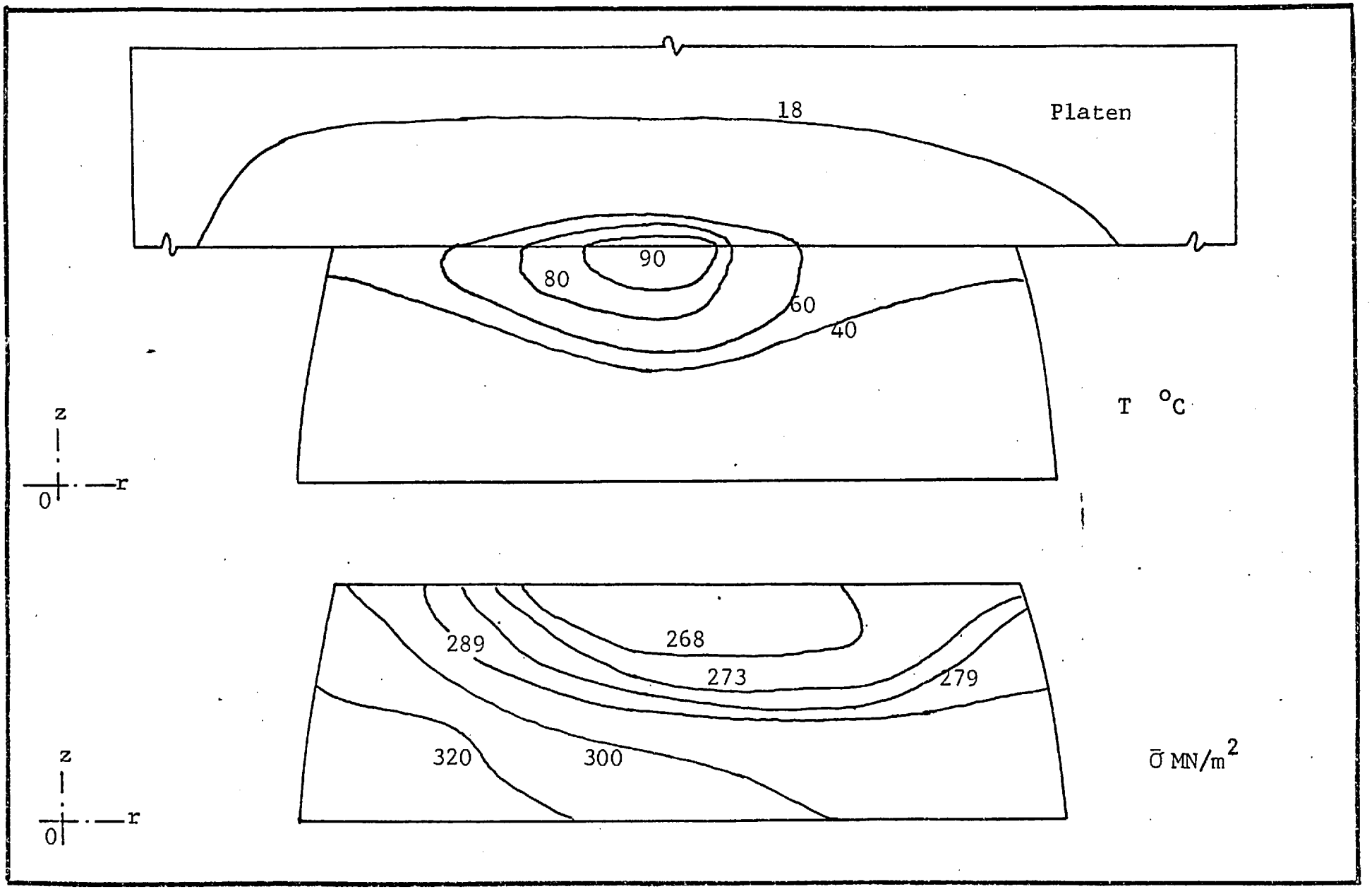

FIG. 7.15 Equivalent Stress and Temperature Fields
(V_I = 5.0 m/s; α = 0.77; 31.5% Deformation).

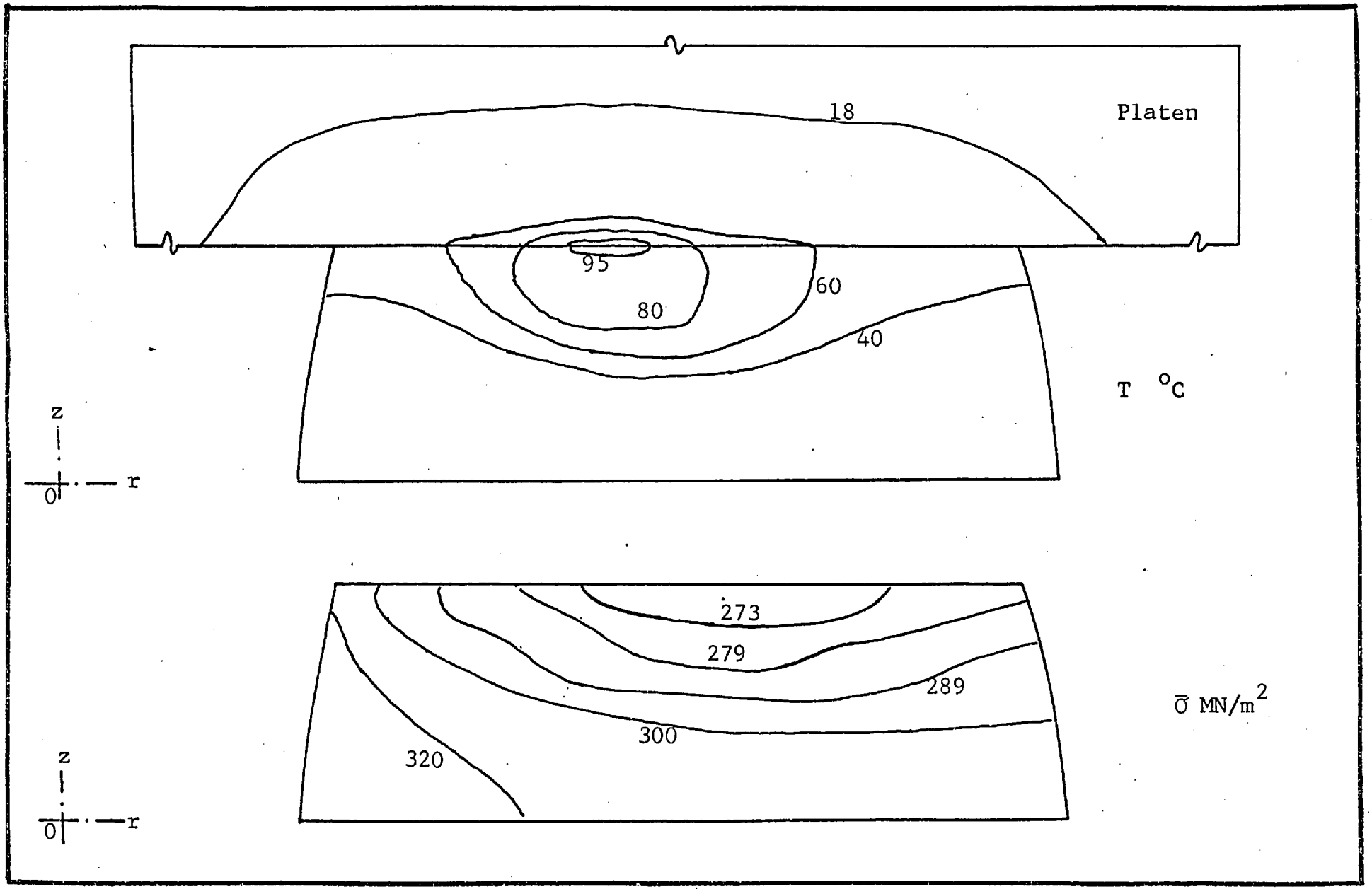

FIG. 7.16· Equivalent Stress and Temperature Fields
(V_I = 10.3 m/s; α = 0.77; 31.5% Deformation).

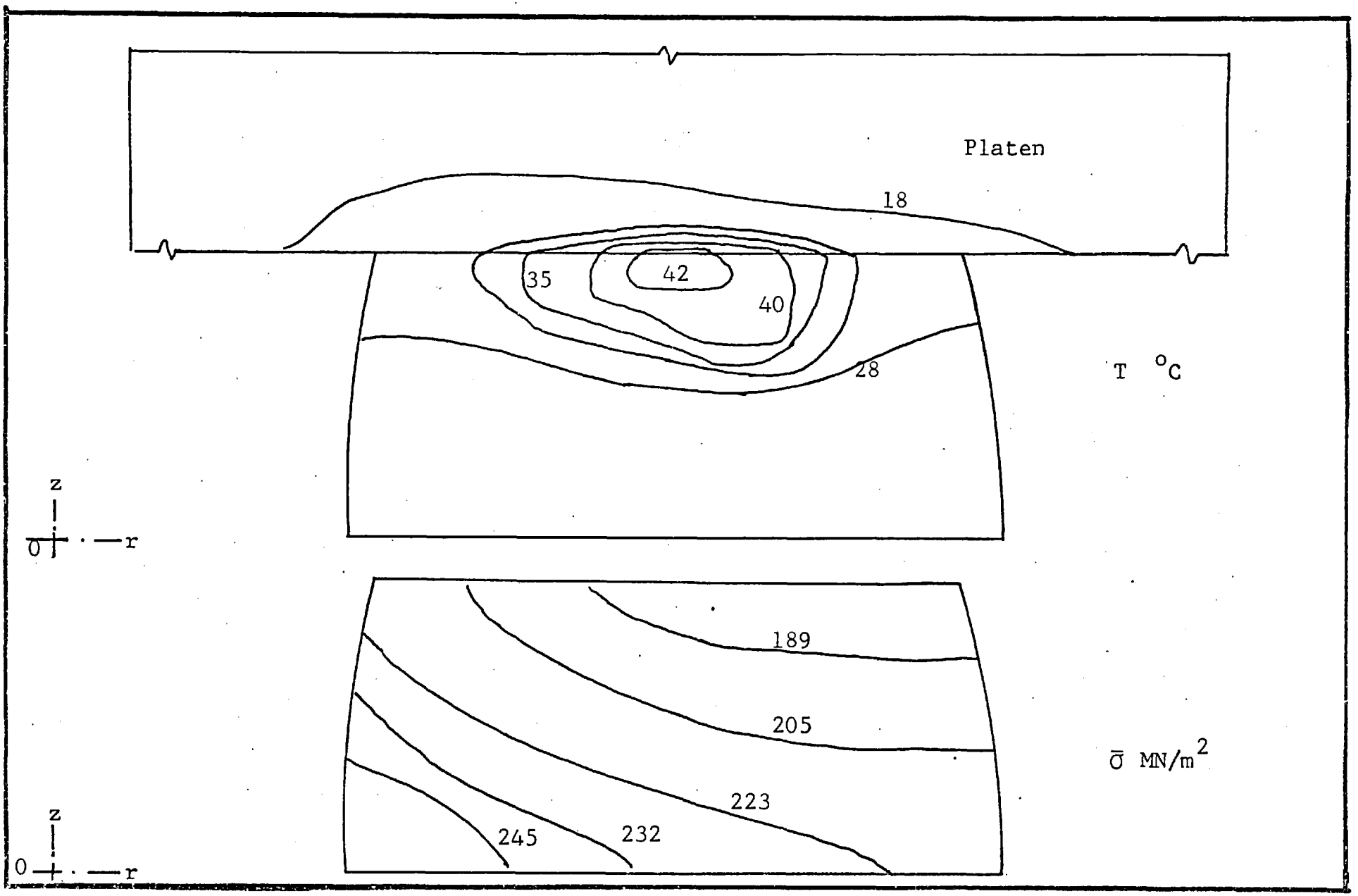

FIG. 7.17 Equivalent Stress and Temperature Fields (V_I = 10.3 m/s; α = 0.77; 15.7% Deformation).

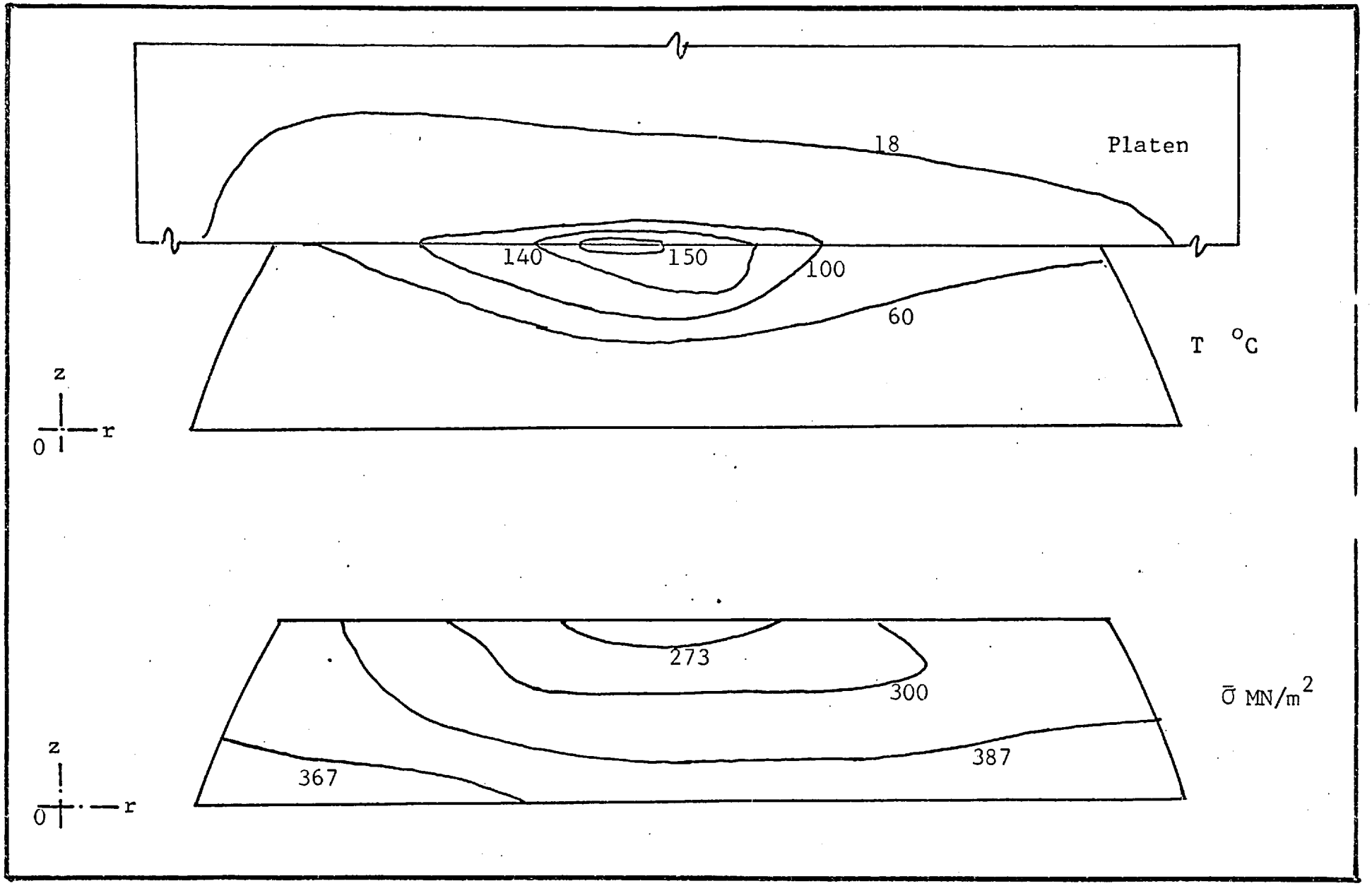

FIG. 7.18 Equivalent Stress and Temperature Fields
(V_I = 10.3 m/s; α = 0.77; 46.8% Deformation).

represents the state of stress at any nodal point and therefore their distributions are included in Figs. 7.13 to 7.18. These have been computed incrementally accounting for thermal softening as explained in Chapter 5. The results demonstrate the fact that the stress field is nearly uniform within the continuum when the friction is low and that they vary within the contimuum more significantly when the friction is high, and that the value of stresses increases with friction.

Comparing Fig. 7.13 and 7.14, the strain rate effects can be observed. At higher deformation velocity the stresses increase as might be expected. The isotherms, particularly 80°C and 70°C, spread deeper into the specimen at higher deformation speed, indicating greater localised heating at the interface. These effects of strain rate are similar in nature when the friction is high. However, as can be seen in Figs. 7.13 to 7.15, the effect of friction by itself is much more pronounced than that of strain rate. As the radial velocity at the interface at an impact velocity of 10.3 m/s is approximately 1.5 times the radial velocity at an impact velocity of 5.0 m/s, and the assumed friction factor ($\alpha = 0.77$) for dry conditions is 5.5 times greater than the friction factor ($\alpha = 0.14$) for the lubricated conditions, the work due to friction given by equation (4.42)

will vary accordingly. It was observed earlier that the conduction of heat into the die surface is slow and the heating is almost adiabatic. On account of these two facts, it is quite plausible that the effects of friction are more pronounced than that of strain rate.

7.4 EQUIVALENT STRESS DISTRIBUTION WITHOUT THERMAL SOFTENING

In order to be able to establish the effect of localised temperature rise due to work of deformation and friction, stress fields were also computed without considering the thermal effects, assuming that the material remained at constant ambient temperature of $18^{o}C$. The equivalent stress distribution is shown in Figs. 7.19 to 7.24.

Conditions of speed and friction correspond to those in Figs. 7.13 to 7.19, so that direct comparison can be made. It is quite evident that the thermal effects are significant.

Comparing Fig. 7.13 and Fig. 7.19, it can be seen that significant thermal softening does occur at the interface and the areas immediately surrounding it as a result of localised heating. This thermal effect is similar in nature at higher speeds and friction, as shown in other

illustrations. At early stages of deformation, Fig. 7.17, this thermal softening is not significant as the increase in temperature is quite small. The increase in stress between 31.5% deformation, Fig. 7.24, and 46.8% deformation, Fig. 7.23, when the thermal softening is neglected is higher than the corresponding increase, Figs. 7.16 and 7.18, when the thermal effects are taken into account. This indicates that thermal softening assumes greater significance as deformation proceeds.

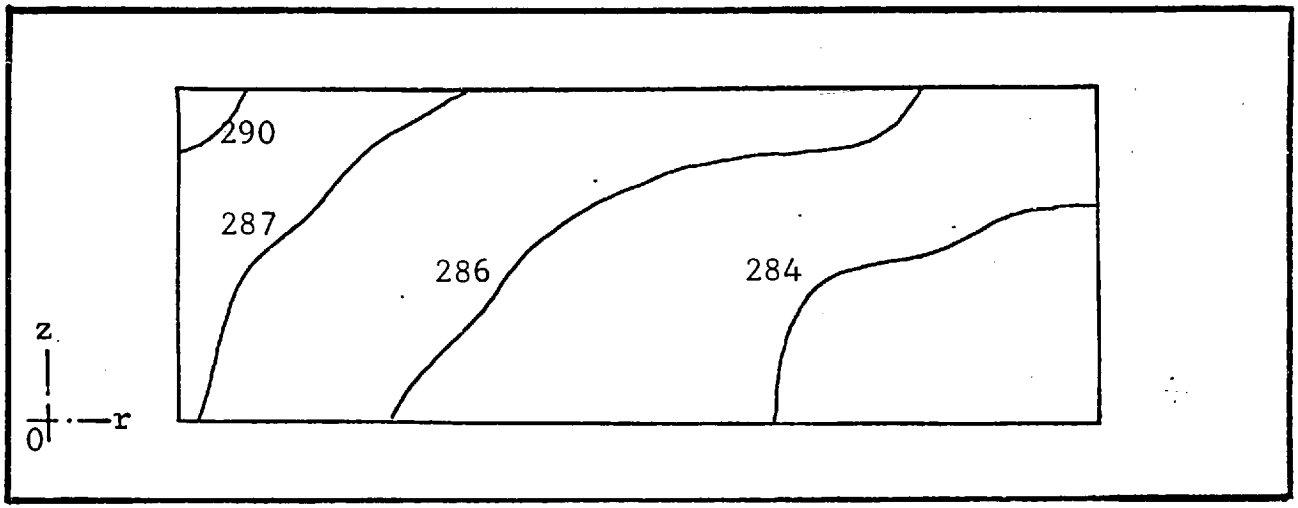

FIG. 7.19 $\bar{\sigma}$ (MN/m^2) Without thermal softening
(V = 5.0 m/s; α = 0.14; 31.5% Deformation).

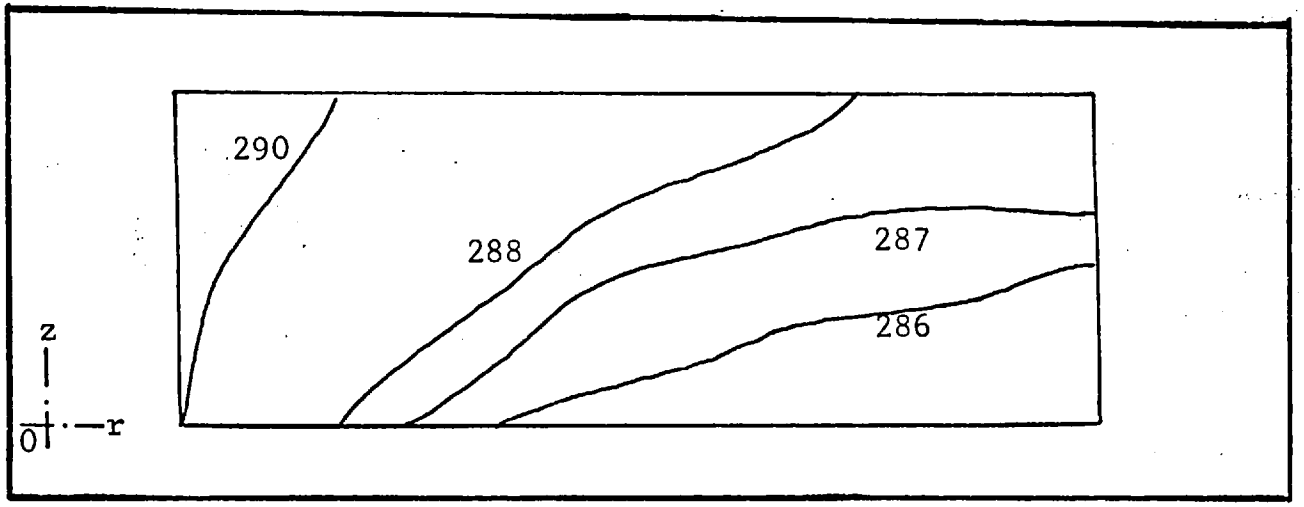

FIG. 7.20 $\bar{\sigma}$ (MN/m^2) Without thermal softening
(V = 10.3 m/s; α = 0.14; 31.5% Deformation).

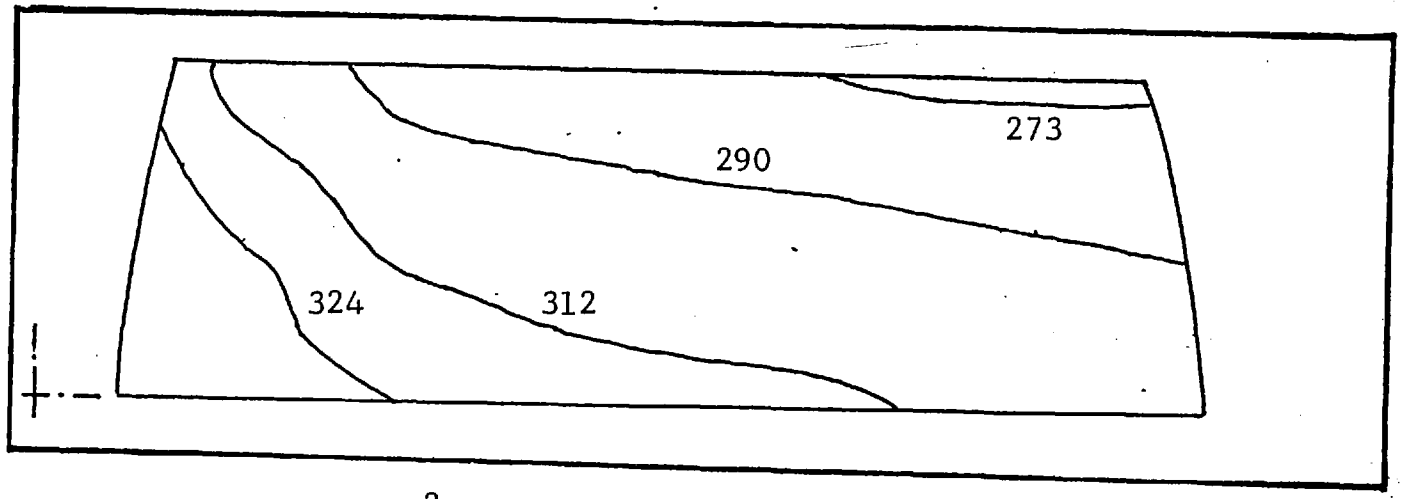

FIG. 7.21 $\bar{\sigma}$ (MN/m^2) without thermal softening (V_I = 5.0 m/s; α = 0.77; 31.5% Deformation).

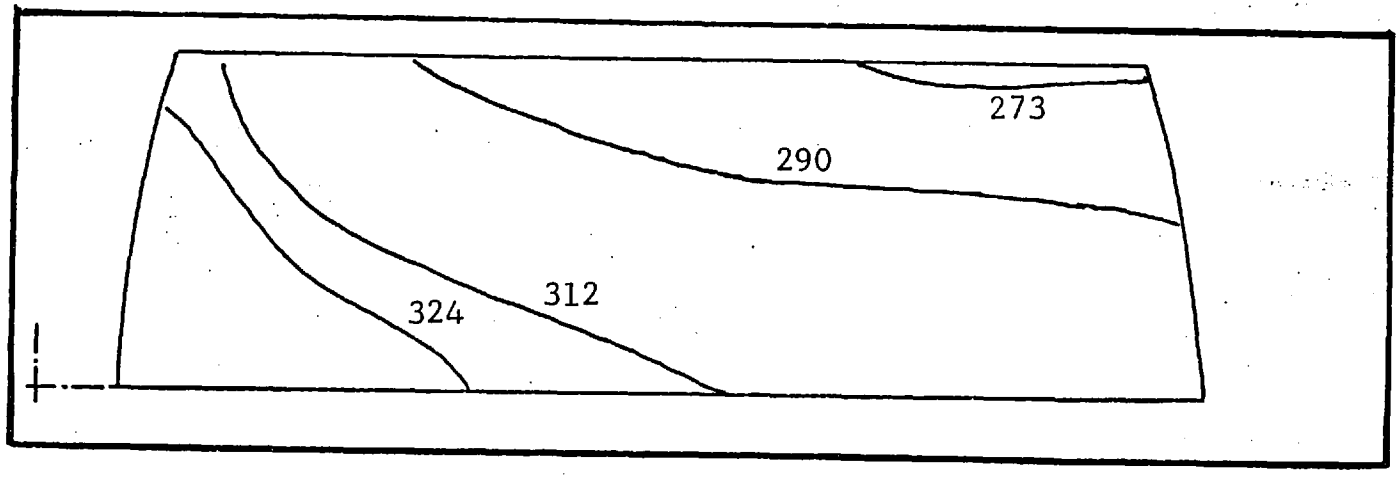

FIG. 7.22 $\bar{\sigma}$ (MN/m^2) without thermal softening (V_I = 10.3 m/s; α = 0.77; 31.5% Deformation).

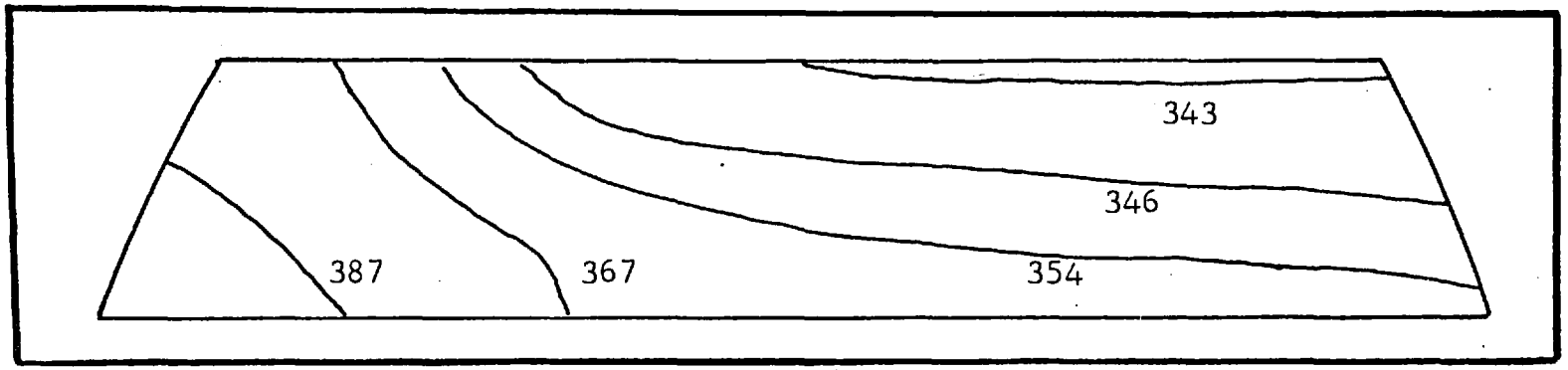

FIG. 7.23 $\bar{\sigma}$ (MN/m^2) without thermal softening
(V_I = 10.3 m/s; α = 0.77; 46.8% Deformation).

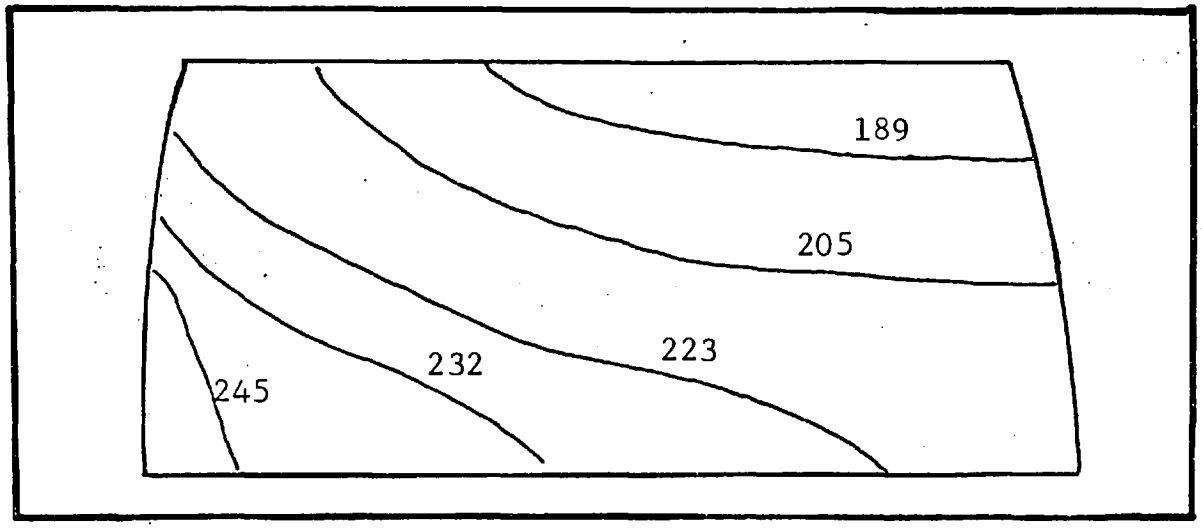

FIG. 7.24 $\bar{\sigma}$ (MN/m^2) without thermal softening
(V_I = 10.3 m/s; α = 0.77; 15.7% Deformation).

7.5 STRESS FIELD

So far only the equivalent stress distributions were discussed as they fully represent the state of stress at a point and can be more meaningfully interpreted. However, for the purposes of illustration, complete stress field for a selected condition is given in Fig. 7.25.

7.6 EFFECTS OF FRICTION AND SPEED

The effects of friction and speed can be more readily assessed by studying the maximum localised temperatures. In Fig. 7.26 it is apparent that the effect of friction on local temperature is more pronounced than that of the speed, particularly at large deformations. It is also observed that in the temperature distributions discussed earlier the temperatures at the tool/specimen interface are much higher than temperatures in the rest of the specimen. However, Figs. 7.27 and 7.28 show that the maximum local temperature rises rapidly with friction up to a particular value $\alpha = .35$ and then becomes more or less steady. This is due to the fact that as friction increases the radial velocity at the interface becomes smaller and hence the work due to friction is less and the temperature rise is due only to plastic work of deformation.

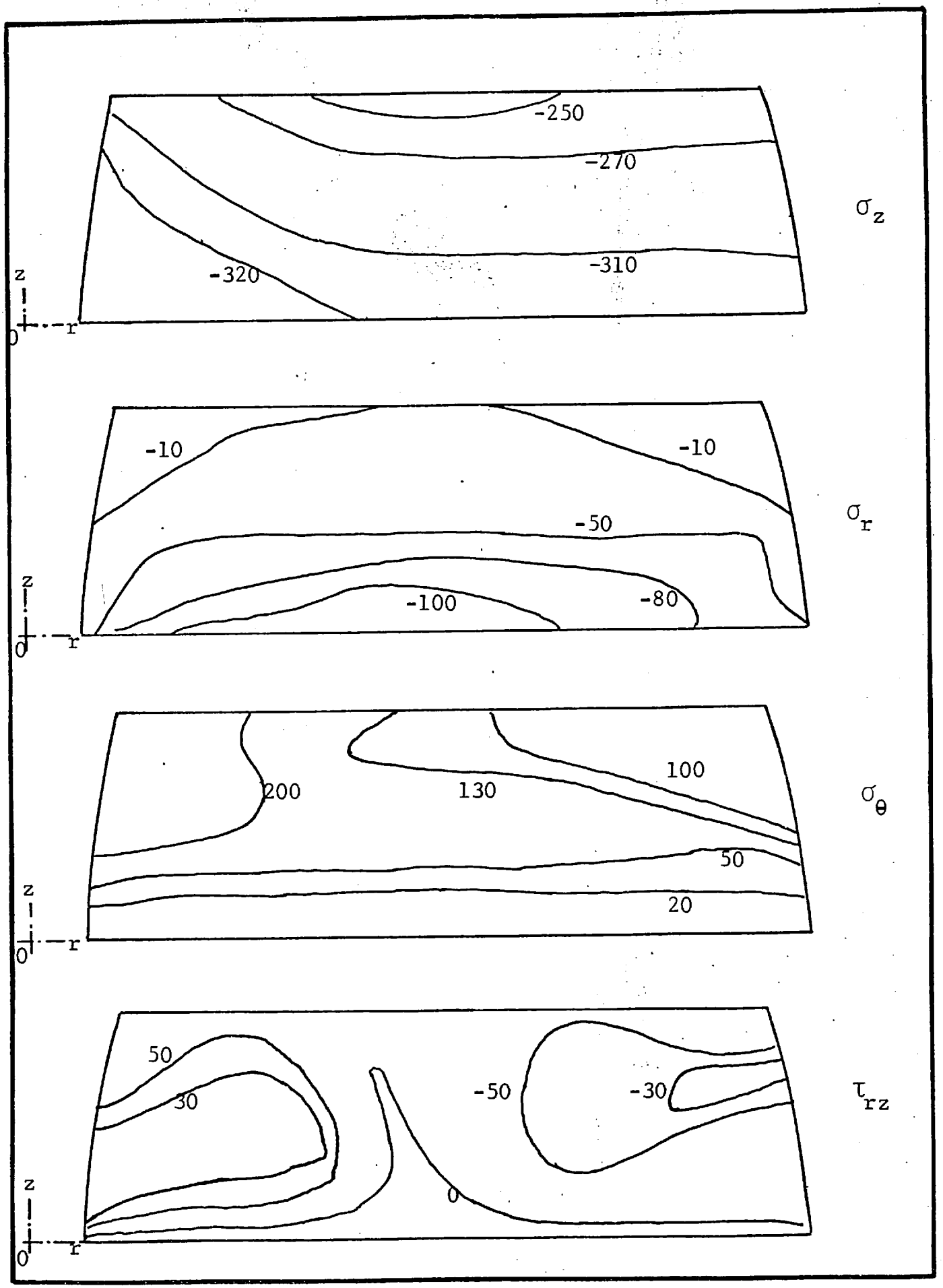

FIG. 7.25 Stress Field (V_I = 10.3 m/s; α = 0.77; 31.5% Deformation).

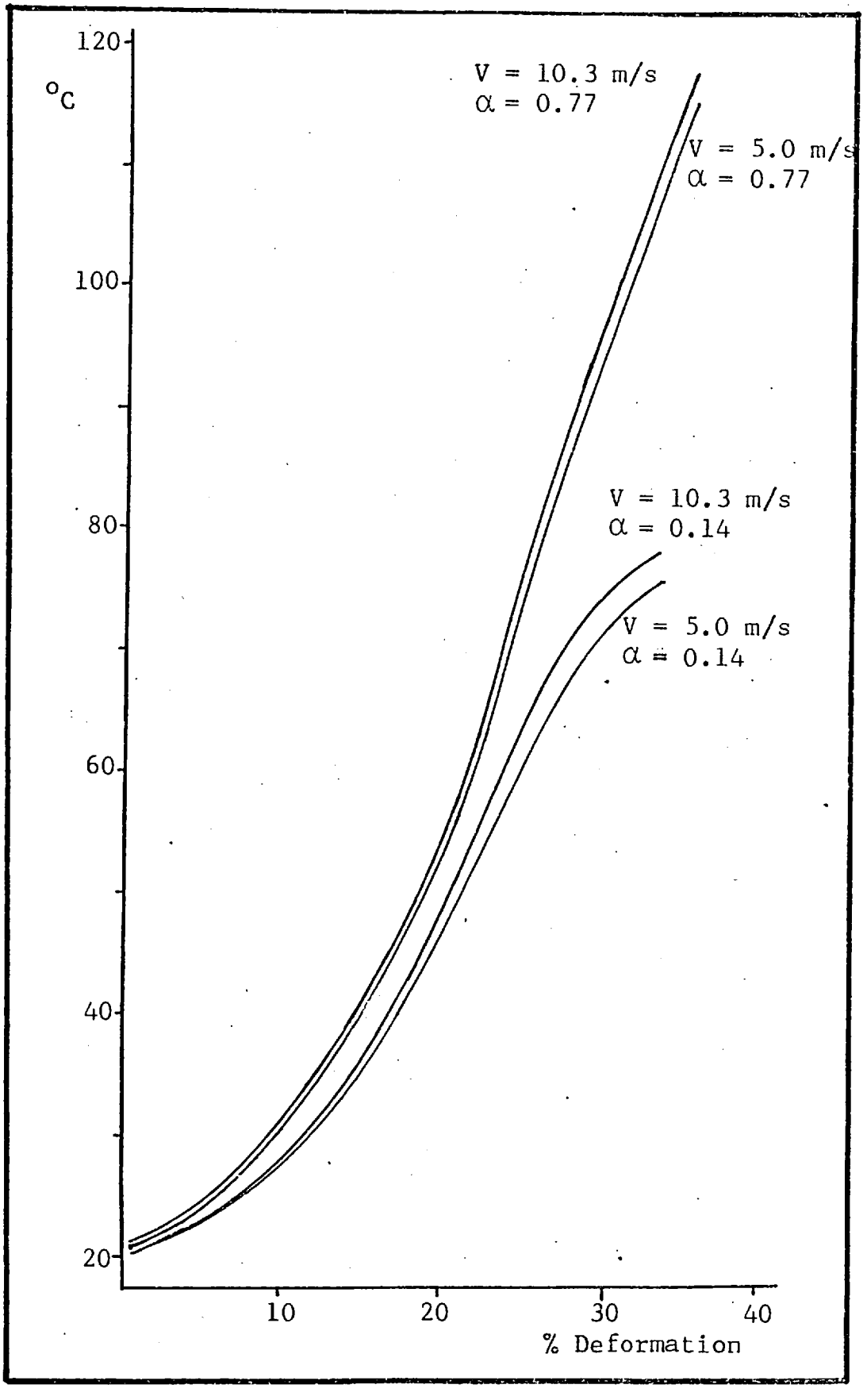

FIG. 7.26 Variation of Maximum Localised Temperature during Deformation.

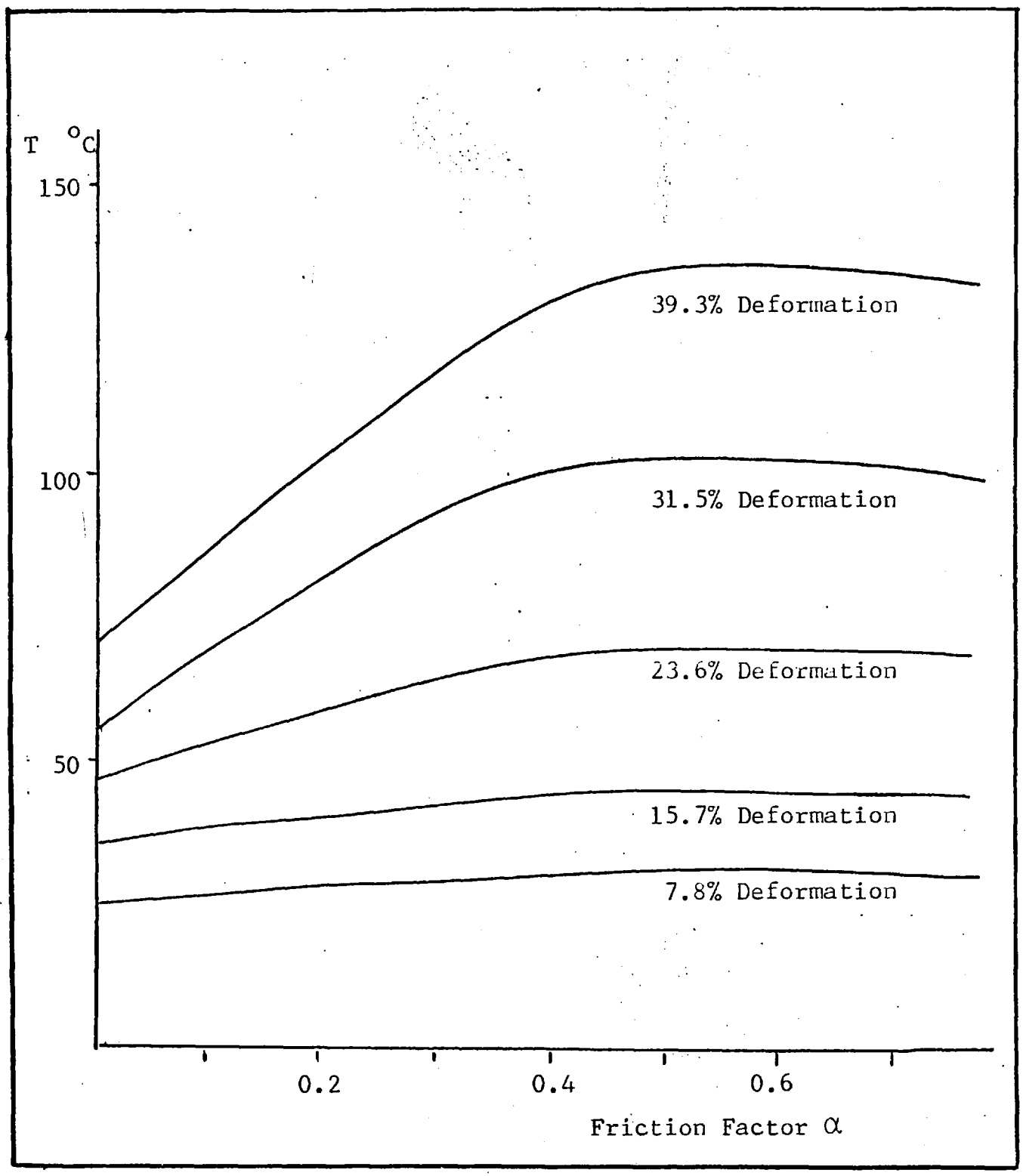

FIG. 7.27 Effects of Friction on Maximum Local Temperature at V_I = 5.0 m/s.

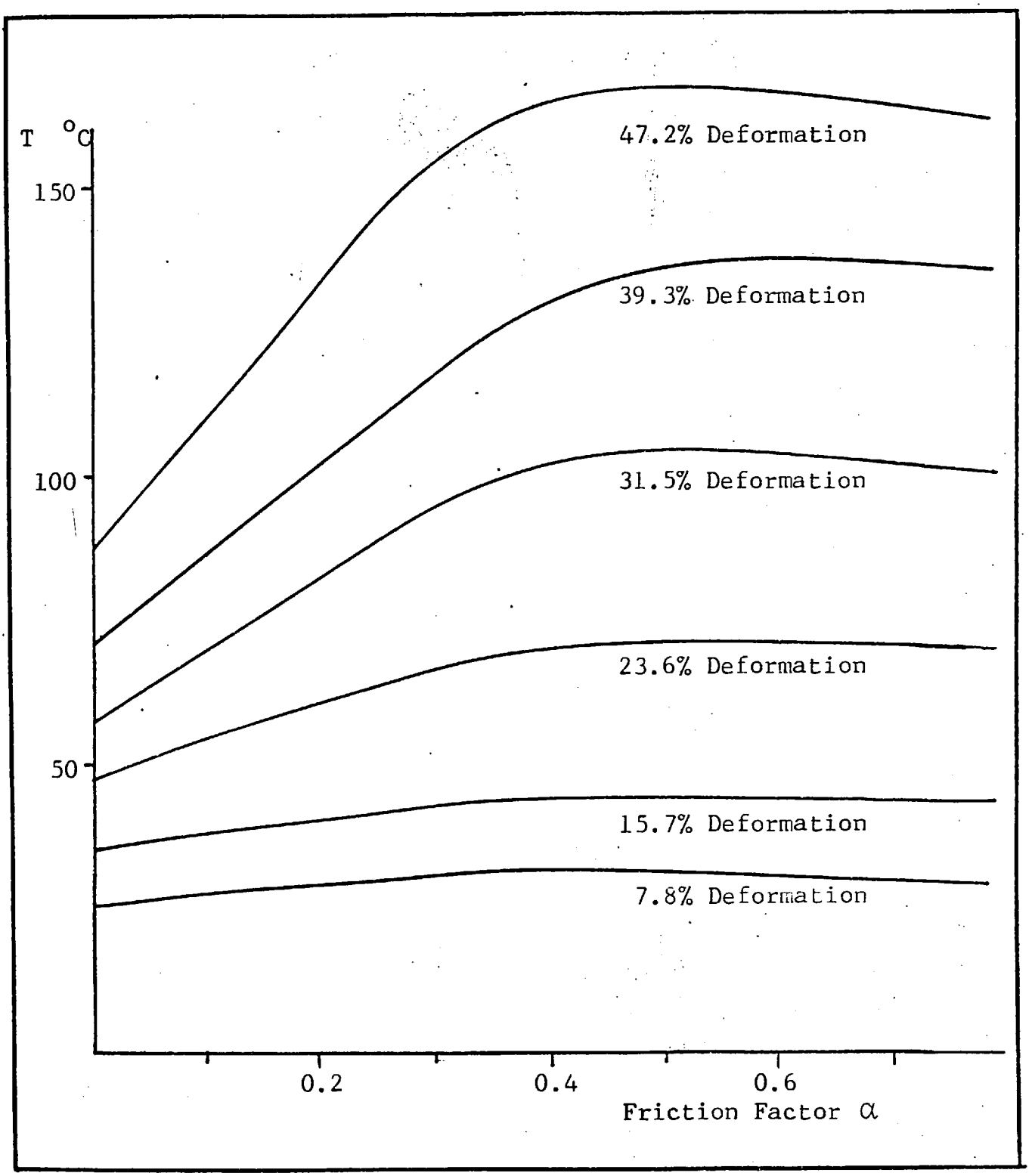

FIG. 7.28 Effect of Friction on Maximum Local Temperature at V_I = 10.3 m/s.

7.7 EQUIVALENT STRESS AND TEMPERATURE DISTRIBUTION (SOLID BILLETS)

The computer programme can be easily adapted to obtain stress and temperature field during upsetting of solid cylindrical billets, as explained in Chapter 5. The equivalent stress and temperature distributions for a particular case are illustrated in Figs. 7.29 and 7.30. The deformation velocity/time relationship was taken from [31] for a copper cylinder 25.4 mm in diameter and height.

7.8 COMPARISON WITH FINITE ELEMENT METHOD

Mohitpur [31] proposed a finite element solution for temperature field during upsetting of solid billets, assuming uniform deformation and Coulomb friction. This makes direct comparison of the results of this work and that of [31] difficult. It is suggested [57] that the average pressures computed using the two theories can be compared and that for any given value of coefficient of friction μ a corresponding value of constant friction factor may be determined so that the average pressure given by the two theories is identical in the region of interest. However, experiments [31] were carried out in dry conditions (without lubricant) and the centre point temperature was

measured during deformation which were compared with the finite element solution which corresponds to a coefficient of friction $\mu = 0.5$. The agreement between the two results was quite good.

The tooling used in this work is the same as that used in [31]; the specimens were machined in the same manner and materials as in Ref. [31] and tests were conducted in similar dry conditions. As observed earlier in Section 7.1 friction factor of $\alpha = 0.77$ adequately described this condition. Therefore this value $\alpha = 0.77$ was used to obtain a weighted residual solution and the temperature field for nearly the same reduction in height is compared with that obtained by the method of weighted residuals and shown in Fig. 7.31. Referring to Fig. 7.32, it is observed that the centre point temperatures agree quite well and that maximum local temperatures as given by the finite element method are very much higher and appear to reach a maximum and then begin to drop. The higher maximum local temperature (at this interface) during early stages of deformation is possibly due to the assumption of uniform deformation, in which case the radial velocity at the interface is much higher and consequently the contribution of work due to friction. This comparison suggests that the assumption of uniform deformation is not realistic.

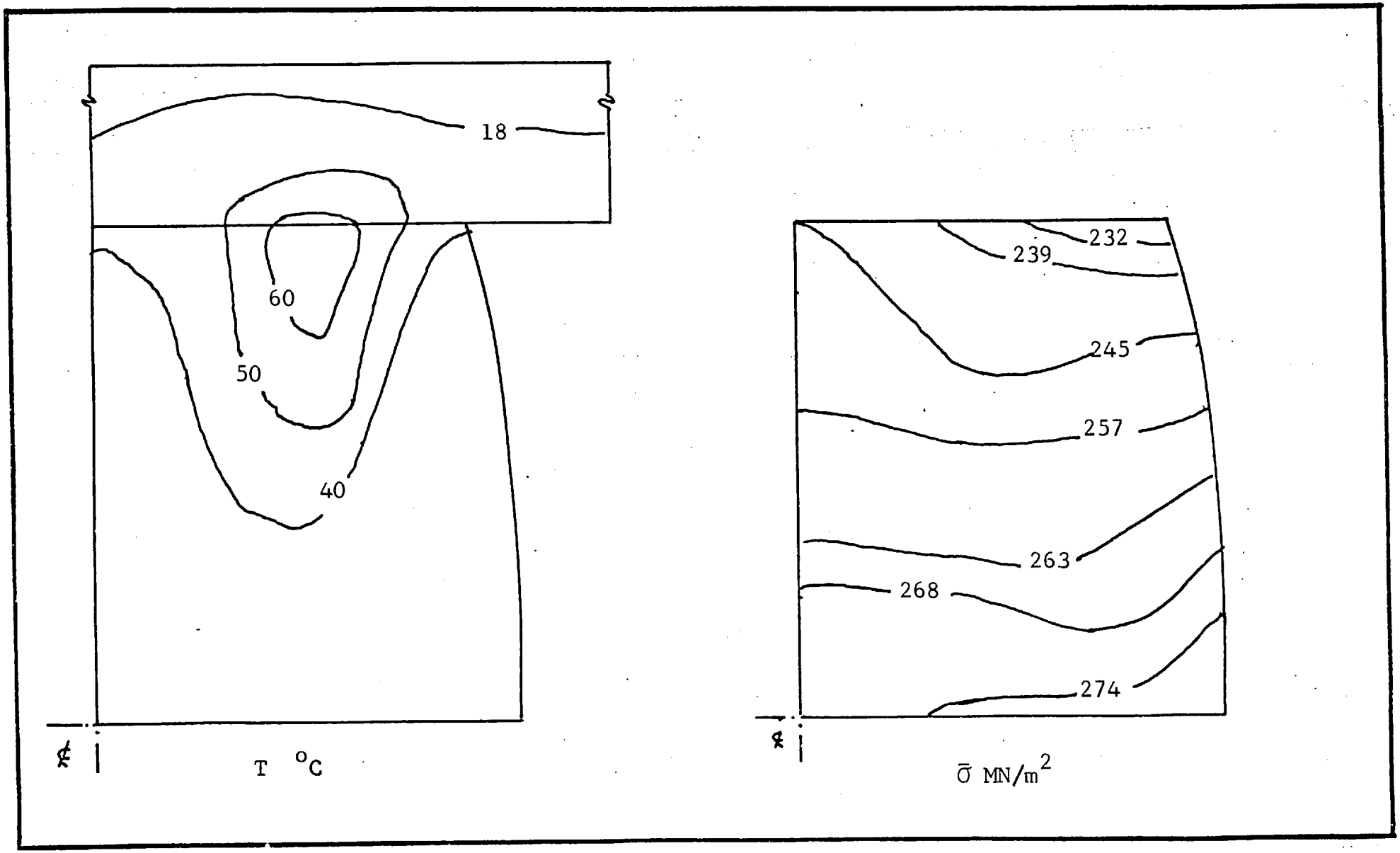

FIG. 7.29 Temperature and Stress Distribution
(V_I = 4.5 m/s; = 0.77; 26.6% Deformation).

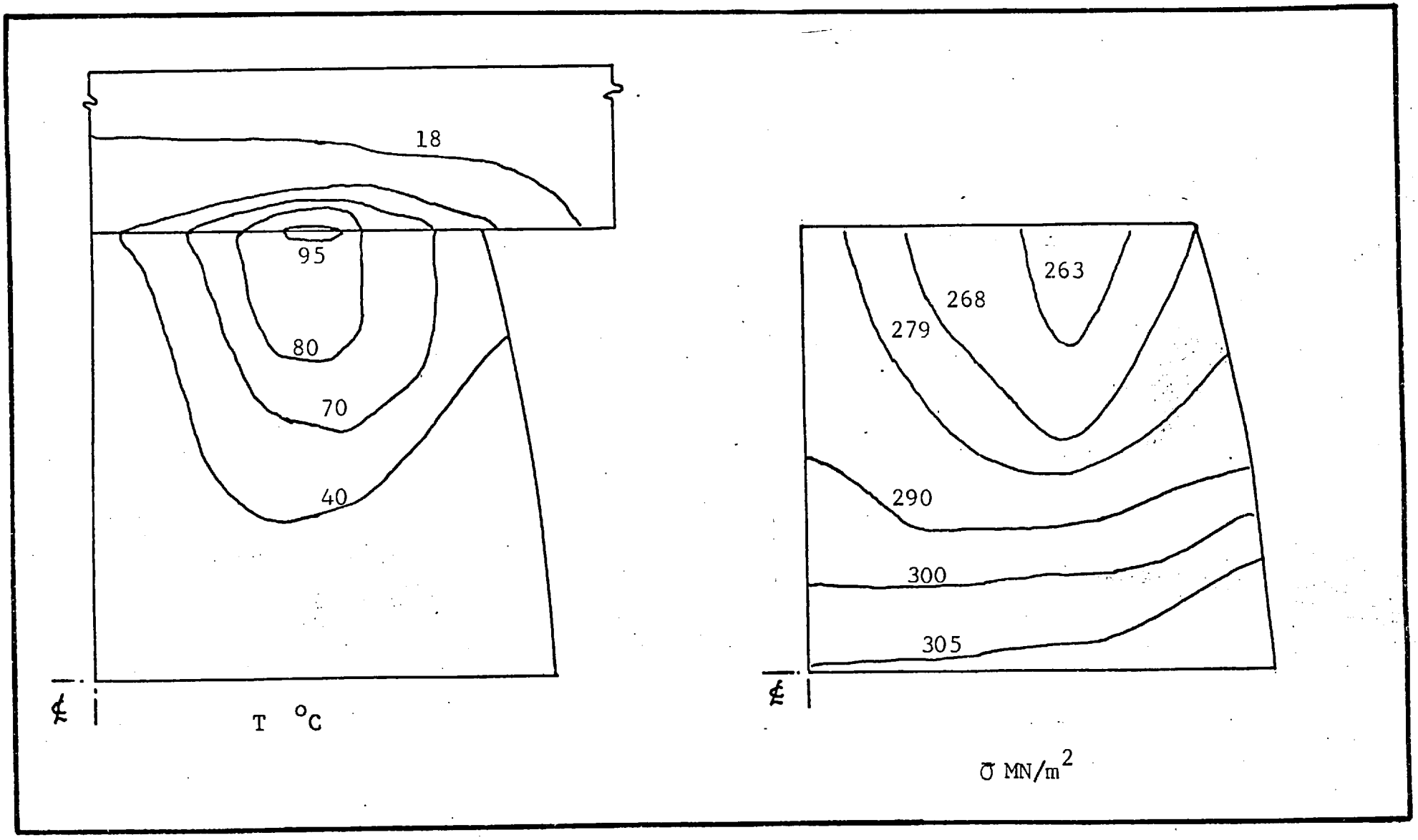

FIG. 7.30 Temperature and Stress Distribution
(V_I = 4.5 m/s; α = 0.77; 34.8% Deformation).

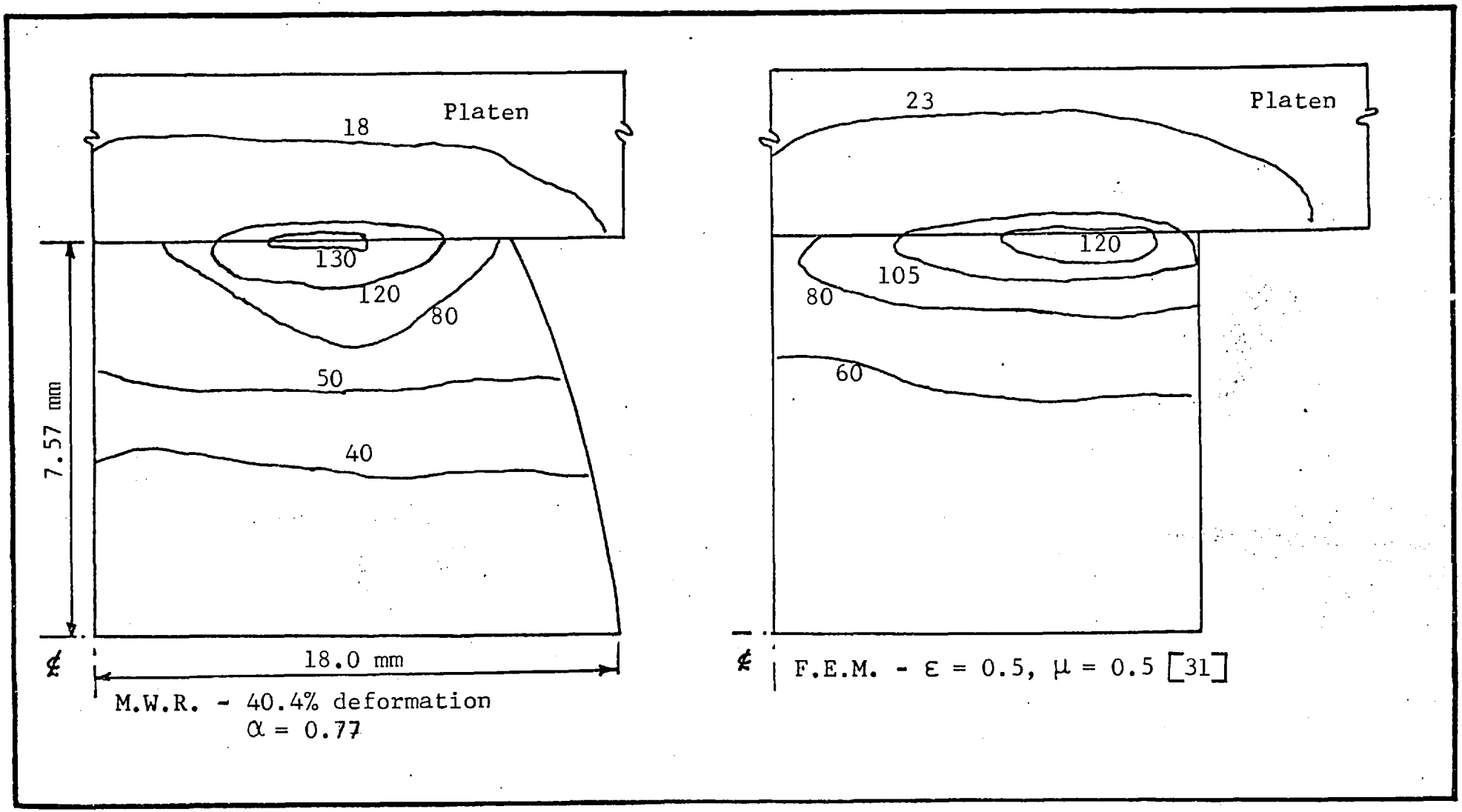

FIG. 7.31 Temperature (^{o}C) distribution (V_I = 4.5 m/s).

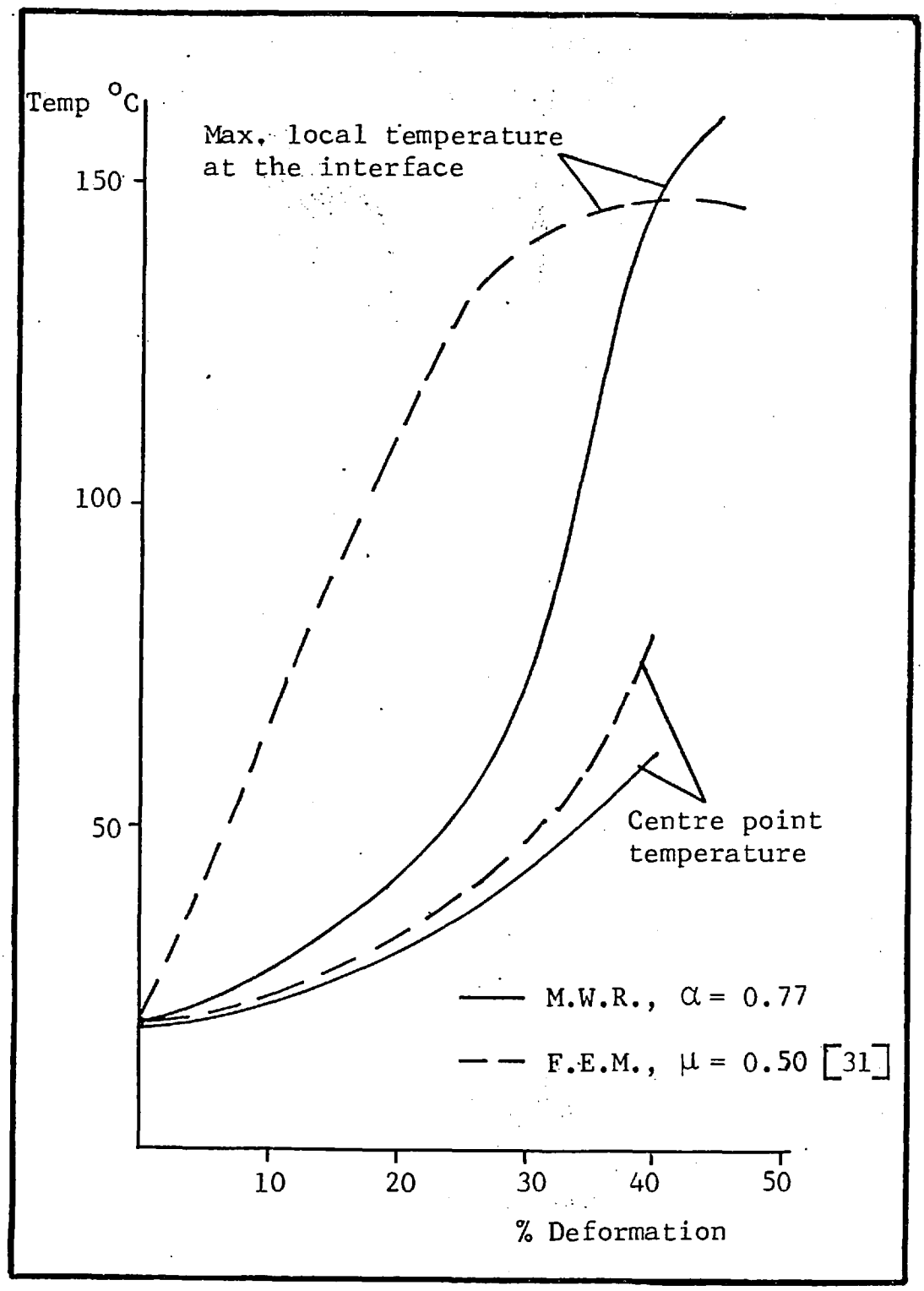

FIG. 7.32 Comparison of local temperatures (V_I = 4.5 m/s).

CHAPTER 8

CONCLUSION

The knowledge of the deformation process of upsetting has progressed in the years as reviewed in Chapter 2. It is evident that strain, strain rate, interface friction and temperature significantly influence the deformation process and that there is interaction between them. Experimental work has led to several empirical formulae which determine the stress/strain relationship, the most important material property from the engineering point of view. Analytical solutions based on simplifying assumptions have been proposed to predict theoretically average values of essential parameters. As the process is far too complex to be fully solved in closed analytical form, numerical solutions have been proposed which determine the velocity, stress and temperature fields so that the variation of these factors within the continuum may be assessed. Numerical methods that are in popular use require much effort and computational facilities and often the effort needed is out of proportion to the advantages that may be gained by applying these sophisticated methods. It is therefore necessary to develop relatively simple, less demanding and sufficiently accurate methods. Judging by the results of this and other work carried out at the Imperial College, London, the method

of weighted residuals appears to be satisfactory.

Analysis of Steck's work [51], the only other known application of the method of weighted residuals to metal-working problems, reveals that it is necessary to assume a velocity field to obtain reliable solutions. The assumed velocity field based on Avitzur's upper bound solution and constant friction factor throughout the deformation describes the process adequately. However, it is desirable to eliminate the need to assume a velocity field and take into account the variation of friction during deformation.

The linear induction motor developed as an experimental forging machine presents interesting possibilities, particularly in view of the fact that the speed of operation could be controlled effectively and economically by a simple system of relays as described in Chapter 6. The measurement system designed to measure the transient phenomenon fully exploits the up-to-date advances in the field of electronics. The digital recording system not only eliminates most of the errors that may arise in a conventional system but also enables data to be processed directly on the computer, resulting in a much more accurate analysis of data. In this particular case, accurate derivatives could be obtained. Precise triggering of the recording system to capture the

transient signal has always been difficult, causing many, otherwise useful, experiments to be discarded. This difficulty has been overcome simply and effectively by using piezoelectric accelerometer as a triggering device.

The results presented for different conditions provide adequate information regarding the effect of speed, friction and temperature rise during upsetting of cylindrical billets at high speeds. Some of the results may be summarised as follows:-

a) Interface friction causes non-uniform deformation resulting in increase in stresses and variation of stresses within the continuum.

b) There is significant rise in temperature due to work of deformation at high speeds.

c) The temperature rise increases with increase in friction due to additional work of friction.

d) The temperature rise also increases to a lesser extent with increase in strain rate.

e) The heating of the specimen due to work of deformation and friction is almost adiabatic.

These findings confirm the results of other numerical solutions found in the literature.

As a result of this work additional conclusions of importance may be made as follows:

a) The temperature rise rapidly increases with friction up to a value of about $\alpha = 0.35$ and thereafter remains more or less steady. As explained earlier, this is due to the fact that the radial velocity at the interface is reduced as sticking begins to occur and work of plastic deformation assumes predominance.

b) The localised temperature rise is significant and considerable thermal softening takes place, particularly at the interface and the areas immediately surrounding them.

So far as is known, this important thermal effect has not been accounted for in the solutions available. In fact, available solutions are either for stress fields or for temperature fields and is not known to have been combined. It is essential that as far as possible all the process variables should be accounted for.

On account of the simplicity of the method of weighted residuals this complex problem could be formulated

and handled with relative ease. To determine temperature and stress field for deformations up to 50% (in ten incremental steps) only 50 seconds of central processing time (CDC 6400) and memory of 20 K was required. This is several orders of magnitude less than the requirements for the finite element solution [31] which requires 60 K memory and processing time of 125 seconds just to obtain the temperature field.

Finally, it is hoped that this work will lay the basis for future work and any further work directed at application and development of this method should be rewarding.

REFERENCES

1. JOHNSON W. (1972) Impact strength of materials. Edward Arnold, London.
2. ALEXANDER, J.M. and BREWER, R.C. (1963) Manufacturing properties of metals. Van Nostrand, London.
3. ROWE, G.W. (1965) An introduction to principles of metal working. Edward Arnold, London.
4. COOK, M. and LARKE, E. (1945) J. Inst. Met., 71, 371.
5. RUMMEL, K. (1919) Stahl und Eisen, 39, 237 and 267.
6. MEYER, H. and NEHL, F. (1925) Ibid, 45, 1961.
7. SIEBEL, E. and POMP, A. (1927) Ibid, 9, 157.
8. SIEBEL, E. and POMP, A. (1928) Ibid, 10, 55.
9. UNDERWOOD, L.R. (1945) Sheet Metal Industries, 22, 1905.
10. TAYLOR, G.I. and QUINNEY, H. (1934) Proc. Royl. Soc., Series A, 143, 307.
11. SACHS, G. (1924) Zeitschrift für Metalkunde, 16, 55.
12. POLAKOWSKI, N.H. (1949) J. Iron. Steel. Inst.
13. KUDO, H. (1960) Some analytical and experimental studies of axisymetric cold forging and extrusion. Int. J. Mech. Sci., 2, 102-127, and 3, 91-917.
14. MALE, A.T. and COCKCROFT (1964-65) J. Inst. Met., 93, 38-46.
15. ROSEN, A. and DORN, J.E. (1964-65) J. Inst: Met, 93, 387.
16. JONAS, J.J. and IMMARIGEON, J.P. (1969) Zeitschrift für Metalkunds, 60, 3, 227.
17. UVIRA, J.L., ALEXRAD, D.R. and JONAS, J.J. (1968) Trans. Japan Inst. Met., 60, 3, 27.

18. MOK, C.H. and DUFFY, J. (1964) J. Inst. Mech. Sci., 6, 161.

19. MANJOINE, M. and NADAI, A. (1940) Proc. Am. Soc. Testing Materials, 40, 882.

20. KOLSKY, H. (1963) Stress waves in solids. New York.

21. McQUEEN, H.J., WONG, W.A. and JONAS, J.J. (1967) Canadian J. Physics, 45, 12 5.

22. TAYLOR, G.I. (1946) J. Inst. Civil Eng., 26, 486.

23. VOLTERA, E. (1948) Nuovo Cimento, 4, 1.

24. LINDHOLM, U.S. (1964) J. Mech. Phys. Solids, 12, 317.

25. MALVERN, L.E. (L965) Behaviour of material under dynamic loading. ASME Pub., New York, 81.

26. SAMANTHA, S. and MAGI, J. (1969) Annals of the CIRP, 17, 463.

27. LENGYEL, B. and KROK, T.V. (1969) Metal forming, 36(6), 172.

28. LENGYEL, B. and STAMELOS, D.C. (1961) Annals of CIRP, 19, 225.

29. PARSON, B., TAYLOR, R. and COLE, B.N. (1965-66) Proc. Inst. Mech. Engrs., 180, 132.

30. COLE, B.N. and PARSONS, B. (1973) Proc. Int. Conf. on the use of high energy rate methods for forming. Leeds University.

31. MOHITPUR, M. (1972) Effects of strain rate, friction and temperature distribution in axisymetric upsetting. Ph.D. Thesis, London.

32. STAMELOS, D.C. (1972) Effects of strain rates on material properties. M.Sc. Thesis, Imperial College.

33. COLE, B.N., DAVIES, S.R., AUSTIN, E.R. and BAKHTAR, F. (1965) Proc. I.M.E., 180, 1.

34. NADAI, A. and MANJOINE, M. (1941) J. Appl. Mech. Trans. ASME, 63, 71.

35. ALDER, J.F. and PHILLIPS, V.A. (1954-55) J. Inst. Metals, 83, 80.

36. JONAS, J.J. McQUEEN, H.J. and WONG, W.A. (1967) Iron and Steel Inst., Report 108, 49.

37. LENGYEL, B. and AGARWAL, B. To be published.

38. DAVIES, R. and AUSTIN, E.R. (1970) Developments in high speed metal forming. Machinery Pub., London.

39. LIPPMAN, H. (1963) Adv. Mach. Tool Des. Res., 53.

40. DEAN, T.A. (1970) Adv. Mach. Tool Des. Res., 13, 761.

41. STURGESS, C.E.N. and JONES, M.G. (1971) Int. J. Mech. Sci., 13, 309.

42. LUDWIK, P. (1909) Elemente der technologischen Mechanik. Springer Verlag, Berlin.

43. SLATER, R.A.C., JOHNDON, W. and AKI, S. (1968) MTDR.

44. MACGREGOR, C.W. and FISHER, J.C. (1946) Trans. Am. Soc. Mech. Engrs., J. Appl. Mech., 13, 1, A11-A16.

45. THOMSEN, E.G., YANG, C.T. and KOBAYASHI, S. (1965) Mechanics of plastic deformation in metal processing. Macmillan & Co., New York.

46. LENGYEL, B. and MOHITPUR, M. (1972) Dynamic stress/strain data to large strains. J. Inst. Met., 100, 2665.

47. NAGAMATSU, A., MUROTA, T. and JIMM, T. (1971) Bull. JSME, 14 (70), 339.

48. SHAH, S.N., LEE, C.H. and KOBAYASHI, S. (1974) Compression of full circular cylinders between parallel flat dies. Proc. Int. Conf. in Prod. Eng., JSPE, Tokyo.

49. POHL, W. (1972) Berechnung der Temperaturverteilung beim Kaltstauchen von Metallen. Industrie Anzeiger, 94, 20, 339.

50. POHL, W. (1972) Ein Näherungsverfahren zur Berechnung der Temperatorverteilung beim Kaltstauchen von Metallen. Annals of CIRP, 21(1), 55.

51. LENGYEL, B. and MOHITPUR, M. To be published.

52. STECK, E. (1971) Numerische Behandlung von Verfahren der der Unformtechnik. Berichte aus dem Institut für Unformtechnik, Stuttgart University, Essen.

53. STECK, E. (1960) Ein Verfahren zur Näherungsweisen Berechnung des Spannungs und Verformungs-anders bei Unfornvorgängen. Annals of CIRP, 18, 251-258.

54. SCHROEDER, W. and WEBSTER, D.A. (1949) J. Appl. Mech., 16, 289.

55. UNKSOV, E.P. (1961) An engineering theory of plasticity. Butterworth, London.

56. AVITZUR, A. (1964) Israel J. Tech., 2, 295.

57. AVITZUR, B. (1968) Metal forming processes and analysis. McGraw-Hill, London.

58. AVITZUR, B. (1969) Bulge in hollow disc forging. AFML-TR-69-261.

59. HAWKYARD, J.B. and JOHNSON, W. (1967) Int. J. Mech. Sci., 9, 163-182.

60. BURGDORF (1967) Industrie Anzeiger, 86 (39), 15.

61. LEE, C.H. and ALTAN, T. (1972) J. Eng. Ind. Trans. ASME, 94, 775.

62. LIU, J.Y. (1972) J. Eng. Ind. Trans. ASME, 94, 1149.

63. LAHOTI, G.D. and KOBAYASHI, S. (1974) Int. J. Mech. Sci., 16, 54-540.

64. HILL, R. (1963) J. Mech. Phys. Solids, 11, 305.

65. JAIN, S.C. and BRAMLEY (1974) Adv. Mech. Tool Des. Res.

66. ABDUL, N.A. and BRAMLEY, A.A. (1974) Adv. Mech. Tool Des. Res.

67. DE PIERRE, V., GURNEY, F. and MALE, A.T. (1969) AFML-TR-72-37.

68. GOSH, T.P. (1974) I.E.(I) Journal, 54, 130.

69. MALE, A.T. (1964-65) J. Inst. Metals, 93, 38,46.

70. MALE, A.T. (1966) J. Inst. Metals, 94, 121.

71. MALE, A.T. and DE PIERRE, V. (1970) J. Lub. Tech. Trans. ASME, 92(3), 389.

72. LIU, J.G. ASME Paper 70-WA/Prod. 28.

73. METZLER, H.J. (1970) Uber den Einfluss der Werkzeug-geschwindigkwit auf den Stauchvorgang. University of Stuttgart.

74. NAGAMATSU, A., MUROTA, T. and JUMMA, T. (1972) Bull. JSME, 15(89), 1339.

75. CRANDALL, S.H. (1956) Engineering Analysis. McGraw-Hill.

76. FOX, L. (1962) Numerical solution of ordinary and partial differential equations. Pergamon Press.

77. ZIENKIEWICZ, D.C. (1971) The finite element method in engineering. McGraw-Hill, London.

78. FENNER, R.T. (1974) Computing for Engineers. Macmillan, London.

79. FINLAYSON, B.B. (1972) The method of weighted residuals and variational principles. Academic Press, London.

80. ZIENKIEWICZ, D.C. and TAYLOR, C. (1973) Weighted residual process in finite element with particular reference to some transient and coupled problems. In Lectures on Finite Element Methods in Continuum Mechanics, Univ. of Alabama Press, 415-418.

81. HELMAN. (1976) Ph.D. Thesis, London University.

82. FINLAYSON, B.A. and SCRIVEN, L.E. (1966) The method of weighted residuals, a version. Appl. Mech. Rev., 19(9), 735-748.

83. REINER, N. (1958) Rheology in Encyclopedia of Physics (S. Flügge ed.). Springer Verlag. 6, 434-549.

84. NEUMAN, C.P. (1974) Recent developments in discrete weighted residual methods. Computational methods in non-linear mechanics. Ed. J.T. Oden. Proc. Int. Conf. on Computational Methods, Univ. Texas, Austin.

85. HODGE, P.G. Jr. (1970) Continuum Mechanics. McGraw-Hill, London.

86. FUNG. (1965) Foundations of Solid Mechanics. Prentice Hall.

87. MENDELSON, A. (1968) Plasticity theory and application. Macmillan & Co., New York.

88. FORD. H. Advanced Mechanics. Longmans (1963).

89. SWEDLOW, J.L. (1973) A review of developments in the theory of elasto-plastic flow. NASA Report CR-2321, U.S.A.

90. CARSLAW, H.S. and JAEGER, J.C. (1959) Conduction of heat in solids. Oxford University Press.

91. ARAPACI, V.S. (1966) Conduction heat transfer. Addison Wesley, Canada.

92. BIRD, B.R., STEWART, W.E. and LIGHTFOOT, E.N. (1960) Transport phenomenon. John Wiley & Sons.

93. ORTIZ, E. Mathematica Department, Imperial College. Personal communication.

94. SLATER, R.A.C., JOHNSON, W. and LAITHWAITE, E.R. (1964-65) An experimental impact extrusion machine driven by linear motor. Proc. Inst. M.E., 179, (1), 15-35.

95. LAITHWAITE, E.R. (1975) Proc. IEEE., 63(2).

96. BOLTON, H. Department of Electrical Engineering, Imperial College. Personal communication.

97. ELMARCHABI, M.S. Department of Electrical Engineering. Imperial College. Personal communication.

98. SUZUKI, H., HASHIZUF, S., YABUKI, Y., ICHIHARA, Y., NAKAJIMA, S. and KENMOCHI, K. (1968) Dept. Inst. Ind. Sci. Tokyo University, 18, (2), 139.

99. GUHA, R.M. (1971) Temperature distribution in hydrostatic extrusion. M.Sc. Thesis, Imperial College.

100. Handbook of Thermal and Physical Properties of Solid Materials. (1965) Pergamon Press, Vol. 1.

101. TOULOUKIAN, Y.S. (Ed.) Thermal and physical properties of high temperature solid materials. Vol. 5. Macmillan & Co., New York.

102. HERCEG, E.E. (1972) Handbook of Measurement and Control. Schaevitz Engineering, Pennsauken N.J.

103. GUHA, R.M. and LENGYEL, B. (1974) J. Inst. Eng. (India), 54, ME3, 117-124.

104. GUHA, R.M. and LENGYEL, B. (1972) Annals CIRP, 21, 1.

105. BISHOP, J.F.N. Quart. J. A. Math., 9, 2, 236.

APPENDIX A

COMPUTER PROGRAMME

The flow charts are given in Chapter V, Fig. (5.5,7,8). The listing of the programme and variable name list are included in this appendix.

Main Programme - compute stress field.

Subroutine VAL - supplies some of the initial values and generates mesh.

Subroutine TEMP - computes temperature field. This subroutine is called after the stress fields have been computed in the main programme.

Subroutine SIMQ - a library procedure for solving a system of equations which employs Gaussian elimination technique. This subroutine is called in the main programme and in the subroutine TEMP.

Subroutine INC - computes flow stress.

A.1 VARIABLE NAME LIST

Main Programme

RTO - outside radius of the specimen at the interface.

RTI	-	inside radius of the specimen at the interface.
RMAX	-	maximum radius (platen).
ZMAX	-	maximum height (platen).
HITE	-	current height of the specimen.
RO	-	equatorial outside radius.
RI	-	equatorial inside radius.
RNUT	-	neutral radius.
BB	-	bulge parameter 'b'.
AKN(N)	-	shear yield stress at a node.
EDOTR) EDOTT) EDOTZ) EDOTRZ)	-	strain rates.
SINVAR	-	second invariant of strain rate tensor.
QG(NN)	-	plastic work of deformation.
SR) ST) SZ) SRZ)	-	deviatoric stresses.
SIGRC) SIGRB) SIGTC) SIGZB) SIGRB) SIGRZB)	-	coefficients of free parameters.
Z(NTT)	-	assembly of coefficients.
A(I,J)	-	corresponds to equation
C(N)	-	after call of SIMQ contains the estimates for free parameters.
SIGMAR) SIGMAZ) SIGMAT) SIGMRZ)	-	stresses.

Subroutine VAL

DEF) DEFVEL)	-	deformation velocity.
DELTAT	-	t (time).
NSTEP	-	number of deformation steps.
SHYLD	-	shear yield stress of the material.
TIME	-	time at any instant.
TI	-	ambient temperature.
ROES	-	density of the specimen.
ROEP	-	density of the platen.
RN) ZN) RNH)	-	parameters for generating mesh.
NODERS	-	number of nodes in the r-direction (specimen).
NODERP	-	number of nodes in the r-direction (platen).
NODEZS	-	number of nodes in the z-direction (specimen).
NODEZP	-	number of nodes in the z-direction (platen).
NSNODES	-	number of nodes in the specimen.
NTNODES	-	number of nodes in the specimen and platen.
KPS	-	total number of terms in the trial function for stress field.
KPT	-	total number of terms in the trial function for temperature field.
RORD	-	r coordinates.
ZORD	-	z coordinates.
MP(N)	-	boundary conditions; see Fig. 5.3 and Fig. 5.6.

Subroutine TEMP

TEMPRT	-	temperature of a nodal point.
SPKS	-	specific heat of the specimen.
SPKP	-	specific heat of the platen.
TKS	-	thermal conductivity of the specimen.
TKP	-	thermal conductivity of the platen.
DTR	-	$\frac{\partial T}{\partial r}$
DTZ	-	$\frac{\partial T}{\partial z}$
DTRR	-	$\partial T^2/\partial r^2$
DTZZ	-	$\partial T^2/\partial z$
DTT	-	$\partial T/\partial T$
T(N)	-	temperature of a nodal point.

```
C       MAIN PROGRAMME

        COMMON    A(32,32),B(1024),C(32),G(6),AKN(200),SINVAR(200),
       1 X( 6,32),IP(200),RORD(200),ZORD(200),ER(10),DEFV(10),
       2VRN(200),VZN(200),E(  200),T(200),RO(200),
       3DEFVEL,DELTAT,NSTEP,SHYLD,CKSPEC, TIME,TT,RODES,RORR,NERRT,NERREN,
       4NODERS,NODEZS ,NODERR,NODEZR, RN,ZN,PIP,QFRIC,PNUT,NSNODE,NTNODE,
       5NODETC,NTERMS ,MATERM,MCTERM,K RS,KP,  NCL, NOM,NON,KPT,KT,BB
        DIMENSION ER(4,200)

C       ASSIGN ALL KNOWN VALUES  AND GENERATE MESH

        CALL VAL
        DO 1E0 NST = 1,NSTEP
        DEFVEL = DEFV(NST)

C       INITIALISE VELOCITIES OF PLATEN NODES

        DO 130 I = (NSNODE+1),NTNODE
        VRN(I) = 0.0
  130 VZN(I) = DEFVEL
        ERROLD = 1.0E26
        ERRTOT = 0.0
        NCYCLE = 0
        RTO = RORD(NSNODE)
        RTT = RORD(NODETC)
        RMAX = RORD(NTNODE)
        ZMAX = ZORD(NTNODE)
        HITE = ZORD(NSNODE)*2.0
        RO = RORD(NODERS)
        PI = RORD(1)

C       SOLID SPECIMEN

        IF(RNH .LT. 0.0000001) GOTO 205
  206 NCYCLE = NCYCLE+1
 9002 FORMAT(8E14.6)
        FROI = RO/RI
        FRTA = RI/RO
        FRTB = FRTA*FRIA
        FRTC = FRTB*FRIA
        FRTD = FRTC*FRIA
        FRA = QFRIC*RO/HITE
        FRB = (0.5/(1.0-(RI/RO))) * ALOG(3.0*FROI*FROI/
       1    (1.0+SQRT(1.0+(3.)*(FROI**4)))))
        IF(FRA .GT. FRB) GOTO 201

C       NEUTRAL RADIUS .LE. INSIDE RADIUS

        XR1 = FROI*EXP(-QFRIC*RO*(1.0-FRIA)/HITE)
        XR = XR1*XR1
        RNUT = RO*SQRT(0.866*(1.0-FRID*XR*XR)/SQRT(XR*(XR-1.0)*(1.0-FRID*
       1    XR)))
        FR0A = RNUT/RO
        FR0B = FR0A*FR0A
        FR0C = FR0B*FR0A
        FR0D = FR0C*FR0A
        FACTA = QFRIC*((FR0B*(1.0-FRIC)/3.0)-(1.0-FRIA))
        FACTB = (RO/(HITE*SQRT(1.0+3.0*FR0D)))*((FR0D*(1.0-FRID)/4.0)
       1 -( FR0B*(1.0-FRID)) + ALOG(FROI))
        BB = FACTA/((FACTA/6.0)+FACTB)
        WRITE(6,9012)FRA,FRB,RNUT,BB,QFRIC,DEFVEL,DELTAT
        GOTO 199

C       NEUTRAL RADIUS .GT. INSIDE RADIUS

  201 ROLD = 0.0047
        DO 110 I = 1,200
        FR0A = ROLD/RO
        FR0B = FR0A*FR0A
        FR0C = FR0B*FR0A
        FR0D = FR0C*FR0A
        RNEW =(HITE/(4.0*QFRID))*((2.0*QFRIC*(RO+RI)/HITE)+
       1   ALOG(ABS (FRTB*(FR0B+SQRT(3.0+FR0D)) / (FR0B+SQRT(3.0*FRID*
       2   FR0D))))
        IF((ABS((ABS(RNEW)-ABS(ROLD))/ABS(RNEW)) .LT. 0.01) GOTO 199
        ROLD = RNEW
        IF(I .EQ. 200) WRITE (6,9003)
 9003 FORMAT(20H  DOES NOT CONVERGE                )
  110 CONTINUE
```

```
  199 RNUT = RNCH
      ERRA = RNUT/RO
      ERRB = ERRA*ERRA
      ERRC = ERRB*ERRA
      ERRD = ERRC*ERRA
      FACTA = (DERIC/ERRA)*(1.7333+(ERRC*(1.0+ERIC)/3.0)-
     1 (ERRA*(1.0+ERIA)))
      FACTB = (RO/(HITE*SQRT(1.0+3.0*ERRD)))*((ERRD*(1.0-ERIC)/4.0)
     1 -( ERRB*(1.0-ERIC)) + ALOG(ERRI))
      BB = FACTA/((FACTA/6.2) + FACTB)
      WRITE(6,9112)ERA,ERB,RNUT,BB,DERIC,DEFVEL,DELTAT
      GOTO 199
  205 BB = ((4.0*DERIC*HITE)/(1.732*RO))/(1.0+((2.0*DERIC*HITE)/
     1  (4.196*RO)))
      RNUT = 0.1
      WRITE(6,9002)BB,DERIC,DEFVEL,DELTAT
  199 WRITE(6,1014)
 1014 FORMAT(//11CH NO          R           Z          VR          VZ
     1EDOTR       EDOTT      EDOTZ     EDOTRZ        I2              /)
      DO 100 J= 1,KP
      DO 100 I = 1,KP
  100 A(I,J) = 0.0
      DO 109 NN = 1,NSNODE
      Z = ZORD(NN)
      R = RORD(NN)
      IF(R .LT. 0.0000001) R = 0.0000001
      IF(Z .LT. 0.0000001) Z = 0.0000001
      R2= R*R
      Z2= Z*Z
      AK= AKN(NN)

C     COMPUTE VELOCITIES AND STRAIN RATES

      ERN = (RNUT/R)*(RNUT/R)
      ERYT = EXP(-BB*Z/HITE)
      ER = EXP(-BB/2.0)
      VR =BB*DEFVEL*R*(1.0-ERN)*ERYT/((1.0-ER)*HITE*4.0)
      VZ = -DEFVEL*(1.0-ERYT)/(2.0*(1.0-ER))
      EDOTR = BB*DEFVEL*(1.0+ERN)*ERYT/(4.0*HITE*(1.0-ER))
      EDOTT = BB*DEFVEL*(1.0-ERN)*ERYT/(4.0*HITE*(1.0-ER))
      EDOTZ=-(EDOTR+EDOTT)
      EDOTRZ = -EDOTT*R*BB/(2.0*HITE)
      SINVAR(NN) = ABS( EDOTRZ*EDOTRZ-EDOTR*EDOTT-EDOTT*EDOTZ-EDOTZ*
     1 EDOTR)
      VRN(NN) = VR
      VZN(NN) = VZ
      SK = AK/SQRT(SINVAR(NN))
      SZCON = - 1.732*AK
      DELTAE = 1.154*SQRT(SINVAR(NN)) * DELTAT
      WRITE(6,1012)NN,R,Z,VR,VZ,EDOTR,EDOTT,EDOTZ,EDOTRZ,SINVAR(NN)
     1    ,DELTAE,ERN(NN)  ,AKN(NN)
 1012 FORMAT(I4,12E11.3)
      WRITE(6,9001)SR,ST,SZ,SRZ,SM,SJ,OG(NN)
 9001 FORMAT(4X,7E11.3)
      ED(1,NN) = EDOTR
      ED(2,NN) = EDOTT
      ED(3,NN) = EDOTZ
      ED(4,NN) = EDOTRZ

C     COMPUTE COEFFICIENTS OF FREE PARAMETERS

      NTT = 0
      NTTT = MATERM
      DO 102 NK = 1,MTERMS
      DO 102 NL = 1,MTERMS
      INDD = NK
      INDE = NL
      INDR = NK
      INDO = NL
      NTTT = NTTT+1
      SIGRC        = (R**(2*INDE-2))*(Z**(2*INDO))
      SIGTC        = SIGRC  * (2*INDR-1)
      NTT = NTT+1
      SIGRR        =(R**(2*INDE-2))*(Z**(2*INDO-2))*(4*INDR*INDR-2*INDD)
      SIGZR = (2*INDE-1)*(2*INDE-2)*(R**(2*INDE-4))*(Z**(2*INDO))
      STGRZR       =-2*INDR*(2*INDE-1)*(R**(2*INDE-3))   *(Z**(2*INDO-1))
      X(1,NTTT) = 0.6667*SIGRC-0.3333*SIGTC
      X(2,NTTT) = 0.6667*SIGTC-0.3333*SIGRC
      X(3,NTTT) = 0.0
      X(4,NTTT) = 0.0
      X(5,NTTT) = STGRC
      X(1,NTT ) = 0.6667*SIGRR-0.3333*SIGZR
      X(2,NTT ) = -0.3333*(SIGRR+SIGZR)
      X(3,NTT ) = STGRZR
      X(4,NTT) = SIGRZR
```

```
      X(5,NTT ) = SIGPR
  102 CONTINUE

C     COMPUTE CONSTANT TERMS

      X(1,KP) = -SK*ZOOTP -3.3333*SZCON
      X(2,KP) = -SK*ZOOTT - 0.7333*SZCON
      X(3,KP) = -SK*ZOOTPZ
      X(4,KP) = +PERIC*AK
      X(5,KP) = 0.0

C     SQUARE RESIDUAL FUNCTION

       DO 120 LT = 1,NERREN
      IF( LT .EQ.4  .AND.  MP(NN) .NE. 2) GOTO 120
      IF( LT .EQ.5  .AND.  MP(NN) .NE. 6) GOTO 120
      DO 101 J = 1,KP
      DO 101 I = 1,KP
  101 A(I,J) = A(I,J) + X(LT,I)*X(LT,J)*G(LT)
  120 CONTINUE
  109 CONTINUE

C     ASSEMBLE SYSTEM OF EQUATIONS

      JJ = 1
      DO 106 J = 1,KPS
      DO 104 I = 1,KPS
      B(JJ) = A(J,I)
      JJ = JJ+1
  104 CONTINUE
      C(J) = A(J,KP)
  106 CONTINUE

C     SOLVE SYSTEM OF EQUATIONS

      CALL SIMQ(B,C,KPS,KS)
      WRITE(6,1013) (C(I),I=1,KPS)
 1013 FORMAT(//4(4X,10E11.3/))
      WRITE(6,1011)
 1011 FORMAT(//125H NO          SRD          STD          SZT          SM       S
     1IGMAR      SIGMAT      SIGMAZ     SIGMAPZ          K          K*K
     1    J2                  /)
      PAW = 0.0
      QTOT = 0.0

C     COMPUTE STRESS FIELD

      DO 213 NN = 1,NSNODE
      Z = ZORD(NN)
      R = RORD(NN)
      IF(R .LT. 0.0000001) R = 0.0000001
      IF(Z .LT. 0.0000001) Z = 0.0000001
      R2= R*R
      Z2= Z*Z
      AK= AKN(NN)
      SK = AK/SQRT(SINVAR(NN))
      SZCON = - 1.732*AK
      NTT = 0
      NTTT = MBTERM
      SIGMAR=0.0
      SIGMAZ=SZCON
      SIGMAT=0.0
      SIGMPZ=0.0
      DO 214 NK = 1,MTERMS
      DO 214 NL = 1,MTERMS
      INDR = NK
      INDZ = NL
      INDP = NK
      INDQ = NL
      NTTT = NTTT+1
      SIGRC        = (R**(2*INDR-2))*(Z**(2*INDQ))
      SIGTC        = SIGRC  * (2*INDP-1)
      NTT = NTT+1
      SIGRB        =(R**(2*INDR-2))*(Z**(2*INDQ-2))*(4*INDP*INDR-2*INDP)
      SIGZB = (2*INDR-1)*(2*INDR-2)*(R**(2*INDR-4))*(Z**(2*INDQ))
      SIGRZB       =-2*INDR*(2*INDR-1)*(R**(2*INDR-3))  *(Z**(2*INDQ-1))
      SIGMAR = SIGMAR+SIGRC* C(NTTT)
      SIGMAT = SIGMAT+SIGTC* C(NTTT)
      SIGMAR = SIGMAR+SIGRB* C(NTT)
      SIGMAZ = SIGMAZ+SIGZB* C(NTT)
      SIGMRZ=SIGMRZ+SIGRZB* C(NTT)
  214 CONTINUE
      SM = (SIGMAR+SIGMAZ+SIGMAT)/3.0
      SR = SIGMAR-SM
      SZ = SIGMAZ-SM
```

```
      ST = SIGMAT-SM
      SJ=-(SR*ST+ST*SZ+SZ*SR)+(STGMRZ*STGMRZ)
      SOK = AK*AK
      VR = VRN(NN)
      VZ = VZN(NN)
      QG(NN) = ED(1,NN)*SR+ED(2,NN)*ST+ED(3,NN)*SZ+ED(4,NN)*SIGMRZ
  215 WRITE(6,1012)NN,SR,ST,SZ,SM,SIGMAR,SIGMAT,SIGMAZ,SIGMRZ,AK,SOK,SJ
  213 CONTINUE

C       COMPUTE TEMPRATURE FIELD

  207 CALL TEMP

C       COMPUTE INCREMENT OF K

      CALL INC
  150 CONTINUE
      STOP
      END



      SUBROUTINE VAL
      COMMON    A(32,32),B(1024),C(32),G(6),AKN(200),SINVAR(200),
     1 Y( 6,32),VR(200),RORD(200),ZORD(200),EG(10),DEFV(10),
     2VRN(200),VZN(200),E( 200),T(200),QG(200),
     3DEFVEL,DELTAT,NSTEP,SHYLD,AKSPEC, TTME,TI,ROES,ROEP,NERET,NERREN,
     4NODERS,NODEZS,NODERP,NODEZP, PN,ZN,RNH,QERIC,PNUT,NSNODE,NTNODE,
     5NODETC,MTERMS ,MBTERM,MCTERM,K PS,KP, NCL,NOM,NON,KPT,KT,BB
      DATA DEFV(I),I=1,10/...,.../
      SHYLD = 110000000.0
      NSTEP = 7
      TI = 18.0
      ROEP = 7850.0
      ROES = 8940.0
      NERET = 3
      NERREN = 5
      NODERS = 10
      NODEZS = 7
      NODERP = 10
      NODEZP = 4
      PN = 0.00052917
      ZN = 0.00052917
      RNH = 0.0047635
      QERIC = 0.14
      TTME = DELTAT
      DEFVEL = DEFV(1)
      SHYLD =(SHYLD+(5300.0*DEFVEL)/(ZN* 2.0*NODEZS))/1.732
      NSNODE = NODERS*NODEZS
      NTNODE = NSNODE + NODERP*NODEZP
      NODETC = NSNODE-NODERS+ 1
      MTERMS=3
      MBTERM=0
      MCTERM=0
      KPS = MBTERM+MCTERM
      KP = KPS+1
      NCL = 3
      NOM = 3
      NON = 3
      KPT = NOM*NON*NCL
      KT = KPT+1
      G(1) = 1.0
      G(2) = 1.0
      G(3) = 1.0
      G(4) = 1.0
      G(5) =1.0
      G(6) = 1.0

C       GENERATE MESH AND ASS IGN BOUNDARY CONDITIONS

      M = 0
      DO 50 J = 1,NODEZS
      Z = ZN*FLOAT(J-1)
      DO 50 I = 1,NODERS
      M = M+1
      RORD(M) = ZN*FLOAT(I-1) +RNH
      ZORD(M) = Z
      SINVAR(M) = 1.0
      AKN(M) = SHYLD
      E(M) = 0.0
      T(M) = TI
      MP(M) = 0
      IF(J .EQ. 1) MP(M) = 1
```

```
      IF(J .EQ. NODEZS) MP(M) = 2
      IF(RNH.LT.0.0001 .O R.I .EQ. 1) MP(M) = 3
   50 IF(I .EQ. 1 .OR. I .EQ. NODERS) MP(M) = 6
      ZZ = ZORD(ISNODE)
      DO 60 J = 1,NODEZP
      Z = ZN*FLOAT(J-1) + ZZ
      DO 60 I = 1,NODERP
      M= M+1
      RORD(M) = RN*FLOAT(I-1)
      ZORD(M) = Z
      MP(M) = 0
      T(M) = TT
      IF(RNH.LT.0.0001 .O R.I .EQ. 1) MP(M) = 3
      IF(J .EQ. 1) MP(M) =4
   60 IF(I .EQ. NODERP .OR. J .EQ. NODEZP) MP(M) = 5
      RETURN
      END



      SUBROUTINE INC
      COMMON    A(32,32),B(1024),C(32),G(6),AKN(200),SINVAR(200),
     1 X( 6,32),MP(200),RORD(200),ZORD(200),EE(10),DEFV(10),
     2VRN(200),VZN(200),E( 200),T(200),QG(200),
     3DEFVEL,DELTAT,NSTEP,SHYLO,CKSPEC, TIME,TI,ROES,ROEE,NERRET,NERRFN,
     4NODERS,NODEZS ,NODERE,NODEZP, RN,ZN,RNH,DERIC,RNUT,NSNODE,NTNODE,
     5NOTETC,MTERMS ,MBTERM,MC TERM,K PS,KP, NCL,NOM,NON,KPT,KT,BB

C     FOLLOWING IS FOR COPPER

      DO 211 NN = 1,NSNODE
      RORD(NN)=RORD(NN)+(VRN(NN)*DELTAT)
      ZORD(NN)=ZORD(NN)+(VZN(NN)*DELTAT)
      DELTAE = 1.1547*SQRT(SINVAR(NN)) * DELTAT
      E(NN) = E(NN) + DELTAE
      EC = E(NN)
      TC = T(NN)
      AK = SHYLO*1.732/1.056
      IF(TC .GT. 100.0) GOTO 212
      TO = TC-18.0
      IF(EC-0.15)11,12,12
   11 AK = AK +(716.0-1.84*TO)*(EC-0.05)
      GOTO 215
   12 AK = AK +(716.0-1.84*TO)*0.1
      IF(EC-0.30)13,14,14
   13 AK = AK+(650.0-1.58*TO)*(EC-0.15)
      GOTO 215
   14 AK = AK+(650.0-1.58*TO)*0.15
      IF(EC-0.50)15,16,16
   15 AK = AK+(265.0-0.97*TO)*(EC-0.3)
      GOTO 215
   16 AK = AK+(265.0-0.97*TO)*0.2
      IF(EC-0.80)17,18,18
   17 AK = AK+(153.0-0.75*TO)*(EC-0.5)
      GOTO 215
   18 AK = AK+(153.0-0.75*TO)*0.3
      AK = AK+( 71.0-0.59)*(EC- 0.8)
      GOTO 215
  212 TO = TC-100.0
      IF(EC-0.15)21,22,22
   21 AK = AK+(565.0-0.94*TO)*(EC-0.5)
      GOTO 215
   22 AK = AK+(565.0-0.94*TO)*0.1
      IF(EC-0.30)23,24,24
   23 AK = AK+(421.0-0.89*TO)*(EC-0.15)
      GOTO 215
   24 AK = AK+(421.0-0.89*TO)*0.15
      IF(EC-0.50)25,26,26
   25 AK = AK+(185.0-0.40*TO)*(EC-0.3)
      GOTO 215
   26 AK = AK+(185.0-0.40*TO)* 0.2
      IF(EC-0.80)27,28,28
   27 AK = AK+(88.00-0.23*TO)*(EC-0.5)
      GOTO 215
   28 AK = AK+(88.00-0.23*TO)*0.3
      AK = AK+(36.00-0.23*TO)*(EC-0.8)
  215 AKN(NN) =(AK/1.732 )*1.0E6
  211 CONTINUE
      RETURN
      END
```

```
      SUBROUTINE TEMP
      COMMON    A(32,32),B(1024),C(32),G(6),AKN(200),SINVAR(200),
     1 X( 6,32),VP(200),ROPD(200),ZORD(200),EP(10),DEFV(10),
     2VRN(200),VZN(200),F( 200),T(200),QG(200),
     3DEFMEL,DELTAT,NSTEP,SHYLD,SKSPEC, TIME,TI,ROES,ROEP,NEREF,NERPEN,
     4NODERS,NODEZS ,NODEPP,NODEZP, DN,ZN,DTH,OFDID,RNUT,NSNODE,NTNODE,
     5NODETC,NTERMS ,NBTERM,NCTERM,K RS,KP, NCL,NOM,NON,KPT,KT,BB
      KPT = NCL*NOM
      KT = KPT+1
      NPNODE = NSNODE+NODEPP
      DO 301 I = 1,KT
      DO 301 J = 1,KT
  301 A(I,J) = 0.0
      DO 302 NN = 1,NTNODE
      RMAX = RORD(NTNODE)
      ZMAX = ZORD(NTNODE)
      HITE = ZORD(NSNODE)*2.0
      TEMPPT = T(NN)
      R=RORD(NN)
      Z=ZORD(NN)
      RIN = RORD(NODETC)
      ROUT = RORD(NSNODE)

C     NODES  ON THE INTERFACE (PLATEN ONLY)

     1   R .LE. ROUT) GOTO 302
      IF(NN .GT. NSNODE .AND. NN .LT. NPNODE .AND. R .GE. RIN .AND.

C     NODES  ON THE R-AXIS

      IF(NN .LE. NODERS ) GOTO 302

C     NODES  ON THE Z-AXIS (SOLID SPECIMENS  ONLY)

      IF(RNU .LT. 0.00001 .AND. MP(NN) .EQ. 3) GOTO 302
      IF(R .LT. 0.0000001) R = 0.0000001
      IF(Z .LT. 0.0000001) Z = 0.0000001
      R2 = R*R
      Z2 = Z*Z
      RF = R2 - RMAX*RMAX
      ZF = Z2 - ZMAX*ZMAX
      AK = AKN(NN)
      VR=VRN(NN)
      VZ = VZN(NN)

C     MATERIAL PROPERTIES

      SPKS=(0.002+(0.002/74.0)*(TEMPPT-TI))*4.186*1000.0
      SPKP= (0.1255+(0.0045/42.0)*(TEMPPT-TI))*4.186*1000.0
      TKS = (340.5-(13.5/98.0)*(TEMPPT-TI))*4186.0/3600.0
      TKP = (30.0-(1.2/82.0)  *(TEMPPT-TI))*4186.0/3600.0
      HEILM = (0.0+0.04*(TEMPPT-TI))*4186.0/3600.0
      BETAS = ROES*SPKS/TKS
      BETAP = ROEP*SPKP/TKS

C     COMPUTE CONSTANT TERMS

      IF(NN .GT. NSNODE) GOTO 351
      IF(NN .GE. NODETC) GOTO 350
      ALPHA = TKS/(ROES*SPKS)
      X(1,KT) = QG(NN)/(ROES*SPKS)
      GOTO 352
  350 ALPHA = (TKS+TKP)/(2.0*(ROES*SPKS + ROEP*SPKP))
      X(1,KT) = (ABS(OFDID*AK*VR*BB/HITE)+QG(NN))*2.0/(ROES*SPKS+
     1   ROEP*SPKP)
      GOTO 352
  351 ALPHA = TKP/(ROEP*SPKP)
      X(1,KT) = 0.0
  352 X(2,KT) = -HEILM*(TEMPPT-TI)/TKS
      X(3,KT) = -HEILM*(TEMPPT-TI)/TKP

C     COMPUTE COEFFICIENTS OF FREE PARAMETERS

      NT = 0
      DO 303  IL = 1,NCL
      DO 303  IM = 1,NOM
      NT = NT+1
      NTM = IM
      NTL = IL
       SER = (R**(2*NTL))*(Z**(2*NTM))
      DTR = ZF*(SER/R)*2.0*(R2+RF*NTL)
      DTRR = ZF*(SER/R2)*2.0*(R2+R2*NTL*4.0+(2.0*NTL-1.0)*RF*NTL)
      DTZ = RF*(SER/Z)*2.0*(Z2+ZF*NTM)
```

```
      DTZZ = RF*(SER/Z2)*2.0*(Z2+Z2*NTM*4.0+(2.0*NTM-1.0)*ZF*NTM)
      X(1,NT) = DTRR+DTZZ+(DTE/R)
      X(2,NT) = DTR
      X(3,NT) = -DTZ
  303 CONTINUE

C     SQUARE RESIDUAL FUNCTION

      DO 300 LT = 1,NERET
      IF(LT .EQ. 1 )GOTO 305
      IF(LT .EQ. 2) GOTO 307
      IF(LT .EQ. 3 )GOTO 306
  307 IF(MP(NN) .NE. 6) GOTO 300
      GOTO 305
  306 IF(MP(NN) .NE. 4 .AND. (R.LT.RORD(NSNODE).OR. R.GT.RORD(NODETO)))
     1   GOTO 301
  305 DO 304 I = 1,KT
      DO 304 J = 1,KT
  304 A(I,J) = A(I,J) + X(LT,I)*X(LT,J)*G(LT)
  300 CONTINUE
  302 CONTINUE

C     ASSEMBLE SYSTEM OF EQUATIONS

      JJ = 1
      DO 242 I = 1,KPT
      DO 243 J= 1,KPT
      B(JJ) = A(I,J)
  243 JJ = JJ+1
  242 C(I) = A(I,KT)

C     SOLVE SYSTEM OF EQUATIONS

      CALL SIMQ(B,C,KPT,KS)
      WRITE(6,1013) (C(I),I=1,KPT)
 1013 FORMAT(//4(4X,10E11.3/))

C     COMPUTE TEMPERATURE FIELD

      DO 253 NN = 1,NTNODE

C     NODES  ON THE INTERFACE ( PLATEN ONLY)

      IF(NN .GT. NSNODE .AND. NN .LT. NPNODE .AND. R .GE. RIN .AND.
     1   R .LE. ROUT) GOTO 253

C     NODES  ON THE R-AXIS

      IF(NN .LE. NODERS ) GOTO 253

C     NODES  ON THE Z-AXIS (SOLID S PECIMENS  ONLY)

      IF(RNN .LT. 0.00001 .A ND. MP(NN) .EQ. 3) GOTO 253
      R = RORD(NN)
      Z = ZORD(NN)
      IF(R .LT. 0.000001) R = 0.0000001
      IF(Z .LT. 0.000001) Z = 0.0000001
      R2 = R*R
      Z2 = Z*Z
      RF = R2 - RMAX*RMAX
      ZF = Z2 - ZMAX*ZMAX
      NT = 0
      DO 252IL    = 1,NOL
      DO 252IM    = 1,NOM
      NT = NT +1
      NTL = IL
      NTM = IM
       SER =  (R**(2*NTL))*(Z**(2*NTM))
      TIN =    RF*ZF*SER*C(NT) + TIN
  252 CONTINUE
      IF(TIN .LT. 0.0) TIN =0.0
      T(NN) = T(NN) + TIN
      WRITE(6,2000) NN,R,Z,T(NN)
  253 CONTINUE
 2000 FORMAT(10(I4,E9.3)/)
      RETURN
      END
```

APPENDIX B

PROPERTIES OF MATERIALS

Mechanical and thermal properties [32,99,102] of the materials used in this work are illustrated in this appendix.

B.1 STRESSES

In Chapter V it was shown that the increment k can be calculated by

$$\Delta k = \frac{2}{\sqrt{3}} \sqrt{I_2}(C_k \Delta t + m)$$

where:

I_2 = second invariant of the strain rate tensor,

Δt = increment in time,

C_k, m = constants.

The stress-strain characteristics of copper and aluminium are graphically represented in Fig. B.1 and Fig. B.4. The curves are divided into segments, within which the slope C_k is assumed to be constant. Similarly this slope is assumed to vary linearly within specified ranges of temperatures. The values of C_{kT} derived in this manner are given in the following tables. The slopes can also be used to calculate flow stress for any given strain.

COPPER - C_{kT}

	$18^{\circ}C < T < 100^{\circ}C$	$100^{\circ}C < T < 400^{\circ}C$
$0.5 < \bar{\varepsilon} < 0.15$	716 - 1.84 (T-82)	565 - 0.94 (T-100)
$0.15 < \bar{\varepsilon} < 0.30$	550 - 1.58 (T-82)	420 - 0.89 (T-100)
$0.3 < \bar{\varepsilon} < 0.50$	265 - 0.97 (T-82)	185 - 0.40 (T-100)
$0.3 < \bar{\varepsilon} < 0.80$	153 - 0.79 (T-82)	88 - 0.24 (T-100)
$0.8 < \bar{\varepsilon} < 1.20$	70 - 0.59 (T-82)	21 - 0.72 (T-100)

Strainrate Sensitivity - m

Copper m = 0.053 (Fig. B.3)

Swedlow [90] used a technique very similar to this and reported them to be satisfactory. The incremental strain

$$\Delta\bar{\varepsilon} = \dot{\bar{\varepsilon}}\,\Delta t$$

therefore

$$\bar{\varepsilon} = \bar{\varepsilon} + \Delta\bar{\varepsilon}$$

If the strain sustained before the incremental step of deformation and strain after the incremental step of deformation are such that they lie in two different regions of linearised segments, then the average slope is used to calculate Δk. As the incremental steps are small, any error that arises from this averaging of slope may be ignored.

B.2 HEAT PARAMETERS

The heat parameters are graphically represented in Figs. B.7 to B.13. They may be numerically represented as follows:

$$T_I = 18^{o}C.$$

Steel (platen)

Specific heat C_p (Fig. B.7)

$$= [0.1055 + 0.000107(T-T_I)]\ 4186\ J/kg.^{o}C.$$

Thermal conductivity k_p (Fig. B.8)

$$= [39 - 0.0146(T-T_I)]\ 1.1627\ J/ms.^{o}C.$$

Copper

Specific heat C_s (Fig. B.9)

$$= [0.092 + 0.000027(T-T_o)]\ 4.86\ J/kg.^{o}C.$$

Thermal conductivity k_s (Fig. B.10)

$$= [349.5 - 0.088(T-T_I)]\ 1.1627\ J/ms.^{o}C.$$

Surrounding medium

Heat transfer from coefficient h_f (Fig. B.13)

$$= [9.9 + 0.057(T-T_I)]\ 1.1627\ J/ms.^{o}C.$$

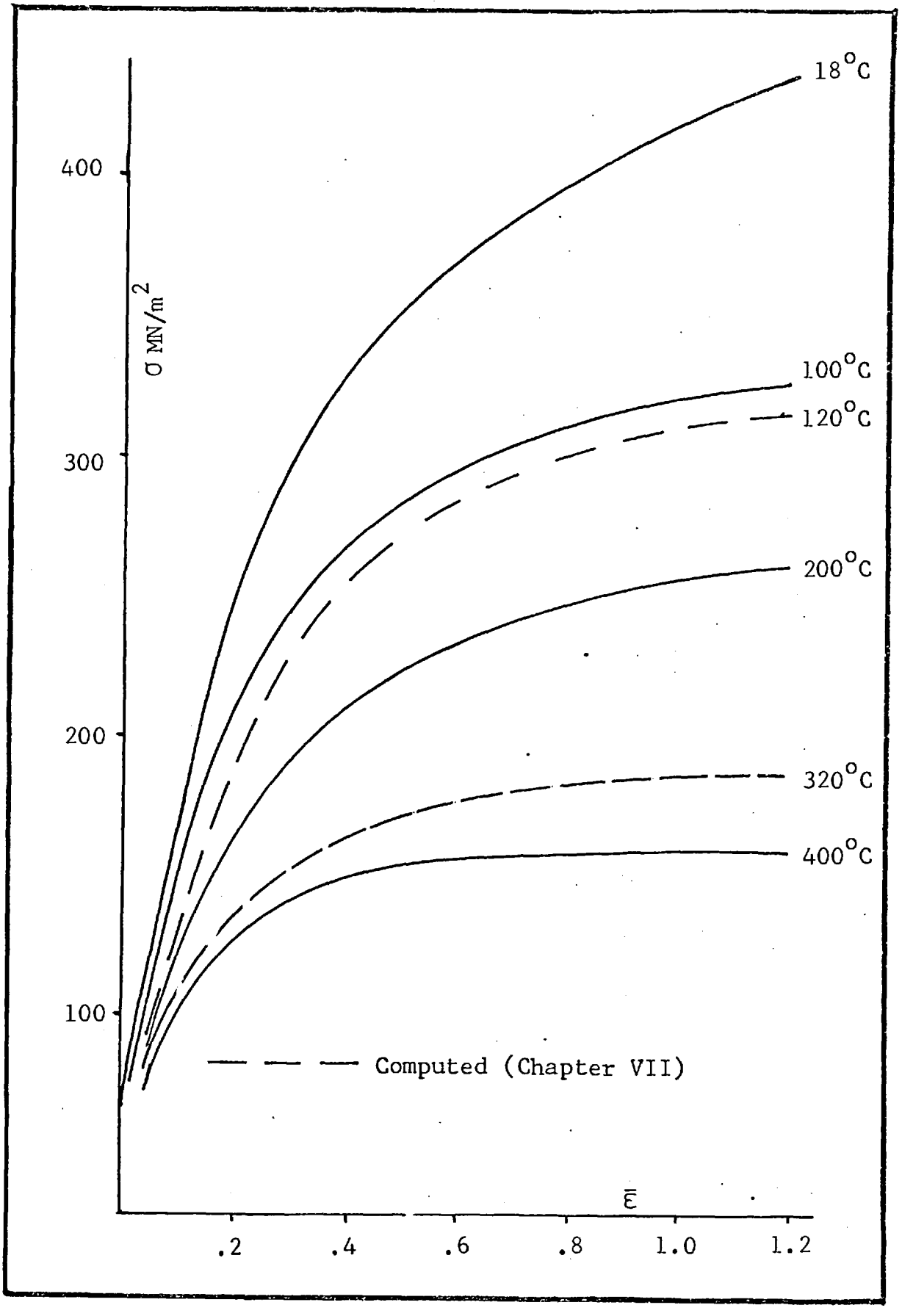

FIG. B.1 Stress/Strain Relationship of 99.9% Cu [32]

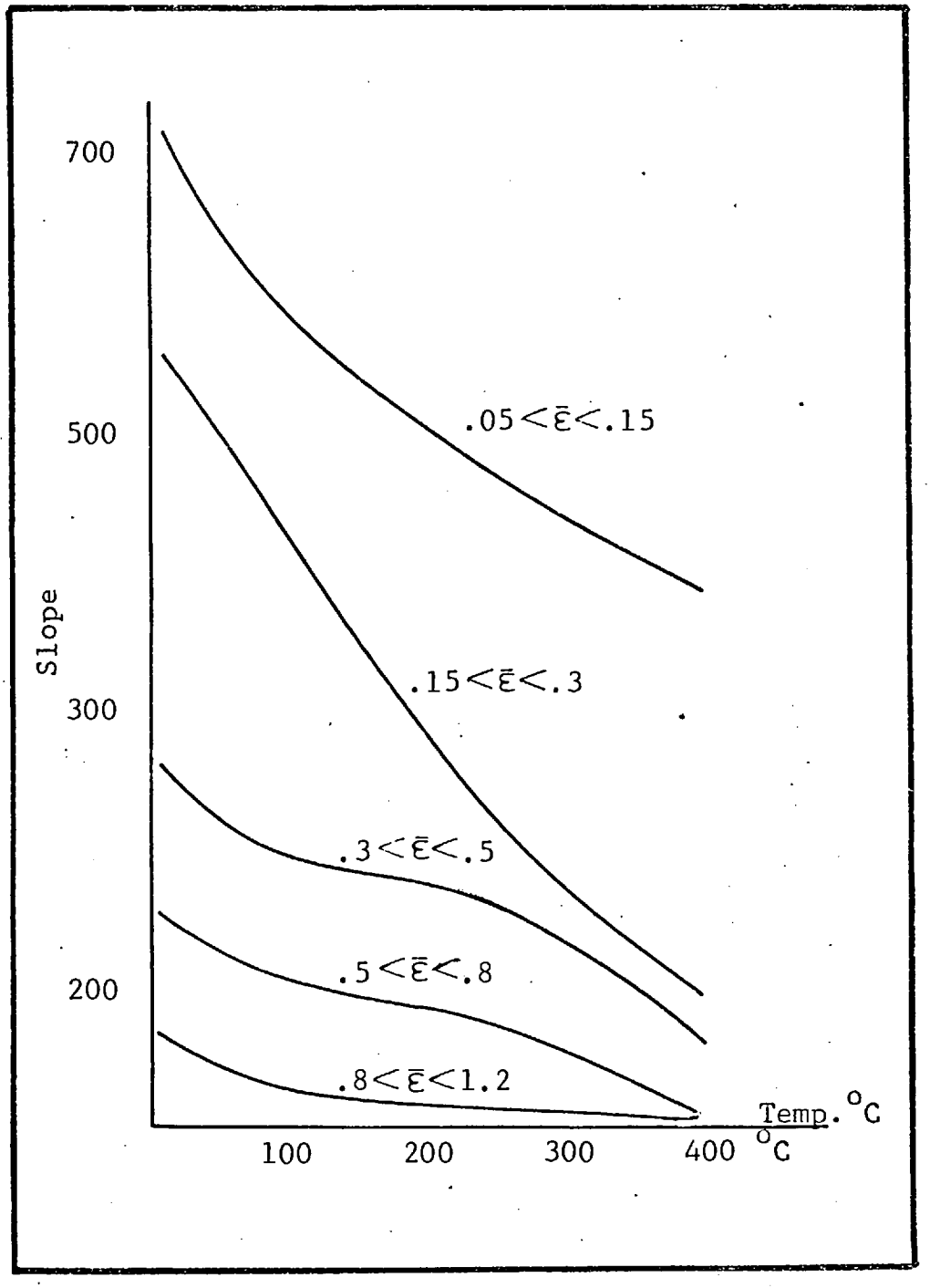

FIG. B.2 Slope of σ/ε Curve/Temperature of Copper [32,99].

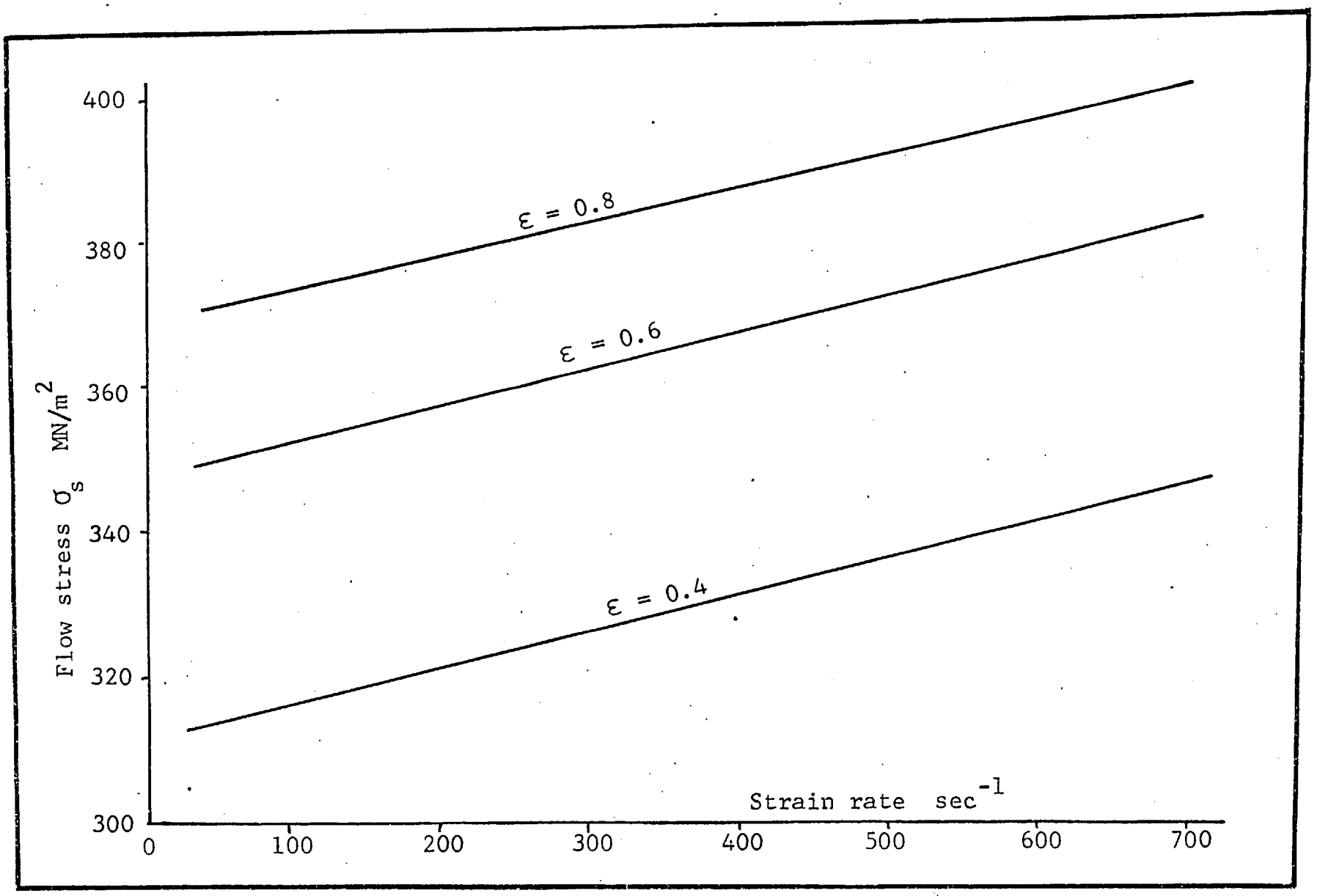

FIG. B.3 Flow Stress/Strain Rate Characteristics of 99.9% Cu [32].

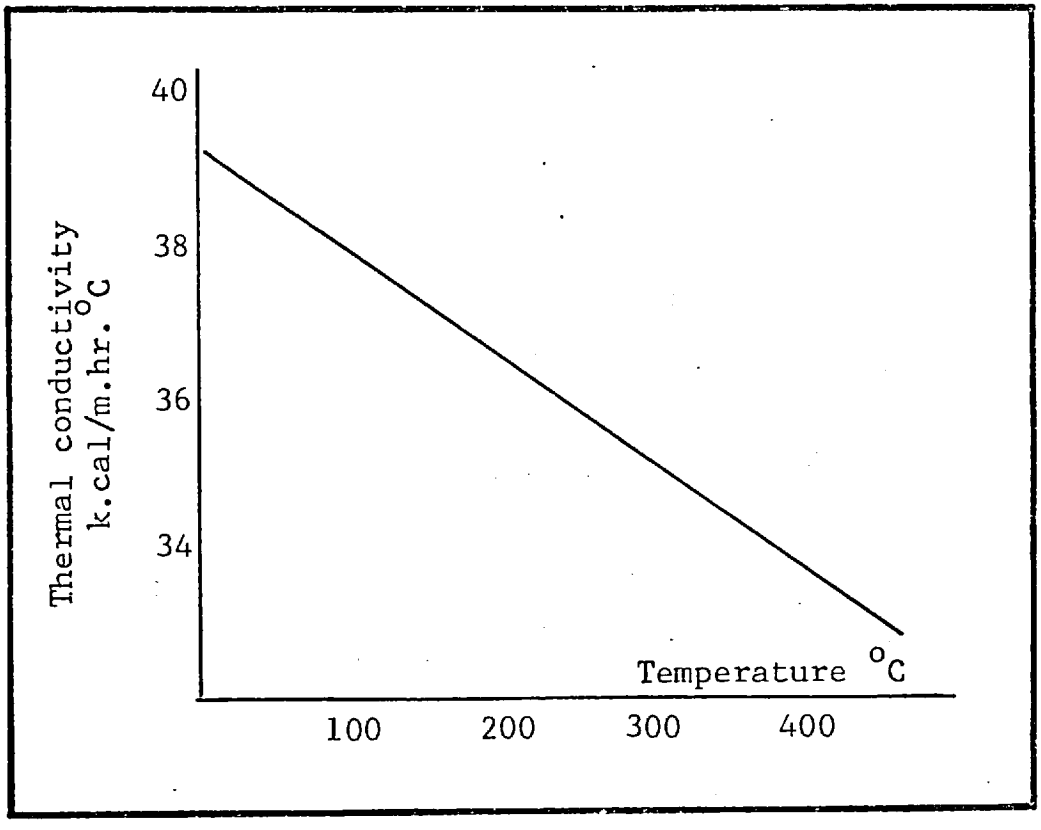

FIG. B.4 Thermal Conductivity of Steel (platen) [101].

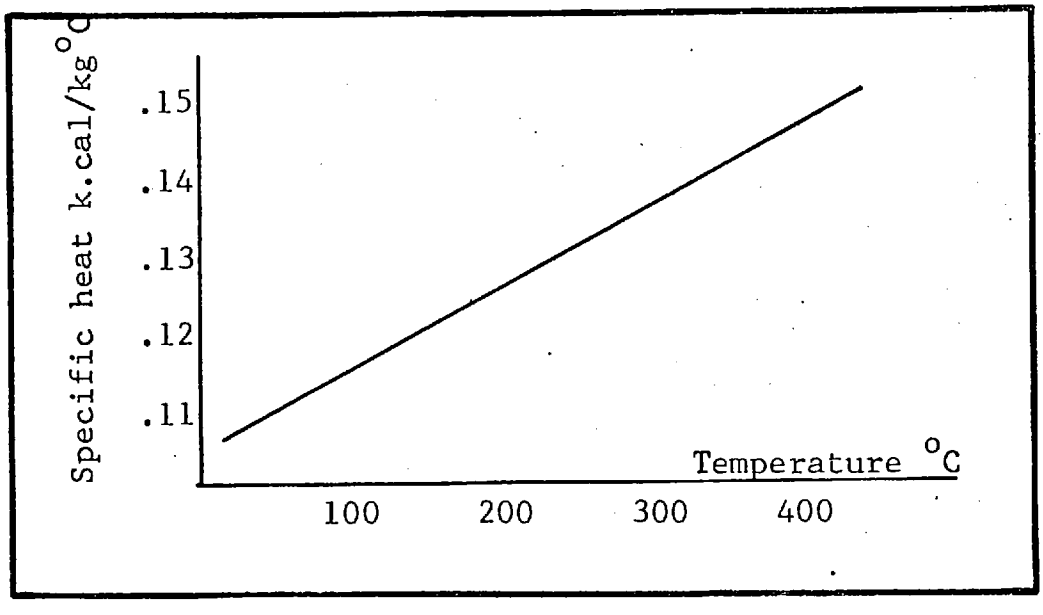

FIG. B.5 Specific Heat of Steel (platen) [101].

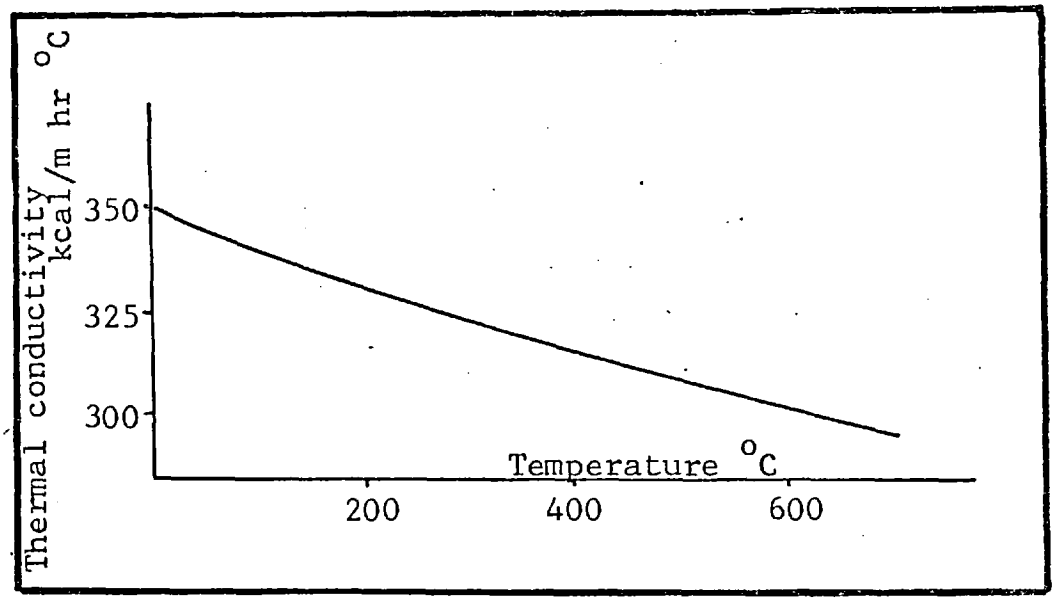

FIG. B.6 Thermal Conductivity of Copper [100].

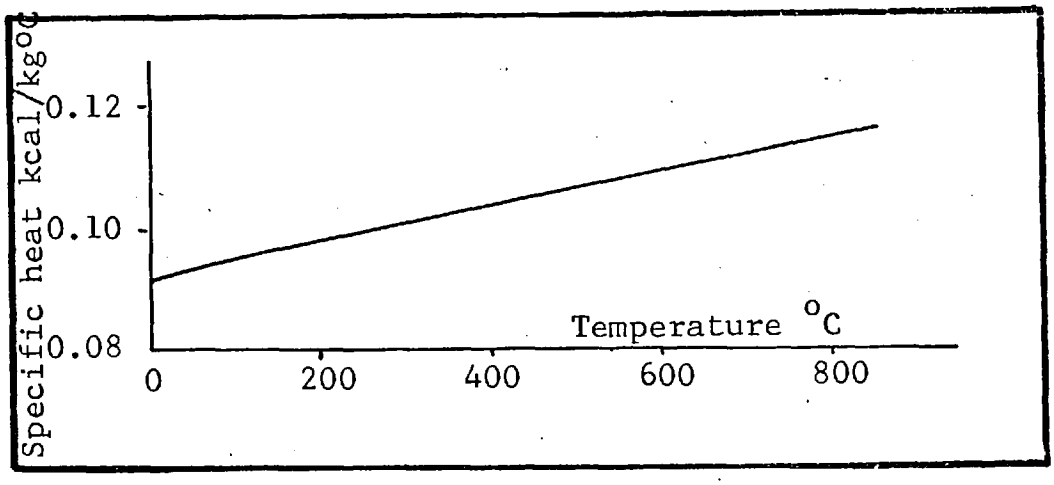

FIG. B.7 Specific Heat of Copper [100].

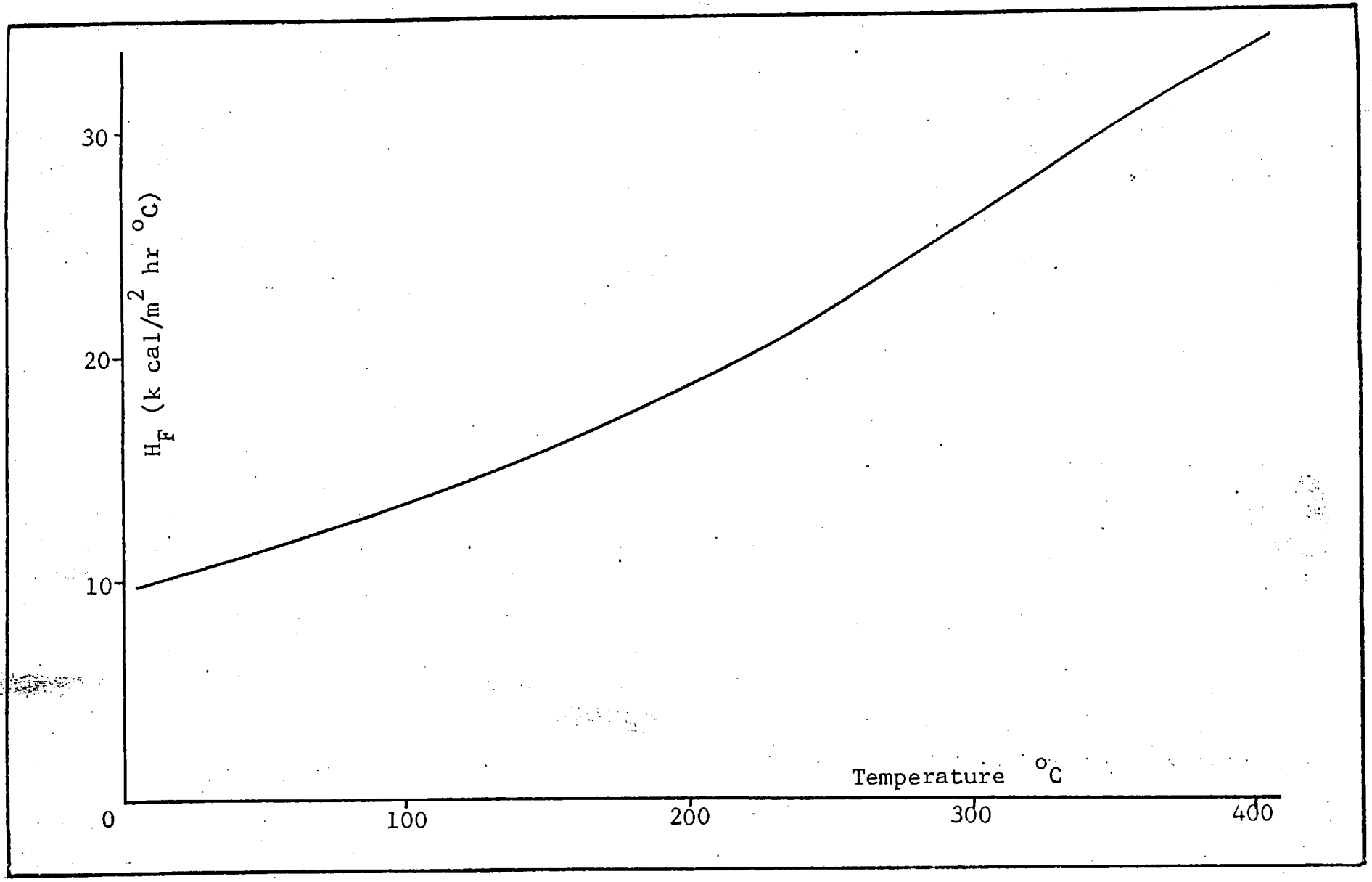

FIG. B.8 , Heat Transfer Film Coefficient [100].